UNIVERSITY OF SOUTHAMPTON

Faculty of Physical and Applied Sciences

Department of Electronics and Computer Science

Supervisor: Prof. Jan Sykulski and Assoc. Prof. Dr Mihai Rotaru

Electromagnetic Compatibility Studies Within Smart Grid Automated Substation

by

Aine Izzati Tarmizi

Thesis for the degree of Doctor of Philosophy

February 2020

UNIVERSITY OF SOUTHAMPTON

ABSTRACT

FACULTY OF PHYSICAL AND APPLIED SCIENCES

DEPARTMENT OF ELECTRONICS AND COMPUTER SCIENCE

Doctor of Philosophy

ELECTROMAGNETIC COMPATIBILITY WITHIN SMART GRID AUTOMATED SUBSTATION

by Aine Izzati Tarmizi

Electromagnetic Compatibility (EMC) is the ability of an equipment or system to function satisfactorily in its electromagnetic environment without introducing intolerable electromagnetic disturbances to anything in that environment. Within the smart grid automated substation, all equipment installed need to be compatible with each other. The electromagnetic environment within high voltage substations needs to be correctly predicted and quantified. This is due to more and more sensitive power electronic devices such as microelectronic equipment that are introduced and other disturbances event in a smart grid system. This trend will only increase with the advent of the 'smart grid'; therefore, there is a need to reassess the substation environment compatibility for current and future circumstances. In this thesis, the numerical calculation method used to determine magnetic field distribution within a substation environment has been reviewed using the input from substation performance in power system software. A new routine developed in-house using Matlab, where a hybrid combination of the Biot-Savart Law (BSL) and Finite Difference Method (FDM) calculating magnetic field within the substation environment. BSL is first used to identify the magnetic field distribution for the whole substation in a large mesh grid. This combination reduced by 50% of the simulation time to predict the magnetic field distribution within the whole substation environment compared to using FDM alone. Specific areas of interest are then identified for more detail study using FDM to produce the magnetic field distribution in a finer mesh grid allows a much better field resolution. The calculation result compared with an experimental measurement done at the same substation environment for validation excellent agreement between the modelling and experiment with 3.5% difference. The result then compared with the recommended safety limit standard. The induced current then generated by the magnetic field distribution around it are calculated, thus allows the user to predict the equipment's compatibility with the distributed field within the substation environment for refurbishment purposes.

Table of Contents

List of Tables

List of Figures

Declaration of Authorship

I, Aine Izzati Tarmizi declare that this thesis entitled ‘Electromagnetic Compatibility within Smart Grid Automated Substation’ and the work presented in it are my own and has been generated by me as the result of my own original research.

I confirm that:

1. This work was done wholly or mainly while in candidature for a research degree at this University;
2. Where any part of this thesis has previously been submitted for a degree or any other qualification at this University or any other institution, this has been clearly stated;
3. Where I have consulted the published work of others, this is always clearly attributed;
4. Where I have quoted from the work of others, the source is always given. With the exception of such quotations, this thesis is entirely my own work;
5. I have acknowledged all main sources of help;
6. Where the thesis is based on work done by myself jointly with others, I have made clear exactly what was done by others and what I have contributed myself;
7. Parts of this work have been published as listed in section 1.4.

Signed:

Date:

Acknowledgements

Alhamdulillah, all praise and thanks to Allah s.w.t. for providing me with this opportunity and granting me the strength, capability and guidance to complete this thesis successfully.

My sincere gratitude to my supervisors, Professor Jan Sykulski, for his immense knowledge, experiences, and countless patients. To my second supervisor, Assoc. Prof. Dr Mihai Rotaru whom always with an answer to my questions, unlimited guidance and non-stop assistance support to finish this thesis writing. I could not have imagined having a better advisor and mentor for my PhD study. I wish they will have all happiness in the world with their families and always in excellent health.

A special thanks to my beloved family members and supportive friends for their continuous prayers and endless encouragement that inspire me to complete this journey.

Words cannot express how grateful I am to my dear husband, Radi Husin for all his help and support, emotionally and knowledge, encouragement and prayer that what sustained me thus far. People said, PhD is a lonely journey, and I think it's not true since I always have you either in good or bad days, this is for both of us. To my lovely daughter Izza Athirah, I am so grateful for your great patience and love, and to my dear Adil Husin for the hope and strength to finish this journey.

Nomenclature

$\nabla \times$	curl
μ	permeability
μ_r	Relative permeability
τ	Time constant
σ	conductivity
$\lvert H \rvert$	Magnitude of magnetic field
$\mathbf{H}$	Magnetic field intensity
$\mathbf{B}$	Magnetic field
$\mathbf{J}_e$	electric current density
$\mathbf{I}$	current
ds	Surface area
δ	skin depth

Abbreviations

BEM	Boundary Element Method
BSL	Biot-Savart Law
DPR	Digital Protective Relays
EMC	Electromagnetic compatibility
EMI	Electromagnetic Interference
FDM	Finite Difference Method
FEM	Finite Element Method
FFT	Fast Fourier Transform
IED	Intelligent Electronic Devices
ICNIRP	International Commission on Non-Ionizing Radiation Protection
PEI	power electronic interface
PLC	Powerline Communication
WHO	World Health Organization

CHAPTER 1

INTRODUCTION

1.1 Background of the Research Area

Electrical power systems is a network that consists of the electrical component to generate the electrical energy then transfer to the user as load, and it is expected to be able to operate under increasingly complex conditions and situations. The recent broad implementation and penetration of renewable generation and demand have introduced new challenges to the operation of the electric grid [1]. With these challenging conditions, the overall system's operation requires new and innovative approaches to enhance the performances of the power grid. One of the novel ways is the concept of a smart grid [2, 3]. Sensing nodes, communication networks and information systems are embedded and integrated into the power network to create a 'smart' grid that can manage almost autonomously all operating conditions by itself [4]. A smart grid is a power system that enables real-time communication and control between the consumer and the utility such that the energy usage is optimised. It is able to consider different aspects; such as cost, technical and environmental constraints when providing optimum power supply to the customer [2].

To operate in such a mode, the smart grid will utilise digital information technology to create a more efficient, reliable and responsive network that is flexible. Communication within a smart grid will not be limited to that between the consumer and the utility only but will include channels between digital relays, so that information could be exchanged between relays without necessarily involving the control centre. This type of network of communication will provide a self-managing capability that will allow the smart grid to develop different strategies in the protection and control of the system. The smart grid architecture aims to provide overall power network monitoring, create control strategies to maintain the system performance, security, reduce the cost of operation, maintenance and system availability planning [5]. The control built within a smart grid will allow the flexibility to handle distributed resources, stochastic demand,

to adapt to new conditions of operation and to respond optimally to smart appliances connected to the grid [2].

Consequently, a smart grid has the potential to improve the efficiency and reliability of the power delivery; however, due to its increased complexity and dependence on technologies that were not previously part of the power grid, the smart grid may be susceptible to factors that will affect negatively it is normal functioning. Some of these factors may result from Electromagnetic Interference (EMI) [6]. The interferences could be from electromagnetic (EM) fields of natural or man-made origin, radiated directly into devices or conducted via the power, signal or ground connections. A smart grid may contain a large number of data communication channels, in support of applications with divergent functions, which can all be degraded by electromagnetic interference [7]. These functions have different reliability requirements, correlating with different levels of data flow reliability, and may require different radiated and conducted immunity levels[6]. Therefore, electromagnetic compatibility (EMC) studies are essential for the latest technology of smart grid within substation environment are crucial to ensure that the compatibility level between each and every component and the overall of the system [8].

1.2 Research Motivation

More development of the current electrical power system into the Smart Grid system implementation is expected to happen rapidly in this near future. This not only the implementation of managing the system is changing, but also many of the component or equipment installed in the system will be evolving to support this new technology too [2, 5]. Electromagnetic compatibility (EMC) studies within smart grid substation environment must be considered to ensure continuous reliable real-time operation between new component and equipment in the smart grid system operation [6].

The main revolution in a smart grid system in power generation will be the rise of renewable energy generation that connected to the grid. With the increment of renewable energy in generating power into the power system such as solar and wind, it leads to new technologies applied into the system and offers an alternative source of unlimited energy and free from pollution. However, there are several potential challenges in integrating renewable energy with the existing grid, which is to keep all component and equipment are electromagnetically compatible not only with each other but to the whole system [6, 8].

The EMC issues include the usage of new power electronic interface (PEI) such as smart meter, power converter and energy storage introduce in the smart grid substation [9]. The installation of photovoltaic plants (PV) itself into the power system to generate power arise the EMC issues, especially when dealing with high-power grid-connected PV plants [10]. The main

topics are radiated and conducted emissions, and immunity problems in electronic equipment. All of this new equipment and component are the source of disturbances towards the smart grid system that lead to the increment of the motivation to study the electromagnetic compatibility of this technology in smart grid substation system [11-13].

Other than the equipment, the substation's daily operation might be the source of EMI such as switching off a circuit breaker [14-16]. This due to the high-frequency transient current produced by this switching activity, will induce electromagnetic interference not only among standard equipment but also the new equipment installed in the smart grid system. The other source of disturbances towards the smart grid system is from the natural event which is lightning strike [17], and the High Power Electromagnetic (HPEM)[18] has been reported in previous research finding. With all EMC issues increasingly occurred in the smart grid system; therefore, it became a motivation to studies the EMC within the smart grid substation by predicting the magnetic field distribution to have a safe and reliable smart grid system.

There are few method and approach has been used in previous research to tackle these issues, such as experimental measurement at the real substation site [19], and the most popular approach is via simulation and modelling using a numerical calculation. Although many research using simulation and mathematical modelling of the magnetic field has been carried out, there are limited studies done for the magnetic field calculation within the large substation environment with the disturbances applied. Thus, the real substation has been modelled and simulated with the source of disturbances to study the EMC condition in the substation. Based on this motivation, a simple simulation used to predict magnetic field distribution induced by current flow during normal operation and the disturbances introduce in the substation circuit. Therefore, this research work focuses on electromagnetic compatibility (EMC) studies within smart grid substation environment. EMC must be considered to ensure continuous reliable real-time operation in the many locations where the Smart Grid equipment will operate [6].

1.3 Objectives of the Research

The objectives of this research work as follows:

1. to model substation performance flow during the nominal working condition and to apply lightning current as a disturbance event in the circuit.
2. to evaluate the magnetic field distribution using the Biot-Savart Law (BSL) within the substation environment and to validate the results with published site measurement data and international standards.
3. to compute magnetic fields using the finite difference method (FDM) in finer mesh grid inside and on the metal box that illustrates the new equipment to be installed in substation.
4. to investigate induced current generated due to the calculated magnetic field distributed around the metal box and penetrate inside the box for shielding effect and electromagnetic compatibility studies.

1.4 Research Contributions

This thesis contribution of research work for electromagnetic compatibility studies within the substation is highlighted as follows:

1. **The distribution of current flow in the substation for magnetic field calculation**. Traditionally, the magnetic field distribution within a substation is determined through experimental measurement, which only quantifies steady-state conditions. This research work introduces a model to simulate the current flow in a substation during a lightning disturbance. Differentiating between steady-state and transient features of current flow in a substation is vital to calculate the magnetic field distribution and identify areas where they are concentrated. This approach enables the prediction of magnetic field profiles within the substation environment and eliminates the needs for extensive installation of expensive measuring equipment.

2. **The hybrid combination of Biot-Savart Law (BSL) and Finite Difference Method (FDM) calculating magnetic field**.
   Applying FDM directly to evaluate the magnetic field distribution for the whole substation would require extensive computation time. Therefore, this research work introduces a new concept where BSL is first used to identify the magnetic field distribution for the whole substation in a large mesh grid. Specific areas of interest are then studied in more detail using FDM to produce the magnetic field distribution in a finer mesh grid. The strength of using this combination is that the simulation time to predict the magnetic field distribution was reduced by 50% compared to using FDM

alone. The result is validated using site measurement data and compared with the recommended limit standard.

3. **Develop a novel "metal box" concept to evaluate the potential EMC and shielding effects on equipment placed at specific areas.**

   To determine whether a specific location is suitable for installing new equipment, the potential EMC effects need to be studied. Currently, there are limited techniques available to model this behaviour during disturbances. By using this concept, the induced current generated by the magnetic field distribution around it can be calculated. This allows the user to predict the equipment's compatibility with the distributed field within the substation environment for refurbishment purposes.

From the research work presented in this thesis, the following papers have been published:

1. **A. I. Tarmizi**; Mihai D. Rotaru; Jan K. Sykulski. Electromagnetic compatibility studies within smart grid automated substations. Power Engineering Conference (UPEC), 2014 49th International Universities. 2014.
2. **A. I. Tarmizi**; Mihai D. Rotaru; Jan K. Sykulski. Magnetic field calculations within substation environment for EMC studies. 2016 IEEE 16th International Conference on Environment and Electrical Engineering (EEEIC).2016.
3. **A. I. Tarmizi**; R.H. Ramlee, Mihai D. Rotaru. Electromagnetic Compatibility Studies of Substation Environment using Finite Difference Method. International Journal of Engineering & Advanced Technology (IJEAT).2019.
4. A. I. Tarmizi; R. H. Ramlee; Hybrid Combination of Biot Savart Law and Finite Difference Method for Magnetic Field calculation within Substation's EMC Studies (Draft)

1.5 Thesis Structure

The thesis consists of five chapters that arranged, and structures as follows:

Chapter 1 gives an introduction and background of the research area, which is focusing on the magnetic field calculation for electromagnetic compatibility within a substation environment. It starts with a description of the research motivation and leads to the objectives of studying the EMC within an automated substation. The chapter also highlights the research contributions together with the list of research publications.

Chapter 2 reviews the literature and theory relevant to the investigation of electromagnetic compatibility (EMC) within the substation. It starts with the basic definition of EMC and continues discussing the characteristic of smart grid systems and the equipment used in the system. Detailed explanations on the automated substation equipment and component that implemented in Smart Grid are given. This chapter also describes previous measurement and numerical calculation methods used to study the electromagnetic field distribution within the substation. At the end of this chapter, EMC limitation guideline and standard also discussed.

Chapter 3 starts with the introduction of the methodology used in this research. Then it provides details of the substation layout used for this whole research, which is the Rosiori substation located in Romania. It is also elaborate detail descriptions of the simulation and calculation methods used and the assumption that has been made together with the modelling procedures adopted.

Chapter 4 discuss the calculation result and the analysis of the research. This result includes those obtained from the substation simulation result using Digsilent PowerFactory software where it used as input to calculate the magnetic field obtained by using the Biot-Savart Law (BSL) within the substation environment. The calculated fields are compared with limitation guideline and validated with published site measurement data. Based on the BSL calculation result, Finite Difference Method (FDM) applied to calculate the magnetic field with the smaller mesh grid at the specific area chosen by refereeing to the earlier finding of the distribution of the magnetic field. Then discuss in details of electromagnetic field prediction with metal box introduction as an illustration of new equipment installed in the smart grid substation environment using FDM calculation. The magnetic field flows inside the metal box and diffuses on the metal box surface were calculated with a cut opening to demonstrate the opening on the real equipment and how the field flows into the box. The magnitude of the calculated magnetic field calculated and compared with the limitation standard that requires for the smart grid system.

Chapter 5 concludes the research study and highlight the recommendations for the future work of this research project.

CHAPTER 2

LITERATURE REVIEW

2.1 Electromagnetic Compatibility within Substation Environment

The ability of an equipment or system to function satisfactorily in its electromagnetic environment without introducing intolerable electromagnetic disturbances to anything in that environment is known as Electromagnetic Compatibility (EMC) [8]. Equipment or system must function satisfactorily in its electromagnetic environment without introducing intolerable electromagnetic disturbance to anything in that environment. The electromagnetic disturbance can propagate from a source to one or several victims, which are the equipment that connected via the electric grid in the power system network. These connections allow the disturbance either from the grid or equipment to propagate between them and eventually will affect the entire system. There are several sources from which disturbances are added, thus jointly contributing to a level of disturbance at a specific site in a grid. Besides, there might be self-produce disturbances by the grids itself, as well as disturbances from other origins outside the grid [20].

As mentioned in the introduction, an understanding of EMC in a power system is essential, especially in the context of a 'smart grid'. For the power system to achieve its optimum EMC, the immunity of equipment connected to a grid should be higher than the electromagnetic disturbance level. Immunity level defined as the maximum level of electromagnetic disturbance at which the device remains able to operate with the required quality level. In a power grid, distribution levels are inconstant, and it will vary with time and location. While for equipment immunity, it may vary with time and depend on the different equipment, as shown in Figure 2-1 [20].

The objective of achieving sufficient EMC level is to meet the protection requirement for equipment, electrical network and the connection system. EMC in the electrical power system achieved when it refers to the voltage quality in the electrical network as limits on the emission and immunity level to connected equipment. This is to make sure the disturbance level in under

susceptibility level. This typical disturbance level is called compatibility level where maximum specified electromagnetic disturbance level to which a device is expected to be exposed in particular operating conditions [21-23]. The finding in this previous research now become the aims of this work.

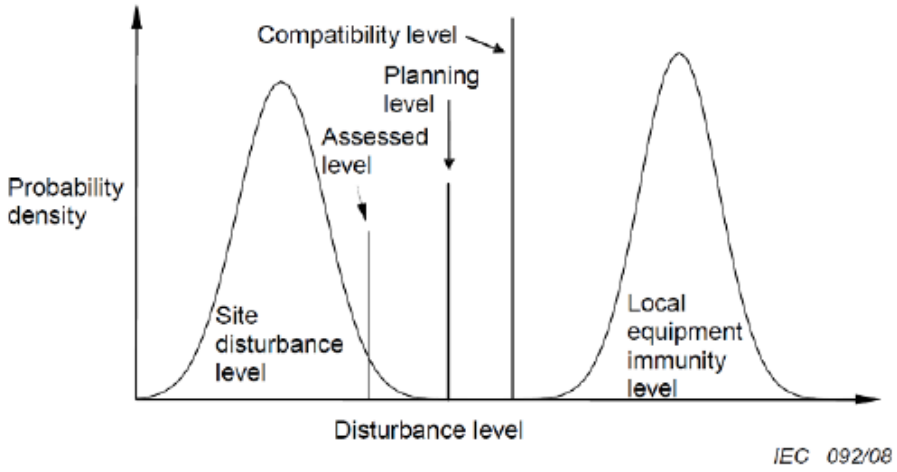

Figure 2.1 Voltage Quality concepts with time statistics on a site within a grid [24]

2.2 Smart Grid System

Currently, the electric power grid usually consists of the following fundamental element; generation, transmission, distribution, and users (residential, commercial and industrial) as illustrated in Figure 2-2 below [3]. For decades, the electric power system is not changing, and however, now it is at a crossroads where it seems that the status quo cannot be kept anymore and substantial changes in the power system are expected. This new development is called the Smart Grid system where not only the implementation of managing the system is changing, but also many of the component or equipment will be evolving too [2, 5].

In modern power systems, the presence of renewable energy such as wind power and solar at both commercial and at residential facilities will become more prevalent. These renewable energies will slowly replace the used of non-renewable energy such as coal, gas and oil, which limited on availability [25, 26]. As this renewable energy increases the percentage of power generated from such renewable source, it is expected to increase; however, their variability will make it more challenging to keep the energy supply and demand in balance. A smarter grid is proposed to alleviate this issue where the balance between the supply and demand achieved by allowing delegation of power flows in the network from parts that do not need the power to parts that need the energy [3, 25].

The main difference between our current grid and a future Smart Grid will be the way that generation and demand kept in balance. In our current system, the high-voltage transmission grid is a sophisticated, highly controlled network that supplies electricity to distribution networks, which can be viewed simplistically as wires delivering electricity to users. The transmission grid must meet whatever demand there is from the distribution system, that is from the users. It does this by controlling the supply from a relatively small number of large power stations.

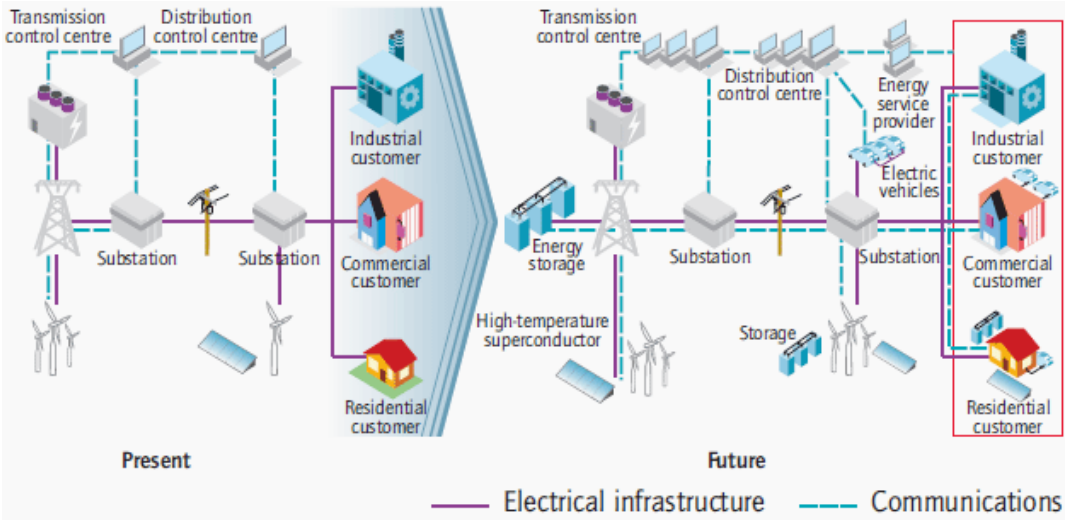

Figure 2.2 Present power system and future smart grid application [3]

Transmission and distribution in a Smart Grid system will have a two-way communication system between demand and supply. There will be a need for more sensors and controls in such a power network. It will be necessary for the utility to control the voltage, current and frequency of the system such the utilities can manage their assets and planning daily operation to increase asset utilisation. New sensors and higher speed communication network will be required to achieve such a goal. There are many advantages of Smart Grid system, as mentioned in [22, 27, 28]. It will increase the grid efficiency where the system controlled by FACTS devices to achieve their optimum power flow. The smart grid will incorporate an energy management system for improving power reliability and quality to get better control of demand. Since the increment of renewable energy production in the smart grid system, it is expected to be able to facilitate expanded deployment of renewable energy sources in the system. Since it is often to be unpredictable, therefore, with a smart grid system, it can enable predictions on the availability of these resources, either renewable or non-renewable energy at any moment and ensure proper energy scheduling decisions are taken. Another significant advantage to both supplier and consumer by using smart metering in the smart grid system is allowed both parties to monitor and administer the power usage and tariffs remotely. These are a few benefits from many more from Smart Grid implementation.

There are a substantial change and development in a smart grid system, both electrical infrastructure and communication system. If every component will be communicating with each other to share the operational data from the energy provider to the consumer, thus the smart grid environment is requirement have optimum levels of EMC. Without this requirement in place, such a system may not run smoothly, and disturbances could lead to interruption, which in the worst case will result in outages. The EMC environment needs to be understood adequately in very early design stages such possible pitfalls could be avoided, and appropriate measures to mitigate any issues are put in place. For example, a substation that has to be part of a smart grid setup. Including all the sensitive electronic communication and sensing equipment without a proper understanding of the EMC environment that will exist with the substation, the yard could lead to problems that are not easily predictable at the time of designing and building the substation. There is a need to assure that all devices and equipment in the system are operating well without being disturbed by any disturbances or will cause disorders to others [29]. These give the motivation to have a better understanding of the electromagnetic environment and the resulting interferences within the new substation system.

2.2.1 Automated Substation in Smart Grid System

The substations in a power network afford one of the most severe electromagnetic environments where the equipment of a smart grid must function correctly and reliably. The term “substation” describes the physical location in the network that contains transformers, circuit breakers, capacitor banks, voltage regulators, sensors, protective relays and other equipment necessary for controlling and distributing electric power. Substations provide critical interconnections and are located throughout the grid for the generation (as part of a power plant), transmission and distribution systems, and for distributed generation (DG) projects. The primary voltages at these substations will vary depending on the location. These substations can be as simple as a few circuit breakers or include complex systems covering large areas. For this electromagnetic interference (EMI) discussion, the substation electromagnetic (EM) environment defined as an area of high EM fields, including transients from switching that are higher than those found in other portions of the distribution system. The physical substation environment is generally the area bounded by a grounded fence around the substation yard and building and the area extending a few meters outside the fence [6]. Substations are very sophisticated in their protection and control schemes.

The microprocessor-based protective relays have recently been replacing electromechanical ones, especially at large substations in the recent development of smart grid substation. These devices not only offer protection but also act as intelligent electronic devices (IEDs) [30] that perform control functions, metering, substation automation, and many more. The

communication between these devices is currently serial using copper wires; the trend, however, is to replace wires between devices with Station Bus technology using Ethernet IP connectivity over fibre-optic cable and to network communication protocols for new or expanded installations. The power line carrier (PLC) transmitters/receivers, microwave and optical fibre communication multiplexers used in conjunction with protective relays to provide pilot protection schemes are now IEDs. This integration of smart electrical equipment increases the ability to monitor their functionality to be able to maintain reliable power, provide quick response, and try to remain cost-competitive, all with fewer resources. This improvement is called automated substations, which can provide the information needed to maintain uninterrupted power to the customer at a lower maintenance cost [31].

Substation automation systems categorised into three hierarchical levels, which are found in most implementations as physical levels, as shown in Figure 2-3[6]. The levels here referred to as the process level, the bay level and the station level. The process level refers to the individual power system equipment in the substation represented by the process interface; circuit breakers, transformers, electronic current transformers (ECT), electronic voltage transformers (EVT) and merging units. The bay level consists of bay protection and control (IEDs) hosting the related functions[30]. The station-level which typically includes of the substation computer with central functions, human-machine interface (HMI) and the gateway to the network control centre. The station and bay levels connected by the station bus. The bay and process levels are nowadays still connected by a lot of parallel copper wires, but soon, as the need for more information exchange increases, these will be replaced by a process bus. A comprehensive set of standards, the IEC61850 series, has been developed to define the requirements for such communication networks and systems in substations [27, 32].

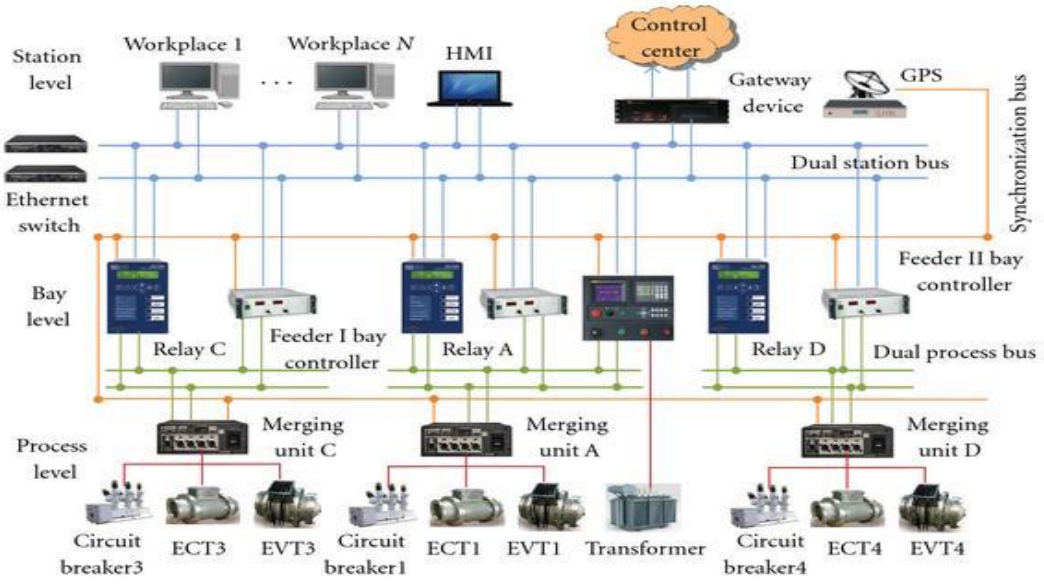

Figure 2.3 System architecture of a substation automation system [6]

Currently, most of the automated substations present a heterogeneous mixture of technologies where the modern IEC61850 structure works in parallel with an analogue instrumentation channel serving a relay which will usually actuate an electromechanical protection device. As mentioned earlier, more and more electromechanical protection relay expected to be replaced with Digital Protective Relay (DPR), especially the new substations. There are significant differences between a conventional relay and DPR. The critical difference is in the communication network, where the method of information being exchanged in the system is different in every way. Therefore, the most affected level in the automated substation is the bay level where all the protection relays are located.

Another essential element of the automated substation is the Merging Unit (MU). The merging units are analogue to digital data collection devices which sample and digitise electrical quantities. The electrical quantities are in analogue or digital signals which are of interest. Analogue quantities include voltage and current signals from Potential Transformers (PTs) and Current Transformers (CTs), transformer temperature signals from Resistance Temperature Detectors (RTDs), transformer turns ratios from potentiometers. Digital quantities include auxiliary contact outputs.

The MUs are located physically close to the signals which they monitor. This arrangement minimises the potential for signal corruption under normal equipment exploitation. The MUs are usually a weatherised exterior suitable for outdoor and extreme physical conditions common in substations. Although these MUs are tested to conform to standards such as IEC 60255-25, IEC 60255-22-4 and IEC 61000-4-3, this may not be enough as field levels that can exist within substations could be larger than the ones specified by the mentioned standards [33, 34].

All of the new component used in the automated substation mentioned above are having a high risk on the exposure of interferences from the disturbance event or the system itself. Thus, all equipment full must fill the immunity test requirement by the given standard, which allows the whole system to operate under actual electromagnetic conditions [35]. In the next subchapter will discuss on the electromagnetic compatibility issues that have been published and reported problems that occur in the smart grid substation environment.

2.3 Disturbances in Smart Grid Substation Environment

The source of disturbances that able to lead into electromagnetic compatibility in a substation is divided into two groups, which are natural sources and human-made sources within a frequency span of 10Hz to 30GHz. From natural causes, the disturbance came of natural phenomena such as lightning strike and solar magnetic storm [36]. For disturbances occur from natural phenomena such as lightning, it might strike the transmission line or directly to the

substation. The lightning pulse can propagate through the line or system and may or may not disturb other equipment or component in the smart grid system [37, 38].

For human-made electromagnetic interferences can be from intentional and unintentional radiation event due to electronics and communication equipment that operate and produce electromagnetic field in the system. In early research of EMC in high voltage substation, the primary source of disturbances is mainly coming from transient current, operation of high voltage insulator, circuit breaker and switching that occur in low voltage circuit[39]. For unintentional disturbances, the emission usually from an electronics and communication equipment which is not expected to disturb others, however, if this happens ideally the affected equipment should have optimum levels of immunity to withstand such emission [20].

In order to understand the EMC problems in the power substation, the sources of disturbances have to be first separated. Another essential aspect that needs to be defined and understood is how the disturbance will propagate and coupled to different parts of the system. There two main mechanisms that need to be considered in the final stage. The first mechanism is conduction and then radiation as the second mechanism. The coupling method can be either capacitive or inductive. Finally, the victim affected by the interferences needs to be distinguished. In general, all equipment or electronic component connected to the system could be a victim of an EMC event from Figure 2-4.

Depending on the frequency of the electromagnetic signal, the disturbances can be in low frequency and high frequency. For low frequency, the range is below 1MHz, and high frequency is higher than 1MHz. These frequency ranges are also divided into radiation and conduction as summarised in the basic electromagnetic interference Table 2-1.

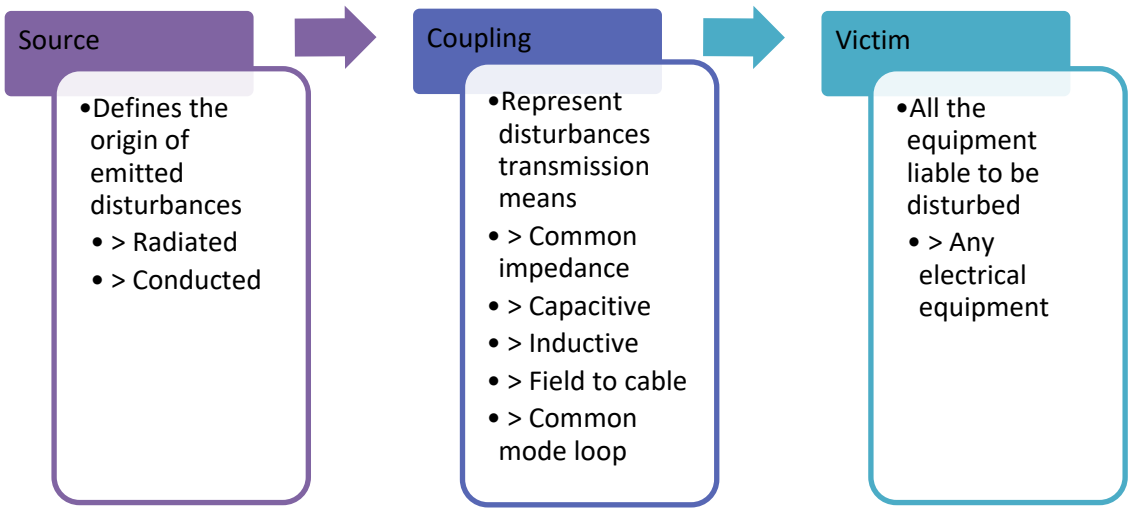

Figure 2.4 Definition of EMC problem in substation [21]

Table 2-1 Basic electromagnetic interference table [40]

	Conduction	**Radiation**
Low frequency	• Harmonics, inter-harmonics • Signal voltage • Voltage fluctuation • Voltage sag and short interruption • Voltage unbalance • Grid frequency change • Low frequency induce voltage DC in AC network	• Magnetic field • Electric field Electrostatic Discharge (ESD)
High frequency	• Continues wave voltage and current induction • Way transient Oscillatory transient	• Magnetic field • Electric field Electromagnetic field (continues wave, transient)

2.4 EMC Issues in Smart Grid Substation Environment

In smart grid implementation, the most significant changes happen in a transmission and distribution substation where new equipment and component installed to operate within the latest intelligent system. Therefore, a few major EMC issues that occur over the years while smart grid substation implementation that deserves serious attention. The source of electromagnetic interference in the smart grid identified to be from high voltage, low voltage equipment, communication system, and natural phenomena reported in [6, 11].

The most mentions problem that occurs in the smart grid substation due to the new technologies that applies and identified as sources of electromagnetic interference. Some of the reported issues are from the application of power electronics interfaces (PEI) such as power converter and smart meter [41-44], powerline communication (PLC) [13, 45-48], Flexible AC Transmission system (FACTS), and the disturbances cause by natural event [17, 49, 50] as listed in Figure 2-5. All of these electromagnetic compatibility issues in the system, it is worth to explore to get a better understanding of these issues. It will help in minimise or solving the problem; thus, the system able to operate in optimal compatibility level.

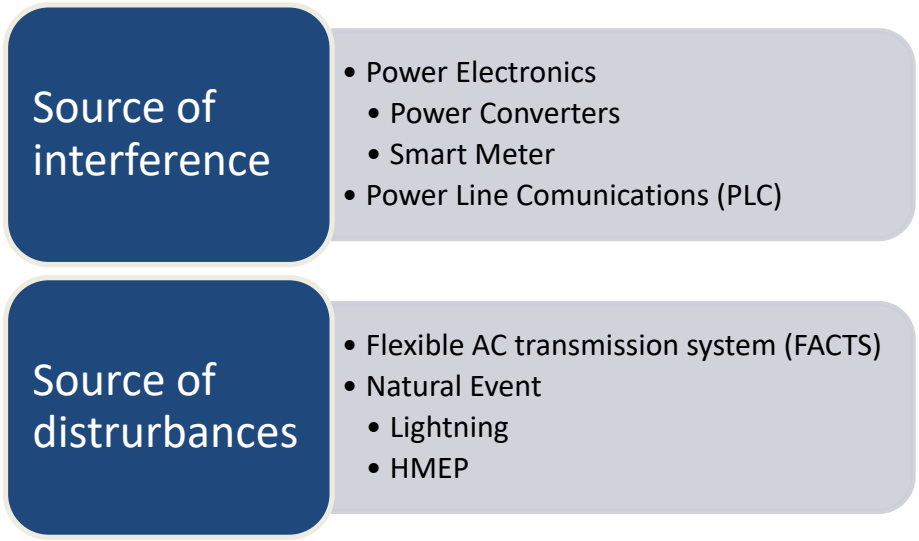

Figure 2.5 Component of EMC Issues

2.4.1 Power Electronic Interface (PEI)

In the smart grid system, the use of renewable energy as a source of energy has experienced one of the most significant growths in percentage. The most exploited renewable energies are solar, hydroelectric, photovoltaic (PV), and wind [1, 9]. Some of the potential challenges in integrating into the system; one of them is the widespread use of power electronic interface (PEI). The application of PEI in the smart grid system such as the used of power converters, smart meter [42, 51-53] and other power electronics component during operation of renewable energy and thus lead to inherent the electromagnetic disturbances and cause the system performance degradation [11, 54].

The EMI issues within smart grid automated substations have been reported to depend on the magnitude of fault currents, their flowing paths and harmonic contents as mention in [55]. The presented results in [54] show that the PEI connected to the low voltage grid may cause a 40-60dB increase in interference at distant points under MV lines. The observed attenuation of the characteristic, oscillatory mode frequency introduced by the converter (equal to 70 kHz) amounted only to 10-20dB for these two distant points. It is important to note that due to the travelling wave, and especially standing wave, phenomena, the measured attenuations should be treated as approximate levels and might change along the line. Interference generated by PEIs might spread over extensive circuits, and medium lines might be a part of its paths. The interference in the low voltage distribution is caused by the four-quadrant converter, which is used commonly as a part of the power electronics interfaces. The interferences coupled by typical

impedance might cause immunity problems not only for low voltage system but medium voltage system that connected by transformer [44].

2.4.1.1 Smart Meter

Smart meters are known as the next generation of electricity and gas meters. The application of smart meters in the smart grid system able to provide real-time energy consumption that automatically initiates the optimisation org generate on power, transmission and distribution based on energy demand. It also will help both consumer and energy supplier on meter reading and estimated bill with precise information on energy that is used [12, 52, 56].

The essential technology that very critical during application of smart meter is communication since the meter needs to communicate reliably and securely all the information. Electromagnetic disturbances that occur in the smart grid might cause interruption to the smart meter operation. The interference that occurs due to the usage of this electronic meters has to lead to inaccurate energy measurement in several cases and transmission of data. A standard requirement needs to be published as a guideline on the immunity requirement and communication guideline to the smart meter application in the smart grid system to prevent this problem from keep happening. It is potential to cost more money since the different type of equipment in the smart grid implementation require different compatibility level [12, 52].

2.4.2 Powerline Communications (PLC)

The next crucial issues related to the smart grid is a communication system, where the technology that uses the same power lines for electric power transmission for data transmission also known as Power Line Communications (PLC) [42]. Based on IEEE Standard for PLC equipment where EMC criteria and consensus test and measurement procedure to make sure communication equipment and installations for broadband over power line (BPL) follow the standard requirement [57].

The main benefits of using PLC in the smart grid system is a low cost, easy to install which is connected directly on the existing power network and it is not concern by high electromagnetic radiation levels as wireless system[45, 46]. Despite all benefit of PLC, it comes with their EMC issues, which is high frequency (HF) and very high frequency (VHF) PLC intended radiation. PLC behave as an actual antenna in HF and VHF band. This due to the EMC compliance for PLC equipment itself is not sufficient. There is a suggestion on how to specify the limit level for symmetrical and unsymmetrical signal done by [46] and force the PLC design to comply with EMC and radio requirement and to make the PLC standardisation easier to achieve [13].

2.4.3 Digital Protection Relay (DPR)

The most fundamental reason for electromagnetic interferences leading electronic equipment to failure is the destruction of electronic components under the energy of electromagnetic interference. The energy produced by electromagnetic interference sources is between 10^{-6} to 10^{-1} Joules, and the interference sources are from electrostatic discharge, over-voltage, secondary lightning and direct lightning strike. Based on the energy range produced by the disturbances, it can be argued that the level of the energy is enough to lead to failure in DPR's components. Table 2-2 shows a list of components found in DPR with their associated failure energy range.

Table 2-2 Failure Energy of Components

Component type	***Failure energy (J)***
Transistor, diodes, and COMS	10^{-6}
High-speed transistors and IC circuit	10^{-5}
Low power transistor and signal diodes	10^{-4}
Medium power transistor and FET	10^{-3}
Zener tubes and rectifier tube	10^{-2}
Power thyristor, power diodes and TVS	10^{-1}

The current state of technologies, silicon-on-sapphire (SOS) used to raise the number to 500 elements per square millimetre of the surface. It is evident that such chips require even lower supply voltages, and it is even more apparent that such improved microelectronics integrity reduces insensitivity of its components to a high-voltage surge due to the diminishing thickness of insulating layers and reduced operating voltage of semiconductor elements. Thus, a faulty substation DPR would work appropriately during laboratory testing, making it impossible to determine the reason for the fault at the substation. There are studies done by Japanese manufacture on the destruction of DPR due to electromagnetic impact, where short-term non-repeated malfunctions of DPRs prevail in most cases. This was also confirmed by another group of researchers [58], according to their data, such faults account for almost 70% of the total amount of DPR damage, while up to 80% of the failures occur in microchips.

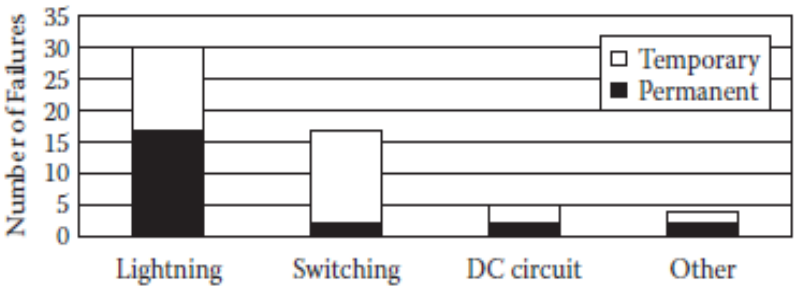

Figure 2.6 Statistics form Japanese manufacturers about the destruction of Digital Protection Relay (DPR) [58]

There have been many cases of DPR failures caused by electromagnetic interference reported as shown in Figure 2-6. Higher numbers of failures are caused by lightning, followed by switching.

2.4.4 Natural Event - Lightning Strike

Lightning or can be called as a transient, high-current electric discharge in the air which typically in tens of kiloamperes and whose length measured in kilometres. The lightning discharge is usually termed as a "lightning flash" or just a "flash." whether it strikes straight to the ground or not. A lightning discharge that involves an object on the ground or in the atmosphere referred to "lightning strike." The four types of lightning, as illustrated in Figure 2-7, are (a) downward negative lightning (b) upward negative lightning, (c) downward positive lightning, and (d) upward positive lightning. Downward flashes exhibit downward branching, while upward flashes are branched upward. The downward negative lightning flashes (type a) which account for about 90% or more of global cloud-to-ground lightning, and that 10% or less of cloud-to-ground discharges are downward positive lightning flashes called type c. Upward lightning discharges which are types b and type d are thought to occur only from tall objects (higher than 100 m or so) or from objects of moderate height located on mountain tops [59].

The terms "stroke" or "component stroke" applies only to components of cloud-to-ground discharges. Most lightning flashes are composed of multiple strokes and all strokes other than the “first” referred to as “subsequent” strokes [59]. Lightning can be modelled by applying to standards. Based on BS EN 61000-4-5 and IEC 62305-1, there are two types of a lightning surge, which is an over-voltage waveform and current surge. The characteristics of the lightning waveform are known as front time and tail time. The front time is the time interval between the instants during the 10%, and 90% of the peak value is reached. Wheres the tail time is the time interval between the virtual origin O_1 and the moment at which the current has decreased to half the peak value on the tail as shown in Figure 2-8 [60, 61].

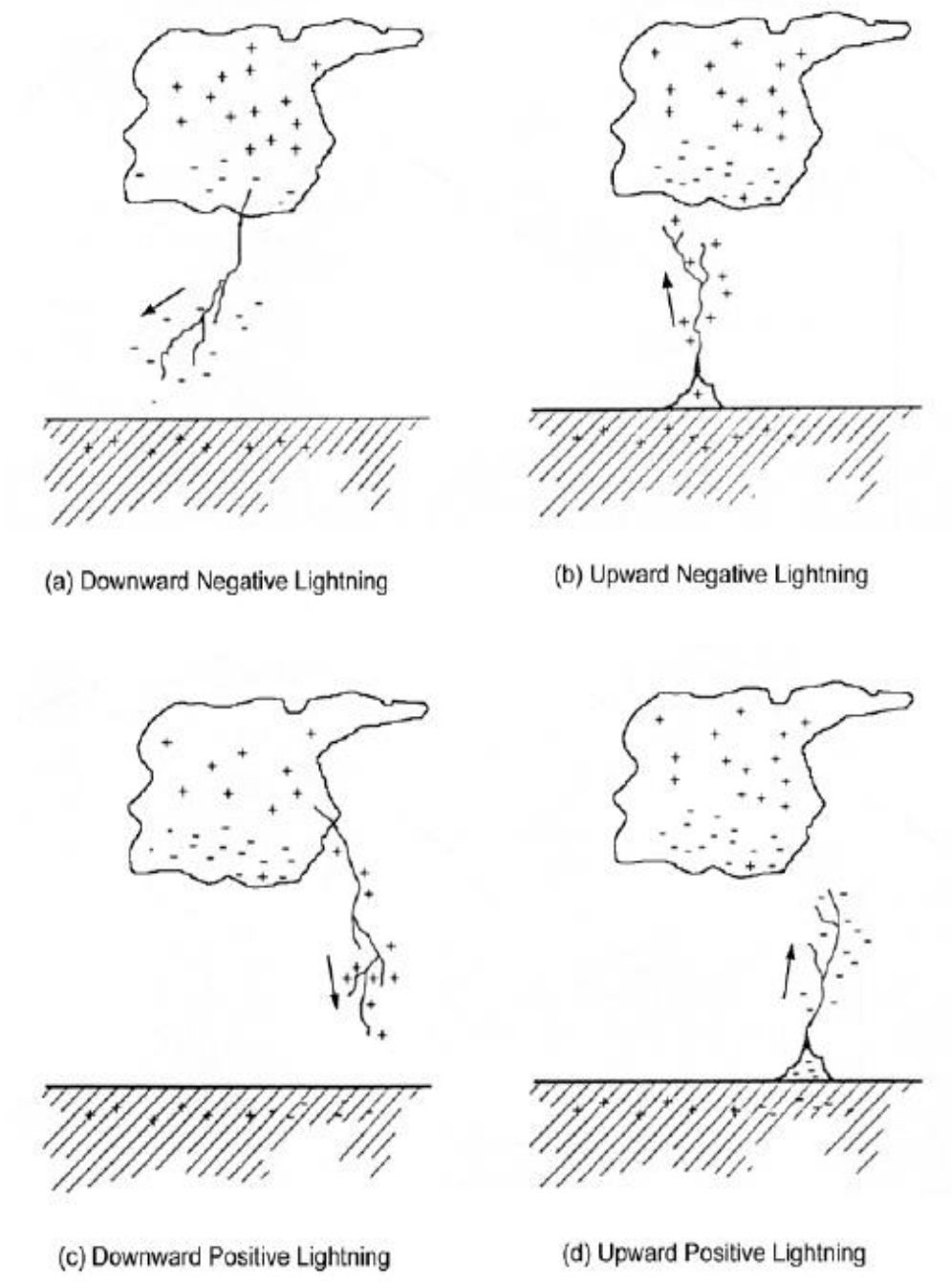

Figure 2.7 Types of lightning

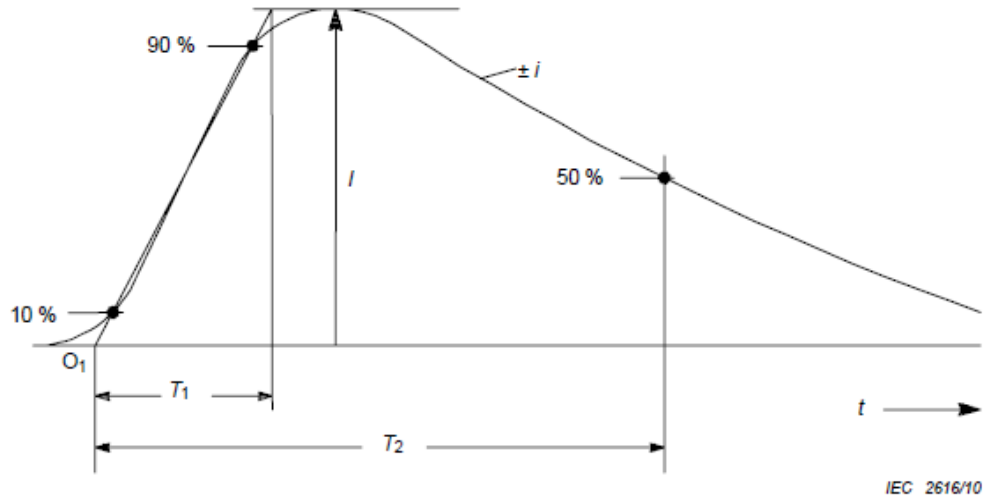

Key

O_1 virtual origin

I peak current

T_1 front time

T_2 time to half value

Figure 2.8 Definitions of impulse parameters [60]

For overvoltage creates by lightning are characterised by 1.2/50μs voltage wave; on the other hand, current surge can be divided into a direct and indirect lightning strike. The direct lightning strikes divided into two current waveshapes which are the first short stroke; 10/350μs and the subsequent short stroke; 0.25/100 μs, on the other hand for the indirect current waveform of 8/20μs applied as mention in IEC 62305-1 [60, 61]. The peak value of the current wave characterises the intensity of the lightning strike.

When lightning strikes the lightning rod, the current flows into the ground and spreads in all directions up to dozens and even hundreds of meters away, resulting in voltage drops due to ground resistance as shown in Figure 2-9. Since the soil layers closest to the current entrance point have the most significant resistance, they also show the highest voltage, where the farther away from the point, the lower the current resistance and voltage [58].

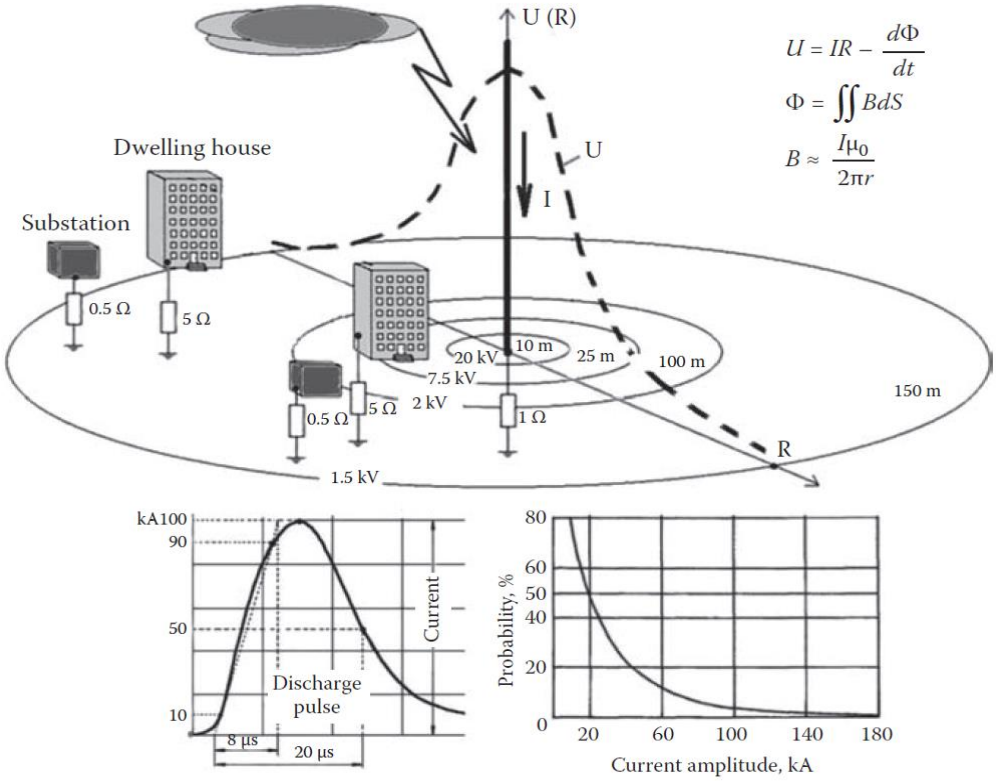

Figure 2.9 Processes occurring in the lightning rod upon a lightning strike [58]

A lightning strike can cause damage or affect an electrical installation. To studies the lightning protection system of electric-power lines or other electrical installation, it is essential to have a model of a lightning strike [62]. The interference from the lightning pulse could be conducted or induced electromagnetic fields immediately into the equipment either by parasitic capacitive and inductive couplings between elements or assemblies of the equipment. These will produce high-frequency transient interference which can propagate into hardware bypassing the filters and protective elements [63].

Lightning discharge interference can penetrate shielding enclosures by the current flowing through the ground metal of equipment, for example on Digital Protective Relay (DPR) casing and grounded shields via connection cables. Therefore, it is complicated to provide a proper level of electromagnetic interference protection. It is particularly challenging to realise at old substations where grounding systems were designed for electromechanical protection, which is much more stable to electromagnetic impact than microprocessor-based ones. Considering that dangerous potential peaks in grounding circuits occur not only upon lightning strikes but also upon emergency shorting in power mains, the problem could potentially become even more complicated. In some cases, grounding rings of power equipment are separated from those of electronic equipment to prevent such potential peaks in electronic equipment circuits. However, such separation is not possible to arrange at existing substations. The only way to avoid the influence of high electromagnetic interference on DPRs is to develop a complex solution [58].

2.4.5 Switching

In dealing with electrical networks, there are two most frequently analysis to be performed in system planning and system operation are the load flow and the short circuit analysis. Typical applications of the short circuit analysis help in system planning include:

- Ensuring that the defined short-circuit capacity of the equipment is not exceeded with system expansion and system strengthening.
- Manage the protective equipment, for example, fuses, over-current and distance relays.
- Locate the earth grounding systems.
- Verification of sufficient fault level capacities at load points
- Verification of admissible thermal limits of cables and transmission lines.

Applications of short circuit analysis in system operation include:

- Ensuring that short-circuit limits are not exceeded with system reconfiguration.
- Determine protective relay settings as well as fuse sizing.
- Calculate fault location for protective relays, which store fault disturbance recordings.
- Analysis of system faults, for example, the malfunction of protection equipment.
- Analyse the possible mutual interference of parallel lines during system faults.

Switching processes and electromagnetic fields generated by operating electrical equipment are the second most influential source of impulse interference affecting the DPR under normal operating conditions. The usual sources of switching noise in the power industry are high-voltage switches and breakers, low-voltage relays and contactors, and controlled capacitor banks. Powerful electric drive frequency converters, corona discharge, and electro spark technologies generate electromagnetic emissions, which are dangerous for electronic equipment. Thus, the routes of interference penetration into DPRs may be very different from direct-induced pickups at low-voltage conductors and substation secondary circuit cables to surge and high-frequency overvoltage occurring in the secondary windings of current and voltage transformers. The lesser the duration of an arc's burning upon disconnection of the high voltage circuit with switching apparatus, the greater the amplitude of an induced voltage surge in the secondary circuits. In general, the highest overvoltage generated by vacuum circuit breakers, second to them is SF6 switches and oil switches, followed by air circuit breakers.

The different amounts of DPR damage resulting from the operation of circuit breakers and disconnections insulated with SF6 gas and air, as shown in Figure 2-10. It should be noted that the high-voltage interference can be induced in the control cables by switching low-voltage circuits, particularly those that contain inductance. The nature of the switching transient process depends on many factors, and therefore the induced voltage can vary significantly even at the

same substation. Since it is rather challenging to make theoretical calculations of such voltage surges, the easiest way to define them is to make direct measurements.

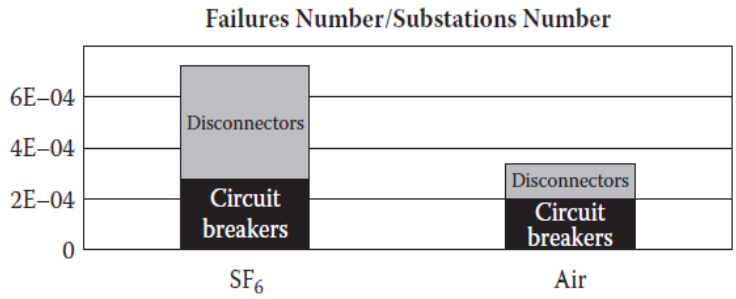

Figure 2.10 A comparative amount of DPR damages resulting from overvoltage upon the operation of circuit breakers and disconnectors with SF6 gas and air insulation.

2.5 Published Literature on Method of EMC Studies within Substation

The previous research work has widely covered EMC in the power system as a subject. However, there has been limited work done on the EMC within an automated substation, especially in the context of smart grid implementation. As mentioned in the previous section, substation automation is a term applied to the electrical substation that managed the operation between distributed intelligent electronic devices (IEDs) interconnected by communication networks [3]. In this context, it is crucial to understand the EMC possible hazard that might be caused by the electromagnetic field interference within a substation environment. The measurements or simulation procedures can be employed to build a picture of the field distribution within the area of interest. However, deciding on which method to use is depends on many factors. Based on previously published work, both approaches commonly used. The computational techniques are used to test cases that are difficult or most likely to be impossible to measure such as lightning strikes event; nevertheless, the numerical method usually is validated against the measured results [64].

2.5.1 Discussion on Published Measurements of EM Field

The experimental measurements of electromagnetic field interference generally applied to an old substation, this is since the substation already ageing and the problem starts to occur. The main reported issues were due to the equipment failure while in working condition or possibility of health hazards that may be created by the operation of substation equipment. There are several significant issues discussed in this area. Health hazard from the exposure to the electric and magnetic field at extremely low frequency is one of the severe problems that have been increasing during the last 20 years, as mentioned in [65, 66]. A similar issue has been studied by research

groups in Malaysia, where they investigated the magnetic field produced by substation equipment in normal operating conditions and explored the ways to minimise the EMI [64, 67]. The measurement of the magnetic field in these particular studies done within the perimeter of the substation area, where most likely to be exposed to the public. The recommendation of the International Commission on Non-Ionizing Protection (ICNRIP) [68] which states that the limit for public exposure is at 1000mG and 5000mG for occupational exposure used as a guideline in this study.

In recent years, there has been an increasing interest in using power electronics equipment in electrical power systems such as converter and control devices. In smart grid application, power electronic equipment needs to be reliable, controllable and have robust communication means associated with it, such it could withstand high electromagnetic emissions that may exist within the environment that these equipment have to function. Thus, it makes the EMC study within the power system, especially in the substation environment are crucial in the development and designing proper smart grid systems [44, 54, 68, 69].

Recent developments in the smart grid have heightened the need for further research and study for EMC within the system. There are few issues highlighted in previous research; one of them is the implementation of Smart Meter where it is the next generation of measuring and metering the electricity and gas. The critical problem with this new technology is communication. It has to communicate reliably and securely to transfer the data to the control centre. Thus, it is crucial to have an optimum EMC level within the environment such that the communication will not interfere with other equipment in the same system [52, 56]. Similar issues have been reported by a researcher in Sweden, after more than five million Automated Meter Reading or smart meter have been installed and implement to the system in this country [70].

Another smart grid characteristic is the power grid will be connected to renewable energy generation such as solar and wind energy. These renewable energies generally offer the alternative source of energy that is pollution-free, environmentally friendly, sustainable and unlimited. Electromagnetic interference still one of the challenges here when dealing with renewable energy with a smart grid system. Other potential problems that will affect the power quality are voltage fluctuation, power system transient and harmonics, reactive power, switching actions, synchronisation, long transmission lines, low power factor, storage system, load management, and forecasting and scheduling [1, 10, 71]. There are a few more EMC issues related to the smart grid such as the impact of high power electromagnetic, corona noise, nuclear electromagnetic pulse and geomagnetic interference [8, 18].

2.5.2 Discussion on Published Numerical Calculation and Simulation EM Field

Electric and magnetic fields of high voltage substation can be computed using the various computational method. In the past few years, different numerical techniques have been used to calculate electric fields that enable designers or utility companies to study the problems that are more difficult or impossible to be solved. There are few numerical methods widely used in previous studies of calculating electric and magnetic field such as Charge Simulation Method (CSM) [72], Finite Element Method (FEM) [73], Boundary Element Method (BEM) [74-76] and Finite difference method (FDM) [77-79]. There are several commercial electromagnetic software has been used to determine the field distribution within the substation environment; for example, the CDEGS software [80, 81]. Each method has its advantages and disadvantages, and it is based on the proposed problem and choosing the most convenient techniques to solve it.

All EMI issues occur to increase the needs and attention of predicting the electromagnetic field in the substation environment. With the prediction of the electromagnetic field, the operation of smart grid systems will be at an optimum level of immunity, despite the disturbances that might exist in that environment. It also helps with designing the automated substation to get all the equipment and component compatible with each other.

2.5.2.1 Finite Difference Method (FDM)

Finite Difference Method (FDM). FDM is a numerical computational method of solving a linear partial differential equation where time has been absorbed into a complex field variable and proceed to an iterative method of solving the resulting matrix equation [78]. The researcher has used this method in the early years of calculation magnetic and electric field for EMC problem [82]. It has been used to predict the sinusoidal steady-state electromagnetic fields penetrating an arbitrary dielectric or conducting body by [83]. Absorbing boundary condition was suggested in [84] to simplify the numerical calculation as the computational technology back then are limited. FDM has been used widely to calculate magnetic and electric field due to interference that occurs in the substation system such as lightning stroke in power substation [85, 86] and switching event that caused transient field [77].

This method of calculation is beneficial for calculating electromagnetic emissions due to disturbances within the large environment because it allows the user to calculate at desire location and not the whole area which will take a long time and need a high specification of the computational processor. FDM simulation also used to estimate field phenomena connected with the propagation of high-frequency electromagnetic waves in building constructions which allows analysing some large-scale models using a local refinement of the differential mesh based on the

adaptation of the rectangular elements [78]. Most of the prediction purpose is to compare with standard and limits for human exposure and electromagnetic compatibility study [87].

2.5.2.2 Finite Element Method (FEM)

Finite element method (FEM) has been used in a few studies of electromagnetic field calculation within the substation. FEM has the dominant position due to its versatility and having strong interchangeability where it can be incorporated into a standard program. Theoretically, FEM can be computed in 3D fields, but in generating a 3D mesh for large size require more time and a high-performance computer processor and memory. This is due to the large size of the matrix coefficient calculation of the system equation.

Although this method is not considered as a convenient technique for electric field computation, there is a study on electric field mapping in high voltage substation using a computational method which is COMSOL, commercial simulation software that based on the FEM[88]. The study aimed to evaluate the distribution of the electric field on the patio and in the vicinity of the substation, whether the values obtained meets the levels of electric field recommended by law. The result shows that the highest exposure point of the electric field. It is suggested that using the simulation, different scenario and arrangement of equipment can be changed and analysed.

2.5.2.3 Boundary Element Method (BEM)

Boundary element method (BEM) also known as Method of Moment (MOM) is a numerical technique used to convert these integral equations into a linear system that can be solved numerically. In solving electrostatic problems, firstly the issue needs to be converted into their respective integral equation into a linear system [89, 90]. In practice, the Laplacian equation is used where the electrical charge enclosed only inside the boundaries of the proposal region and volume charge density in the region is equal to zero or negligible.

There were few studies done based on BEM to calculate the electric field in the substation. One of the researches in the estimation of the electric field in high voltage substation using BEM applied together with the Charge Simulation Method (CSM). Both methods used to determine the 3D electric field inside the high voltage substation. These approaches are useful for designing power equipment and for the use of environmental protection authorities [91]. The same author developed his own software package BEM solver 3D to study the exposure of electromagnetic emission during working with power equipment [75].

Boundary element method is also used in calculating the electric field in a transformer substation. The results obtained were used to understand where in the substation, the ‘hot spots’

were, and the model was used to show how these ‘hot spots’ could be reduced. In this research, the indirect boundary integral equation is used for the fundamental solution of point charges and the superposition principle to establish the boundary integral equation. The results showed that in this 500kV substation the power frequency electric field calculated depend mainly on the height of the busbar. It is suggested to increase the height of the busbar in order to decrease the reduce the field intensity on the areas where human operators might be present [74]. Then the same method can be applied to the automated substation in order to study its EMC. However, few considerations have to be made to consider the extra equipment or new component installed at the substation to achieve the functionality required by the smart grid.

2.6 Calculation Method Used to Calculate Magnetic Field in this Research

Based on the review off all the calculation method available mention earlier, two mathematical calculation has been combined to predict the magnetic distribution within the substation environment for this research. Under normal operating conditions, magnetic and electric fields exist around the current carrying equipment within the substation. It is expected that the highest magnitude of the fields will be observed around the paths that carry the highest currents. However, there are various factors affecting the level of the fields, such as current magnitude, phase spacing, bus height, phase configuration, and distance from the source. It is rather difficult to predict the distribution of the magnetic field in the substation environment using popular numerical methods, such as finite differences and finite elements directly. Mainly because of the large size of the electromagnetic problem to be solved; these methods will struggle with meshing large domains such as the whole substation environment. The Biot-Savart Law (BSL) employed directly at first to identify an overall overview of magnetic field distribution for the whole substation in a large mesh grid because of its simplicity and computational efficiency. All components and equipment structure and dimensions need to be included.

Based on the entire field distribution in the substation environment, the focus area is chosen to get the much closer and detail look at the distribution of the field. Specific areas of interest are then studied in more detail using the Finite Difference Method (FDM) to produce the magnetic field distribution in a finer mesh grid. Applying FDM directly to evaluate the magnetic field distribution for the whole substation would require extensive computation time. The detail resolution of the magnetic field, the current induced by the generated field were calculated to relate with shielding effect in the substation environment. This allows the user to predict the equipment’s compatibility with the distributed field within the substation environment for refurbishment purposes. Mathematical descriptions of both methods will be discussed in the next subtopic.

2.6.1 Biot-Savart Law (BSL) Mathematical Description

Various factors are affecting the level of the fields, such as current magnitude, phase spacing, bus height, phase configuration, distance from the source and the phase unbalance. The magnetic field intensity can be linked to the factors mentioned above through the Biot-Savart equation, which is very similar in its format with the Coulomb's law for electric fields. However unlike in the case of the Coulomb's law where the charges can be treated as separate, here in Biot-Savart equation a differential length of current needs to be introduced to play the role of the charge in the Coulomb's law.

Biot-Savart law states that the differential magnetic field dH generated by a steady current $\boldsymbol{I}$ flowing through a different length $\boldsymbol{dl}$ is given by [92]. The current $\boldsymbol{I}$ flowing in the substation simulated in the previous chapter will be the input to predict the distributed field.

$$dH = \frac{I}{4\pi}\frac{dl \times \hat{R}}{R^2} \tag{1}$$

Where R is the distance vector between dl and the observation point $\boldsymbol{P}$, as shown in Figure 2-11 below, if the distance of the observation point to the conductor is changing, it is changing proportionally the calculated magnetic field induced by the current.

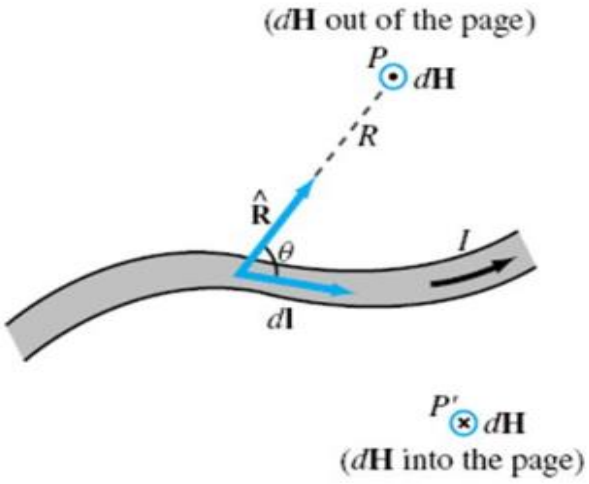

Figure 2.11 Linear conductors of the length of $\boldsymbol{l}$ carrying the current I [92]

According to the Biot-Savart Law, the magnetic field due to a current element of length dl is given by [92]. A simple MATLAB routine was developed to calculate the field in three dimensions (3D) within the air environment. The total magnetic field intensity, H, at each position (x, y, z) and at any instant of time, t is then given by equation 3. And superposition applied at every location. Rosiori substation in Romania used in the simulation to illustrate the approach as

mention in details in the previous chapter. The magnitude of the magnetic field is written as equation 4.

$$H = \frac{I}{4\pi}\int_{l} \frac{dl \times \hat{R}}{R^2} \tag{2}$$

$$H(x, y, z, t) = \hat{x}H_x(t) + \hat{y}H_y(t) + \hat{z}H_z(t) \tag{3}$$

$$|H| = \sqrt{H_x^2 + H_y^2 + H_z^2} \tag{4}$$

2.6.2 Finite Difference Method (FDM) Mathematical Description

FDM is a numerical computational method of solving a linear partial differential equation. It starts with applying Maxwell's equation for magnetic field component in 3D, where **B** and **H** are magnetic field quantities, **E** and **D** is electric field quantities as written in equation 5 until equation 8, **J** is the current density per unit area, and ρ_v .

On the other Electric and magnetic field quantities interrelated by $\mathbf{B} = \mu\mathbf{H}$ with μ being the magnetic permeability of the material [92, 93].

$$\nabla \cdot \mathbf{D} = \rho_v \tag{5}$$

$$\nabla \times \mathbf{E} = -\frac{\partial \mathbf{B}}{\partial t} - \mathbf{J}_m \tag{6}$$

$$\nabla \cdot \mathbf{B} = 0 \tag{7}$$

$$\nabla \times \mathbf{H} = \mathbf{J}_e + \frac{\partial \mathbf{D}}{\partial t} \tag{8}$$

Where $\mathbf{J}_e$is the electric current density in amperes per square meter and σ is the magnetic resistivity in ohms per meter, it shows in equation 9 below.

$$\mathbf{J}_e = \sigma\mathbf{E} \tag{9}$$

In a static case where all charges are permanently fixed in space, or they move at a steady rate thus J is constant in time, $\partial\mathbf{D}/\partial t = 0$. It will lead equation 11 to equation 13 below, where

the value of the magnetic field, **H** in (H_x, H_y, H_z). This will separate the electric field and magnetic field interconnection, which will allow to study electricity and magnetism as two separate phenomena [93].

$$\nabla \times \mathbf{H} = \mathbf{J}_e \tag{10}$$

Since Maxwell's equation are a first-order differential equation, it is challenging to solve the boundary-value problem; therefore the first-order equation needs to be decoupling to obtain the wave equation. It is more useful in solving a problem with a second-order differential equation. To get the wave equation for a linear problem, take the curl of both sides of equation 11.

$$\nabla \times \nabla \times \mathbf{H} = \nabla \times \mathbf{J}_e \tag{11}$$

Applying the vector identity,$\nabla \times \nabla \times \mathbf{F} = \nabla(\nabla . \mathbf{F}) - \nabla^2 \mathbf{F}$ and equation 12 and into equation 15

$$\nabla \times \nabla \times \mathbf{F} = \nabla(\nabla . \mathbf{F}) - \nabla^2 \mathbf{F} \tag{12}$$

$$\nabla(\nabla . \mathbf{H}) - \nabla^2 \mathbf{H} = \sigma(\nabla \times \mathbf{E}) \tag{13}$$

Then by applying another vector identity,$\nabla(\nabla . \mathbf{H}) = 0$, and equation 14 will give the equation as written below which call diffusion equation:

$$-\nabla^2 \mathbf{H} = -\frac{\partial \mathbf{B}\sigma}{\partial t} \tag{14}$$

The vector B and H are connected by permeability and the equation now is simplified as

$$\nabla^2 \mathbf{H} = \sigma \mu_\circ \mu_r \frac{\partial \mathbf{H}}{\partial t} \tag{15}$$

From the simplified equation, it can be described in partial differential equation for the magnetic field in three dimensional as below:

$$\left[\frac{\partial^2}{\partial x^2} + \frac{\partial^2}{\partial y^2} + \frac{\partial^2}{\partial z^2}\right] \mathbf{H}^m_{(x,y,z)} = \sigma \mu_0 \mu_r \frac{\partial \mathbf{H}}{\partial t} \tag{16}$$

$$\frac{\partial^2 \mathbf{H}^m_{(x,y,z)}}{\partial x^2} + \frac{\partial^2 \mathbf{H}^m_{(x,y,z)}}{\partial y^2} + \frac{\partial^2 \mathbf{H}^m_{(x,y,z)}}{\partial z^2} = \sigma \mu_0 \mu_r \frac{\partial \mathbf{H}}{\partial t} \tag{17}$$

For equation at right-hand-side, it is expended for tree dimensions, (*x*,*y*,*z*) to be as below:

$$\frac{\partial^2 \mathbf{H}^m_{(x,y,z)}}{\partial x^2} = \frac{\mathbf{H}^m_{(k+1,j,i)} - 2\mathbf{H}^m_{(k,j,i)} + \mathbf{H}_{(k-1,j,i)}}{\Delta x^2} \tag{18}$$

$$\frac{\partial^2 \mathbf{H}^m_{(x,y,z)}}{\partial y^2} = \frac{\mathbf{H}^m_{(k,j+1,i)} - 2\mathbf{H}^m_{(k,j,i)} + \mathbf{H}^m_{(k,j-1,i)}}{\Delta y^2} \tag{19}$$

$$\frac{\partial^2 \mathbf{H}^m_{(x,y,z)}}{\partial z^2} = \frac{\mathbf{H}^m_{(k,j,i+1)} - 2\mathbf{H}^m_{(k,j,i)} + \mathbf{H}^m_{(,j,i-1)}}{\Delta z^2} \tag{20}$$

While, $\Delta x = \Delta y = \Delta z = h$, and at left-hand-side, the equation solved using explicit method for three-dimensional problem varied with time.

$$\sigma\mu_0\mu_r \frac{\partial \mathbf{H}}{\partial t} = \sigma\mu_0\mu_r \frac{\mathbf{H}^{m+1}_{(k,j,i)} - \mathbf{H}^m_{(k,j,i)}}{\Delta t} \tag{21}$$

The equation then was simplified as equation 22 and equation 23 to achieve constant value, C.

$$\begin{aligned} H^m_{(k+1,j,i)} - 6H^m_{(k,j,i)} + H^m_{(k-1,j,i)} + H^m_{(k,j+1,i)} + H^m_{(k,j-1,i)} + H^m_{(k,j,i+1)} + H^m_{(k,j,i-1)} \\ = \frac{\sigma\mu_0\mu_r h^2}{\Delta t}(H^{m+1}_{(k,j,i)} - H^m_{(k,j,i)}) \end{aligned} \tag{22}$$

$$C = \frac{\Delta t}{\sigma\mu_0\mu_r h^2} \tag{23}$$

To make the equation more comfortable to understand, it re-arranges into initial value and current value as mention in equation 24 and 25 below.

$$\begin{aligned} \mathbf{H}^{m+1}_{(k,j,i)} = \mathbf{H}^m_{(k,j,i)} + C[\mathbf{H}^m_{(k+1,j,i)} - 6\mathbf{H}_{(k,j,i)} + \mathbf{H}_{(k-1,j,i)} + \mathbf{H}_{(k,j+1,i)} + \mathbf{H}_{(k,j-1,i)} \\ + \mathbf{H}_{(k,j,i+1)} + \mathbf{H}_{(k,j,i-1)}] \end{aligned} \tag{24}$$

$$H^{m+1}_{(0)} = H^m_{(0)} + C[H^m_1 - 6H^m_0 + H^m_2 + H^m_3 + H^m_4 + H^m_5 + H^m_6] \tag{25}$$

Within a nonmagnetic conductor of conductivity, $\boldsymbol{\sigma}$ where the material constants used in calculation listed in the appendix and mesh length $\boldsymbol{h}$, the finite difference equation reduces to the simplest form as written in equation 26 and equation 27 below. To calculate the current value of **H** at any point, it will use an initial value around it, and the value of constant, C. The iteration will go on until all value of **H** is determine for all point in the dimension set earlier.

$$H_0 = C(H_1 + H_2 + H_3 + H_4 + H_5 + H_6) \tag{26}$$

$$C = (6 + j\omega\sigma\mu_0 h^2)^{-1} \tag{27}$$

The substation's focus area then divided into sub-segments in the ***x,y,z*** coordinate system by square cells and having mesh length ***h***, as shown in Figure 2-12. Value of the field at the surface node only applied at the interior nodes. For three-dimensional problem, the surface node becomes cube nodes as illustrated in Figure 2-12. With this algorithm, the density of the calculation points can be easily modified to focus on regions of higher interest.

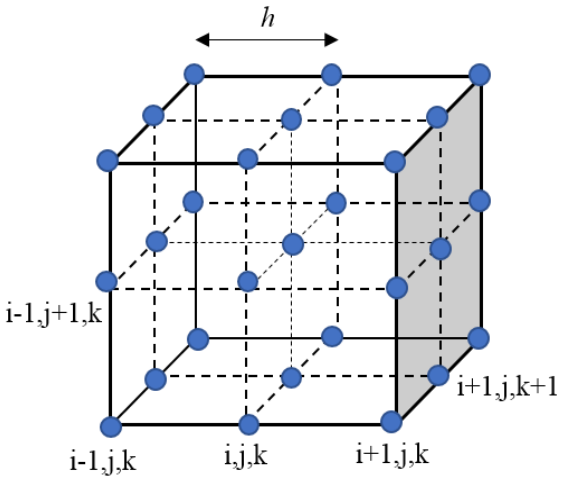

Figure 2.12 Uniform mesh in a 3-D grid point

2.6.3 Induced Current Mathematical Description

According to Ampere's law, induced current in the conductor able to calculate by apply numerical calculation, curl of **H** to get current density, **J** as mention in equation 28 below.

$$\nabla \times \mathbf{H} = \mathbf{J} \text{ (A/m-2)} \tag{28}$$

Taking the equation 28 and curl on both side and gives

$$\nabla(\nabla . \mathbf{H}) - \nabla^2 \mathbf{H} = \nabla \times \mathbf{J} \tag{29}$$

Assuming the Gauss's law for magnetism $\nabla . \mathbf{H} = 0$, it simplified the equation to be

$$-\nabla^2 \mathbf{H} = \nabla \times \mathbf{J} \tag{30}$$

Then, using the Ohm's law to relate the material conductivity, $\boldsymbol{J} = \sigma \mathbf{E}$, $\mathbf{B} = \mu \mathbf{H}$ and the differential form of Faraday's law equation below,

$$\nabla \times \mathbf{E} = -\sigma \frac{\partial \mathbf{B}}{\partial t} \tag{31}$$

This gives a diffusion equation of **H**.

$$-\nabla^2 \mathbf{H} = -\sigma\mu \frac{\partial \mathbf{H}}{\partial t} \tag{32}$$

This diffusion equation used to calculate the magnetic field diffuse on the metal surface by the magnetic field distributed in the air. To solve this diffusion equation, the finite different method (FDM) applied as mention in subchapter 2.63, in the final equation 26 and 27. After having a magnetic field on the metal surface calculated, as discuss detail in subchapter 4.5.2, the current induced by this magnetic field able to determine by introducing the Ampere's law again (equation 28). Since the H are calculated in *x*, *y*, and *z* directions, thus to calculate the current component in *x*, *y*, and *z* directions, complete expression of curl **H** is for each axis need to be apply, for example, H_x is the component of curl in *x*-direction where its perpendicular to the surface and in the same direction as $\mathbf{J}_x$ as shown in equation 33 below.

$$\nabla \times \mathbf{H} = \hat{x}\left[\frac{\partial H_z}{\partial y} - \frac{\partial H_y}{\partial z}\right] + \hat{y}\left[\frac{\partial H_x}{\partial z} - \frac{\partial H_z}{\partial x}\right] + \hat{z}\left[\frac{\partial H_y}{\partial x} - \frac{\partial H_x}{\partial y}\right] \tag{33}$$

$$\mathbf{J} = \hat{x}\boldsymbol{J_x} + \hat{y}\boldsymbol{J_y} + \hat{z}\boldsymbol{J_z}$$

Then from the result of curl, the equation was integrated at both side over an open surface, S that based on Ampere's law its state that

$$\int (\nabla \times \mathbf{H}).\,\mathbf{ds} = \int \mathbf{J}.\,\boldsymbol{ds} \tag{34}$$

The current induced, **I** was calculated by integration of current density on the closed contour bounding all sub-area surfaces, *ds* of the box for all component in *x*, *y*, *z* axis

$$\mathrm{I} = \int \mathbf{J}.\,ds \tag{35}$$

The thickness of the metal box was set to be 9mm to compare the effect of skin depth on this calculation.

2.7 EMC Limitation Guidelines and Standard

High voltage substation system generates electric and magnetic fields up to 300 GHz during normal operation or during disturbances that occur in the systems. These electromagnetic field disturbances might affect the overall system compatibility and affect the health safety of the public and occupational exposure. Thus, electromagnetic compatibility limitation guidelines and standard apply for high voltage substation divided into two main categories, the limits guidelines for human health and safety and the compatibility of the equipment. For health and safety point of view, national guidelines are set by the International Commission on Non-Ionizing Radiation Protection (ICNIRP) [68] which is recognised by the World Health Organization (WHO) as a non-governmental organisation.

On the other hand, every system has its limitations and optimal acceptance level towards electromagnetic interference. The standard immunity requirement for equipment will be referring to BS EN 61000-4 [94], and IEC 61000-4 series [95] provide the information and guidance on EMC basic standard. The basic standard related to immunity test that applied for electrical and electronic equipment, including systems. The standards are used to assist all related bodies, both user and manufacturer in considering and determining the immunity test methods and limits that applicable to their products and relevant to the electromagnetic environment that intended to be used. Details of these standards and limits guidelines will be discussed in the next subchapter.

2.7.1 International Commission on Non-Ionizing Radiation Protection (ICNIRP)

The International Commission on Non-Ionizing Radiation Protection (ICNIRP) is an independent organisation that provides scientific advice and guidance on the health and environmental effects of non-ionizing radiation (NIR) to protect people and the environment from detrimental NIR exposure. These generated fields should be within the range of health regulations and EMC standards, although different countries able to be setting their national standards based on these guidelines. These guidelines will be periodically revised and updated as advances are made in identifying the adverse health effects. Importantly, their guidelines are not intended to be a complete system for protecting the public that should be applied in different countries as it stands. The guidance considers only the science, and Governments will need to look at other factors before deciding whether and how to implement the guidelines. The limits of the electric and magnetic field for 50 Hz system within the environment which recommended by the ICNIPR [68] and WHO [96] as summarised in Table 2-3.

Table 2-3 ICNIRP exposure guidelines at power frequency 50Hz [68]

	Electric field (V/m)	***Magnetic flux density (μT)***	***Magnetic field strength (A/m)***
Public exposure	5 000	100	80
Occupational exposure	10 000	500	400

Indirect effects of electric and magnetic fields may result from physical contact, for example, touching or brushing between a person and an object. The consequence of such contact that might have accumulated on the object or the body of the person. The range of threshold that causing an indirect effect to the body of individual summarised in Table 2-4 is the frequency range up to approximately 1MHz. Threshold values for these effects are frequency-dependent, with the lowest threshold occurring at frequencies between 50 and 1MHz. Therefore, for an engineer or administrative control are advised to wearing personal protective clothing that can prevent these problems from occurring.

Table 2-4 Range of threshold current for indirect effects [68]

Indirect effect	***Threshold current (mA) at frequency:***			
	50/60 Hz	***1 kHz***	***100 kHz***	***1 MHz***
Touch perception	0.2-0.4	0.4-0.8	25-40	25-40
Pain on finger contact	0.9-1.8	1.6-3.3	33-55	28-50
Painful shock/let-go threshold	8-16	12-24	112-224	Not determined
Severe shock/breathing difficulty	12-23	21-41	160-320	Not determined

The reference levels for contact current are given above which caution must be exercised to avoid shock and burn hazards. The point contact reference levels are presented in Table 2-5. Since the threshold contact currents that elicit biological responses in children and adult women with approximately one-half and two-thirds, respectively of adult men, therefore the reference levels for contact current for the general public are set lower by a factor of two than the values for occupational exposure.

Table 2-5 Reference current induced at frequencies between 10 and 110 MHz [68]

	Reference levels current induced in any limb (mA)
Public exposure	45
Occupational exposure	100

2.7.2 British Standard EN 61000 Electromagnetic Compatibility (EMC)

The standard BS EN 61000 is the same standard from IEC 61000, and it is published in series which is separate parts which are Part 1 is General, Part 2 Environment, Part 3 Limits, Part 4 Testing and Measurement Techniques, Part 5 Installation and Mitigation Guidelines, Part 6 Generic Standard and Part 9 Miscellaneous. By refereeing to the standards, it provides information and guidance on EMC applied to electrical and electronic equipment, including systems [95]. The object of this part of IEC 61000 [35] is to assist the technical committees of IEC or other bodies, users and manufacturers in considering and determining the immunity test methods applicable to their products and for the electromagnetic environment in which their products are intended to be used. The standard presents the immunity requirement of equipment under operating condition towards magnetic disturbances at 50 HZ and 60Hz. The standard related to:

1. Residential and commercial locations
2. Industrial installation and power plants
3. Medium voltage and high voltage substation

Items of equipment are installed and implemented within power stations and substations according to the rules/guidelines given by the manufacturers. It is essential that these items of equipment operate according to the specified performances when exposed to the variety of electromagnetic phenomena, conducted and radiated, typical of these installations. The electrical power system equipment can be installed in control centres, radio repeaters, or low voltage distribution points in industrial, commercial or residential areas, as shown in Figure 2-13. The general standard and product standard should be to cover the placement of equipment in those areas. In some cases, special mitigation measures often use, for example, specialised cabling, shielding of some regions are taken to create a "protected" environment and to reduce the immunity requirements accordingly. This allows using equipment not meeting the specifications of this standard. A protected environment can be created employing mitigation measures to

minimise immunity requirements to the immunity levels of product standards or universal standards [35].

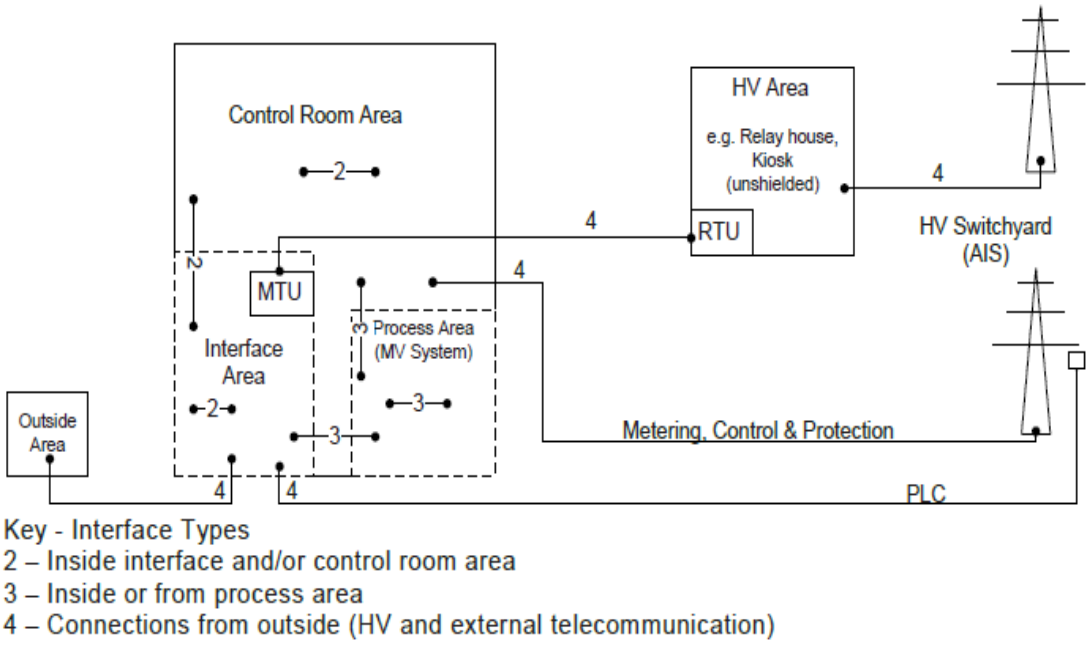

Figure 2.13 The situation of a power station [35]

This research will be focusing on the standard for medium voltage and high voltage substation. The magnetic field strength is express in A/m, where 1A/m corresponds to a free space magnetic flux density of 1.26μT [97]. In the substation environment magnetic field is dependent on the configuration of the high voltage line, load, fault condition. It is significant to know the field profile in the electromagnetic environment exposure towards equipment. Thus, the values of the magnetic field within the substation area based from the standard will be used to compare the EMC as tabulated in Table 2-6.

Table 2-6 Values of the magnetic field in high voltage substation areas [97]

Substation	**220kV**	**400kV**
Under the bus-bars near connection to a line carrying about 0.5 kA	14 A/m	9 A/m
In the relay room (kiosk)	Near event recorders at about 0.5 m distance: 3.3 A/m Near measurement voltage transformer: d = 0.1 m: 7.0 A/m d = 0.3 m: 1.1 A/m	

In the equipment room	Maximum 0.7 A/m

The magnetic field within the substation environment determined by the proposed calculation method compares with the standard given to ensure the EMC level for the system in optimum level. The equipment installed in the substation needs to satisfy its functional requirement and able to operate with or without electromagnetic interference in the system.

These limits will be used as guidelines for electric and magnetic field calculations in this research to ensure the safety of the environment not only for workers but for the public as well. As mentioned in Chapter 2, the transformation of the current electrical power system into a smart grid system with the introductions of new power electronic equipment required higher immunity level towards electromagnetic interference due to sensitivity issues. One of the many latest equipment installed in the smart grid system is a digital protective relay (DPR). The most critical disadvantages towards DPR is that the microprocessor technologies applied in DPR are fragile and more sensitive towards electromagnetic interference penetrating from the operating power circuit, voltage circuits and current transformers then traditional electromechanical relays.

These malfunctions are due to insufficient EMC and DPR interference sensitivity, which is much higher than traditional electromechanical protection relay. For electromechanical relay operation, 10^{-3} joules is the energy that could trigger a false trip, meanwhile in the case of a microelectronic controlled device, energy of 10^{-7} joules would be capable of creating a malfunction. The difference is about four orders of magnitude, or 10,000 times [58, 98]. The energy is translated into electric and magnetic fields as shown in Table 2-7 for further analysis on compatibility and sensitivity of the DPR.

Table 2-7 Energy trigger false trip in terms of magnetic and electric fields

	Energy (Joules)	***Magnetic field (μA/m)***	***Electric field (kV/m)***
Electromechanical relay operation	*10^{-3}*	*50.132*	*15.029*
Microelectronic controlled device	*10^{-7}*	*0.5132*	*0.1503*

The system must at the optimum level of immunity towards the interference occur in the environment. With the information of electromagnetic compatibility in the substation, it also helps in designing the automated substation itself. It is to ensure that both new and old equipment and component are compatible with each other. Therefore, there is a need to develop methodologies and simulation tools that allow prediction and calculation of electromagnetic field emissions in such environments.

2.7.2.1 Design Principle for Shielding

The mitigation of radiated or conducted disturbances might be required if EMC between an apparatus is not achieved. Mitigation can be attained by using an electromagnetic barrier between the source and the victim. For conducted disturbances, this barrier can be a filter or other decoupling device, and for radiated disturbances, it can be an electromagnetic shield and perhaps a filter as needed, the attenuation of which is compatible with that of the shield in the frequency range considered at least equal to the difference between the disturbance level and the immunity level of the apparatus to that disturbance [99].

According to uncertainties on disturbance levels and immunity levels, a margin should be considered as well and added to the basic attenuation needed. This margin generally depends on the criticality of the equipment. As discussed in IEC 61000-5-1[100], it is useful to extend the concept of the enclosure as being the boundary of a facility. An enclosure may be envisioned as a complete building, a room, a rack, a single cabinet and even, by extension of the concept, as an individual apparatus or a circuit board within an apparatus. This facility interfaces with its environment by "ports" as shown in Figure 2.14 provides further discussion of the concept of ports.

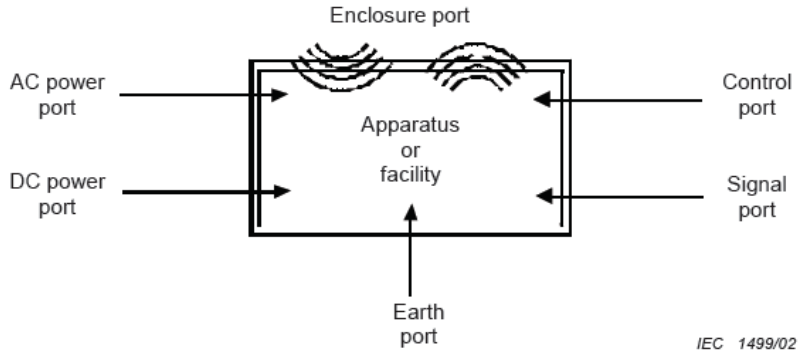

Figure 2.14 Ports of an apparatus or facility [99]

Electromagnetic shielding of buildings, rooms, compartments, cabinets, rack chassis and equipment makes it possible to ensure compliance with the EMC for equipment exposed to radiated disturbances[99]. Screening of rooms and cabinets with appropriate penetration protection is only one of several actions that may be used to limit the effect of radiated electromagnetic disturbances. Obtaining a satisfactory result may involve other actions such as

a) selecting correct cabling and wiring by adding a screen jacket over cables or wires
b) applying good cable layout and management

c) implementing good earthing and bonding practices
d) using devices limiting the emissions or increasing the immunity

The standard provides guidance for the main arrangements used in mitigation methods involving screening of installations. It introduces the concept of mitigation zones and review of the corresponding types of shielded enclosures. I also provide the guidance on the preservation of shielding effectiveness for housings (shielding) with openings based on a set of standard EMC rules. It also presents the information on the implementation of screening, progressing from the sensitive apparatus to the complete building, as well as on the means of dealing with the unavoidable opening apertures or penetrations[99].

To ensure shielding effectiveness, many parameters need to be considered. In real practice, the effectiveness of an enclosure with penetrations of all types will be reduced and limited by these penetrations. For practical purposes, the shielding effectiveness of a solid metallic cabinet or enclosure is mainly determined by the following factors[99]:

- the disturbance currents need to be connected to the earth/ground
- the installation of penetrating cables, should be earthed directly to the cabinet
- the electrical length of seams of all parts of the enclosure should be as small as possible
- the size of holes should be as small as possible

2.8 Summary

After going through all the all findings in the literature review regarding the electromagnetic compatibility within substation environment, it has been found that previous electrical power system is transforming into the system that much more intelligent called Smart Grid System. There is a substantial change and improve development in a smart grid system, both electrical infrastructure and communication system. The presence of renewable energy generation at both commercial and residential facilities will become more prevalent. However, their variability will make it more challenging to keep the energy supply and demand in balance. A smarter grid is proposed to alleviate this problem; thus, the balance between the supply and demand is achieved by allowing delegation of power flows in the grid.

Supply and demand are connected by transmission and distribution system in a smart grid, which two-way communication system that has been implemented in the system. There will be a need for more electronic sensors and controls equipment or system for the utility company to be able to manage their assets and planning daily operation to increase asset utilisation. With all of the new component used in the system, it is more likely to expose the equipment and system to interferences. It might be from the disturbance event or even from the system itself. To understand

the effect of electromagnetic interference towards any equipment or system, one has to know the sources of disturbances, method of coupling and finally the victim. These interferences that occur in the system lead to electromagnetic compatibility studies are becoming more crucial.

The most mention EMC issues within substation were published and discussed the implementation of several new types of equipment such as power electronic interfaces and power line communication system. The disturbances due to natural phenomena such as lightning strike at the substation also invest in EMC problem within the smart grid implementation, and there are few other issues. Although the previous research work has widely covered the EMC issues in previous power system, there has been limited work done on the EMC within an automated substation, especially in the context of smart grid implementation.

Two main approaches have been used to study the electromagnetic compatibility within the substation environment, which is via experimental measurement and simulation either using commercial software or numerical calculation. Deciding on which method to use depends on many factors, but the most important is the problem itself. Experimental measurements of electromagnetic interference were done usually at old substations, which already were having problems. These are to get a clear picture of the substation's performance during normal operation. The substation performance during disturbances event occurs very hard to study in real-time. Thus, the computational simulation methods are used to test cases that are difficult or impossible to measure, such as lightning event.

There are several numerical calculation methods previously used in electric and magnetic field calculation within the substation. The most common calculation method used is the Finite Difference Method (FDM), Boundary Element Method (BEM) and Finite Element Method (FEM). Both have their advantages and disadvantages, depending on the objective of the research studies. For this research, numerical calculation using the Finite Difference Method (FDM) will be used to calculate the distributed magnetic field in the substation environment with lightning as a source of interference. Based on the review of all calculation method, it is has been chosen to combine two methods of calculation to determine the magnetic distribution within the substation environment for this research which is Biot Savart Law (BSL) directly to determine the magnetic field within a large substation environment. The second part of the study is applying the Finite Difference Method (FDM) to determine the magnetic field distribution at the focus area

In the next chapter will be explaining the methodology used for this research. It starts by explaining the details on chosen substation layout component that applied for this whole research. Then the method is divided into four parts, and every section will explain in further information on the step by step of the modelling procedure and assumption made.

CHAPTER 3

RESEARCH METHODOLOGY

3.1 Overview

In this chapter will explain in details the flow and methodology of this research work. Generally, the research methodology is divided into four parts to fulfil the written objectives in Chapter 1. The main goal of this research is to determine the magnetic field generated within the substation environment due to the current input during the normal operating condition and while disturbances occurred via power system simulation. The magnetic field distribution within the substation environment is compared with standard and limits requirement, to ensure the compatibility level of the whole system. The overall methodology summarised in the flow chart in Figure 3-1.

This chapter begins with a discussion in details regarding the chosen substation structure located in Romania at Rosiori for the research study. The first part of the research is to construct a substation model in Digsilent PowerFactory software. The substation performance was studied during the steady-state which is before applying any disturbances, and while a lightning strike event. The result from the substation performance will be used as an input for the next stage of research. The following part involves calculating the magnetic field within the substation environment based on the current flow in power system simulation. The magnetic field was calculated first by applying Biot Savart Law (BSL) to investigate the overall distribution of the magnetic field within the substation environment. Then based on the overall distribution of calculated magnetic field, then the Finite Difference Method (FDM) adopted into determine the field distribution at the desired focus area and evaluating the electromagnetic compatibility within the environment. All the details on the methodology of this research will be discussed in the next subtopic.

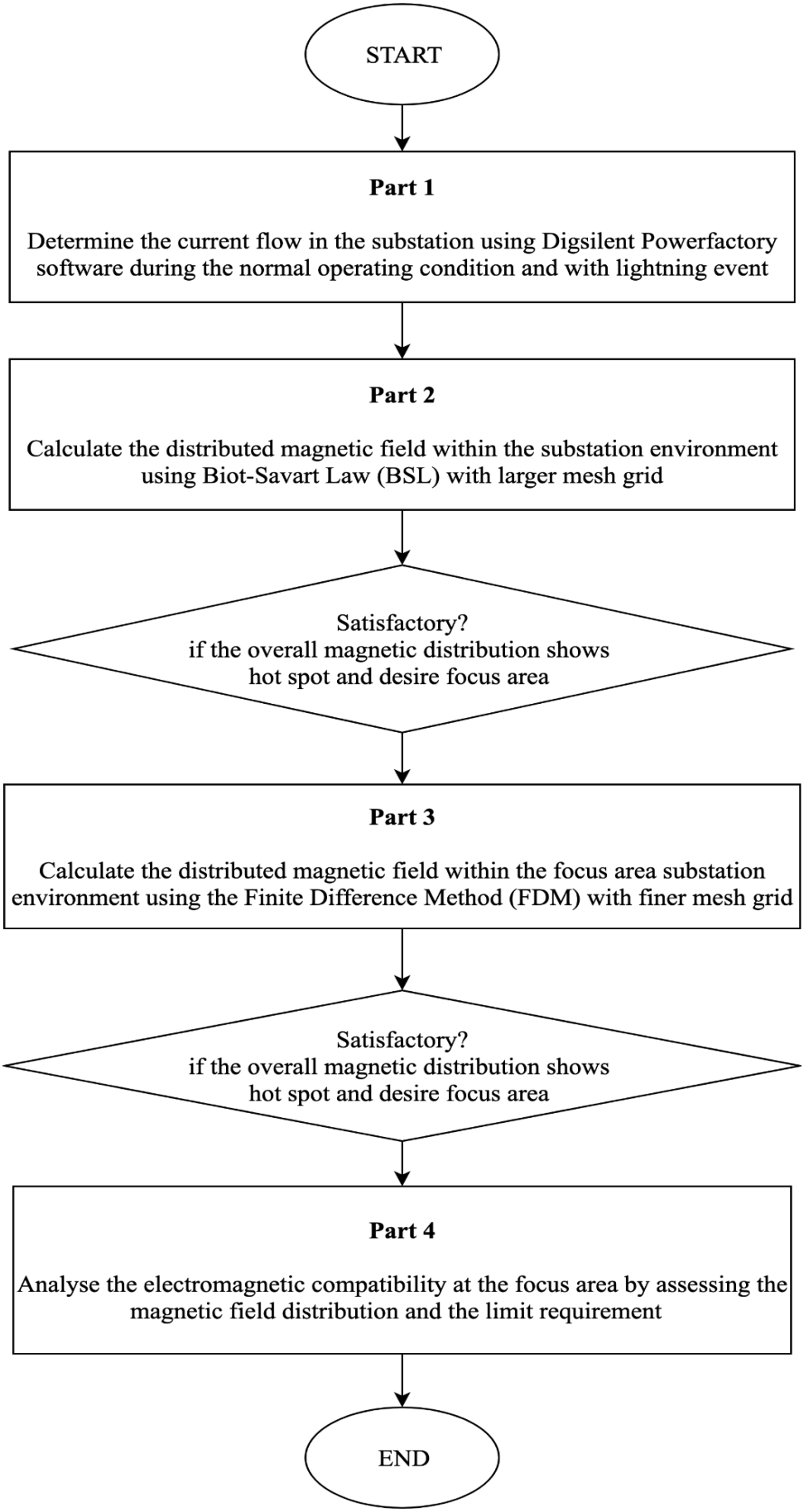

Figure 3.1 Flow chart of the research methodology

3.2 Description of Rosiori Substation Model Structure

The layout of the substation details provided by our collaborators at the Technical University of Cluj, Faculty of Electrothechnics. Figure 3.2 shows the design and features of substation used. The Rosiori substation consists of three outgoing feeders which are Gadalin, Mukacevo, and Oradea and one compensation coil at 400kV double busbar. It is connected to autotransformer to step the voltage down to 220kv and finally three outgoing feeders which are Vertis, Baia Mare1 and Baia Mare 2. Details of Rosiori power station 400/220kV [101] as listed in Table 3-1:

Table 3-1 List of the component in the Rosiori Substation

Component of 400kV Substation Station	***Component of 220kV Substation Station***
1. Overhead line 400kV Gadalin 2. Overhead line 400kV Mukacevo 3. Overhead line 400kV Oradea 4. Autotransformer 400/220kV, S = 400MVA 5. Reactance coil 400kV, Q = 100MVAr	1. Overhead line 220kV Vertis 2. Overhead line 220kV Baia Mare – double circuit

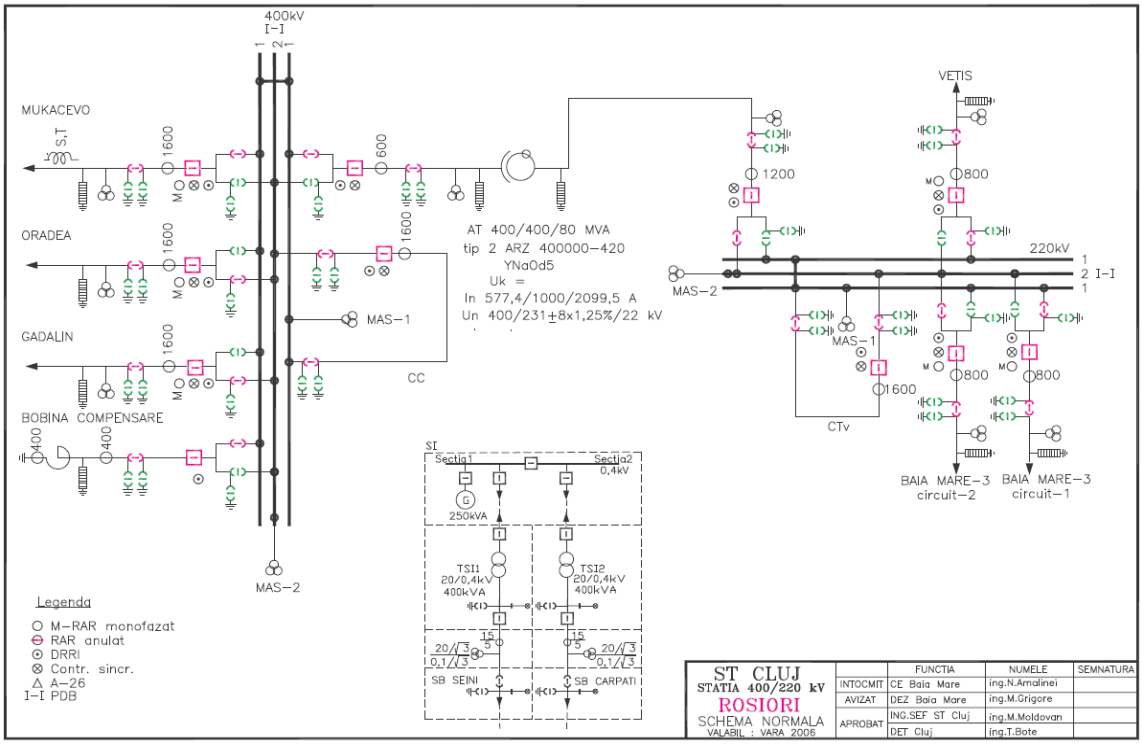

Figure 3.2 Romania's Substation Layout, Rosiori

The structural layout of a Rosiori substation area with the measured dimension of 12m height, 250m length and 140m wide as shown in Figure 3-3. Detail dimensions of the substation layout attached in the appendix for further references.

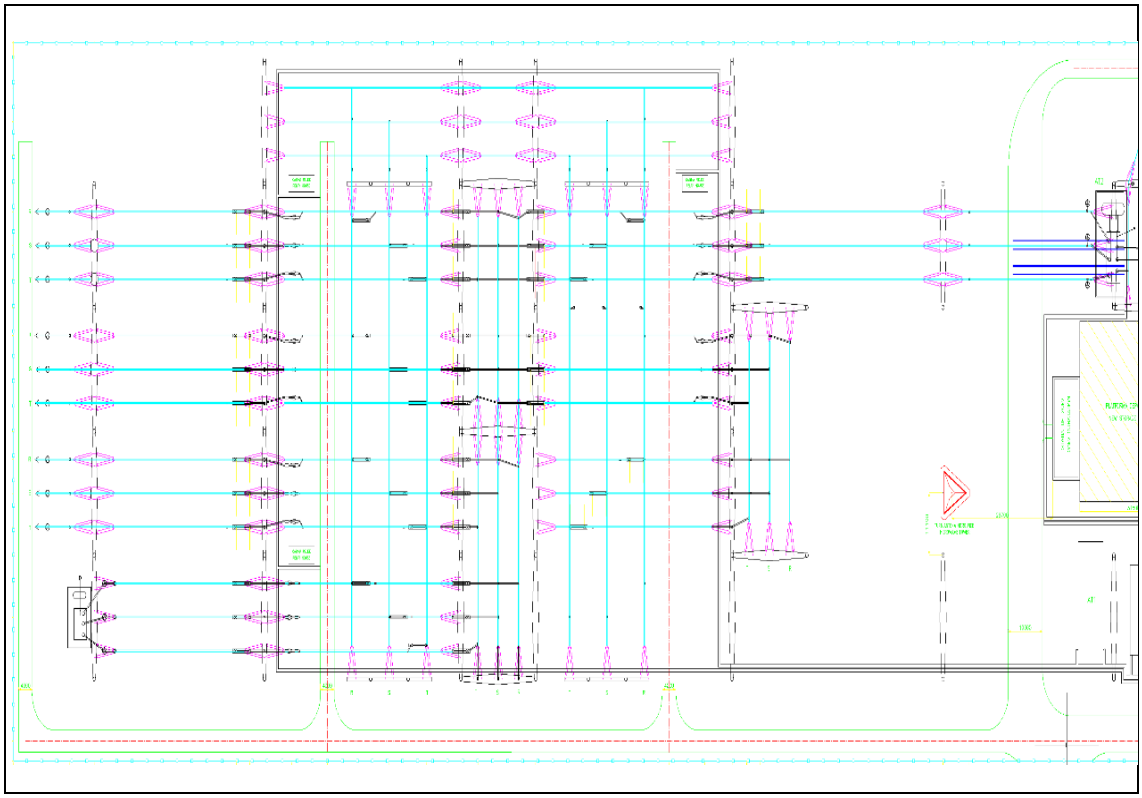

Figure 3.3 Layout drawing of Rosiori substation for the 400kV side

Since there is quite an intensive study done by the group from Technical University Cluj on electric and magnetic field distribution either in prediction via numerical calculation or experimental measurement on this particular substation in [102-105], this will help in validating the model with previous measurement data.

3.3 Part 1 – Substation Performance During Normal Operating Condition and With Disturbances of Lightning Strike Event

The objectives of this part are to study the performance of substation during the normal operating condition, and the effect of lightning event occurred in the substation using Disgsilent Powerfactory software. With the information on the Rosiori substation given by collaborators at the Technical University of Cluj, Faculty of Electrothechnics, the substation will be used to be modelled in the software. From the substation layout in Figure 3-3, first, it will be translated into single line diagram in the Digsilent PowerFactory software. After translating the drawing layout into a single line diagram, all the components in the substation are set up as required in the software. This particular software was selected due to the capability to simulate the substation circuit at normal condition, and the ability to apply disturbances such as lightning pulse into the simulation circuit.

3.3.1 Normal Operating Condition

As mention earlier, the Rosiori substation has the 400kV side connected to three loads, a shunt reactance and an autotransformer to step down the voltage to 220kV. The normal operating currents at the frequency of 50Hz for each load, as listed in Table 3-2. The circuit layout of the modelled substation in the Digsilent PowerFactory software shown in Figure 3-4. Since there is no detail information on the capacity and numbers of power supply by the generator connected to the substation, the load supplied by external networks called the External Grid element. The External Grid element modelled as a voltage source with an internal impedance, and the mechanical equations are for synchronous machine [106]. The circuit model, the main focus of the study, is at the steady-state condition and the substation behaviour due to applied disturbances.

Table 3-2 Operating currents of the Rosiori station 400kV side

Load component	***Operating current (A)***
Load 1(Mukacevo)	200
Load 2 (Oradea)	90
Load 3 (Gadalin)	28
Shunt reactance	147

The first analysis that has been done before applying any disturbances in the circuit is a load flow analysis is done to know few steady-state condition requirements as below:

1. Electricity generations sufficient for the consumer, including loses.
2. Bus voltage magnitude operated at rated values.
3. Generator operated within specified real reactive power limits
4. Transmission lines and transformer are not overloaded.

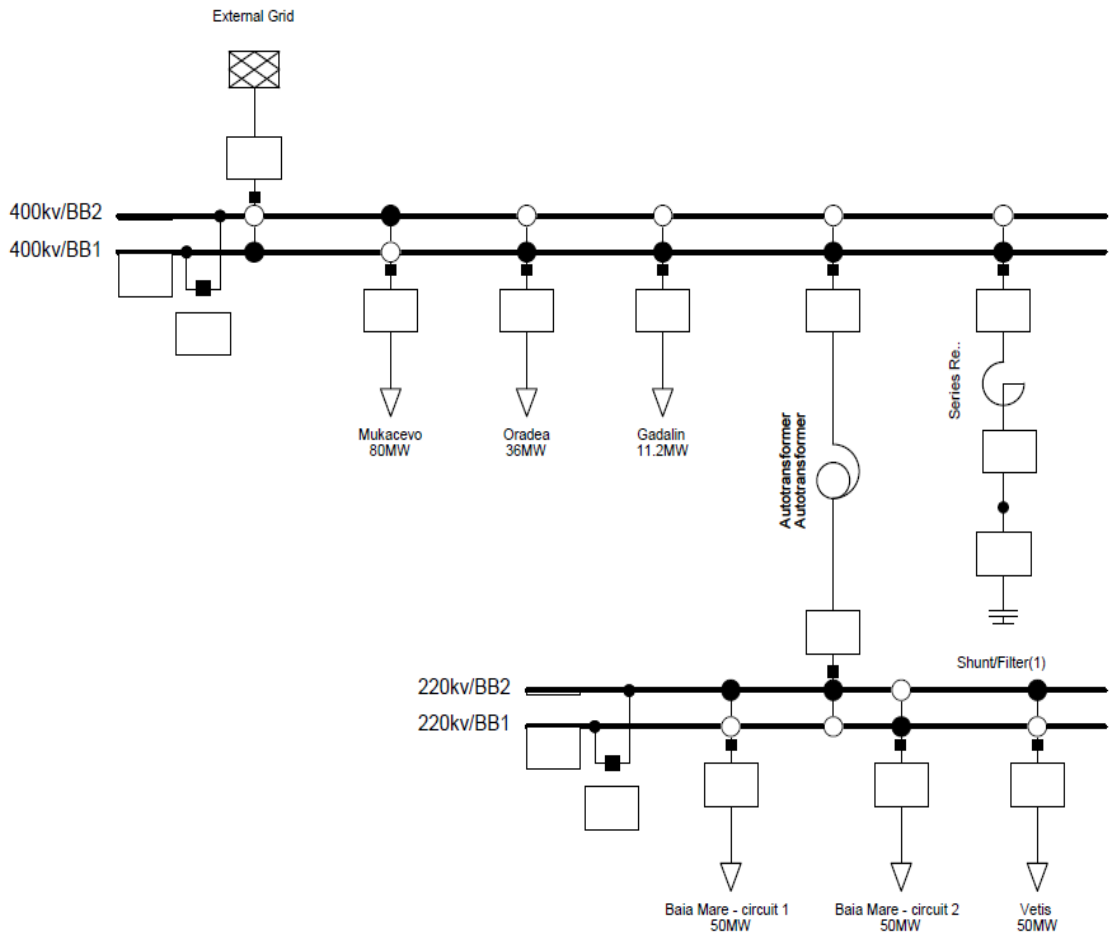

Figure 3.4 Rosiori substation build in DigSilent Power Factory software at steady state

3.3.2 Disturbances of Lightning Strike Event

Since the research aim is to replicate the environment during interference occur in the substation environment, a direct lightning strike on a conductor of power line or substation can cause problems in the distribution network. It will generate extremely high voltage pulses at the strike point propagate as travelling waves into the distribution network [49]. Theoretically, the crest of the voltage can be calculated as equation 36 below, where V is the peak voltage, I is the peak lightning current and Z is the impedance seen by the pulse along the direction of travel.

$$V = I \times Z \tag{36}$$

The lightning waveform based on standard IEC 62305-1 [60] implemented in the DigSilent software described by the equation (37). Where I is the peak current in kA, k is the correction factor for the peak current, t is the time, τ_1 is the front time constant in μs, τ_2 is the front time constant in μs, and n is exponent or steepness factor (10) [62, 107]. A first short stroke lightning current pulse with the magnitude of 200kA and waveform of 10/350μs (front and tail times) was injected as a disturbance to illustrate the worst-case scenario of the lightning strike. The impulse parameter set in the software, as shown in Figure 3-5. The lightning current waveform applied to the substation circuit is illustrated in Figure 3-6 [60]. The current waveshape was chosen because the first stroke of lightning will cause more damage to the system compared to the subsequent stroke that mitigates after the first stroke.

$$i = \frac{I}{k} . \frac{\left(\frac{t}{\tau_1}\right)^n}{1 + \left(\frac{t}{\tau_1}\right)^n} . \exp\left(-t/\tau_2\right) \tag{37}$$

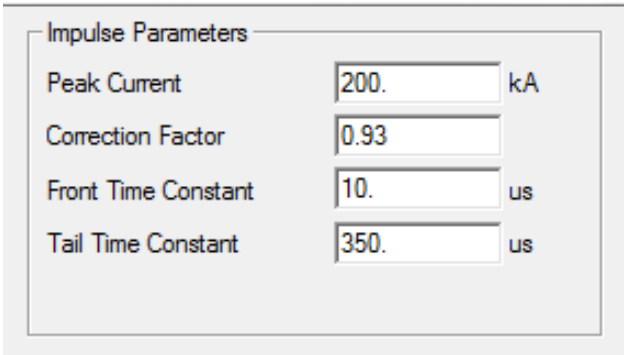

Figure 3.5 Impulse Parameter setting

The current impulse source element used to represent a lightning strike current waveform in Power Factory software. It is a single-phase, single-port element, and it connected to any AC Terminal [62]. The lightning pulse currents were injected straight into the 400kV busbar (400kV/BB1) in the substation model, as shown in Figure 3-7. This is because of the height of 400kv busbar are typically located at 8m from the ground, including structure height is adjusted, making ground clearance more than 2.5m [108]. At this height, it is inviting the lightning to strike straight to the busbar. Thus, the worst-case scenario could be replicated to predict the field generated by this such event.

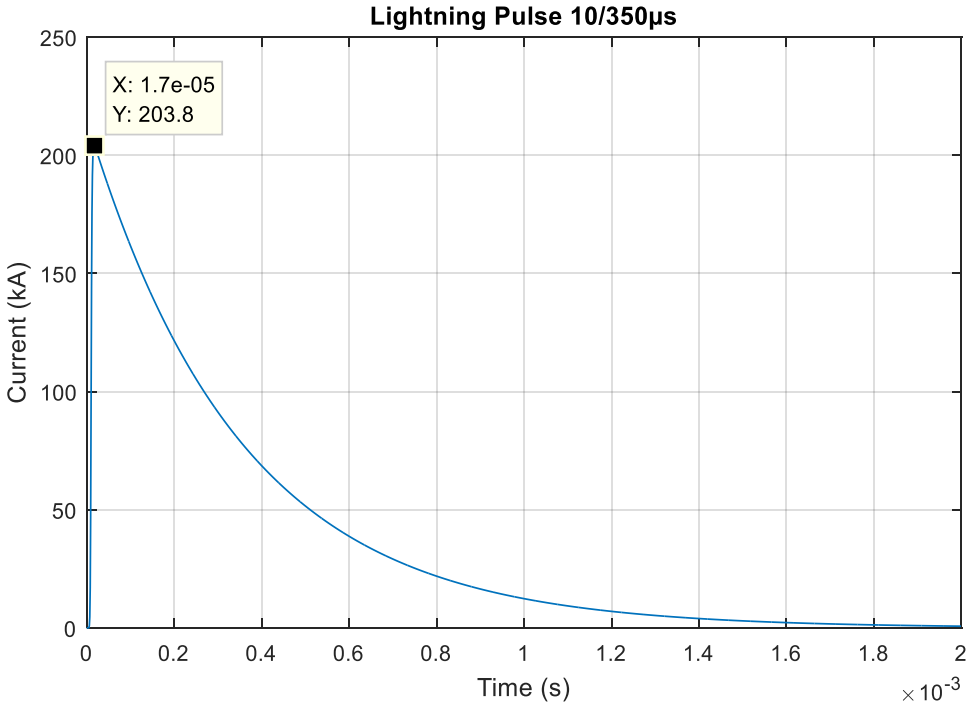

Figure 3.6 Lightning pulse 10/350µs injected to the substation (IEC62305-1)

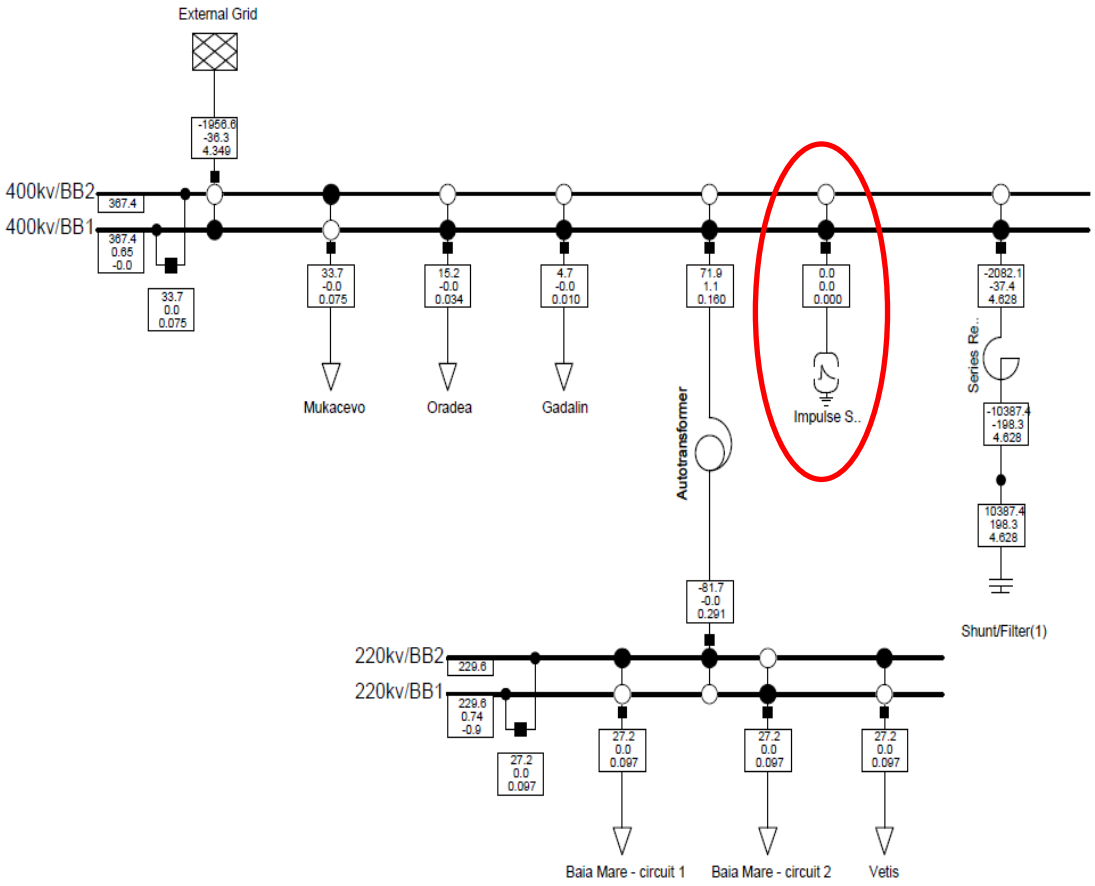

Figure 3.7 Substation circuit with IEC62305-1 applied at 400kV (BB1)

3.3.3 Input Current Assumption for the Magnetic Field Calculation

During a normal operating condition of a substation, alternating current (AC) flowing through the wire and busbar, where the value of current is changing through time. Since the substation environment is normally a large area, a few simplifications have to be made in the calculation in order to determine the magnetic field distribution within the whole area. In order to apply Biot-Savart's Law (BSL) in this context, the current flow of every line connected to the substation is done at specific time frames. In this way, the AC nature of the current flow is treated as having DC characteristics. For each time frame, the magnetic field intensity, H was calculated for the whole predefined area to obtain a coarse evaluation of the worst-case scenario (i.e. the maximum value of H). This value will then be used as a base to conduct FDM to get finer H resolution at specific areas. Significant computation time is reduced using this method. These assumptions aligned with the experimental measurement setup on real substation environment during steady-state condition[19, 109]. The result of the calculated magnetic field using BSL calculation will be compared with the published experimental measurement data done for the same substation.

3.4 Part 2 – Calculation of Magnetic Field Using Biot-Savart Law (BSL)

In this part, the magnetic field calculated numerically by applying BSL using the previous result from the substation simulation. The current flow during both normal condition and with a lightning strike into the substation used as input. The algorithm is written in Matlab software calculate the distributed magnetic field within the substation environment, and the computed result eventually compared with the limits and standard. Figure 3-8 shows the steps in Part 2 of this research work.

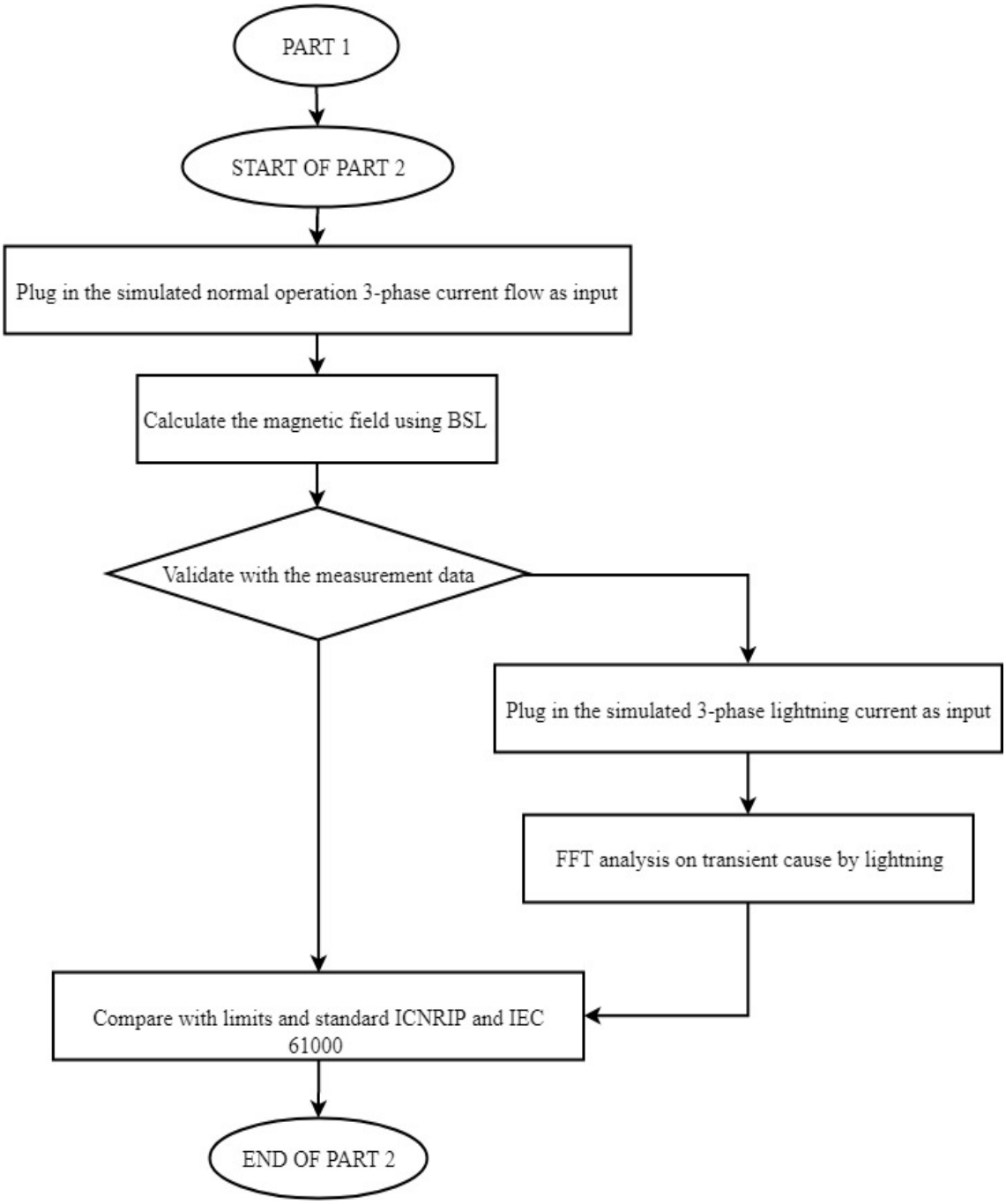

Figure 3.8 Flow chart of Part 2

There are many different numerical calculation techniques have been used to compute electric and magnetic fields, but the most suitable calculation method of the magnetic field for the large area specifically in substation by employed Biot-Savart Law (BSL) directly. The size of the substation's environment usually is enormous, and it is difficult or nearly impossible to determine the magnetic distribution by other methods. BSL is a fundamental equation that used to calculate the magnetic field generated by a steady-state current, *I* flow through a conductor. The current from load flow analysis in the previous part is used as an input to determine the magnetic field distribution within the high voltage substation environment.

The algorithm is created based on the BSL mathematical description was explained in the previous chapter 2.6.1. High voltage substation produces electric and magnetic fields where the strongest fields come from transmission and distribution lines entering and leaving the substation [110]. The magnetic field is produced whenever current is flowing through a conducting channel. A few assumptions have to be made to keep the procedure of modelling and calculation simplified. Then the result of the calculated magnetic field will be discussed. Lastly, the result will be compared with the experimental measurement as validation in the last section of this chapter.

3.4.1 General Substation's Modelling Assumption

All the assumption are made to simplify the substation model, and it will be used for the calculation and prediction of the magnetic field for Rosiori Substation in the next chapter. Only the conductor in the substation included in the calculation model with three-phase currents flowing for each load. Since the power transformer also been neglected to simplify the calculation, the calculation stops at the conductor that connected to the power transformer where it will step down the 400kV to 220kV. The calculation focusses only on the 400kV substation system.

It is decided to be focusing only on the primary sources of the magnetic field and thus neglect the less critical influences to make the modelling more efficient. The first simplification was to include only the conductors above the ground, with the substation busbars treated effectively as transmission lines and currents and voltages of each branch computed. All other equipment, as well as the insulators, are neglected. Thus, only the magnetic field produced by the conductors in the substation is considered. Although there are some differences in the results while comparing the case which more details are accounted for, as discussed in[91], the errors are relatively minor; hence the simplification is considered acceptable. The main difference being observed and reported in[10] is not the overall field distribution, but instead, it is done in the finer details of the results. The closeness of the maximum field to the substation equipment where if the magnetic field is calculated far enough from the current paths the assumption used here is justified.

Another important substation component which would generally be considered is the transformer. The transformers installed in substations, however, are usually very well shielded, so that most of their magnetic field is confined within their casing; consequently, their contribution to the magnetic field of the outer environment is relatively small. It would be costly computationally to simulate the whole transformer [111]; therefore, for this particular research study, only the connections between the transformer terminals and the cables are considered. This simplification appears to be fully justified for the normal operation of the system. Still, it may need to be reconsidered in the case of a lightning strike situation, especially when the strike is close to the transformer.

3.4.2 Modelling Procedures

The algorithm consists of two main steps. First, the geometry (and topology) of the substation is introduced to identify all conducting paths. Each path is then divided into sub-segments in the *x,y,z* coordinate system and currents are applied to each conductor. This information would usually come from a power flow solution provided by the appropriate modeller, which is Digsilent PowerFactory software [112] for normal operating conditions. The Biot-Savart Law is then applied to calculate the magnetic field generated by the applied currents. For the illustrative example reported in this thesis, a plane grid of 6674 calculation points is arranged where a matrix of 94×71 in *x*-axis and *y*-axis for the substation environment for magnetic field calculations. Along the *x*-axis, the increment is a 3m interval (*x*+3), and for the *y*-axis, it is a 2m interval (*y*+2) as illustrated in Figure 4-2. With this algorithm, the density of the calculation points can be easily modified to focus on regions of higher interest.

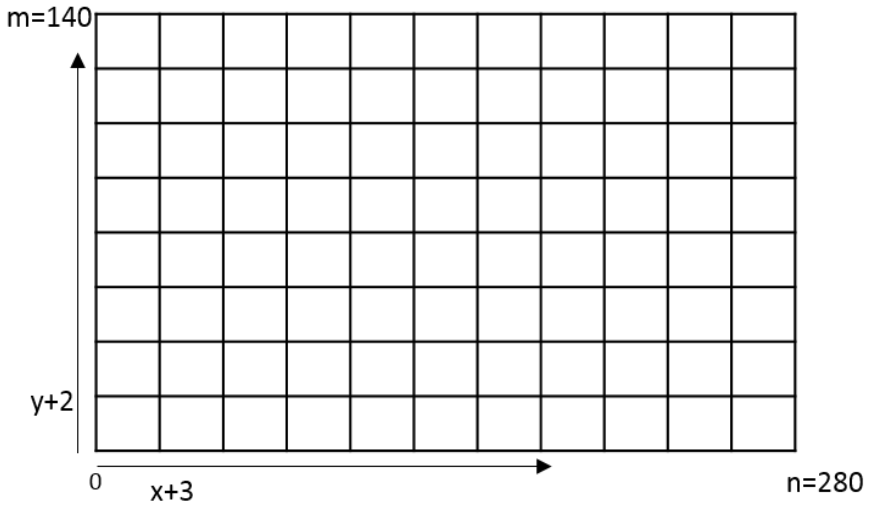

Figure 3.9 Illustrated grid for magnetic field calculations for a substation.

The substation measurement considered as 280m long, 140m wide and the conductors located at the height of 12m above the ground (on the 400kV side). For such a large site, it takes almost 6 hours for a computer with Intel (R) Core (TM) 3.4GHz processor with 16GB of RAM to complete the magnetic field calculations for a matrix of points 94×71 in *x*-axis and *y*-axis, respectively. The generated magnetic field is studied at different levels from the ground by setting the height for *z*-axis in the algorithm. The magnetic field was measured at three different heights based on the human body measurements, namely: the feet at 0m, the waist at 1m and the head at 1.75m [113]. The computing times will depend on the number of current inputs that plug in the calculation.

Two cases of magnetic field calculation have been considered. For the first case, a normal distribution of three-phase currents is assumed resulting from a load flow analysis. The second case introduces a lightning strike, and associated current injected into substation conductors. Thus, both the steady-state and a disturbance have been considered. Although for the case of the lighting strike the assumptions introduced earlier on maybe a little too restrictive, the results will nevertheless demonstrate the capability of the algorithm to cope with transient as well as steady-state currents. The frequency-domain analysis was also implemented to show the capability of frequency analysis in the results of magnetic field intensity. The results are presented and compared with the time-domain analysis.

3.4.3 Validation with Experimental Data

The result of the calculated magnetic field using BSL calculation will be compared with the published experimental measurement data done for the same substation. Rosiori substation is one of many substations that will be refurbished by the utility company in Romania. Before any new implementation, the Technical University of Cluj, Faculty of Electrothechnics have been appointed to perform a study of the substation to plan and design the substation refurbishment[101].

The experimental was perform to measurement electric and magnetic field covering the whole surface with a mesh grid of the substation environment that the distance between two adjacent test points on a measurement line was 3m. The device placed at 1.7m height above the ground. The field measurement was done with more than 3000 test points, and the measurement lines have been selected such way that they passed in closed vicinity to the main power equipment. The experiment is only was done during a normal operation condition [104]. These measurements data will be used to compare and validate the result of in-house BSL calculation algorithm.

3.5 Part 3 – Magnetic Field Calculation using FDM

After solving magnetic field using Biot-Savart law (BSL) in larger resolution scale within the whole substation environment in the previous chapter, the next step is to get the detailed analysis on a specific area within the substation environment using Finite Difference Method (FDM). FDM is a numerical computational method of solving a linear partial differential equation where time has been absorbed into a complex field variable and proceed to an iterative method of solving the resulting matrix equation [78].

Thus, a numerical algorithm model using approximated methods based on Maxwell's equations has been developed in Matlab to perform detailed analysis and magnetic field distribution prediction within the specific area in the substation environment. The result of the calculation of developed algorithm FDM was compared with those obtained using BSL in the previous chapter. The comparison between BSL and FDM will validate the FDM calculation method and set as a boundary area for further analysis on the EMC of equipment installed in the substation environment in Chapter 4.4. It would be helpful to the user or utility company by providing the information on electromagnetic compatibility location to install new equipment.

3.5.1 Modelling Structure and Assumption

Based on the FDM mathematical description for magnetic field calculation, the simulation model developed to predict the magnetic field at focus area within the substation environment in three-dimension (3D). The focus area first to be chosen by refereeing to overall magnetic field distribution at 1.7m above the ground calculated from the previous calculation using BSL for the whole substation with larger mesh grid solution as shown in Figure 3-10. Details on the BSL magnetic field calculation method were discussed in Chapter 3.4. Based on the initial value of calculated magnetic field distribution in the substation environment, a suitable location is chosen to be the focus area for further details study as a potential location to install new equipment. It is best to choose the location that has low field distribution so that the new equipment able to operate compatibly within the environment with low disturbances [13, 114].

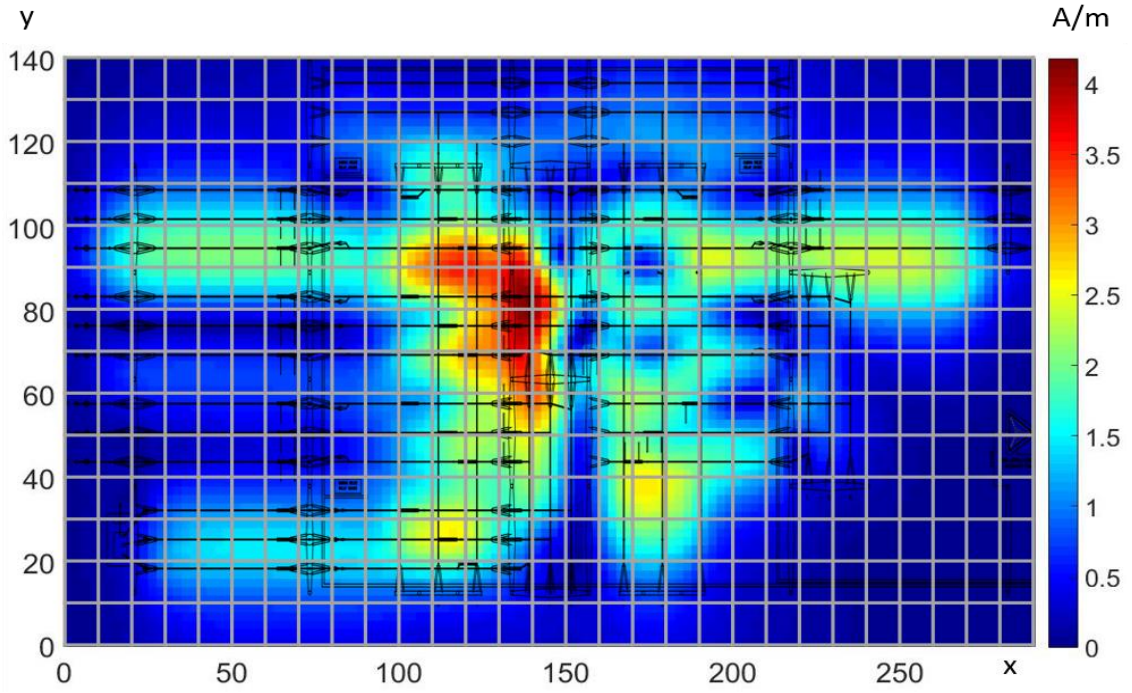

Figure 3.10 Substation area with calculated magnetic field in grid square cell

After the desired location of the focus area within the substation environment has been determined, the size, dimension and resolution of this area in terms of mesh grid as illustrated in Figure 3-10 need to be plug-in the FDM algorithm. For this particular case, the coordinate of the focus area chosen to be at [102,22,2], where it is not the hottest spot in the environment. The size of this area is set to be 5m x 5m x5m in length, width and height. It is unnecessary to calculate the distributed magnetic field for the whole dimension of the substation area, which will require extremely large computational data processor and storage. Thus, by focusing on limited area size, which contains the interference and set as a boundary condition on the outer surface of the mesh. Such that the unbounded surrounding is modelled as accurately as possible [84].

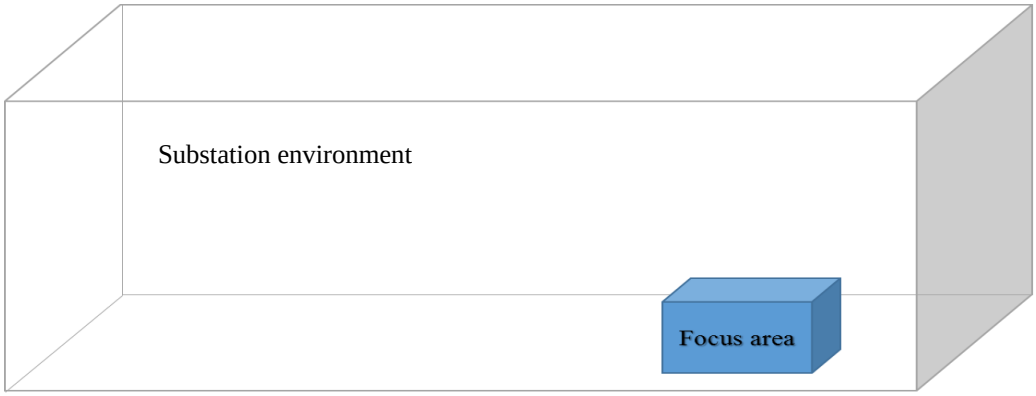

Figure 3.11 Illustration of substation environment and focus area.

To understand the FDM calculation process in the algorithm, magnetic field, **H** was calculated for the focus area based on the initial value of the distributed magnetic field earlier

using BSL. From Figure 3-12 shows the rectangular coordinates system formed by simple mesh or grid of (*x*,*y*,*z*) axis and the nodes are address by (*i*,*j*,*k*) represent the magnetic field at that node at the cross-section of the z-axis. Each rectangular cell formed by the mesh has associated with its constant conductivity and permeability. The mesh grid coloured in blue represent the chosen focus area, and the white grid will be the substation environment with an initial calculated magnetic field from the previous calculation.

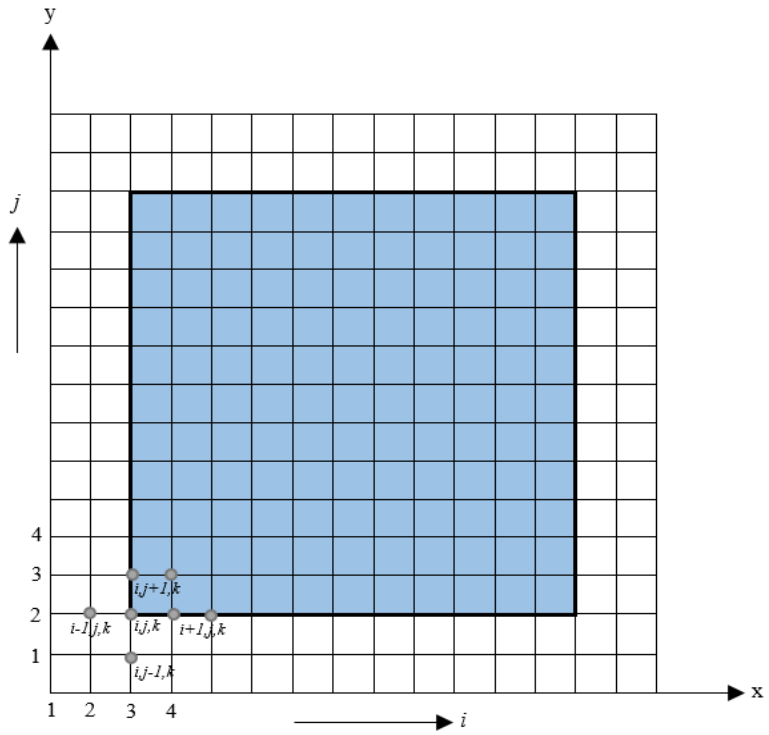

Figure 3.12 Finite difference grid or mesh in 2D (cross-section of z-axis)

By using equation 26 and 27 from Chapter 2.6.2, the magnetic field $\mathbf{H}_{(i,j,k)}$ were calculated by taking previous initial value until alliteration for every node is done. It is much easier to calculate at a smaller focus area with a finer resolution of the mesh grid rather than calculated the whole substation environment. The bigger the model is built, the more computational time and the complexity of the problem is increased. The results are plotted using colour contour in 3D for the whole targeted focus area, and the reading of the magnetic field value taken in a table and explain in the next subchapter.

3.6 Part 4 – Shielding Effect in the Substation Environment

The EMC and immunity studies on the component or equipment are usually done by setting up an experimental test to learn their ability and compatibility in the electromagnetic environment. This was by the test equipment will be arranged to be put under induced disturbances by radio frequency to see their immunity level [13]. Measurement experiment also has been done on measuring the electric and magnetic field within the substation environment during substation's regular operation [65, 104, 115]. It is difficult to setup up a test environment to study EMC within substation with actual interference injected into the system. Thus, most of the previous research done by producing mathematical numerical modelling to calculate the EMC problem of power substation during disturbances occur [86, 116, 117].

This part of the research will combine both situations, whereby the equipment's EMC performance during disturbances occur within the substation environment will be predicted. To illustrate the real equipment that installed in the substation environment, a metal box is modelled in using the algorithm and simulated within the calculated magnetic field environment. The magnetic field induced from the substation environment is expected to travel inside the equipment box. A concept of 'metal box' model to illustrate shielded enclosures, builds with opening apertures to illustrate any holes that made in the equipment for any connecting power supply and control buttons on the equipment. Magnetic flux that could be generated by the induced current on the surface of the box will be calculated based on the parameter of the box which will be regulated in the model are the dimension, location, and material of the desired by used. The same numerical calculation method as previous which is FDM will be used.

The result of the magnetic field penetrates the metal box will be illustrated using the quiver plot from Matlab. It is to shows the movement of the magnetic field penetration into the box and the field concentration area as well. The reading inside the box is taken, and compare with standard immunity level for smart grid equipment to get better information on the distributed magnetic field. All equipment installed in the substation environment expected to have standard immunity requirement to withstand any interference occur in the system as stated in IEC 61000 [97, 118].

3.6.1 Modelling Assumption and Geometric Description

As mention earlier, the box could be located at desired substation's environment; ideally, the box should be placed in the area that has the lowest magnetic field interference which is suggested in IEC 61000-5-6 standard[99]. It will reduce the electromagnetic compatibility issues due to the magnetic field disturbances towards the new equipment that will be installed [13, 118].

Using the simulation algorithm, the size and location of this box can be adjusted to any measurement and could be set to anywhere in the substation environment to suite the user needs.

The first assumption made for this part of the simulation is, the same focus area will be used to apply the concept of 'metal box' (in red) as illustrated shielding effect [99] as shown in Figure 3-13. For this particular case, the coordinate of the focus area assumed to be at [102,22,2] where it is not the hottest spot in the environment based on the previous numerical calculation result. The size of the fixed focus area is 5m cubic area and act as the boundary condition. The metal box with the dimension of 0.5m for length, width and wide is located in the middle of the focus area with the calculated magnetic field as it will be the initial value at the boundaries and is assumed to be fixed due to the changes in the subdomain. The thickness of the metal box is set to be 9mm, considering the skin depth where the penetration depth for a good conductor at 50Hz can be calculated from the following equation 38. These dimension chosen are based on the typical size of equipment that might be installed in the substation control room area.

$$\delta = \frac{1}{\sqrt{\pi f \sigma \mu}} \tag{38}$$

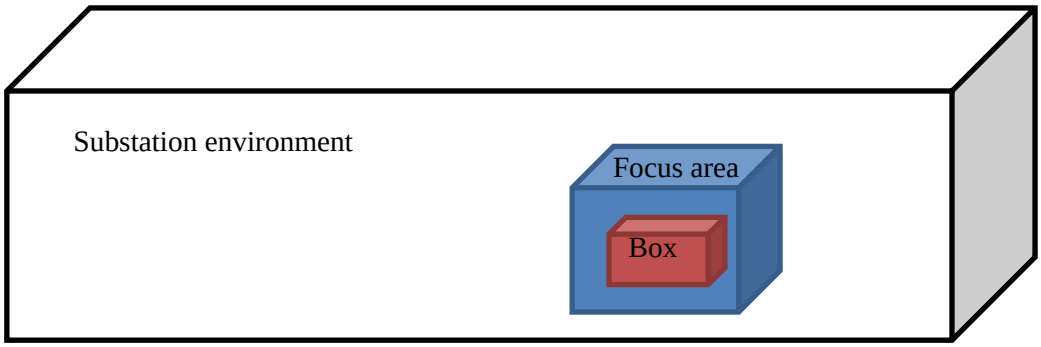

Figure 3.13 Overall illustrations of introducing a metal box in the substation

The developed FDM applied to every node in the mesh grid to calculate the magnetic field within the metal box. Figure 3-14 shows the grid or mesh in 2D where the cross-section of the metal box. Every node (*i*,*j*,*k*) are divided into the region into several subdomains. The blue mesh is set as a focus area which calculated earlier, the grey mesh will be the metal box, and the white will be air. All parameter that associate to every node applied to the finite difference equation.

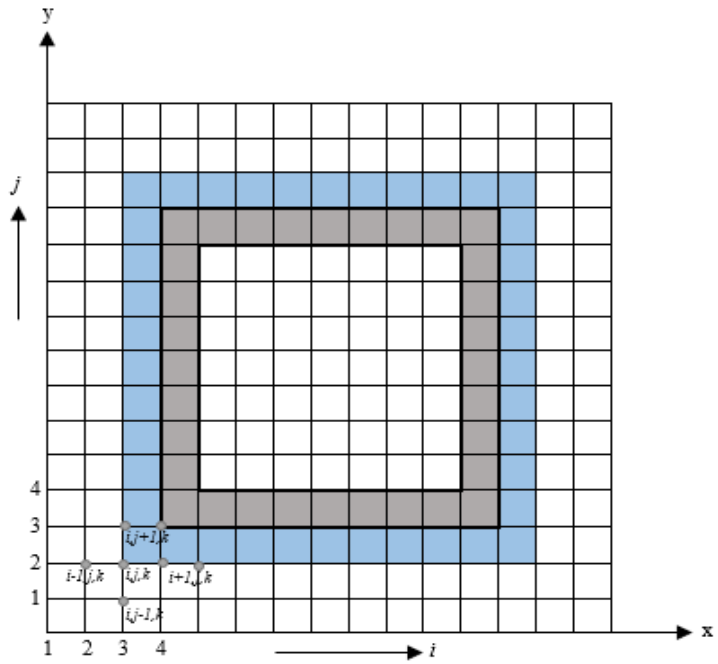

Figure 3.14 Finite difference grid or mesh in 2D (cross-section) with metal box

The magnetic field was calculated inside the box for every 20mm point at each axis for different opening positions where makes the mesh for *x,y,z* axis to be 30x30x30. That makes the total array to be 27000 to calculate. With the limitation of computational resources, all the calculation is done by using a computer with the specification of Intel (R) Core (TM) 3.4GHz processor with 16GB of RAM. To represent the real equipment that will be installed in the substation environment, the metal box model as the equipment under test should have a cut opening on the surface usually are for power supply connection or control button. The manufacturer will try to make it as small as possible to avoid any interference propagate into the equipment. Due to that, to study the pattern of magnetic field propagation due to an opening on the box, a few cases scenario was developed in the model to have different opening position and area sizes. The details set up for each case are tabulated in Table 3-3 below. Another important assumption needs to be applied in all the modelled of this metal box is grounding. On one of the bottom corners was set to be having zero voltage potential, (v=0) and infinite current (I=∞) to act as ideal grounding termination point as recommended in [99, 119].

Table 3-3 Details on the scenario set up for each case

Scenario	No of opening	Size	Location
Case 1	1	$16cm^2$	Horizontally
Case 2	3	$16cm^2$	Vertical

Case 3	3	4cm^2	Vertical

The model is set to have three different apertures positions horizontally at A, B, and C with the area size of 16cm^{2,} as illustrated in Figure 3-15. The magnetic field generated from the substation environment expected to penetrate into the box through the opening apertures [99]. These three openings located at different height of the box which to illustrate the location of the opening might influence the amount of field that penetrates in the metal box. The magnetic field predicted that would have higher field density at the opening of the box.

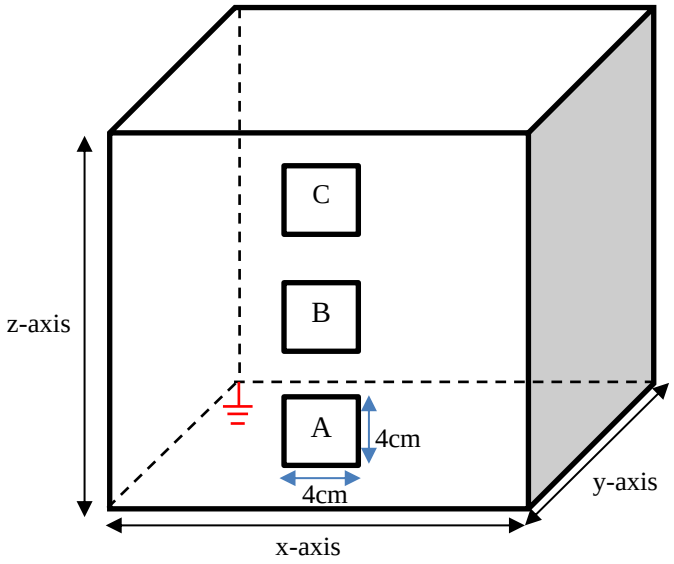

Figure 3.15 Illustration of the grounded box with opening (Horizontal)

For further investigation, the metal box are modelled by having multiple opening that located at the bottom of the metal box's surface with two different area size of 16cm^2 and 4cm^2 as shown in Figure 3.16 and Figure 3.17. These will allow researcher to study the amount of field entered the metal box effected by the numbers of opening and the size of opening area on the metal box as suggested in standard discuss previous in Chapter 2.7.2. With the smaller opening area, it might limit the magnetic field entered the metal box hence the effect of magnetic disturbances able to be reduced[99].

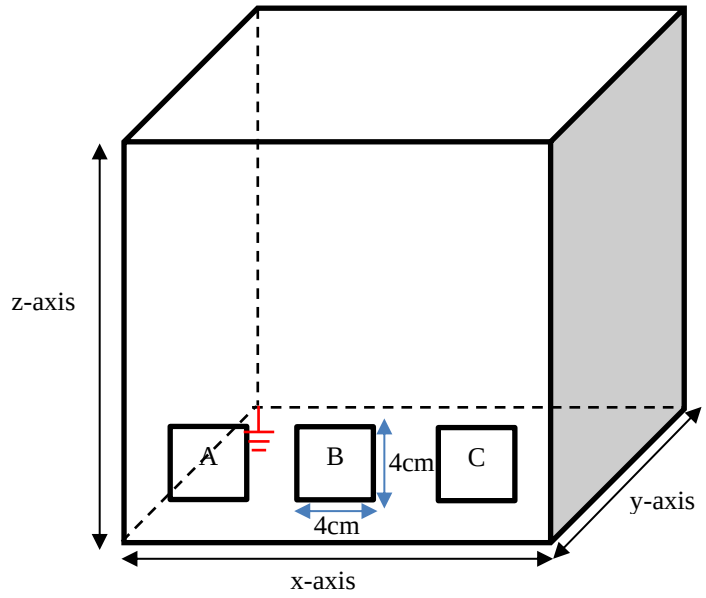

Figure 3.16 Illustration of the grounded box with all three opening (Vertical)

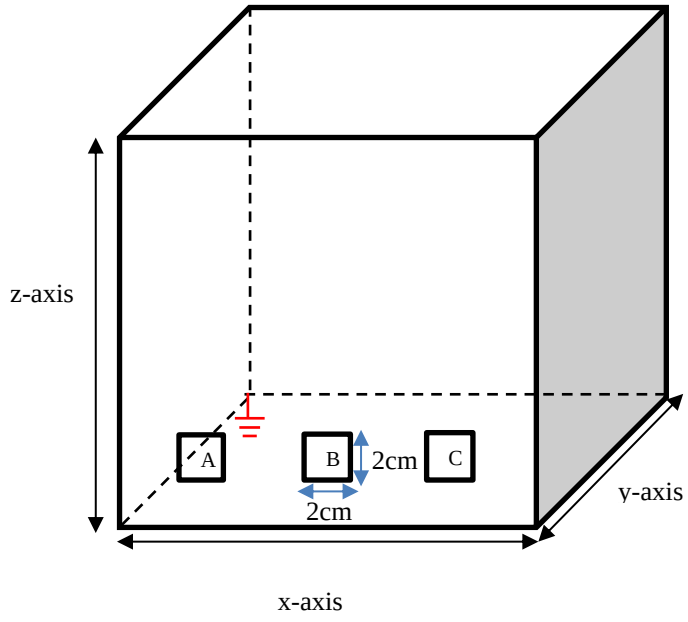

Figure 3.17 Illustration of the grounded box with the smaller opening (Vertical)

There is another vital justification to be made before installing new equipment in the substation, are the function and the connection of the equipment to the substation need to be at optimum immunity level and cost-friendly. The other parameter that needs to be considered is the type of material[99] which represents the magnetic field equation as permeability, μ and conductivity of the material, as shown in equation 30. Using this algorithm model, the size and location of this box can be adjusted to any measurement and could be set to anywhere in the substation environment to suit the user desires to fit the equipment that installed in the substation.

With this calculation and prediction of the magnetic field within the operated substation, the result would be useful not only for safety assurance but it also will help utility company to design a new automated substation or refurbish the old one with an optimum immunity level. The information on the calculated magnetic field that penetrates inside the box will be compared to the specification of several new types of equipment for smart grid system such as a digital protective relay. Detail data and information on the equipment specification will be gathered to make detail analysis; hence, comparison can be made. The equipment specification that needs to be concentrate on are the dimension of the equipment and immunity level towards magnetic field disturbances.

3.7 Summary

The methodology adopted in this research has been described in detail in this chapter. The description of the substation used presented at the beginning of this chapter. The substation detail was used in all other parts of this research. It starts with determining the performance of the substation using Digsilent PowerFactory software for both normal operations and with lightning disturbance applied, then using the result as input to the calculation of the magnetic field distribution. The magnetic field calculated for both conditions within the substation environment. The Biot Savart Law (BSL) first adopted to compute the magnetic field for the whole substation environment with large resolution. Then, the Finite Difference Method (FDM) was applied to obtain the magnetic field for the focus area based on the previous distributed magnetic field for three different cases. Lastly, the induced current was calculated to study the shielding effect on the focus area desired. For further investigation, the shielding effect on multiple opening of the box was studied to achieve a stronger conclusion.

CHAPTER 4

RESULT AND DISCUSSION

4.1 Overview

In this chapter will be discussing in detail all the results obtained in this research. The results are presented divided into four parts in this research, which starts with Part 1, determine the current flow and substation performance during the normal operating condition and during the lightning event applied in the substation circuit. By using the simulation result in the first part as input to calculate the magnetic field by adopting the Biot Savart Law (BSL) within the substation environment was discussed in Part 2. In Part 3 of this research involves the field calculation of the Finite Difference Method (FDM), and the result was compared with limits and standard for electromagnetic compatibility within the substation environment. Finally, in Part 4 discuss the shielding effect towards the simulated model metal box that illustrates the equipment in the substation environment. The key findings of each phase are summarized at the end of each section in this chapter.

4.2 Part 1: Substation Simulation Using Digsilent Powerfactory

The load flow analysis applied to the Rosiori substation to determine its performances. The substation layout transferred to the single-line diagram in Digsilent PowerFactory software. The circuit model was set to be at their steady-state operating current, which is for Mukacevo's load for 200A, Oradea at 90A, Gadalin at 28A and lastly for the current flowing through the shunt reactor to be at 147A. All the current flow in the substation circuit simulation are in a three-phase system. The substation performance will be presented during the normal operating condition, and during a lightning event applied to the circuit in the next subchapter.

4.2.1 Result of Substation Performance During Normal Operating Condition

For steady-state condition, DigSilent functions determine the initial condition for all power system elements which represent the steady-state operating point at the beginning of the simulation. Line voltage measured at 400kV busbar to be at 399.9kV at 1pu and current flowing through the busbar at 0.182kA. The transformer stepping down 400kV voltage to 220kV and at 220kV busbar, line voltage measured to be 219.9kV with the current of 0.18kA as illustrated in Figure 4-1. The three-phase current flowing in the substation will be using in the next part of research to as input calculate magnetic field.

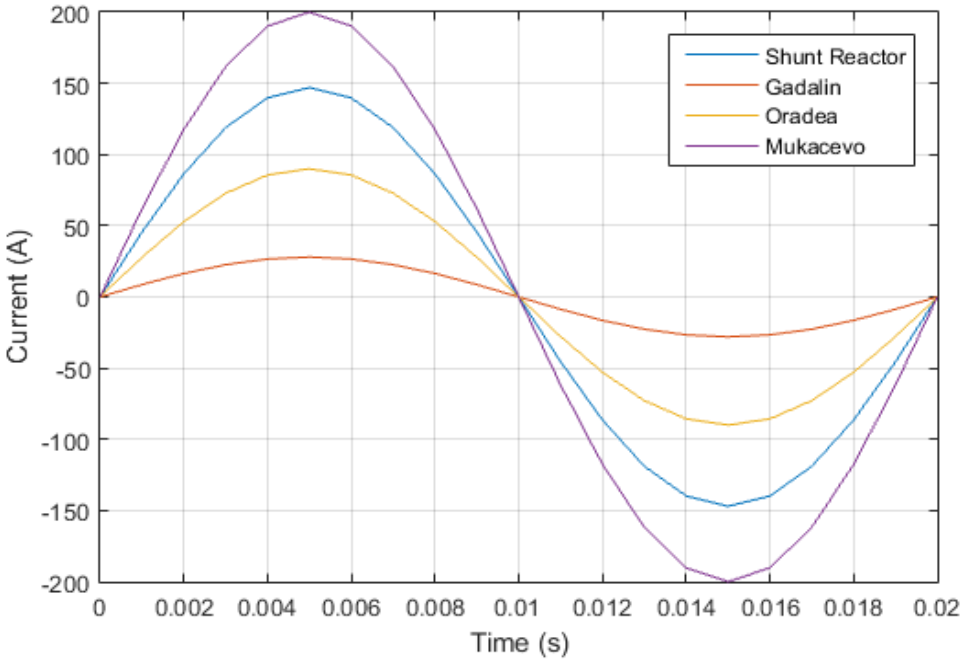

Figure 4.1 Input current for Rosiori Substation

To study the effect of disturbances applies to the circuit, a lightning strike was set up in the DigSilent environment. As explained in the previous chapter, lightning events have the potential

to cause high-frequency interference that able to couple into a low voltage control circuit and electronic equipment unless they are protected [120].

4.2.2 Result of Substation Performance with Lightning Strike

Using the Power Factory software [121], the load flow in the substation was supplemented by the addition of a lightning pulse injected at 0s at one of the 400kV busbars. The time step of this transient analysis is one of the essential parameters that need to be correctly set to achieve meaningful results. The time step will influence the length of the simulation; thus, it is crucial that not set to a very small value. The smaller is the time step, and it takes a longer time to run the simulation. With appropriate time step on plotting the data, it is expected to provide much more accurate result as the data is taken within a small gap of time Thus, to decide on a suitable timestep value, several simulations with different time step were set up and run.

The results in terms of the currents flow in one of the loads (Mukachevo) are shown in Figure. 4-2 for four different time steps: 0.1μs, 1μs, 5μs, and 10μs, respectively. It is clear that a 10μs time step is not sufficient and the peak current calculated using 5μs and 1μs steps is about 5% larger; moreover, the time at which the maximum current is reached is also different. When the time step was further reduced to 0.1μs, there are no significant differences observed compared with the 1μs case. Consequently, for the simulations presented here, a 1μs time step was used. The currents flow of each load with the lightning pulse injected in the substation were plotted in Figure 4-3. The highest current magnitude in the system at 0.02s was 64kA at Mukacevo.

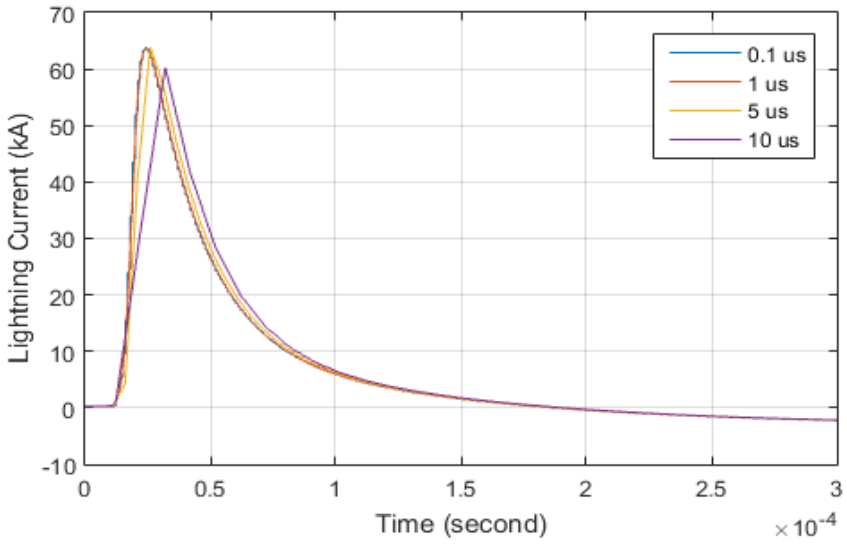

Figure 4.2 Lightning current at one of the load (Mukachevo) for four different time steps.

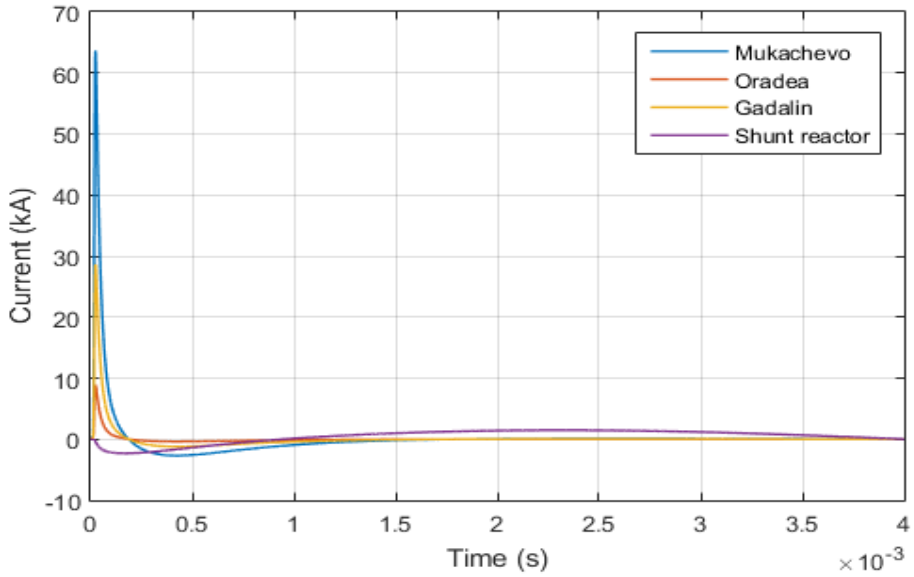

Figure 4.3 The current waveforms when a lightning pulse is added.

The magnetic field distribution in the substation due to the lightning pulse can be considered in two different ways, in the time domain and frequency domain. Both approaches have been applied and compared in the next subchapter.

4.2.2.1 FFT Analysis

The work presented in this section compares the effect of using different models for the lightning strike in terms of the resultant induced voltage into the 400kV busbar. For further analysis Prony Analysis and Fast Fourier Transform (FFT), the frequency analysis tools from the Digsilent Power Factory [121], were used. Prony Analysis was used to decompose the signal into damped sinusoidal oscillations to determine the exact value of the essential harmonic signals over a range of frequencies. These results compare well with the existent data in the public domain that the induced currents due to the lightning strike have the frequency ranging from 100kHz to 120MHz [122]. The magnitude and frequencies decomposed from each three-phase load currents using Prony Analysis, as shown in Figure 4-4. The important frequencies are f1, the fundamental frequency at 50Hz, f2 at 70kHz, f3 at 100kHz, f4 at 150kHz, f5 at 200kHz, and lastly f6 at 250kHz.

The wavelength of an electromagnetic wave at 100 kHz is approximately 3km, which is much larger than any features that will exist in the substation; hence it is very unlikely that any of the energy available after the lightning strike will be radiated away. It is expected that most of the electromagnetic coupling will take place through conducting means. Another possible issue that may need attention when a 100kHz wave is excited in a substation is the possibility of that wave to propagate along the high voltage transmission lines connected to the substation. There

may be a possibility to create secondary effects due to the reflection of that wave one any impedance discontinuity encounter before the energy is dissipated into a surge arrester. Therefore, the network structure around the substation may be considered when a more detailed analysis is done.

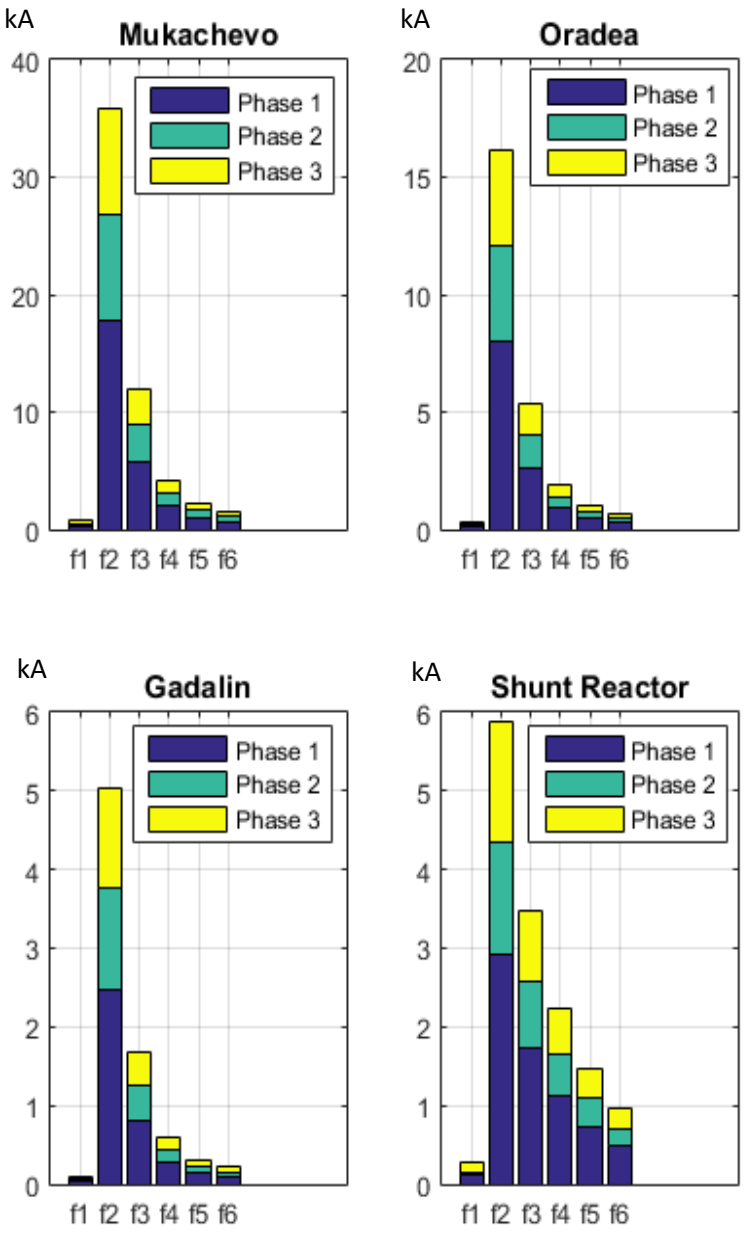

Figure 4.4 The important harmonics of each three-phase current at every load.

4.2.3 Summary of Part 1 Findings

This chapter described in detail of the substation performance during steady-state and during applying the disturbances lightning in the simulation that was used to illustrate the lightning pulse injected into the substation circuit. Using the Power Factory software, the load flow in the substation supplemented by the addition of a lightning pulse injected at the time of 0s at one of the 400kV busbars. A first short stroke lightning current pulse with the magnitude of 200kA and waveform of 10/350μs (front and tail times) was injected to illustrate the worst-case scenario of the lightning strike.

The time step of this transient analysis is one of the crucial parameters that need to be correctly set to achieve meaningful results. The time step will influence the length of the simulation; thus, it is essential to choose the appropriate value. Several simulations with different time step were set up and run to decide on a suitable timestep value. Consequently, for the simulations presented here, a 1μs time step was used since there was no significant difference between 0.1μs and 1μs time step.

For the substation performance during lightning disturbances occurrence, simulated result in Digsilent PowerFactory are in the time domain. To study the value of the essential harmonic signals over a range of frequencies during a lightning event, FFT is applied to the result. The important frequencies are f1, which is the fundamental frequency at 50Hz, f2 at 70kHz, f3 at 100kHz, f4 at 150kHz, f5 at 200kHz, and lastly f6 at 250kHz. Based on the result of calculated FFT, the crucial components of harmonics produced by lightning able recognise and percussion step can be taken accordingly.

In the next part, the magnetic field distribution will be calculated using BSL due to the normal operating current, and during a lightning event apply to the substation. The lightning pulse case can be considered in two different ways, in the time domain and frequency domain. Both will be compared together. This approach enables the prediction of current flow during the normal condition and while disturbances occur within the substation environment, thus eliminates the needs for extensive installation of expensive measuring equipment.

4.3 Part 2: Magnetic Field Calculation Using Biot Savart Law (BSL) within Substation Environment

The simulation for magnetic field distribution result for two particular cases of magnetic field calculation has been studied in Part 2. For the first case, a normal distribution current is assumed resulting from a load flow analysis. BSL applied by using the current flow of every line connected to the substation is done at specific time frames. Thus, the alternated current nature of the current flow is treated as having DC characteristics. For each time frame, the magnetic field intensity, H was calculated for the whole predefined area to obtain a coarse evaluation of the worst-case scenario (i.e. the maximum value of H)

The second case introduces a lightning strike, and associated current injected into substation conductors. Although for the case of the lighting strike the assumptions introduced earlier on maybe a little too restrictive, the results will nevertheless demonstrate the capability of the algorithm to cope with transient as well as steady-state currents. Frequency domain analysis was also implemented to show its capability, and the results in terms of magnetic field intensity are presented and compared with the time-domain analysis.

4.3.1 Magnetic Field Calculation with Nominal Input Current

To calculate the magnetic field, the three-phase operating current flowing in the substation will set into the model for all loads, which is for Mukacevo's load for 200A, Oradea at 90A, Gadalin at 28A and lastly for the current flowing through the shunt reactor to be at 147A as plotted in Figure 4-1. The algorithm calculated the magnetic field at every grid point in three axes (x,y,z) during the highest value of current flowing in the substation.

The substation measurement considered as 280m long, 140m wide and the conductors located at the height of 12m above the ground as illustrated in Chapter 3.42. For such a large environment, it takes almost 6 hours for a computer with Intel (R) Core (TM) 3.4GHz processor with 16GB of RAM to complete the magnetic field calculations for a matrix of points 6671 arrays in x-axis and y-axis, respectively. The generated magnetic field is studied at different levels from the ground by setting the height for z-axis in the algorithm. The magnetic field was measured at human head level for safety assurance which is at 1.7m [113]. The computing times will depend on the number of current inputs that plug in the calculation.

The computed results for the calculated magnetic field at the normal operating currents are presented in Figure 4-5. The computed result and the layout of the substation were combined to get a better illustration of distributed fields since the calculated result are based on the real

dimension of the substation area. It shows that the predicted highest value of the magnetic field is 4.164A/m located along busbar 1, where it is connected to Load 1 with 200A.

The result of the calculated value was depicted in a table and to show the intensity of the field, it is overlapped on the substation blueprint. The magnetic field distribution can be evaluated at different heights from the ground, but for this particular substation, this was calculated and plotted only at the height of 1.7m since the measurements were done at this height so that it is appropriate to make a fair comparison between both calculation and measurement [104]. The predicted and experimental distributions of the magnetic field also will be compared in the context of the exposure limits.

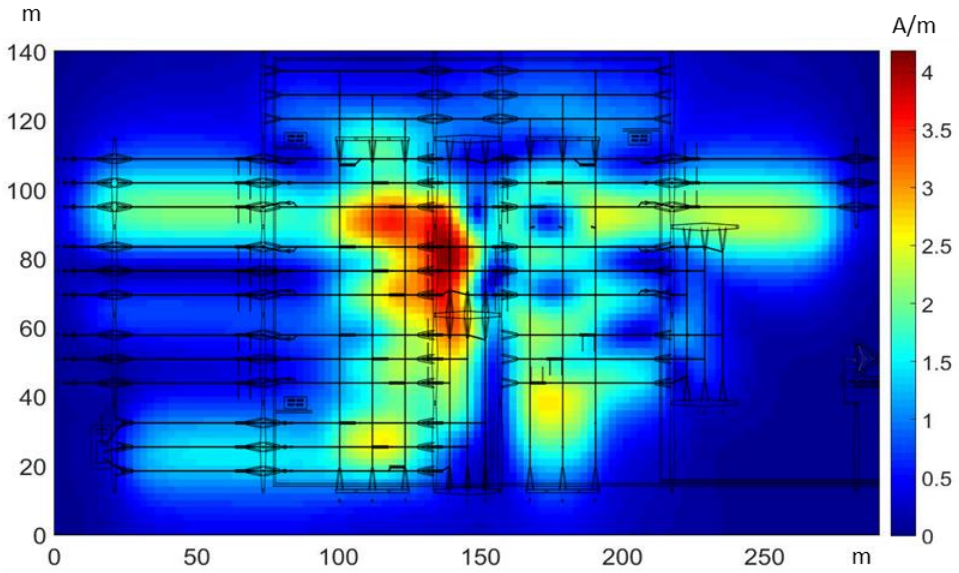

Figure 4.5 Calculated Magnetic Field at the Rosiori substation at 1.7m above the ground

Based on the calculation result, the magnetic field is below the limits recommended by ICNIRP and WHO for both public and occupational exposure limits[96] as tabulated in Table 4-1. Thus, to make a clear comparison, the percentage difference of the magnetic field was calculated as in equation 39 below. It shows that during normal operation of the substation, the magnetic field was -94.79% below public exposure limit and -98.95% below the occupational exposure limit. Based on this information, the substation environment is safe during the normal operational condition.

$$Percentage\ difference = \frac{New\ value - Old\ value}{|Old\ value|} \times 100\% \tag{39}$$

Table 4-1 Comparison calculated magnetic field with ICNIRP limits

	Magnetic field strength (A/m)	***Calculated magnetic field (A/m)***	***Percentage difference %***	***Status***
Public exposure	80	4.164	-94.79%	Within limits
Occupational exposure	400		-98.95%	Within limits

4.3.2 Validation Using Published Experimental Measurement Data

The published data from the experimental measurement was used to validate the previously calculated result. A colour contoured maps give the result for experimental measurement of the magnetic field, and 2D plots are built along measurement lines, as shown in Figure 4-4. The result then compares with the human exposure limits and the professional exposure limits for safety analysis. The experimental result shows that the highest magnetic field value measured in the experiment below the human exposure limits with 4A/m. The area that indicates the highest magnetic field generated is located at shunt reactor and the Mukacevo power line [104]

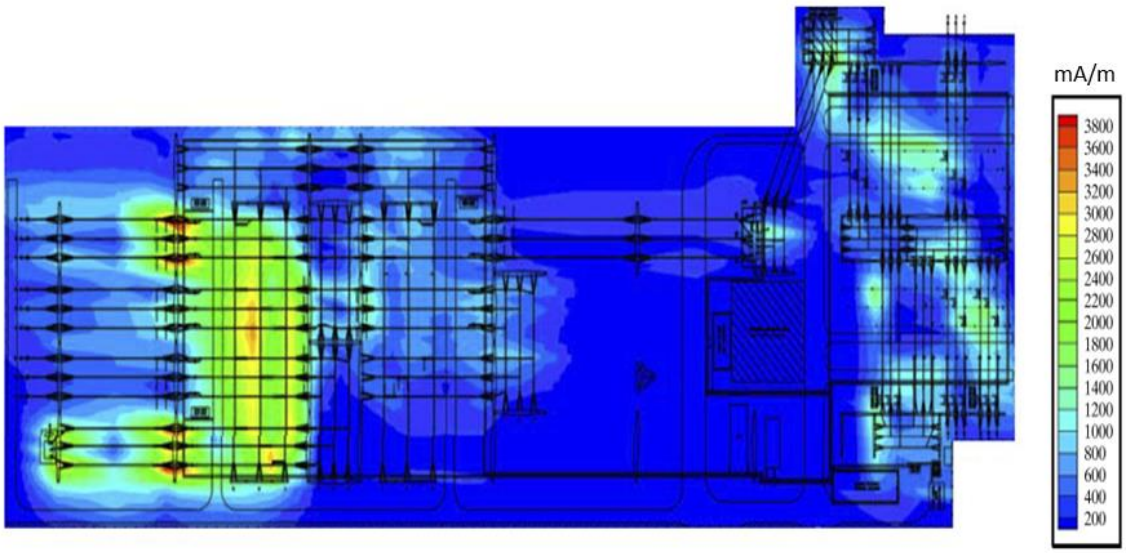

Figure 4.6 Measured magnetic field in the 400/220 kV Rosiori substation [104]

The measurements were performed under normal working conditions and by monitoring the current flow in all bays. The highest magnetic field measured was 4A/m; thus, the prediction is within 3.5% percentage difference of the estimated maximum as shown in Table 4-2, and both values are within the public exposure limits. The excellent agreement between the modelling and experiment increases confidence in the results and provides some justification for the assumptions made. This approach enables the prediction of magnetic field profiles within the substation

environment and eliminates the needs for extensive installation of expensive measuring equipment [19].

Table 4-2 Comparison of the calculated and experimental measured magnetic field

Calculated magnetic field (A/m)	*Measured magnetic field (A/m)*	*Percentage difference %*
4.164	4	3.5

4.3.3 Single Lightning Strike as Input Current

During lightning pulse injected directly to the substation, it shows that the magnitude of the magnetic field predicted increased. This is due to the high magnitude of the lightning pulse flowing within a short time. By knowing the electromagnetic field generated by operating substation or with disturbances, it is now possible to predict the magnetic flux on any equipment installed due to the magnetic source. This simple and low-cost procedure would prevent the extended stay of workers in these environments, thus, mitigating the cumulative effects of exposure to the field on them. The three-phase currents flowing in each load with the lightning pulse were used as the input to predict the magnetic field distributions, as shown in Figure 4-3. The charge conservation is enforced within the model. The total currents flowing in and out of the substation need to ensure sum up to zero. The magnetic field distribution in the substation due to the lightning pulse can be considered in two different ways, in the time domain and the frequency domain. Both approaches have been applied and compared.

4.3.3.1 Magnetic Field Calculation: The Time Domain Approach

The current flow with a lightning pulse added varies in time as illustrated in Figure 4-1, thus the magnetic field changes with time too. Since the lightning current is changing fast, the current element needs to be small enough to capture this fast-transient situation; however, it has been found that a 1m long element is sufficient to yield excellent precision of the result. The time step used for this simulation was 1μs, and the total time of the simulation 0.0003s. The highest magnetic field is plotted in Figure 4-7 and is obtained at the time of 24μs. The field is plotted at 1.7m from the ground, and the maximum magnitude of the calculated magnetic field is 1282A/m.

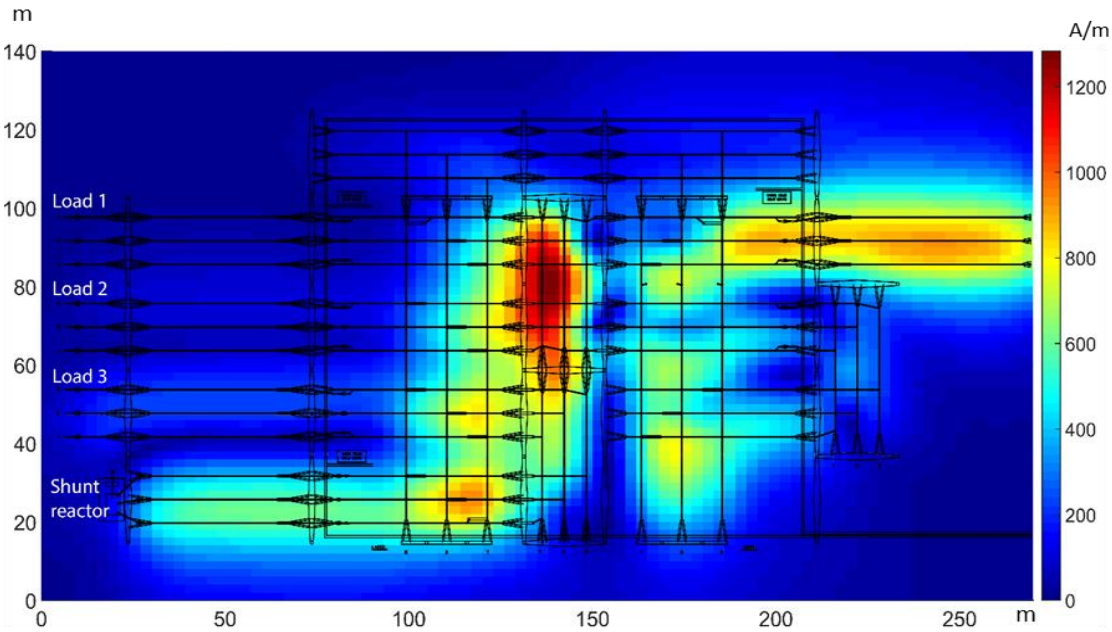

Figure 4.7 Distribution of the magnetic field due to a lightning strike in the time domain

Substation environment is not a safe place to be during lightning event occur. The field may be harmful to the equipment in the proximity of the hot spots. The magnetic field calculated shows that the maximum magnetic field value exceeds the public limit with 93.75% above the limit and the occupational exposure limit with 68.79% above the set limit by ICNIRP [96] as shown in Table 4-3.

Table 4-3 Comparison of the calculated magnetic field during lightning with ICNRIP limits

	ICNRIP Limits Magnetic Field (A/m)	***Calculated Magnetic Field (Lightning) (A/m)***	***Percentage difference %***	***Status***
Public exposure	80	1282	93.75	Exceed limit
Occupational exposure	400		68.79	Exceed limit

With the ability to predict magnetic field distribution during the lightning event provide a better understanding of the substation condition with or without the disturbances occur. The calculated magnetic field could be used for further electromagnetic compatibility analysis and immunity test [118] for equipment that will be installed in the substation in the next chapter. The magnetic field will be predicted at the chosen focus area with smaller mesh grid to get better resolution of distributed fields[19]. This information will allow further study on define ascertain optimal equipment placement so that the effect of the magnetic field is minimised[11].

4.3.3.2 Magnetic Field Calculation: The Frequency Domain Approach

Based on the FFT analysis from the previous subchapter, the magnitude and frequencies decomposed from each three-phase load currents using Prony Analysis are shown in Figure 4-4 will be used to calculate magnetic field induced in the substation. The important frequencies that were used in the magnetic field calculations are, f_1, the fundamental frequency at 50Hz, f_2 at 70kHz, f_3 at 100kHz, f_4 at 150kHz, f_5 at 200kHz, and lastly f_6 at 250kHz.

The model was then excited separately by each of these harmonics with their respective amplitude. The magnetic field for each frequency was then computed. Finally, the results were combined by adding all the fields, in terms of *x*, *y* and *z* components from all harmonics. A typical result is shown in Figure 4-6 and 4-7. The highest magnetic field computed using this approach is 1166A/m; this value is 9.04% smaller than the value obtained from the time-domain analysis, as shown in Table 4-4.

Table 4-4 Comparison of magnetic field calculation between time and frequency domain

	Time domain	***Frequency domain (all component)***	***Percentage difference %***
Magnetic Field (A/m)	1282	1166	9.04%

The difference in the calculated magnetic field can be attributed to the fact that there are only considering six harmonics, whereas, in the time domain, all the harmonics carrying power are accounted for. Nevertheless, the approach allows us to separate the effects of each of these harmonics. For example, in Figure 4-6, the magnetic field intensity plot without the 70kHz harmonic is presented: the maximum magnetic field only reaches 436.4A/m, as shown in Table 4-5. Therefore, if the 70kHz harmonics were to be filtered out, a reduction of more than half could be achieved. An appropriate filter may be sufficient to apply for protection of sensitive electronic equipment in the substation environment.

Table 4-5 Magnetic field calculation in frequency with all component and without 70kHz

	Magnetic field strength (A/m)	***Percentage difference %***
Frequency domain (all component)	1166	62.57%
Frequency domain (without 70kHz)	436.4	

Both analyses, the time domain and frequency domain predict the hot spot in the same location, which gives confidence in the proposed methodology and the computational tool. The hot spot for the Rosiori substation, studied here, is close to the connection towards the autotransformer. As demonstrated, this relatively simple approach allows the calculation of the magnetic field within the substation and could be used by the utility companies to predict the field distribution following any disturbance and thus assist in the planning for the future substation refurbish or upgrade.

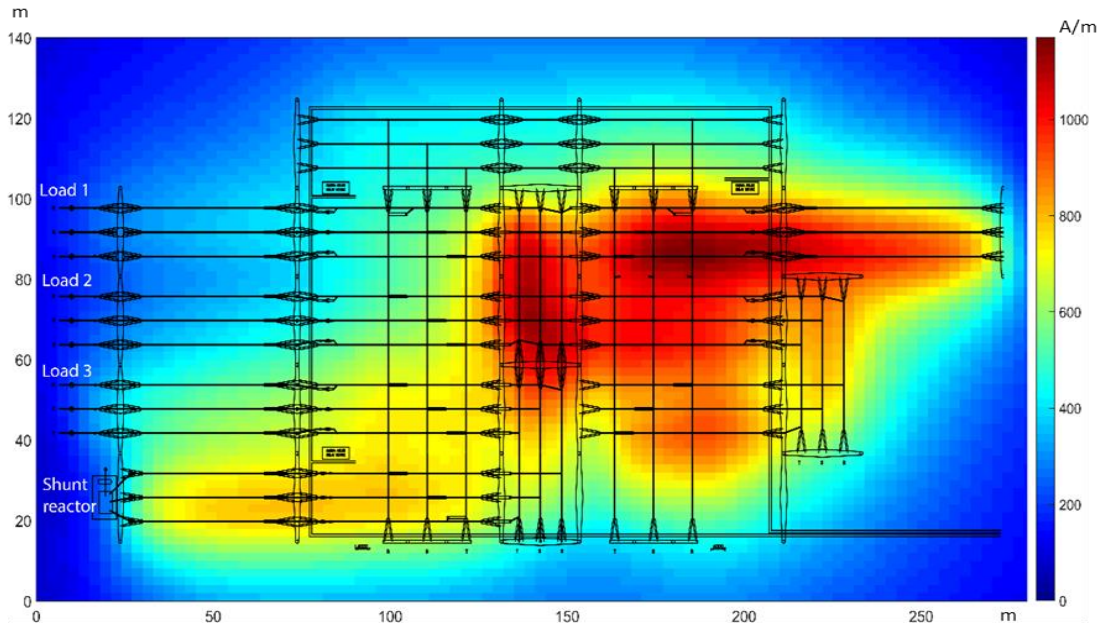

Figure 4.8 Magnetic field distribution due to a lightning strike (all frequency component)

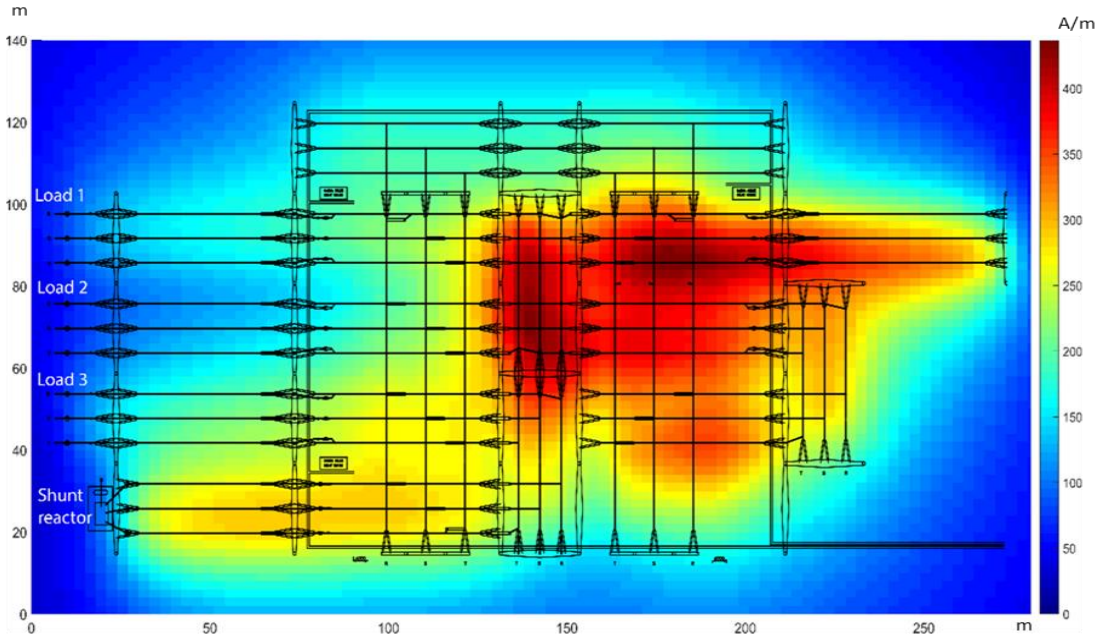

Figure 4.9 Magnetic field distribution in the frequency domain without a 70kHz harmonic

4.3.4 Summary of Part 2 Findings

In this chapter, a simple computational approach has been proposed for predicting magnetic field distribution within the substation environment. The magnetic field was calculated using Biot Savart Law (BSL) to define the field generated by current flowing through a conducting wire. To make the modelling to be an efficient tool, a few simplifications to be made, it is decided to focus on the primary sources of the magnetic field and thus neglect the less critical influences. The alternated current nature of the current flow is treated as having DC characteristics. For each time frame, the magnetic field intensity, H was calculated for the whole substation area to obtain an overall view of the worst-case scenario.

The magnetic field calculated for two different input, which is during normal operating current and with lightning injected into the system. For the normal operation conditions, the maximum values of the calculated magnetic field were 4.164A/m, and it is below public exposure limits. Based on this result, the substation environment is safe during the normal operational condition. To ensure that the magnetic field was predicted correctly, the result was validated with the published experimental measurement data from the same substation. The excellent agreement between the modelling and experiment with 3.5% difference, thus, it instantly increases confidence in the results and provides some justification for the assumptions made.

The magnetic field was then calculated for the cases when a lightning pulse was injected to the substation as a disturbance using the same algorithm. Since there is a high-frequency component in lightning pulse, FFT analysis was done, and the model able to calculate the magnetic field using two different approaches, in the time domain and the frequency domain. Both methods yield very close results and predict that the maximum magnetic field value exceeds the public limit with 93.75% above the limits and 68.79% above the occupational exposure limit set by ICNIRP. For a lightning strike in the substation, a smaller time step in the current load flow analysis is required to predict the peak current magnitude and to capture the fast transient so that the magnetic field could be calculated accurately.

Using the frequency domain approach facilitates the understanding of how each important frequency harmonic influences the field distribution within the substation, and this can be used to design more efficient EMI protection for sensitive electronic and digital equipment. The method has been verified through direct comparison with test results conducted at a particular substation during working conditions, and good agreement is observed with 9.04% difference. By knowing the electromagnetic field generated by operating substation or with disturbances, it is now possible to predict the magnetic flux on any equipment installed due to the magnetic source. This simple and low-cost procedure would prevent the extended stay of workers in these environments, thus, mitigating the cumulative effects of exposure to the field on them.

4.4 Part 3: Magnetic Field Calculation Using the Finite Difference Method (FDM)

After identifying the magnetic field distribution for the whole substation area in a large mesh grid using BSL, specific areas of interest are then studied in more detail using FDM to produce the magnetic field distribution in a finer mesh grid. Since the input is in three-phase current and keeps changing through time as plotted in Figure 4-1, assumption needs to be made to simplify the numerical calculation. Three value of current at different time frame used to calculate steady-state magnetic field distribution within the substation environment. The calculation result was plotted in figure 4-10 until 4-12. The result shows that the calculated magnetic field distributed is changing at a different time due to the magnitude of current flow in the substation system.

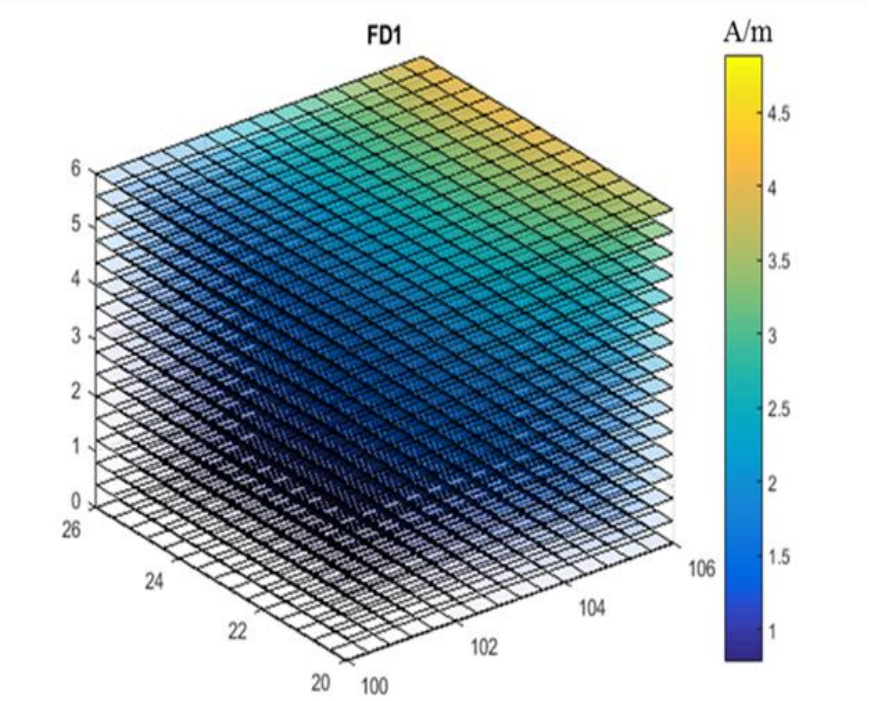

Figure 4.10 Calculated magnetic field distribution at focus area using FDM at t=1

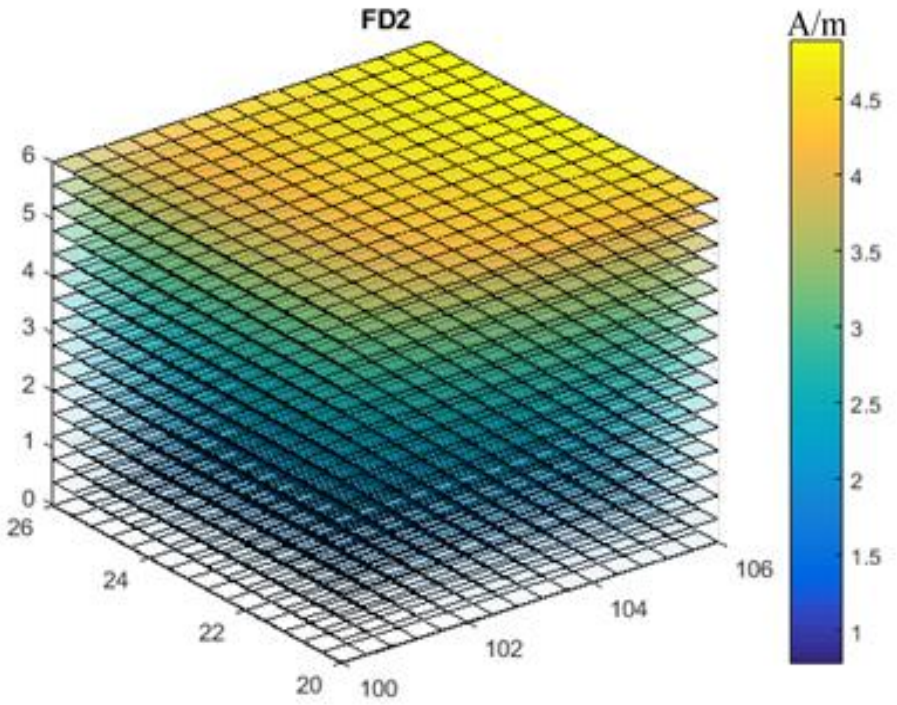

Figure 4.11 Calculated magnetic field distribution at focus area using FDM at t=2

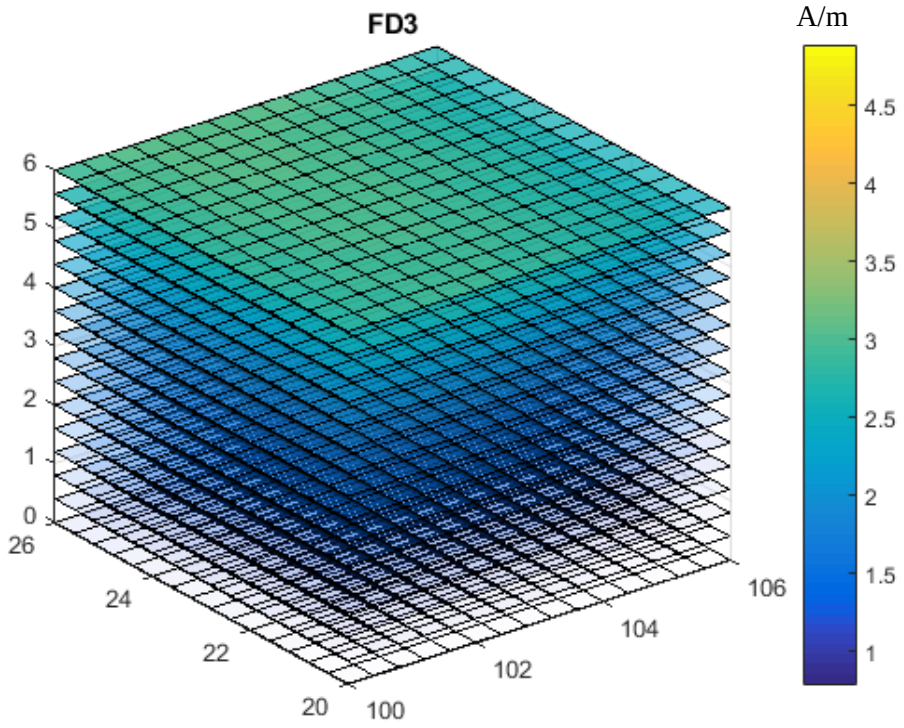

Figure 4.12 Calculated magnetic field distribution at focus area using FDM at t=3

Based on all three figure, the highest magnetic field was calculated to be nearly 5A/m which is below ICNIPR exposure guideline for public and occupational, as shown in Table 4-6 [96]. The result also shows that the substation environment is safe for humans during normal operation condition.

Table 4-6 Comparison of the calculated magnetic field using FDM with ICNRIP limits

ICNRIP Limits	***Magnetic field strength (A/m)***	***Calculated magnetic field -FDM (A/m)***	***Status***
Public exposure	80	5	Within limit
Occupational exposure	400		Within limit

The calculated magnetic field in this focus area will be used in the next chapter for EMC study on equipment that will be installed in the substation environment.

4.4.1 Comparison Between FDM and BSL Calculation Method

After calculating the magnetic field using FDM as described earlier, the same initial value was used to estimate distribution magnetic field using BSL. The BSL algorithm was validated by comparing the result of the calculated magnetic field with the published experimental measurement data, and it shows a good agreement between the modelling and experiment [116]. It is convinced that the BSL algorithm can predict the magnetic field close enough to real measurement value. Thus, to make sure FDM are producing the proper magnetic field value, the same parameter was used to calculate the magnetic field using BSL so that both calculation methods, BSL and FDM validate each other.

The result from the calculation using FDM and BSL were plotted at three different time and line up side to side as shown in Figure 4-13 until Figure 4-15, and the maximum magnetic field calculated both 5A/m. From this figure, it shows that the computed value of **H** for both methods are almost the same, and it is difficult to do the comparative analyses. The percentage differences for every point between FDM and BSL are calculated and plotted, as shown in Figure 4-16. Then the algorithm calculates the magnetic field start from initial value towards the inside for the whole area with the resolution of 0.02m for every axis (x,y,z). From the figure, it shows that the initial magnetic field value, which starts from outer points of the focus area is the same for both calculation method with 0% difference. The differences between both calculation methods are getting more significant as it calculates far apart from the initial value. It shows that the centre of the focus area has the highest with 1.01% percentage difference.

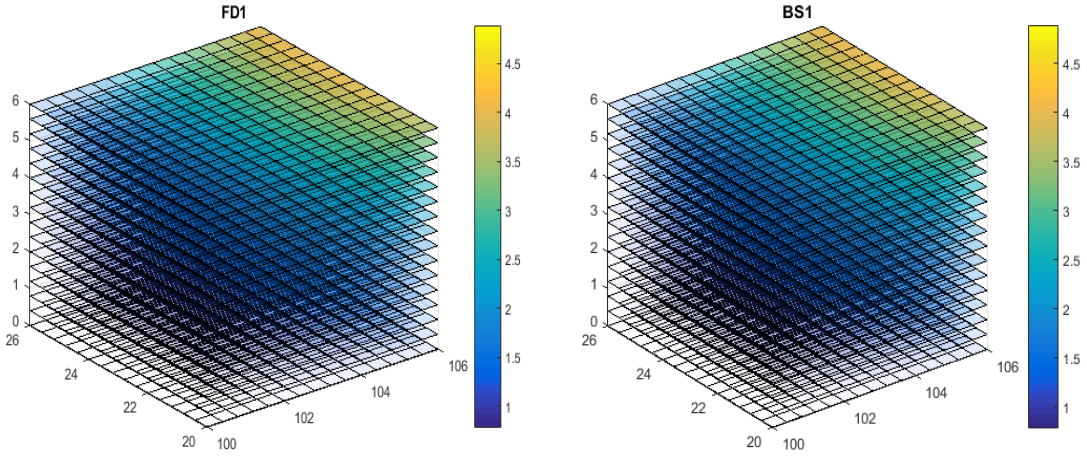

Figure 4.13 FDM vs BSL at t=1

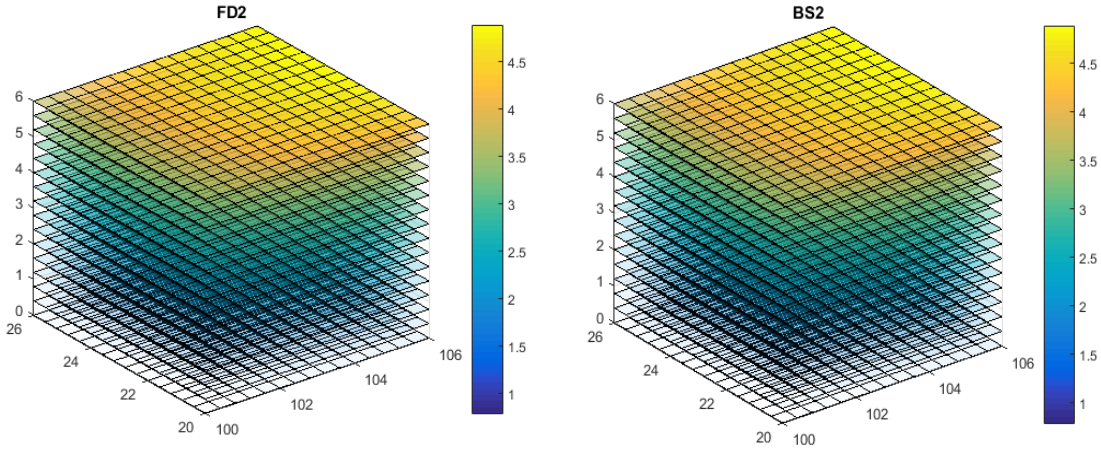

Figure 4.14 FDM vs BSL at t=2

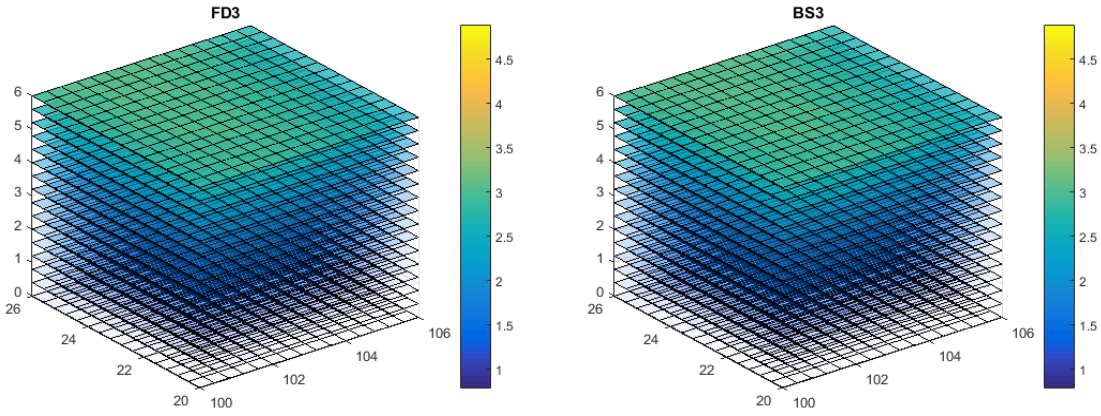

Figure 4.15 FDM vs BSL at t=3

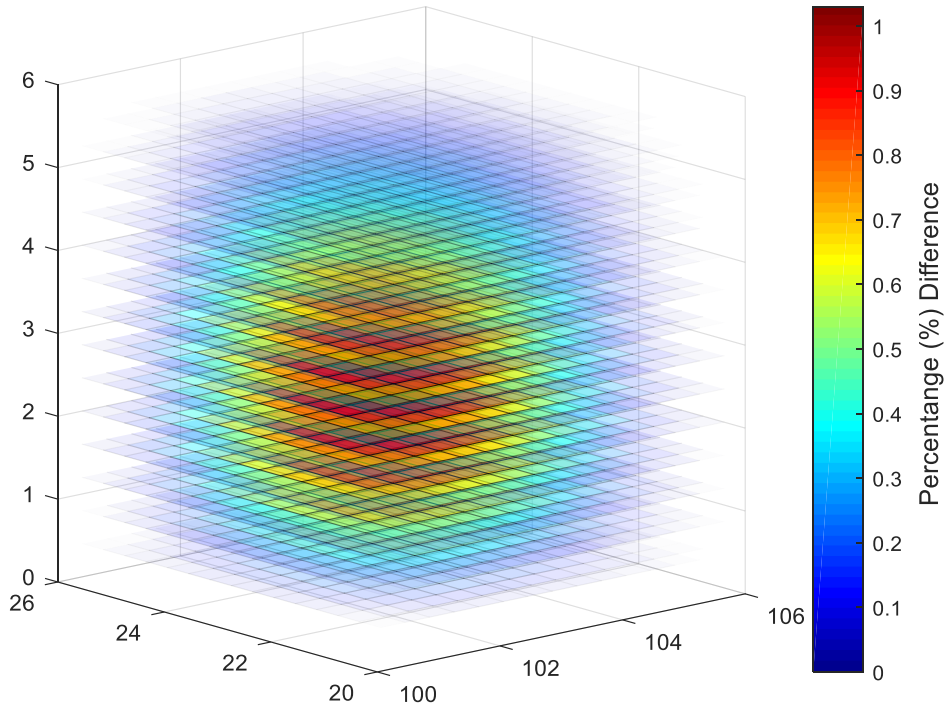

Figure 4.16 Percentage in different between FDM and BSL

A cross-section of Figure 4-16 plotted in Figure 4-17 and Figure 4-18 to get a better view of the percentage difference between both numerical calculation methods. The figures show that the cross-section calculated magnetic field at 2.8m, which is in the middle of the focus area. Both figures show that the maximum value of percentage difference error is 1.012% located in the middle of the calculated area. The differences for both calculation methods gradually increase as it calculates the magnetic field towards the centre of the area. Thus, with the low percentage of difference, it is confident that both numerical method able to predict magnetic field distributed in the environment correctly

The main advantages of applying FDM for the magnetic field calculation is on the algorithm effectiveness were FDM takes less time to compute the result, whereas the BSL calculation takes more time. For this particular case (with the smaller resolution), calculation using FDM takes only six hours whereby the BSL need twelve hours to compute the same setting. This is because BSL compute the magnetic field directly from the source of current to the points of interest. The distance of the observation point to the conductor is changing need to be calculated first, and it is changing proportionally the calculated magnetic field induced by the current. The calculation time could be reduced by setting the point of interest to be in a larger mesh. Thus, BSL is suitable for predicting an overall picture of magnetic field distribution in the whole substation area with larger mesh grid. Specific areas of interest are then studied in more detail using FDM to produce the magnetic field distribution in a finer mesh grid. The FDM was

introduced, where the magnetic field was calculated using the previously calculated value of **H** as the initial value to get the latest magnetic field value for the whole focus area as mention in equation 29. For further analysis, other material such as a metal box that represent new equipment that will be installed for the smart grid system in the substation. This will allow a utility company to predict and determine the most suitable location to place the new equipment for the smart grid system.

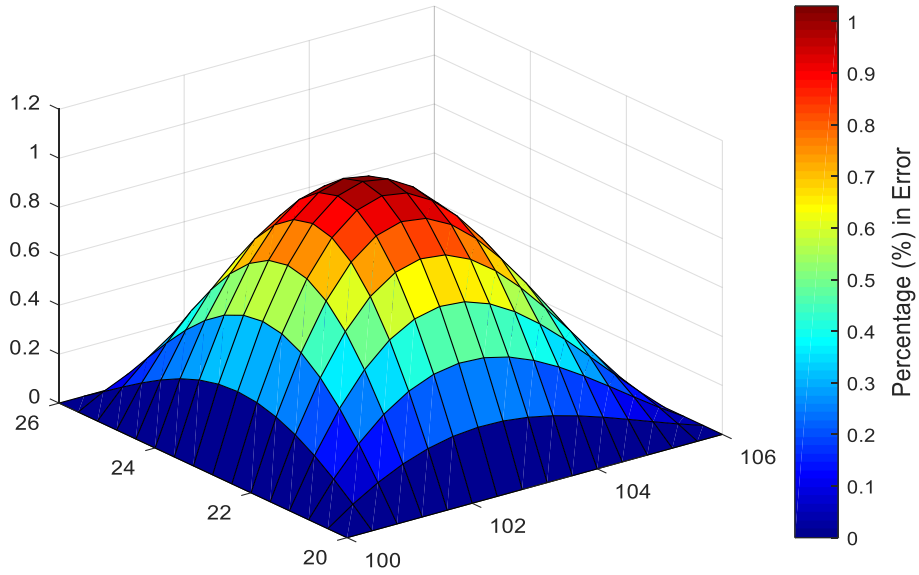

Figure 4.17 Percentage difference at the cross-section of the focus area.

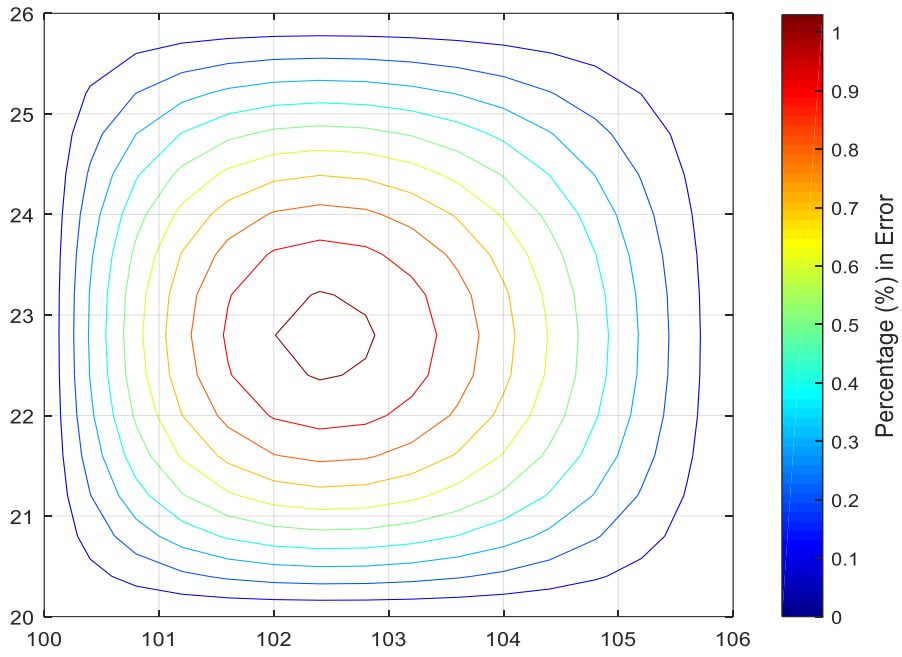

Figure 4.18 Percentage difference at 2.8m cross-section of the focus area

4.4.2 Summary of Part 3 Findings

In this part, the FDM equation has been introduced to calculate the magnetic field in the focus area within the substation environment. In early of this chapter, were first discuss the mathematical description of the FDM equation for calculating the magnetic field. The simulation model developed to predict the magnetic field in the focus area within the substation environment in three-dimension (3D). The focus area was chosen by refereeing to overall magnetic field distribution at 1.7m above the ground calculated from the previous calculation using BSL for the whole substation with more extensive mesh grid solution.

The result shows that the calculated magnetic field distributed is changing at a different time due to the magnitude of current flow in the substation system. The highest magnetic field was calculated to be nearly 5A/m which is below ICNIPR exposure guideline. The substation is a safe place to be during the normal operating condition. The same parameter set in BSL calculation was used to calculate the magnetic field using FDM so that both calculation methods can be compared together to make sure FDM are producing the proper magnetic field value. The result from the calculation using FDM and BSL were plotted at three different time and compare side to side, and the maximum magnetic field calculated both 5A/m. The percentage difference between both methods calculated for every point in the focus area. A cross-section of the area was plotted to get a better view of the percentage difference calculation result, and the maximum value of the percentage difference is 1.012%.

By using FDM in the calculation algorithm, any magnetic field reading at any point inside the box can be calculated to help predict the level of the magnetic field that enters the box. The calculated value will be able to compare with the standard immunity or electromagnetic compatibility level of the equipment and help in the planning of the new equipment installed in the substation environment in future.

For further analysis, other material such as a metal box that represent new equipment that will be installed for the smart grid system in the substation. This will allow the utility company to predict and determine the most suitable location to place the new equipment for the smart grid system. FDM used to perform a detailed analysis of the box that will be located in the substation environment to illustrate the new equipment that planned to install.

4.5 Part 4: Shielding Effect in the Substation Environment

The developed tools are used to calculate the distributed magnetic field in the substation environment by applying the Finite Difference Method (FDM) for few cases scenario. Based on the previous result, the magnetic field generated from the substation environment penetrate the box via the opening cut on the model box and the field travelled inside the box freely. The magnetic field was calculated for two different input current, which is during normal operating current and lightning strike into the substation circuit using FDM method calculation algorithm. The magnetic field was calculated inside the box for every 20mm point at each axis for different opening positions and size where makes the mesh for *x*,*y*,*z* axis to be 30x30x30. That makes the total array to be 27000 to calculate. The calculated result of the magnetic field was generated and distributed into the metal box and on the wall were plotted and discussed in detail in the next subchapter.

4.5.1 Calculated Magnetic Field Flowing Inside the Metal Box

The magnetic field was calculated using FDM calculation algorithm developed in Matlab. First, the algorithm calculates the magnetic field during normal operation of the substation by using the input current from the earlier simulation result. The magnetic field was calculated at the opening area are listed in Table 4-7 for all three cases, as mention in subchapter 3.6.1. The highest magnitude of the magnetic field was calculated at opening C, which is located on the highest of the metal box's surface with 0.46563A/m. The calculated magnetic field decreased as the locations of the opening change to location A and B. The value decreases 3% from location C to B and 6% for location C to A. It is expected that the result shows the highest magnetic field where the opening is located at the highest of the metal box surface. This is due to the source of the magnetic field are coming from the transmission line cable above the box.

Table 4-7 Maximum calculated magnetic field flowing into the opening during normal operation

Opening Location	**$\bar{H}$ Max (A/m)**		**$\bar{H}$ Min (A/m)**	
A	0.39367-0.19119i	0.43764	0.11242-0.25912i	0.28246
B	0.40619-0.19699i	0.45143	0.11243-0.25912i	0.28246
C	0.41883-0.20344i	0.46563	0.11242-0.25912i	0.28246

The magnetic field flowing from the environment towards inside of the metal box gradually reduce as the opening getting further away from the source, as plotted in Figure 4-19 until Figure 4-21. From the result, it shows that the calculated magnetic field having a higher intensity

concentrating at the opening of the box which is expected as the source of the magnetic field are entering from the opening area.

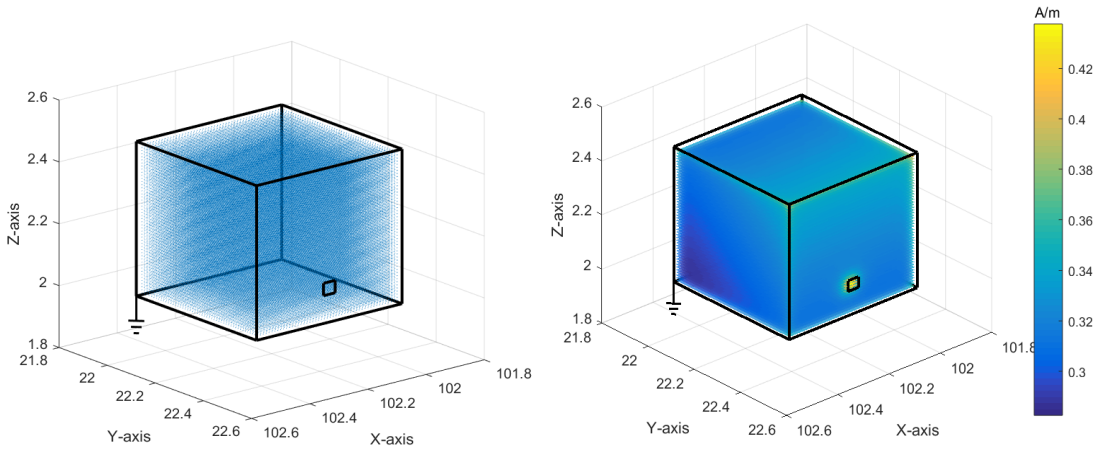

Figure 4.19 Magnetic fields inside the metal box with an opening at A (normal condition)

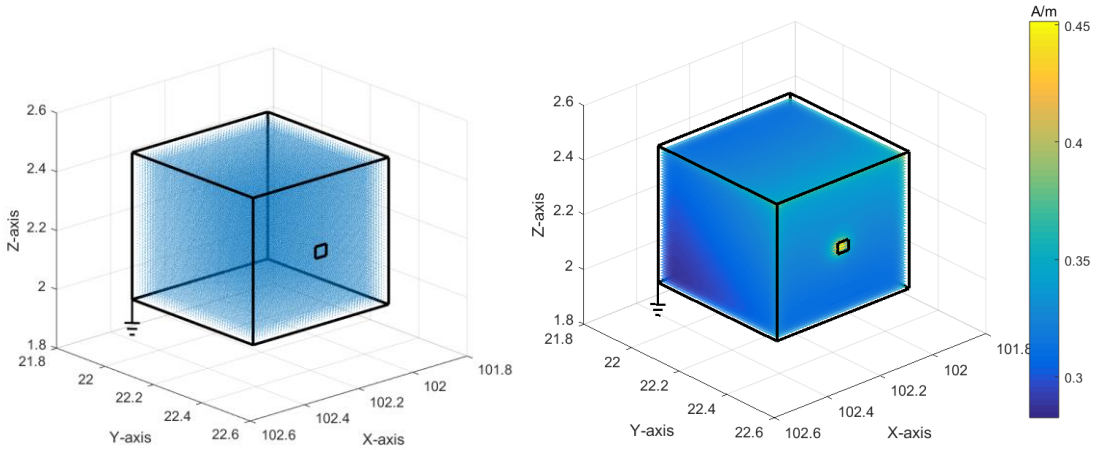

Figure 4.20 Magnetic fields inside the metal box with an opening at B (normal condition)

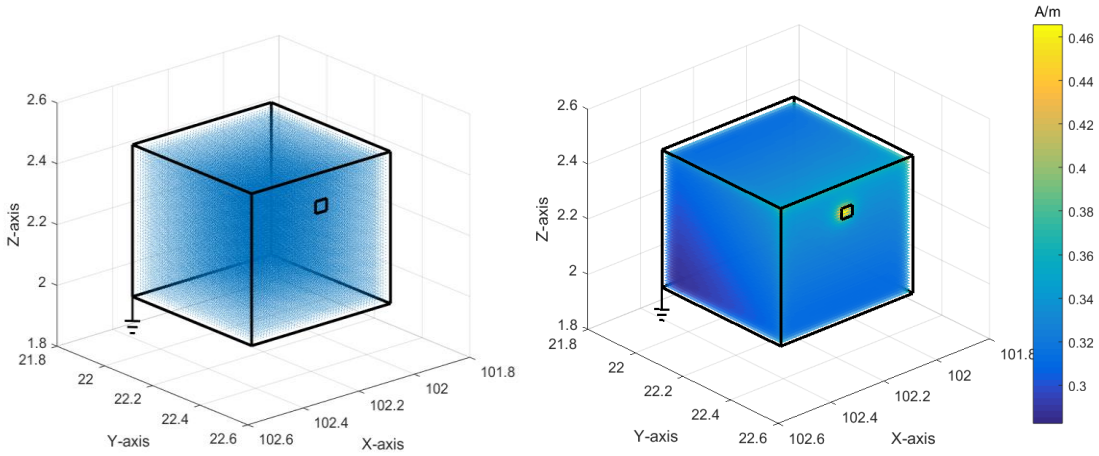

Figure 4.21 Magnetic fields in the metal box with an opening at C (normal condition)

As mention earlier, the magnetic field concentrating on the opening area, which is coming from the source of the field. It is gradually decreasing as it is getting further away from the opening. Based on this value, the predicted magnetic field was below the safety guidelines exposure limit for both public and occupational [68]. The field interference occurs might safe to human (ICNIRP standard) but, it might cause compatibility issues towards the equipment installed in the substation and the system. Thus the result was compared with the standard of the magnetic field in high voltage substation areas [97].

During the normal operation condition, it essential to satisfy the standard requirement for equipment to operate compatibly within its electromagnetic environment, as shown in Table 4-8. Based on the standard, in the equipment room of the substation environment, the maximum magnetic field value that suggested by IEC is 0.7A/m. All three calculated magnetic field compared with the standard requirement where 37.48%, 35.51%, and 33.48% below the limit required. This to ensure that all equipment installs in the equipment room compatible with each other during the working condition. If the calculated magnetic field above the limits, it shows that the magnetic field needs to be mitigated therefore, EMC between apparatus could be achieved[99].

Table 4-8 Comparison calculated magnetic field with IEC limits

	Calculated $\bar{H}$ (A/m)	**IEC61000 [97] (A/m)**	**Percentage difference %**	**Status**
A	0.43764	0.7	37.48%	Within limit
B	0.45143		35.51%	Within limit
C	0.46563		33.48%	Within limit

The magnetic field distribution inside the box calculated using the same FDM for the current flow due to lightning flowing within the substation circuit. It is evident that in the result shows that the higher field density located at the opening of the box as plotted in Figure 4-22 until Figure 4-24, where the cut opening at three various places. The results were plotted using quiver function, and it used magnitude and vector of each node to view as an arrow which indicates that the field flowing from outside and fill up the entire metal box with higher magnitude. The magnitude of field generates from the range of 910A/m at the opening area and gradually reduce to 620A/m as it distributes inside the box for all three cases during lightning current flowing in the substation environment.

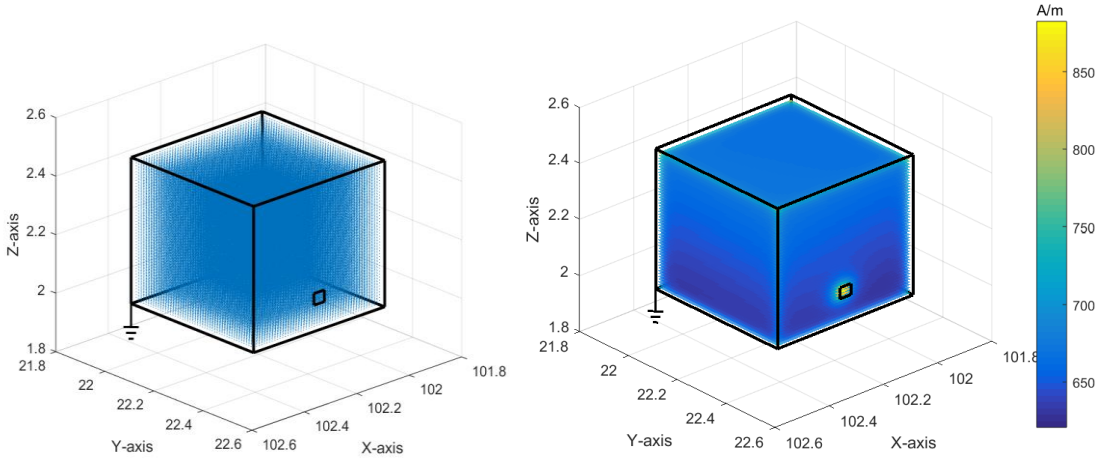

Figure 4.22 Magnetic field distributed in the metal box with an opening at A (lightning)

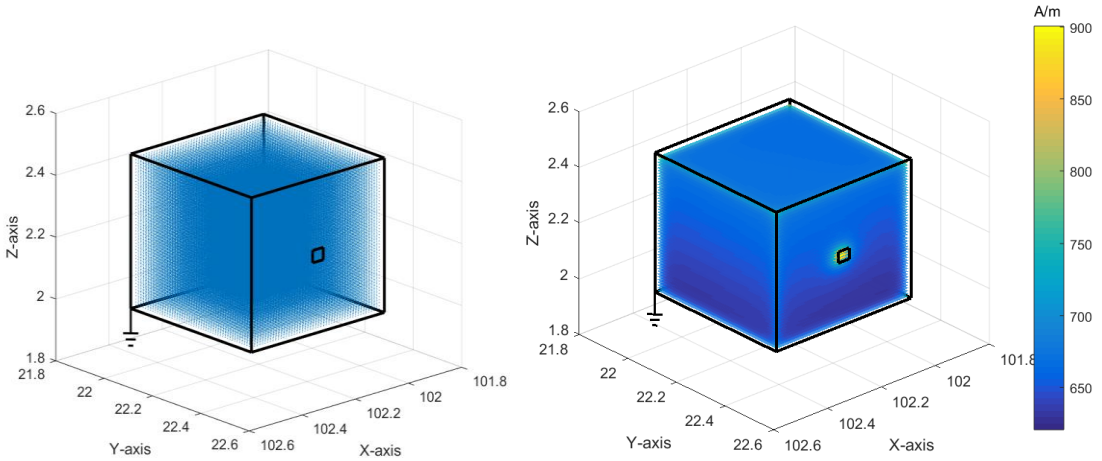

Figure 4.23 Magnetic fields distributed inside the metal box with an opening at B (lightning)

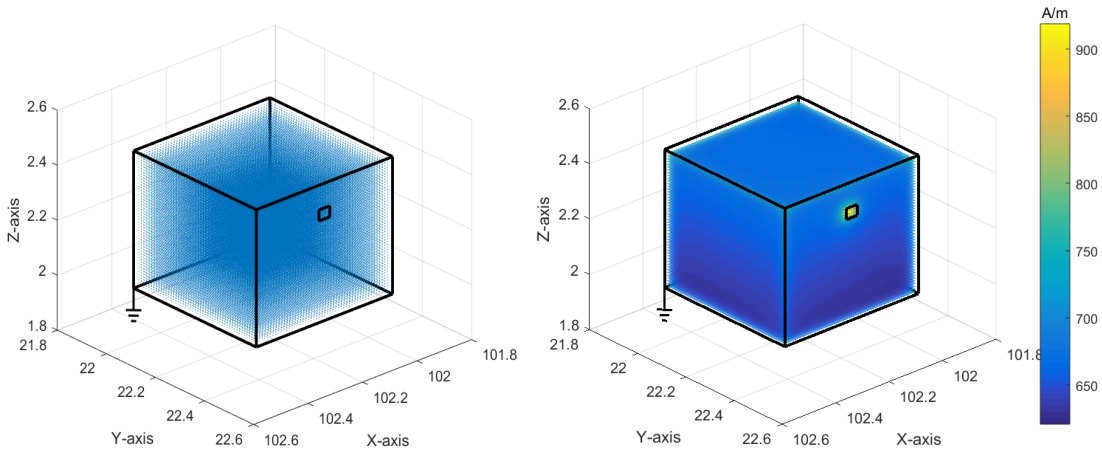

Figure 4.24 Magnetic fields distributed inside the metal box with an opening at C (lightning)

The calculated magnitude of the magnetic field is listed in Table 4-9 for all three cases of opening. Based on the table, it shows that the highest magnitude of the magnetic field is 918.793A/m at the opening located at C and gradually flow into the box. Same as the previous case, the calculated magnetic field decreased as the locations of the opening change from C to location A and B. The magnetic field value decreases 1.98% from location C to B and 3.96% for location C to A. This is due to the high lightning currents flow through the transmission line in the substation. Since the magnetic field is induced from current with a lightning strike in the substation, it is generated a much higher magnitude of fields compare with the normal operating current.

Table 4-9 Maximum calculated magnetic field flowing into the opening during a lightning event

Opening Location	**$\bar{H}$ Max (A/m)**		**$\bar{H}$ Min (A/m)**	
A	793.1027-386.8647i	882.426.	247.7069-569.0925i	620.665
B	809.6097-394.3496i	900.544	247.7077-569.0922i	620.665
C	825.7602-402.8657i	918.793	247.7258-569.0673i	620.649

The comparison of the calculated magnetic field during a lightning event with the standard limits listed in Table 4-10. Based on this calculated value, the predicted magnetic field are not fulfilling the safety guidelines exposure limit for health and safety, both public and occupational by ICNIRP [68, 96], which is recommended to be below 400A/m for occupational and 80A/m for public exposure. It also shows that during the lightning event, the substation environment is not a safe place for anyone. Nevertheless, the equipment in the substation is included at risk, where the maximum magnetic field needs to be 0.7A/m in the equipment room (IEC61000). With that calculated field, it does not fulfil the compatibility requirement by IEC61000[57, 97] within the substation environment.

Table 4-10 Comparison calculated magnetic field with IEC limits during lightning [97]

	$\bar{H}$ (Lightning) (A/m)	***Public exposure (A/m)***	***Occupational exposure (A/m)***	***IEC61000 (A/m)***	***Status***
A	882.426	80	400	0.7	Exceed limit
B	900.544				Exceed limit
C	918.793				Exceed limit

Usually, during the lightning event, the protection system in the substation should be operated instantaneously to protect the equipment and component from lightning pulse flowing in. However, the magnetic field generated by this high current might cause electromagnetic compatibility issues in the system[17]. Especially with the latest development of smart grid substation, were new power electronic equipment installed in the system [49, 123]. To ensure the system operate within the optimal compatibility level, it needs to satisfy the standard requirement by IEC61000 [57, 97]. The immunity requirement of equipment is there to assure under operating condition towards magnetic disturbances. In order to achieve optimum immunity for all apparatus while disturbances occur, is with mitigating the field disturbances by implementing proper shielded area thus, all equipment or apparatus able to operate compatibly[99].

The main important practical advantages of using FDM is the inclusion of boundary condition is inherent in the method. By using FDM allows the subdivision of region graded to give small element where it desired that the field is varying rapidly[93]. With the initial value calculated earlier, the magnetic field is able to be predicted for the smaller mesh located at the desired area. However, the difficulties of FDM is that the resulting matrix equation usually requires compact storage for the coefficient matrix, and require large computational storage. Thus this makes the calculation method increasingly sophisticated due to the expense of programming complexity[93, 124].

Applying FDM directly to evaluate the magnetic field distribution for the whole substation would require an extensive computation time. Therefore, the hybrid combination of BSL and FDM are crucial used to predict the magnetic field in such area. BSL is first used to identify the magnetic field distribution for the whole substation in a large mesh grid. With that information allows the user to choose the focused location in calculating the magnetic field values by applying FDM directly to evaluate the magnetic field distribution with much smaller resolution. The strength of using this combination is that the simulation time to predict the magnetic field distribution was reduced by 50% compared to using FDM alone. With three-dimensional simulation, it might require computer running times, but the result able to represent in both direction and magnitude of the calculated field at the desired location. The result is validated using site measurement data and compared with the recommended limit standard. For the next part, the magnetic field flowing in the air used to calculate the magnetic field that diffuses on the wall of the metal box.

4.5.2 Further Investigation of the Metal Box with Multiple Opening

Based on the predicted magnetic field in chapter 4.5.1, further investigation has been done where the magnetic field flowing inside the metal box was calculated with multiple opening that located at the bottom of the metal box surface. The openings located at the bottom of the box because based on the previous result, the lowest opening area will have the lowest magnetic field penetrate as suggested as well in the standard [99]. This is due to the location of the current source located above the metal box. The size of the opening area will be set for $16cm^2$ and $4cm^{2,}$ as illustrated previously in Figure 3.16 and Figure 3-17. The magnetic field calculated during the normal operating condition and lightning disturbances occur.

The calculated magnetic field due to normal operating condition with multiple opening areas (three) was each area is a size of was $16cm^2$ plotted in Figure 4-25. It shows that magnetic field flowing inside the box via all the opening is the highest with 0.43931A/m. Whereas the highest magnetic field travel into the smaller opening area ($4cm^2$) which is 0.40763A/m at each of the opening areas, as shown in Figure 4-26. The calculated magnetic field was decreased 5.98% by having 75% reduction of the opening areas size, which is from $16cm^2$to $4cm^2$. The calculated result is listed in Table 4-17.

Table 4-11 Magnetic field due to having different size opening at normal operating condition

Area Size	**$\bar{H}$ Max (A/m)**		**$\bar{H}$ Min (A/m)**	
$16cm^2$	0.39545-0.19136i	0.43931	0.11244-0.25913i	0.28247
$4cm^2$	0.17745-0.36698i	0.40763	0.11242-0.25912i	0.28246

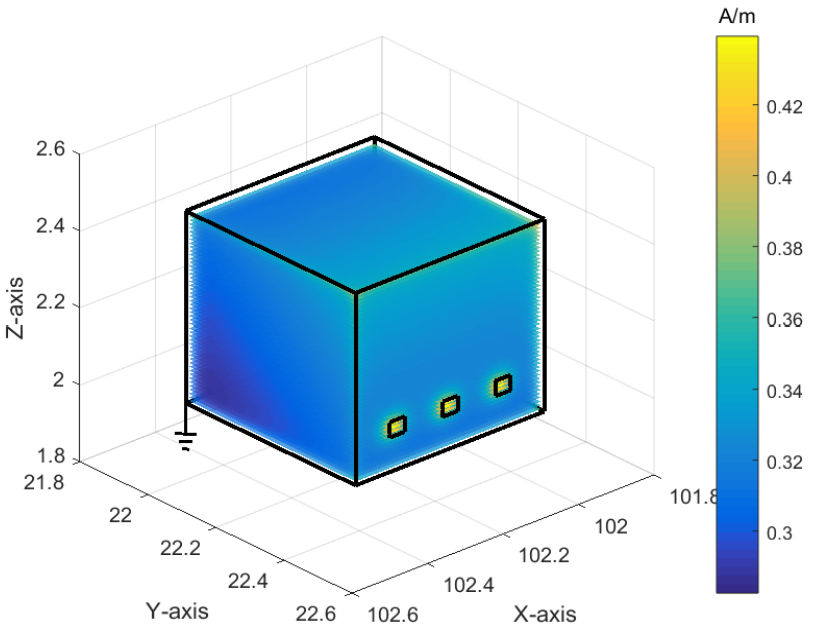

Figure 4.25 Magnetic field with multiple opening area (16cm^2) due to normal condition

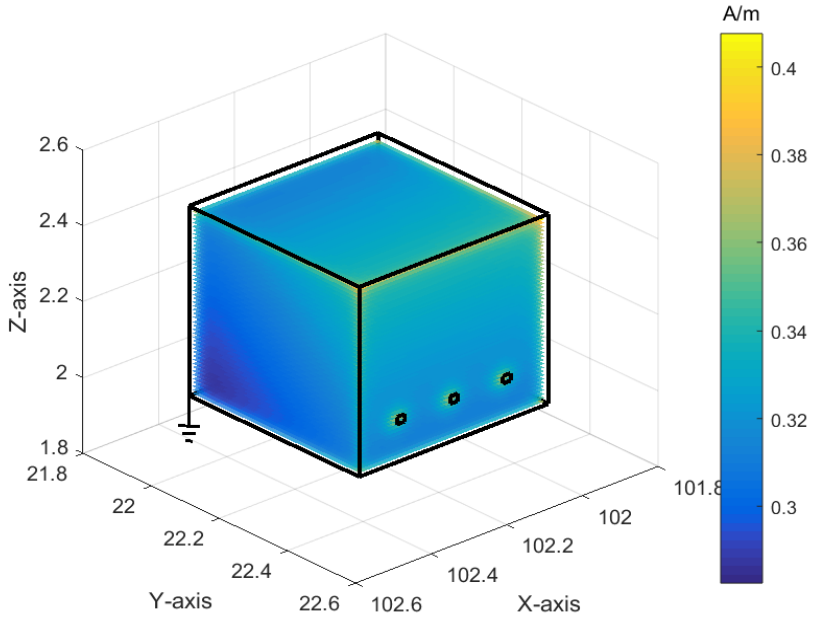

Figure 4.26 Magnetic field with multiple opening areas (4cm^2) due to normal condition

The same model used to calculate the magnetic field distribution during the lightning event for both opening size which is 16cm^2 and 4cm^2. The calculated magnetic field is shown in Figure 4-27 for the multiple opening with a larger size. The highest magnetic field is located at each of the opening areas with 886.8646A/m. The lowest magnetic field is 620.6993A/m, which obviously located inside the box. A slightly lower magnetic field was determined with the smaller opening area (4cm^2) with 799.8579A/m, as shown in Figure 4-28. The calculated magnetic field

was decreased 9.8% by having 75% reduction of the opening areas size, which is from 16cm^{2}to 4cm^2. The calculated result is listed in Table 4-18.

Table 4-12 Magnetic field due to having different size opening at during lightning

Area Size	**$\bar{H}$ Max (A/m)**		**$\bar{H}$ Min (A/m)**	
16cm^2	797.1562-388.6783i	886.8646	247.6759-569.1435i	620.6993
4cm^2	347.8746-720.2472i	799.8579	247.6963-569.0944i	620.6625

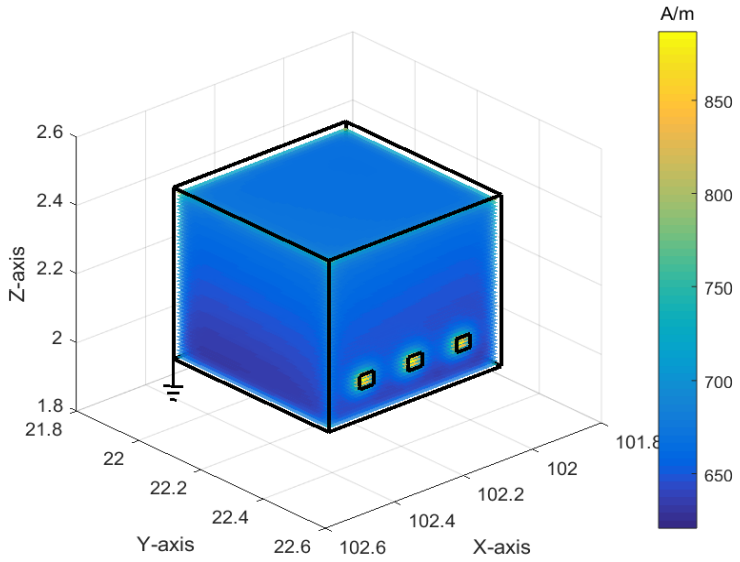

Figure 4.27 Magnetic field with multiple opening area (16cm^2) due to lightning

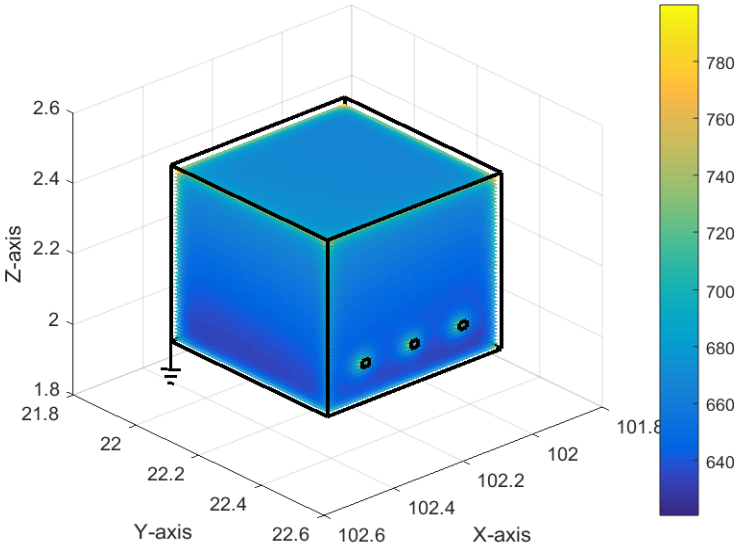

Figure 4.28 Magnetic field with multiple opening area (4cm^2) due to lightning

The amount of field entered the metal box are affected by the numbers of opening and the size of it[99]. With larger multiple opening area on the box's surface, it allows the magnetic field to penetrate easily. However, by having smaller area sizeable to limits the magnetic field entered the box, thus reduced the risk of electromagnetic compatibility issues occurs to the equipment installed in the shielded metal box. The generated magnetic field disturbances need to be mitigated to ensure the electromagnetic compatibility between equipment and the whole system are achieved especially during disturbances occur such as lightning strike[99].

4.5.3 Magnetic Field Diffuse on the Metal Box's Surface

The magnetic field diffused on the surface of the wall were calculated using the initial magnetic field flowing in the air using the same calculation method. Since the material of the metal box were set as copper, the conductivity, σ were changed to $5.8x10^7$ in equation 30. Detail list of constant parameters used in this calculation listed in Appendix A. The magnetic field calculated for both cases, normal operation and lightning disturbances occur.

During normal operation of the substation, the magnetic field was calculated. The maximum and minimum value of the magnetic field are listed in Table 4-13 for three different cases. The three cases were the different cut opening on the surface of the box. The maximum magnetic field diffused on the surface of the metal box wall is 0.42856A/m, and the lowest is 0.28044A/m was the opening located at C. Based on generic standards of immunity for power station and substation environments IEC 61000-6-5 [35], the maximum value stated in the standard where the maximum limit for the magnetic field in the equipment room is 0.7A/m. Thus, in this case, the predicted magnetic field is within the limit required during the normal operating current.

Table 4-13 Magnetic fields diffused on the metal box's surface at normal operation

Location	**$\bar{H}$ max (A/m)** 0.075472		**$\bar{H}$ min (A/m)**	
A	0.19501-0.38162i	0.42856	0.11074-0.25765i	0.28044
B	0.19501-0.38162i	0.42856	0.11074-0.25765i	0.28044
C	0.19501-0.38162i	0.42856	0.11074-0.25765i	0.28044

The calculated magnetic field on the metal box with opening apertures then plotted in Figure 4-29 until Figure 4-31 to get a better view of the field distribution on the surface of the box. The highest magnetic field located at the surface near the box opening of the box, where the source of the magnetic field flowing into the box.

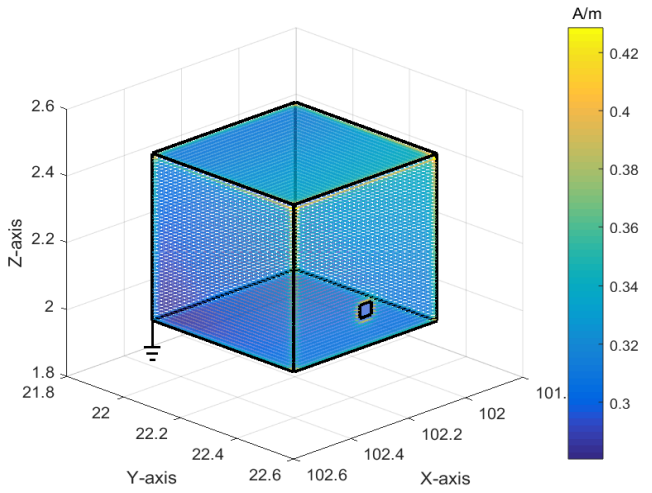

Figure 4.29 Magnetic field diffuse on the wall with opening A (normal condition)

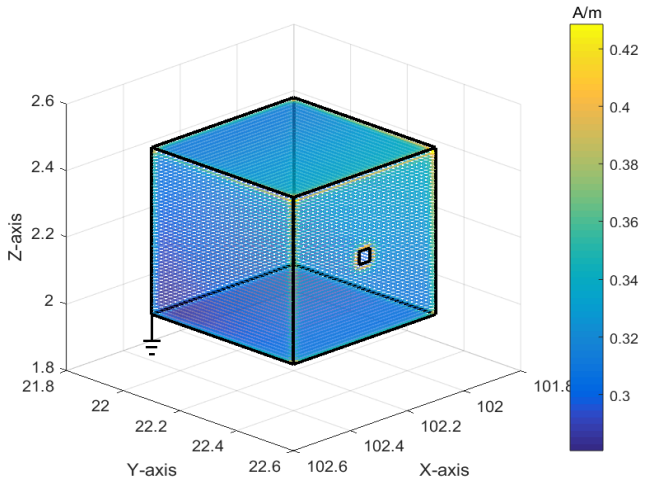

Figure 4.30 Magnetic fields diffuse on the wall with opening B (normal condition)

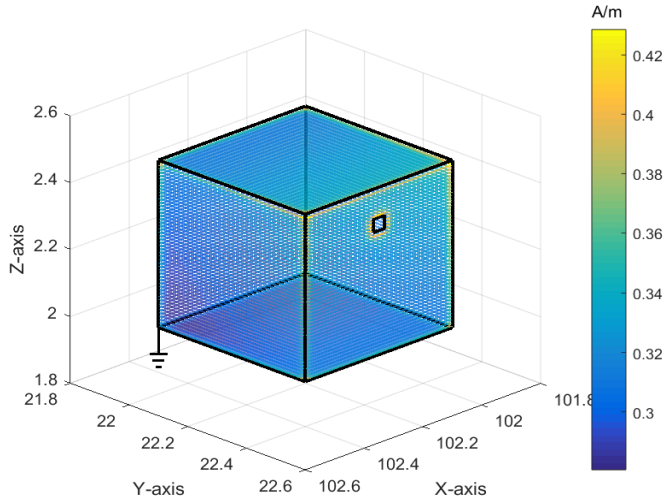

Figure 4.31 Magnetic fields diffuse on the wall with opening C (normal condition)

Next, the magnetic field diffuse on the metal box will be calculated using the input where the lightning pulse is injected into the substation circuit. This will show the performance of equipment installed in the substation during a lightning event where the equipment and component should be able to tolerate in the electromagnetic field generates in the system. The maximum and minimum calculated magnetic field are listed in Table 4-14, where the maximum magnetic field calculated is 840.271A/m and 618.247A/m at minimum value during lightning event.

Table 4-14 Maximum and minimum of the calculated magnetic field due to lightning

	$\bar{H}$ minimum (A/m)		$\bar{H}$ max (A/m)	
A	245.0452-567.6109i	618.247	382.0439-748.3972i	840.271
B	245.0454-567.6112i	618.2473	382.0438-748.3982i	840.272
C	245.0445-567.6093i	618.245	382.0435-748.4005i	840.274

The calculated magnetic field on the metal box then plotted in Figure 4-32 until Figure 4-34 to get a better view of the distribution on the surface of the box during lightning event occurs. The highest magnetic field was located at the opening of the box which the source of the magnetic field flowing into the box. The calculation result, the magnetic field generated during normal operation and lightning occur in the substation were compared with ICNIRP exposure limit for health and safety [68, 96], and standard requirement by IEC61000 [57] to ensure the system compatibility.

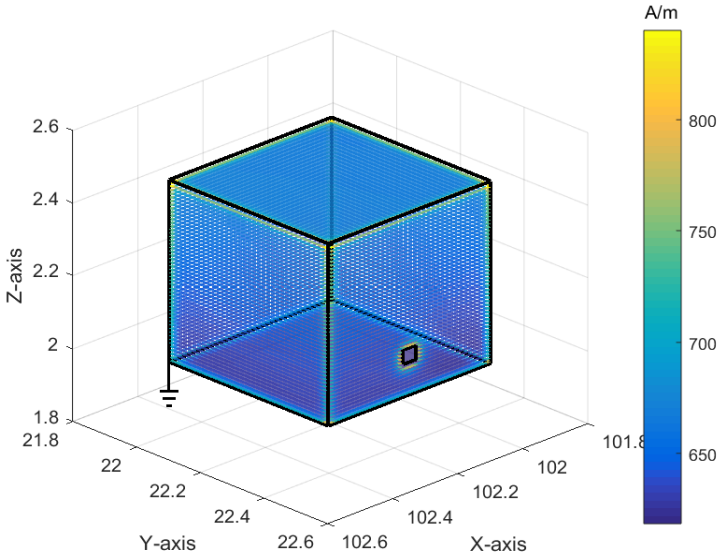

Figure 4.32 Magnetic field diffuse on the wall of a metal box with opening A (due to lightning)

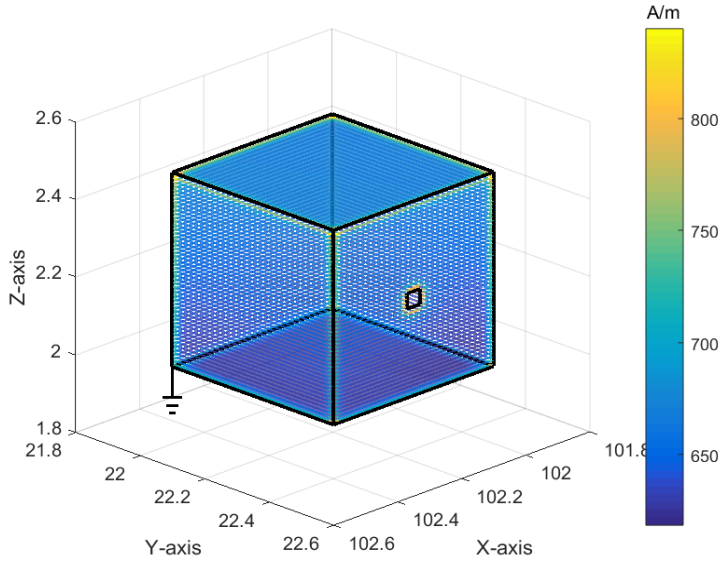

Figure 4.33 Magnetic field diffuse on the wall of a metal box with opening B (due to lightning)

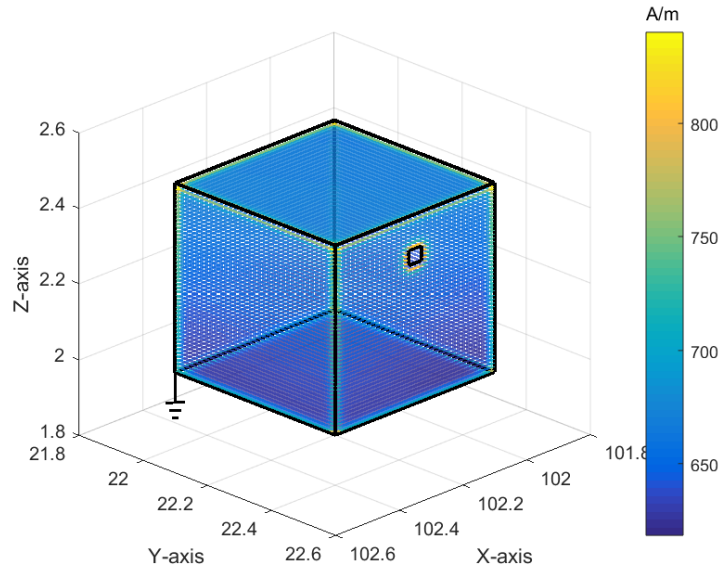

Figure 4.34 Magnetic field diffuse on the wall of a metal box with opening C (due to lightning)

Based on both calculation result, the magnetic field has a higher value with the opening located at C, where it is the nearest to the source on which is located above the box. Therefore, it is suggested for any equipment to have the cut opening for any incoming cable input or button to be at very bottom of the box since it will be further away from the primary source of the magnetic field. This will help in increasing the compatibility level of equipment installed in the substation towards the magnetic field disturbances.

The high current from lightning strike causes disturbances into the system, but normally the protection system will operate, but for the disturbances causes by generated magnetic field

will affect the compatibility of other sensitive electronic equipment or the operating system. With this information, the limitation of certain equipment's immunity level towards electromagnetic interference could be compared and thus, help the utility company to plan in designing the substation equipment installation location and attained mitigation between the source and the victim [99].

With the limitation of computational resources, all the calculation is done by using a computer with the specification of Intel (R) Core (TM) 3.4GHz processor with 16GB of RAM. The mesh chosen to be 30x30x30 makes 27000 array of data which takes 6hour to simulate. If the mesh is set to be finer, it requires longer computing hours, for example, the mesh would be set as 60x60x60 that will make 276000 arrays of data It may consume long processing time, where it is predicted to run the simulation ten times longer. Thus, the user must consider this computational limitation while running the simulation.

4.5.4 Comparison of Magnetic Field Distribution with and without Shielding

In the high voltage substation environment, there will be some electromagnetic disturbances even during normal operation, or unwanted interferences occurs. In a standard case, all the equipment should be shielded from the exposure of disturbances so that the system could operate compatibly[99]. Thus, the calculated magnetic field compared between the magnetic field distribution without and with shielding within the substation environment as in Table 4-15. The table shows that with shielding in the area, the calculated magnetic field was reduced significantly both during normal operation and during lightning event occur. During the normal operation, the magnetic field was calculated to be 5A/m and reduced 91.4% to 0.42856A/m with the shielding applied. For the lightning event, the magnetic field predicted to be 1282A/m then reduced to 840.271A/m with 34.4% reduction. Even though the result of the reduction of the calculated magnetic field with shielding apply in the substation environment, during the lightning strike the magnetic field predicted are still high, although further action could be taken to mitigate the distributed field. Thus, further analysis prediction can be made to improve the effectiveness of shielding in the substation.

Table 4-15 Comparison of the calculated magnetic field without and with the shielding effect

Condition	***Without shielding (A/m)***	***Shielding – in the box (A/m)***	***Percentage difference %***
Normal	5	0.42856	91.4%
Lightning	1282	840.271	34.4%

The effectiveness of shielding depends on many parameters. In theory, a shielded enclosure may be designed to produce attenuation frequency up to 10GHz. For practical purposes shielding effectiveness primarily determine by following factors which is the disturbance current, cable installation, length of penetrating cable, and electrical length of seams of the enclosure and the size of opening apertures should be small as possible [99].

4.5.5 Induced Current Calculation Result and Discussion

After knowing the magnetic field that travels inside and diffuses on the wall of the metal box, it is helpful to calculate the current induced by the magnetic field on the surface of that box to understand the conducted disturbances as the electromagnetic phenomena in the power substation. The conducted disturbances in the range of direct current to 150 kHz include the power frequency which coming from induction from industrial electronics, filters leakage current, fault current at the power frequency, etc [35]. With the information on the calculated induced current were compare with limitation guideline by ICNIRP [68] for public and occupation safety. For electromagnetic compatibility in the substation, the calculated induced current compare with the standard from BS EN 61000-6-5 [35] where it is for electromagnetic compatibility on immunity for power station and substation environments. This information is very useful in predicting the placement of smart equipment and component in the smart substation. For the next simulation, the magnetic field, **H** flow in the metal box and on the surface of the box were gathered from the previous chapter will be using them to calculate induced current.

The induced current was calculated from the magnetic field diffuse on the wall of the metal box during normal operating current and due to lightning disturbance flowing the substation as shown in previous subchapter 4.3.3. At first, the metal box is not grounded, thus to represent the standard engineering practice, one of the bottom corners to act as ideal grounding termination point [99, 119] by the assumption of having zero voltage potential, (v=0) and infinite current (I=∞). The magnitude of the calculated induced current is listed in Table 4-16 for all box's surfaces with both assumptions of grounded and ungrounded during normal condition.

Table 4-16 Induced current during normal condition ungrounded and grounded

SURFACE	***Induced Current, I (mA) Ungrounded***	***Induced Current, I (mA) Grounded***	***Percentage difference %***
I_ileft	0.08582	0.012888	84.9%
I_iright	0.084273	0.019228	77.2%
I_jbottom	0.033305	0.0065707	80.3%
I_jtop	0.026762	0.0037269	86.1%
I_klow	0.074655	0.00067822	99.0%
I_khigh	0.09187	0.00077409	99.1%

The result shows that the calculated induced current on the ungrounded metal box is much higher compared to grounded. The percentage difference between them is within the range of 77.2% to 99.1% induced current decreases. Induced current due to the lightning disturbances are calculated for the same model. The result in Table 4-17 shows that another significant difference for induced current that generated while lightning disturbance occurs. The highest induced current due to lightning calculated to be 119.3A without grounding whereas with grounding assumption it decreases up to 96.6% less. By making the grounding assumption on the metal box, it is allowing the current to flow out to the ground, this to ensure the safety of equipment that might be installed in the metal box from access current flow[99].

Table 4-17 Induced current during lightning occur ungrounded and grounded

SURFACE	***Induced Current, I (A) Ungrounded***	***Induced Current, I (A) Grounded***	***Percentage difference %***
I_ileft	115.1778	13.8522	87.9%
I_iright	119.3117	9.826	91.8%
I_jbottom	97.0283	8.2817	91.5%
I_jtop	103.0690	8.2535	91.9%
I_klow	96.5953	4.3121	95.5%
I_khigh	110.0375	3.6621	96.6%

The calculated induced current compared to the limits required to ensure public and occupational safety [68] as shown in Table 4-18. During the normal operating condition, the calculated induced current is within the reference level for both public and occupational exposure for grounding metal box, which is proposed to be under 100mA. Whereas during the lightning event, the current induced were calculated to be 119.3115A without grounding and reduced to 13.85A with grounding, but it is still definitely beyond the exposure limit. This excess current flowing might cause adverse health effects towards human and might as well cause disruptions to the equipment immunity.

The established guidelines for limiting EMF exposure will protect against it. Studies on both direct and indirect effects of EMF are described as direct effects result from direct interaction of fields with the body and indirect effects involve interactions with an object at a different electric potential from the body.

Table 4-18 Comparison of calculated induced current with exposure limits

Induced Current, I Ungrounded		***Induced Current, I Grounded***		***Induced Current Exposure Limits [68]***	
Normal condition (mA)	***Lightning (A)***	***Normal condition (mA)***	***Lightning (A)***	***Public exposure (mA)***	***Occupational exposure (mA)***
91.87	119.3117	19.228	13.8522	45	100

To represent the calculation result in their magnitude and direction where the direction of current depending on the direction of the calculated curl of **H** at all three axes (*x*, *y*, *z*). The result in Figure 4-35 plotted to visualises the flow of current induced on the metal box's surfaces due to the distributed magnetic field during the normal operation, and Figure 4-36 is due to lightning disturbances occur. In the figure, it shows that the direction of current flow on the surface opposes with the magnetic field that causes it, and with the opening on the surface, the current flowing by avoiding the opening and move around to other surfaces without laminations. This induced current is also known as eddy current, where it cannot be eliminated completely, but they surely can be reduced greatly.

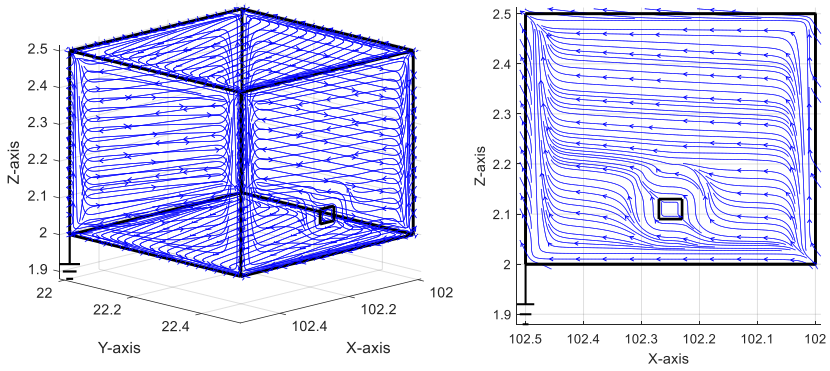

Figure 4.35 Calculated induced current with an opening at A (normal operating condition)

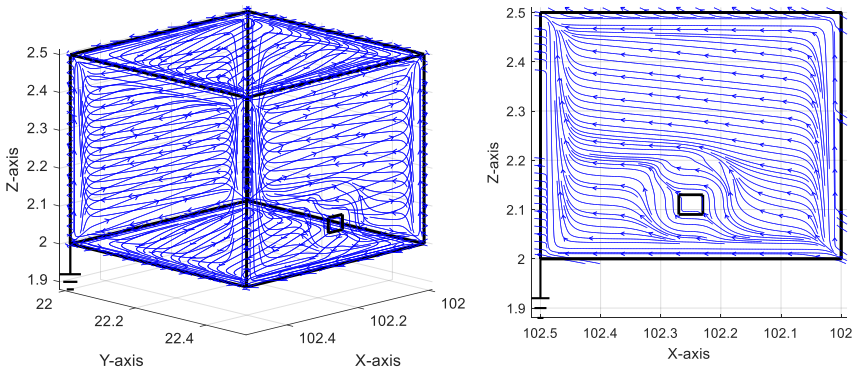

Figure 4.36 Calculated induced current with an opening at A (lightning)

Considering this magnitude of current-induced are generated by magnetic field during lightning around the substation, it is very high even though this calculation is done by assuming that the metal box grounded and ungrounded condition. The grounded metal box shows that the induced current is significantly less then ungrounded. With grounding, the results are much more resemble the application in engineering practice to make a further judgement. To reduce physical damage and failure of the electrical and electronic system in the substation equipment that connected to the smart grid, these are the protection measures could be implemented in the substation [60, 125].

By applying this numerical calculation, it allows evaluating the equipment immunity level within the simulated substation environment. The equipment or component could be planned to install based on its sensitivity level to the environment with protective zones [35]. It is essential for the equipment operates according to the specific performance while exposing to conducted or radiated electromagnetic disturbances. In some cases, special mitigation measure is needed to allow using the equipment that was not meeting the specification; thus, reduce immunity, a protective environment needs to be set up.

It is essential to consider the electromagnetic compatibility within the environment for new electronics component that will be introduced widely to the substation facilities and user facilities in developing the smart grid system [114]. Thus, the calculation of the magnetic field and the induced current on a metal box illustrate the equipment will be installed in the substation environment are used to study the electromagnetic compatibility. With all calculated value will help in determining the suitable location and the protection system required due to disturbances that occur for the equipment to function compatibly within the system.

4.5.6 Summary of Part 4 Findings

This chapter described the calculation of the magnetic field with a shielding effect which the introduction of a metal box that illustrates the new equipment that will be installed in the substation environment by using FDM calculation method. The magnetic field was predicted at the desired area with smaller resolutions for a better view of the field distribution. Using the developed algorithm tools, the size and location of this box can be adjusted to any measurement and could be set to anywhere in the substation environment to suite the user needs.

The magnetic field flowing inside the metal box and diffuse on the metal box surface were calculated with different location of the opening area on it. The calculation result is plotted in 3-D to view the field distribution inside the box and freely the box's surfaces. The magnitude of the fields that effected on the surfaces of the box is plotted using contour to provide better graphic on field distribution. The calculated magnetic field decreased as the locations of the opening change, and the result shows the highest magnetic field where the opening is located at the highest of the metal box surface. This is due to the source of the magnetic field are coming from the transmission line cable which located above the box.

The calculated magnetic field then compared between the magnetic field distribution without and with shielding within the substation environment as in Table 4-13. The table shows that with shielding in the area, the calculated magnetic field was reduced significantly both during normal operation and during lightning event occur. This will help in the study the effect of magnetic field exposure to the box and hence to determine the most suitable location for installing new equipment in the substation environment. It also used as a tool to predict the electromagnetic compatibility of equipment or component due to difference disturbances occur in the substation environment.

For the next calculation, the induced current from the distributed magnetic field on the metal box will be calculated on every surface. This summarises that the induced current generates from the calculated magnetic field. The induced current was calculated on the wall of the metal box due to the normal operating current and with lightning disturbance current input flowing in the substation. The magnitude of the calculated induced current listed in Table 4-14 and 4-15 for every metal box's surfaces. The calculated induced current compared to safety and limits for both cases where during the normal condition, the calculated induced current are within the reference level for occupational exposure. While the lightning event, the current induced were calculated to be 119.3115A at first, which is beyond the exposure limit. By making the grounding assumption on the metal box, it is allowing the current to flow out to the ground and reduced the induced current up to 96%. This to ensure the safety of equipment that might be installed in the metal box from access to current flow. The result also shows the direction of the current flow on the surface

was avoiding the opening and move around to other surfaces. From the simulation result, the information used to study the compatibility of the substation towards magnetic field disturbances. The suggestion of locating the equipment at a suitable location could be made based on the information given.

Further investigation has been done where the magnetic field flowing inside the metal box was calculated with multiple opening that located at the bottom of the metal box surface. The openings located at the bottom of the box because based on the previous result, the lowest opening area will have the lowest magnetic field penetrate. This is due to the location of the current source located above the metal box. The size of the opening area will be set for $16cm^2$ and $4cm^2$. By having smaller area sizeable to limits the magnetic field entered the box, thus reduced the risk of electromagnetic compatibility issues occurs to the equipment installed in the shielded metal box.

4.6 Summary

The findings obtained in this research have been presented and discussed in detail in this chapter and organised by the parts involves in this research.

In Part 1, determination of substation performance via Digsilent Power Factory software simulation during normal operation and with lightning strike applied. Three-phase current flow in the substation circuit was determined both using time-domain and frequency domain analysis. Differentiating between steady-state and transient features of current flow in a substation is vital to calculate the magnetic field distribution and identify areas where they are concentrated. This approach enables the prediction of magnetic field profiles within the substation environment and eliminates the needs for extensive installation of expensive measuring equipment.

Part 2 discussed the calculation result of the magnetic field using the Biot Savart Law (BSL) within the substation environment would be based on the previous result in Part1. Both the normal operating condition and with a disturbance applied in the system have been considered. The calculated magnetic field was compared with the limits and standards guidelines, additionally validated with published experimental data which is shown an excellent agreement between the modelling and experiment with 3.5% difference. Therefore, it instantly increases confidence in the results and provides some justification for the assumptions made.

Previously, BSL is first used to identify the magnetic field distribution for the whole substation in a large mesh grid. In Part 3, specific areas of interest are then studied in more detail using the Finite Difference Method (FDM) to produce the magnetic field distribution in a finer mesh grid. The result is compared with the BSL method to validate the algorithm on predicting the magnetic field. The main advantages of applying FDM for the magnetic field calculation is on the algorithm effectiveness were FDM takes less time to compute the result.

Finally, in Part 4 involved the shielding effect in the substation environment where a metal box is introduced, and the magnetic field penetrated inside the box was calculated. The calculated magnetic field then compared the magnetic field distribution without and with shielding within the substation environment. Based on the results, it can be concluded that the magnetic field predictions within the substation environment are very crucial issues, especially during the occurrence of disturbances such as a lightning strike. It is shown that the needs of equipment shielding in the harsh atmosphere like substation are very crucial for a compatible system. With these developed tools, it will help the utility company to plan in substation restoration or refurbishment. Overall, by using this combination algorithm allow the user to identify the magnetic field distribution for the whole substation in a large mesh grid by adopting BSL, then for specific areas of interest are then studied in more detail using FDM to produce the magnetic field distribution in a finer mesh grid with less extensive computation time.

CHAPTER 5

CONCLUSION AND FUTURE WORK

5.1 Conclusions

The main revolution of power system network is the implementation of new electronic equipment and penetration of renewable generation and demand have introduced new challenges to the operation of the electric grid. With these challenging conditions, the overall system's operation requires new and innovative approaches to enhance the performances of the power grid, which is the Smart Grid. To operate in such a mode, the smart grid will utilise digital information technology to create a more efficient, reliable and responsive network that is flexible. This not only the implementation of managing the system is changing, but many of the component or equipment installed in the system will also be evolving to support this new technology too. Therefore, electromagnetic compatibility (EMC) studies within smart grid substation environment must be considered to ensure continuously, reliable real-time operation between new component and equipment in the smart grid system operation.

This research aims to develop a simple but reliable simulation algorithm as a tool which will help in monitoring the electromagnetic field interferences towards new equipment within the substation environment. It has been established that disturbances occur in the operated substation could generate electric and magnetic field interference in the system. Thus, the electromagnetic field within the substation will make sure the level of interferences exposure to other equipment within the optimum level, and more importantly, exposure to the occupational and public exposure are below limit requirement. Since the substation installing more new equipment and electronic component to integrate with a smart grid system, it is becoming more relevant to monitor the electromagnetic field in the substation environment. It is easily able to help in deciding on the location for installing new equipment within the substation environment.

The substation structure used in this research which is Rosiori substation from Romania which kindly provided by our collaborators at the Technical University of Cluj, Faculty of Electrothechnics. Substation performance during steady-state and during applying the disturbances lightning in the simulation that was used to illustrate the lightning pulse injected into the substation circuit. Using the Power Factory software, the load flow in the substation was inserted by the addition of a lightning pulse injected at 0s at one of the 400kV busbars. The magnetic field distribution in the substation due to the lightning pulse can be considered in two different ways, in the time domain and the frequency domain. Both approaches have been applied and compared. The current flow of every line connected to the substation at specific time frames was used to calculate the magnetic field intensity, **H** for the whole predefined area to obtain a coarse evaluation of the worst-case scenario which is the predicting the maximum value of **H** distributed within substation environment. Thus, this approach enables the prediction of current flow during the normal condition and while disturbances occur within the substation environment, thus eliminates the needs for extensive installation of expensive measuring equipment.

A simple computational approach has been proposed for predicting magnetic field distribution within the substation environment using Biot Savart Law (BSL) generated by current flow to identify the magnetic field distribution for the whole substation in a large mesh grid. The magnetic field was calculated for two different input current flow, which is during normal operating current and with lightning injected into the system. For the normal operation conditions, the maximum values of the magnetic field were found to be below public exposure limits with 4.164A/m. The excellent agreement is shown between the modelling and experiment, with 3.5% of difference; therefore, it instantly increases confidence in the results and provides some justification for the assumptions made. The Rosiori substation is one of many substations in Romania that will be refurbished by the utility company, thus by knowing the electromagnetic field generated by operating substation or with disturbances, and now possible to predict the magnetic flux on any equipment installed due to the magnetic source. This simple and low-cost procedure would prevent the extended stay of workers in these environments, thus, mitigating the cumulative effects of exposure to the field on them.

Using the frequency domain approach facilitates the understanding of how each important frequency harmonic influences the field distribution within the substation, and this can be used to design more efficient EMI protection for sensitive electronic and digital equipment. The method has been verified through direct comparison with test results conducted at a particular substation during working conditions, and good agreement is observed with 9.04% difference. Using the frequency domain approach facilitates the understanding of how each important frequency harmonic influences the field distribution within the substation, and this can be used to design more efficient EMI protection for sensitive electronic and digital equipment. By knowing the electromagnetic field generated by operating substation or with disturbances, it is now possible

to predict the magnetic flux on any equipment installed due to the magnetic source. This simple and low-cost procedure would prevent the extended stay of workers in these environments, thus, mitigating the cumulative effects of exposure to the field on them.

Specific areas of interest are then studied in more detail using FDM to produce the magnetic field distribution in a finer mesh grid based on the previous calculation using BSL for the whole substation. The strength of using this combination is that the simulation time to predict the magnetic field distribution was reduced by 50% compared to using FDM alone. The result from the calculation using FDM and BSL were plotted at three different time and compare side to side, and the maximum magnetic field calculated both 5A/m. The percentage difference between both methods calculated for every point in the focus area for validation. A cross-section of the area was plotted to get a better view of the percentage difference calculation result, and the maximum value of the percentage difference is 1.012%. Therefore, the calculations algorithm are convinced to provide magnetic field reading at any point inside the box can be calculated to help predict the level of the magnetic field that enters the box. The calculated value will be able to compare with the standard immunity or electromagnetic compatibility level.

To illustrate the real equipment that installs in the substation environment, a novel "metal box" concept introduced to evaluate the potential EMC and shielding effects on equipment placed at specific areas. The magnetic field generated from the substation environment is expected to travel inside the equipment box. The metal box model builds with an opening aperture to illustrate any holes built in the equipment for any connecting power supply and control buttons on the equipment. The result shows the highest magnetic field where the opening is located at the highest of the metal box surface with 3% - 6% magnetic field decreases while changing the location of the opening. This is due to the source of the magnetic field are coming from the transmission line cable above the box. All three calculated magnetic field compared with the standard requirement where 37.48%, 35.51%, and 33.48% below the limit required. The magnetic field was concentrating on the opening area, which is where the source of the field comes from. It is gradually decreasing as it is getting further away from the opening. Therefore, it is suggested for any equipment to have the cut opening for any incoming cable input or button to be at very bottom of the box since it will be further away from the primary source of the magnetic field.

The amount of field entered the metal box are also affected by the numbers of opening and the size of it. The calculated magnetic field was decreased 5.98% by having 75% reduction of the opening areas size, which is from $16cm^2$to $4cm^2$. With larger and multiple opening area on the box's surface it allows the magnetic field to penetrate easily, however, by having smaller area sizeable to limits the magnetic field entered the box, thus reduced the risk of electromagnetic compatibility issues occur to the equipment installed in the shielded metal box. The generated magnetic field disturbances need to be mitigated to ensure the electromagnetic compatibility

between equipment and the whole system is achieved, especially during disturbances occur such as a lightning strike.

In a standard case, all the equipment should be shielded from the exposure of disturbances so that the system could operate compatibly, and thus during the normal operation, the magnetic field was calculated to be 5A/m and reduced 91.4% to 0.42856A/m with the shielding applied. For the lightning event, the magnetic field predicted to be 1282A/m then reduced to 840.271A/m with 34.4% reduction. Even though the result of the reduction of the calculated magnetic field with shielding apply in the substation environment, during the lightning strike the magnetic field predicted are still high but further action could be taken to mitigate the distributed field. Thus, further analysis prediction can be made to improve the effectiveness of shielding in the substation.

After knowing the magnetic field that travels inside the box and diffuses on the wall of the metal box, it is helpful to calculate the current induced by the magnetic field on the surface of that box to understand the conducted disturbances as the electromagnetic phenomena in the power station and substation. To represent the standard engineering practice, one of the bottom corners to act as ideal grounding termination point [99, 119] by the assumption of having zero voltage potential. It is shown that the calculated induced current on the ungrounded metal box is much higher compared to the grounded. The percentage difference between them is within the range of 77.2% to 99.1% induced current decreases. Induced current due to the lightning disturbances are calculated for the same model. The result shows that another significant difference for induced current that generated while lightning disturbance occurs with the highest induced current due to lightning calculated to be 119.3A without grounding whereas with grounding assumption it decreases up to 96.6% less. During the normal operating condition, the calculated induced current is within the reference level for both public and occupational exposure for grounding metal box, which is proposed to be under 100mA. Whereas during the lightning event, the current induced were calculated to be 119.3115A without grounding and reduced to 13.85A with grounding, but it is still definitely beyond the exposure limit. This excess current flowing might cause adverse health effects towards human and might as well cause disruptions to the equipment immunity.

Overall, the research presented in this thesis has succeeded in making a contribution to understanding the importance of the electromagnetic compatibility within the environment for new electronics component that will be introduced widely to the substation facilities and user facilities in developing the smart grid system. By applying this numerical calculation, it allows evaluating the equipment immunity level within the simulated substation environment. The equipment or component could be planned to install based on its sensitivity level to the environment with protective zones. It is essential that the equipment operates according to the specific performance while exposing to conducted or radiated electromagnetic disturbances. In some cases, special mitigation measure is needed to allow using the equipment that is not meeting

the specification, thus, reduce immunity, a protective environment needs to be set up. Finally, with predicted magnetic field distribution within the substation environment, the suggestion on locating the equipment based on the result was made together with the protection measures that could apply to enhance the safety of the equipment in the substation environment.

5.2 Future Work Recommendations

The Smart Grid system will keep moving forward towards implementing more intelligent equipment and component and used the intelligent system soon. Further development and improvement of the established calculation method of the magnetic field within the substation model will take place. At this stage, the developed simulation coding in MATLAB has its limitation. All conductors in the substation have to be entered in the model one at a time, which is not user-friendly and time-consuming. This simulation coding can be improved by normalising the standard substation structure so that it can be easily used for calculation.

Since the power flow simulation of the substation used to generate input in magnetic field calculation done separately, it would be great features if both power system simulation and Matlab could be connected by designing the graphical user interface (GUI). With GUI, all the parameter such as the focus area, size of equipment, resolution of the simulation and input file could be easily key into the coding. The result will be set to be plotted in various ways to get a better view of the field distribution by the user and the result of the simulation able to display automatically.

To improve the calculation so that it more realistic, the grounding features should be improved in the numerical calculation by including the capability of real grounding parameter. Thus, the calculated induced current able to generate more accurate and realistic current flow on the equipment for electromagnetic compatibility studies. These features will improve the shielding effect analysis within the substation environment.

References

[1] G. Shafiullah, A. M. T. Oo, D. Jarvis, A. S. Ali, and P. Wolfs, "Potential Challenges-Integrating Renewable Energy with The Smart Grid," *20th Australasian Universities Power Engineering Conference (AUPEC)*, pp. 1-6, 2010.

[2] "What is a Smart Grid," *The IET 2013*, 2013.

[3] E. Csanyi. (2012). *Smart Grid Concept and Characteristics*.

[4] K. Vu, M. M. Begouic, and D. Novosel, "Grids get smart protection and control," *IEEE Computer Applications in Power*, vol. 10, no. 4, pp. 40-44, 1997.

[5] M. Amin and B. F. Wollenberg. (2005) Toward a Smart Grid - Power Delivery for the 21st Century. *IEEE Power & Energy Magazine*.

[6] SGIP Electromagnetic Interoperability Issues Working Group, "Electromagnetic Compatibility and Smart Grid Interoperability Issues," *Smart Grid Interoperability Panel*, 2012.

[7] S. P. Verma, P. Kumar, and Noor-ul-Islam, "Smart Grid, Its Power Quality and Electromagnetic Compatibility," *MIT International Journal of Electrical and Instrumentation Engineering*, 2012.

[8] Working Group C4.208, "EMC within Power Plants and Substations," CIGRE2013.

[9] M. Liserre, T. Sauter, and J. Y. Hung. (2010) Future energy systems - Integrating Renewable Energy Sources into The Smart Power Grid Through Industrial Electronics. *IEEE Industrial Electronics Magazine*.

[10] R. Araneo, S. Lammens, M. Grossi, and S. Bertone, "EMC Issues in High-Power Grid-Connected Photovoltaic Plants," *IEEE Transactions on Electromagnetic Compatibility*, vol. 51, no. 3, 2009.

[11] A. E. Shadare, M. N. O. Sadiku, and S. M. Musa, "Electromagnetic compatibility issues in critical smart grid infrastructure," *IEEE Electromagnetic Compatibility Magazine*, vol. 6, no. 4, pp. 63-70, 2017.

[12] P. Kotsampopoulos *et al.*, "EMC Issues in the Interaction Between Smart Meters and Power-Electronic Interfaces," *IEEE Transactions on Power Delivery*, vol. 32, no. 2, pp. 822-831, 2017.

[13] D. D. C. Antonio Cataliotti, Giuseppe Marsala, Antonella Ragusa, "Electromagnetic Immunity Analysis of a New Interface Device with Power Line Communication for Smart Grid and Energy Storage Applications," *IEEE 17th International Symposium on Power Line Communications and Its Applications*, 2013.

[14] B. Filipović-Grčić, I. Uglešić, V. Milardić, and D. Filipović-Grčić, "Analysis of electromagnetic transients in secondary circuits due to disconnector switching in 400 kV air-insulated substation," *Electric Power Systems Research*, vol. 115, pp. 11-17, 10// 2014.

[15] W. Siew, Y. Liu, B. Musa, F. Mir, and Y. Wang, "Basis For a Wireless Network For EMC Measurements In Electric Substations," *IEEE International Symposium on Electromagnetic Compatibility (EMC 2007)*, 2007.

[16] B. U. Musa, W. H. Siew, and M. D. Judd, "Computation of Transient Electromagnetic Fields Due to Switching in High-Voltage Substations," *IEEE Transactions on Power Delivery*, vol. 25, no. 2, 2010.

[17] S. Gu, D. Li, X. Zeng, J. Su, Y. He, and Z. Zhao, "Analysis of the characteristics and impact of lightning on smart substations," in *2017 IEEE 5th International Symposium on Electromagnetic Compatibility (EMC-Beijing)*, 2017, pp. 1-6.

[18] W. A. Radasky and R. Hoad, "An Overview of the Impacts of Three High Power Electromagnetic (HPEM) Threats on Smart Grids," *International Symposium on Electromagnetic Compatibility (EMC EUROPE)*, pp. 1-6, 2012.

[19] C. P. Nicolaou, A. P. Papadakis, P. A. Razis, G. A. Kyriacou, and J. N. Sahalos, "Experimental measurement, analysis and prediction of electric and magnetic fields in open type air substations," *Electric Power Systems Research*, vol. 90, pp. 42-54, 9// 2012.

[20] M. Olofsson and U. Grape, "Framework for Electromagnetic Compatibility in Electric Power Systems," *VIII International Symposium and Exhibition on Electromagnetic Compatibility and Electromagnetic Ecology*, 2009.

[21] P. Montignies and B. Jover, "Electromagnetic compatibility of digital protective relays installed in medium voltage switchgear," in *2008 5th Petroleum and Chemical Industry Conference Europe - Electrical and Instrumentation Applications*, 2008, pp. 1-11.

[22] M. Olofsson, "Power Quality and EMC in Smart Grid," *10th Intenational Conference Electrical Power Quality and Utilisation*, 2009.

[23] L. Y. Liu Yucheng, "Design Strategy of Anti-Electromagnetic Interference for Microcomputer Relay Protection System," *International Forum on Information Technology and Applications*, 2010.

[24] *Electromagnetic Compatibility (EMC) – Part 3-6: Limits – Assessment of emission limits for the connection of distorting installations to MV, HV and EHV power systems*, 2008.

[25] "What is A Smart Grid," *The Institution of Engineering and Technology 2013*, 2013.

[26] X. Yu, Carlocecati, T. Dillon, and M. G. Simoes. (2011) The New Frontier of Smart Grids. *IEEE Industrial Electronics Magazine*.

[27] E. Chikuni, "Power System and Substation Automation."

[28] X. Fang, S. Misra, G. Xue, and D. Yang, "Smart Grid-The New and Improved Power Grid- A Survey.," *IEEE Communications Surveys & Tutorials*, vol. 14, no. 4, 2012.

[29] Q. Huang, Y. Song, X. Sun, L. Jiang, and P. W. T. Pong, "Magnetics in Smart Grid," *IEEE Transactions on Magnetics*, vol. 50, no. 7, pp. 1-7, 2014.

[30] D. Ishchenko and M. J. Mousavi, "Automated event management in IEC 61850 substations," in *2013 IEEE Power & Energy Society General Meeting*, 2013, pp. 1-5.

[31] S. Bricker, T. Gonen, and L. Rubin, "Substation automation technologies and advantages," *IEEE Computer Applications in Power*, vol. 14, no. 3, pp. 31-37, 2001.

[32] X. Lu, WenyeWang, and JianfengMa, "Authentication and Integrity in the SmartGrid : An Empirical Study in Substation Automation Systems," *International Journal of Distributed Sensor Networks*, 2012.

[33] M. V. M. M. K. Kostin, A. Ovsyannikov, V.S.Verbin, S. Zhivodernikov, "Some Results of EMC Investigations in Russian Substations," *CIGRE*, 2002.

[34] C. W. G. 36.04, "EMI Characterization of HVAC Substations – Updated Data and Influence on Immunity Assessment," *CIGRE*, 2002.

[35] *Draft BS EN 61000-6-5 Ed.1.0 Electromagnetic compatibility (EMC) - Part 6-5: Generic standards - Immunity for power station and substation environments*, 2013.

[36] W. G. Duff, *Fundamentals of Electromagnetic Compatibility* (A handbook series on electromagnetic interference and compatability, no. 1). Gainesville, Va.: Interference Control Technologies, 1988, p. 457 p. in various pagings.

[37] G. Xuehai and H. Jinliang, "Electromagnetic Interference on Secondary Systems of Substation Caused by Incoming Lightning Stroke," in *2007 International Symposium on Electromagnetic Compatibility*, 2007, pp. 212-216.

[38] J. Takami, S. Okabe, and E. Zaima, "Study of Lightning Surge Overvoltages at Substations Due to Direct Lightning Strokes to Phase Conductors," *IEEE Transactions on Power Delivery*, vol. 25, 2010.

[39] G. Pellegrini, A. Raimo, and C. Reynaud, "EMC Problems in H.V. Substations," in *IEEE 1976 International Symposium on Electromagnetic Compatibility*, 1976, pp. 1-4.

[40] L. Yucheng and L. Yubin, "Design Strategy of Anti-Electromagnetic Interference for Microcomputer Relay Protection System," *International Forum on Information Technology and Applications*, 2010.

[41] I. Roasto, E. Romero-CadavaI, J. Martins, and R. Smolenski, "State of The Art of Active Power Electronic Transformers for Smart Grids," *IECON 2012 - 38th Annual Conference on IEEE Industrial Electronics Society*, pp. 5241 - 5246, 2012.

[42] P. Kotsampopoulos *et al.*, "EMC issues in the interaction between smart meters and power electronic interfaces," *IEEE Transactions on Power Delivery*, vol. PP, no. 99, pp. 1-1, 2016.

[43] F. Benyoubi, L. Pichon, M. Bensetti, Y. L. Bihan, and M. Feliachi, "An Efficient Method for Modeling the Magnetic Field Emissions of Power Electronic Equipment From Magnetic Near Field Measurements," *IEEE Transactions on Electromagnetic Compatibility*, vol. 59, no. 2, pp. 609-617, 2017.

[44] R. Smoleński, M. Jarnut, G. Benysek, and A. Kempski, "Power Electronics Interfaces For Low Voltage Distribution Generation-EMC Issues," *7th International Conference-Workshop Compatibility and Power Electronics (CPE)*, 2011.

[45] Z. Yuan, J. Liu, and B. Zhao, "Low-voltage Power Line Channel Environment and the Application Analysis in Smart Grid," in *2012 China International Conference on Electricity Distribution (CICED 2012)*, 2012.

[46] A. Alain and L. Frank, "Electro-magnetic emission of power line communiation system: Intended or not intended radiation?," in *2017 International Symposium on Electromagnetic Compatibility - EMC EUROPE*, 2017, pp. 1-5.

[47] S. Galli, A. Scaglione, and Z. Wang, "For the Grid and Through the Grid- The Role of Power Line Communications in the Smart Grid," *Proceedings of the IEEE,* vol. 99, no. 6, 2011.

[48] Q. L. W. H. Siew, Martin G. Stewart, Keith Walker, and Chris Piner, "Measurement of electromagnetic emissions from FACTS equipment operational within substations-part I," 2005.

[49] Y. Yang, Z. Zhao, S. Gu, D. Li, and X. Zeng, "Analysis of the impact of direct lightning smart substation overhead ground wire on the station smart components," in *2016 Asia-Pacific International Symposium on Electromagnetic Compatibility (APEMC)*, 2016, vol. 01, pp. 927-929.

[50] S. Gu *et al.*, "Evaluation method of lightning performance on low voltage system in smart substation," in *2016 Asia-Pacific International Symposium on Electromagnetic Compatibility (APEMC)*, 2016, vol. 01, pp. 896-898.

[51] J. Liu, Y. Zhu, Q. Xu, and Q. Huang, "Simulation analysis of power-frequency electromagnetic field interference on smart meters," in *2015 IEEE PES Asia-Pacific Power and Energy Engineering Conference (APPEEC)*, 2015, pp. 1-5.

[52] M. Tyndall, R. Marshall, K. Armstrong, and C. Marshman, "Potential EMC Implementation Problems of Smart Metering, Display and Communications," *2nd IEEE PES International Conference and Exhibition on Innovative Smart Grid Technologies (ISGT Europe)*, 2011.

[53] S. d. Miguel-Bilbao *et al.*, "Electromagnetic exposure hot-spots in a healthcare environment, caused by smart metering to control public utilities," in *2017 E-Health and Bioengineering Conference (EHB)*, 2017, pp. 603-606.

[54] R. Smolenski, A. Kempski, J. Bojarski, and P. Lezynski, "EMI Generated by Power Electronic Interfaces in Smart Grids," presented at the IEEE International Symposium on Electromagnetic Compatibility (EMC EUROPE), 2012.

[55] A. I. Tarmizi, M. D. Rotaru, and J. K. Sykulski, "Electromagnetic compatibility studies within smart grid automated substations," in *49th International Universities Power Engineering Conference (UPEC)*, 2014, pp. 1-6.

[56] S. T. Mak, "Smart Meters Serving as Synchro-Sensors for Smart Distribution Grid Applications," *IEEE Power and Energy Society General Meeting*, 2011.

[57] *IEEE Standard for Power Line Communication Equipment— Electromagnetic Compatibility (EMC) Requirements—Testing and Measurement Methods*, 2010.

[58] V. Gurevich, *Digital Protective Relays - Problems and Solutions*. Taylor and Francis Group, LLC, 2011.

[59] *Lightning Parameters for Engineering Applications - Working Group C4.407*, 2013.

[60] *IEC 62305-1 Protection against lightning – Part 1: General principles*, 2010.

[61] *BS EN 61000-4-5:2014 Electromagnetic compatibility (EMC) Part 4-5: Testing and measurement techniques — Surge immunity test*, 2014.

[62] D. PowerFactory, "DIgSILENT PowerFactory Technical Reference Documentation-Impulse Source ElmImpulse," ed: DIgSILENT GmbH, 2014.

[63] M. Ianoz, "Developments in the Study of Lightning Electromagnetic Effects with Applications to the Protection of Distribution Power Lines," 2006.

[64] I. Said, H. B. Hussain, and V. Dave, "Characterization of Magnetic Field at Distribution Substations," *9th International Conference on Environment and Electrical Engineering (EEEIC)*, pp. 423 - 426, 2010.

[65] A. S. Safigianni and A. Kostopoulou, "Electric and Magnetic Field Measurements in an indoor Electric Power Substation," *Journal of Materials Processing Technology*, vol. 181, no. 1-3, pp. 126-130, 2007.

[66] R. D. Miller *et al.*, "Possible Health Hazards from Exposure to Power-Frequency Electric and Magnetic Fields - A Comar Technical Information Statement," (in English), *IEEE Engineering in Medicine and Biology Magazine*, vol. 19, no. 1, pp. 131-137, Jan-Feb 2000.

[67] I. Said, A. S. Farag, H. Hussain, and N. A. Rahman, "Measurement and Simulation of Magnetic Field of a 132 kV Air-Insulated Substation in Malaysia," *39th International Universities Power Engineering Conference, (UPEC 2004)*, vol. 1, 2004.

[68] *ICNIRP Guidelines For Limiting Exposure to Time-Varying Electric, Magnetic And Electromagnetic Fields (Up To 300 GHz)*, 1998.

[69] R. Smolenski, M. Jarnut, A. Kempski, and G. Benysek, "Compensation of CM Voltage in Interfaces for LV Distributed Generation," *IEEE International Symposium on Electromagnetic Compatibility (EMC)*, 2011.

[70] A. Mannikoff and H. Nilsson, "Sweden-Reaching 100% 'smart meters' July 1, 2009," *Power & Energy Society General Meeting, 2009. PES '09. IEEE*, 2009.

[71] Z. Ming, H. Lixin, Y. Fan, and J. Danwei, "Research of the Problems of Renewable Energy Orderly Combined to the Grid in Smart Grid," *Asia-Pacific Power and Energy Engineering Conference (APPEEC)*, 2010.

[72] H. Singer, H. Steinbigler, and P. Weiss, "A Charge Simulation Method for the Calculation of High Voltage Fields," *IEEE Transactions on Power Apparatus and Systems*, vol. PAS-93, no. 5, pp. 1660-1668, 1974.

[73] L. Hasselgren, E. Moller, and Y. Hamnerius, "Three Dimensional FEM Calculations on Shielding of Power Frequency Magnetic Fields from a Substation," *IEEE International Symposium on Electromagnetic Compatibility*, 1993.

[74] T. Ling, W. Xiaoyu, Q. Liang, S. Lu, and Y. Fan, "Calculation of Power frequency Electric Field in HV Substation Using BEM," *Asia-Pacific Power and Energy Engineering Conference (APPEEC), 2011*, 2011.

[75] W. Krajewski, "BEM analysis of 3D EMC problem with consideration of eddy-current effects," *IEE Proceedings - Science, Measurement and Technology*, vol. 153, no. 3, pp. 101-107, 2006.

[76] J. Deng *et al.*, "A Wavelet Transform Boundary Element Method for Electric Field Problem Inside Substations," *IEEE Transactions on Electromagnetic Compatibility*, vol. 54, no. 1, 2012.

[77] B. U. Musa, W. H. Siew, M. D. Judd, T. Wang, and Q. M. Li, "Application of Finite Difference Time Domain Method to High Voltage Substations: Switching Transient Fields," *International Journal of Engineering Science and Innovative Technology (IJESIT)*, vol. 2, no. 5, 2013.

[78] A. Choroszucho and B. Butrylo, "Implementation of the variable density mesh within the finite difference frequency domain algorithm to analysis of electromagnetic field in building constructions," in *2016 17th International Conference Computational Problems of Electrical Engineering (CPEE)*, 2016, pp. 1-5.

[79] LeiLiu, X. Cui, and L. Qi, "Simulation of Electromagnetic Transients of the Bus Bar in Substation by the Time-Domain Finite-Element Method," *IEEE Transactions on Electromagnetic Compatibility*, vol. 51, no. 4, 2009.

[80] M. Stojkov, D. Sljivac, and L. Jozsa, "Electric And Magnetic Field Computation Of 35 Kv Voltage Level Of Transformer Substation 35/10 Kv Using The CDEGS Software," *Acta Electrotechnica et Informatic*, vol. 10, no. 4, pp. 64–68, 2010.

[81] S. Nikolovski, P. Maric, Z. Baus, and B. Stefic, "Computation of Electromagnetic Field of Transformer Station 110/10(20) kV Using the CDEGS software," in *EUROCON 2007 - The International Conference on "Computer as a Tool"*, 2007, pp. 1360-1365.

[82] I. Rumsey and M. Piket-May, "Application of the finite difference time domain (FDTD) method to a challenging real-world EMC problem," in *1999 IEEE International Symposium on Electromagnetic Compatability. Symposium Record (Cat. No.99CH36261)*, 1999, vol. 2, pp. 679-683 vol.2.

[83] A. Taflove, "Application of the Finite-Difference Time-Domain Method to Sinusoidal Steady-State Electromagnetic-Penetration Problems," *IEEE Transactions on Electromagnetic Compatibility*, vol. EMC-22, no. 3, pp. 191-202, 1980.

[84] G. Mur, "Absorbing boundary conditions for the finite-difference approximation of the time-domain electromagnetic field equations," *IEEE Transactions on Electromagnetic Compatibility*, 1981.

[85] R. M. e. S. d. Oliveira and C. L. d. S. S. Sobrinho, "Computational environment for simulating lightning strokes in a power substation by finite-difference time-domain method," *IEEE Transactions On Electromagnetic Compatibility*, vol. 51, 2009.

[86] D. S. Shishigin and S. L. Shishigin, "Numerical modeling in EMC problems of electric power substations when lightning strikes," in *2017 IEEE International Conference on Environment and Electrical Engineering and 2017 IEEE Industrial and Commercial Power Systems Europe (EEEIC / I&CPS Europe)*, 2017, pp. 1-5.

[87] M. Zang, C. Cimala, M. Clemens, J. Dutiné, T. Timm, and B. Schmuelling, "A Co-Simulation Scalar-Potential Finite Difference Method for the Numerical Analysis of Human Exposure to Magneto-Quasi-Static Fields," *IEEE Transactions on Magnetics*, vol. 53, no. 6, pp. 1-4, 2017.

[88] R. M. R. BARROS and E. G. d. COSTA, "Electric Field Mapping in High Voltage Substation Using the Finite Elements Method," *22nd International Conference on Electricity Distribution*, 2013.

[89] W. C. Gibson, *The Method of Moments in Electromagnetics*. Taylor & Francis Group, LLC, 2008.

[90] L. N. Dworsky, *Introduction to Numerical Electrostatics Using MATLAB®*. John Wiley & Sons, Inc., Hoboken, New Jersey, 2014.

[91] W. Krajewski, "Numerical modelling of the electric field in HV substations," *IEE Proceedings - Science, Measurement and Technology*, vol. 151, no. 4, pp. 267-272, 2004.

[92] F. T. Ulaby, *Electromagnetics for Engineers*. Pearson Education, 2005.

[93] M. N. O. Sadiku, *Numerical Techniques in Electromagnetics with MATLAB*. CRC Press, Inc, 2009.

[94] *Electromagnetic compatibility (EMC) Part 4-8: Testing and measurement techniques — Power frequency magnetic field immunity test*, 2001.

[95] *IEC TR 61000-4-1 Electromagnetic compatibility (EMC) – Part 4-1: Testing and measurement techniques* 2016.

[96] (2007, 23-Mac-2017). *Electromagnetic fields and public health - Exposure to extremely low frequency fields*. Available: http://www.who.int/peh-emf/publications/facts/fs322/en/

[97] *Electromagnetic compatibility (EMC)Part 4-8: Testing and measurement techniques — Power frequency magnetic field immunity test*, 2010.

[98] V. Gurevich, *Cyber and Electromagnetic Threats in Modern Relay Protection*.

[99] *IEC 61000-5-6 Electromagnetic compatibility (EMC) Part 5-6: Installation and mitigation guidelines* 2002.

[100] *BS IEC 61000-5-1:1996 Electromagnetic compatibility (EMC)— Part 5:Installation and mitigation guidelines* 1996.

[101] D. N. FÎTA, L. Muresan, C. Cheleman, and M. Grebenisan, "The Modelling of Rosiori Power Station 400/220/20 KV Retechnologized of Transelectrica Company. The Simulation of the Permanent Regime With EDSA Programme," *6TH International Conference Electromechanical dan Power Systems*, 2007.

[102] C. Munteanu, V. Topa, A. Racasan, I. T. Pop, and E. Merdan, "Study of the Electric Field Distribution Inside High Voltage Substations," *International Symposium on Electromagnetic Compatibility (EMC Europe 2011),*, 2011.

[103] C. Munteanu, V. Topa, I. T. Pop, A. Racasan, and E. Merdan, "Advances on the Electromagnetic Field Distribution Analysis inside High Voltage Substations," *International Universities' Power Engineering Conference (UPEC 2011)*, 2011.

[104] C. Munteanu, G. Visan, and I. T. Pop, "Electric and Magnetic Field Distribution Inside High Voltage Power Substations. Numerical Modeling and Experimental Measurements," *IEEJ Transactions on Electrical and Electronic Engineering*, vol. 5, no. 1, pp. 40-45, 2010.

[105] C. P. Nicolaou, A. P. Papadakis, P. A. Razis, G. A. Kyriacou, and J. N. Sahalos., "Measurements and Predictions of Electric and Magnetic Fields From Power Lines," *Electric Power Systems Research*, vol. 81, no. 5, pp. 1107-116, 2011.

[106] W. K. Daily and F. Dawalibi, "Measurements and Computations of Electromagnetic Fields in Electric Power Substations," *IEEE Transactions on Power Delivery*, vol. 9, 1994.

[107] Y. Xiao, Communication and Networking in Smart Grids, Y. Xiao, ed.: CRC Press Taylor & Francis Group, 2012. [Online]. Available.

[108] A. Eqbal. (2016, 1 Oct 2019). *Clearance Requirements In EHV AIS Substation You MUST Respect*. Available: https://electrical-engineering-portal.com/clearance-requirements-ehv-substation

[109] C. D. A. Silveira, C. A. D. Costa, R. D. C. E. Silva, L. R. Soares, and J. C. P. Guimaraes, "Electromagnetic Environment Measurement under Steady-State Conditions in Utility Substations," in *2006 IEEE/PES Transmission & Distribution Conference and Exposition: Latin America*, 2006, pp. 1-6.

[110] U. M. Peterlin and T. Živic, "Electromagnetic compatibility levels in power plants and substations," in *2015 IEEE International Symposium on Electromagnetic Compatibility (EMC)*, 2015, pp. 266-270.

[111] A. P. P. Charalambos P. Nicolaou, Panos A. Razisa, George A. Kyriacou, John N. Sahalos, "Simplistic numerical methodology for magnetic field prediction in open air type substations," *Electric Power Systems Research,* vol. 81, pp. 2120-2126, 2011.

[112] "DIgSILENT PowerFactory 15," in *User Manual*, 15 ed. Gomaringen, Germany: DIgSILENT GmbH, 2015.

[113] C. P. Nicolaou, A. P. Papadakis, P. A. Razis, G. A. Kyriacou, and J. N. Sahalos, "Experimental measurement, analysis and prediction of electric and magnetic fields in open type air substations," *Electric Power Systems Research,* vol. 90, 2012.

[114] W. A. Radasky, "Immunity for power station and substation environments," in *IEEE International Symposium on Electromagnetic Compatibility & Signal/Power Integrity (EMCSI)*, 2017, pp. 1-25.

[115] Y. Ma, G. G. Karady, J. R. Hunt, and B. L. Priest, "Measurement and Prediction of Electrical Substation Generated Electromagnetic Field," *IEEE Power and Energy Society General Meeting*, 2011.

[116] A. I. Tarmizi, M. D. Rotaru, and J. K. Sykulski, "Magnetic field calculations within substation environment for EMC studies," in *IEEE 16th International Conference on Environment and Electrical Engineering (EEEIC)*, 2016, pp. 1-6.

[117] M. Purcar, C. Munteanu, A. Avram, and F. Miron, "CAD/CAE Modeling of Electromagnetic Field Distribution in HV Substations and Investigation of The Human Exposure," in *2016 International Conference on Applied and Theoretical Electricity (ICATE)*, 2016, pp. 1-5.

[118] *Electromagnetic compatibility (EMC) Part 4-9: Testing and measurement techniques — Impulse magnetic field immunity test*, 2016.

[119] M. S. N. V. Kamaraju, *High Voltage Engineering*. Mc Graw Hill, 2006.

[120] C. Imposimato, J. Hoeffelman, A. Eriksson, W. H. Siew, P. H. Pretorius, and P. S. Wong, "EMI Characterization of HVAC Substations - Updated Data And Influence On Immunity Assessment," *CIGRE Working Group 36.04,* 2002.

[121] "DIgSILENT PowerFactory 15 User Manual," ed: DIgSILENT GmbH, 2015.

[122] M. O. Durham and R. A. Durham, "Lightning, Transient & High Frequency Impact on Material Such As Corrugated Tubing," *Frontiers of Power,* 2008.

[123] Q. Song *et al.*, "Smart substation integration technology and its application in distribution power grid," *CSEE Journal of Power and Energy Systems*, vol. 2, no. 4, pp. 31-36, 2016.

[124] J. FAIZ and M. OJAGHI, "Instructive Review of Computation of Electric Fields using Different Numerical Techniques," *International Journal of Engineering Education*, vol. 18, no. 3, pp. 344-356, 2002.

[125] *CISPR Guidance document on EMC of equipment connected to the SmartGrid*, 2014.

Appendix A: Coefficient

Table 5-1 Conductivity, σ of used materials [92]

Material	Conductivity, σ
Copper	5.8×10^{7}
Air	3×10^{-15}
Aluminium	3.5×10^{7}

Table 5-2 Relative Permeability, μ_r of used materials

$\mu = \mu_o \times \mu_r$ and $\mu_o = 4\pi \times 10^{-7}$

Material	Relative Permeability, μ_r
Copper	$0.99999 \cong 1$
Air	$1.000004 \cong 1$
Aluminium	$1.000002 \cong 1$

Appendix B: Matlab Coding

```
clc
clear all
close all force
%myCluster=parcluster('local');
N=myCluster.NumWorkers; parpool(myCluster,N)
% === IMPORTANT!!! ==================
% EDIT THIS PART FOR DIFFERENT INPUT
% ====================================
% load ('lightninginput7_temp1.mat');
% ilightnum = 7;

% Nx=100:0.25:106;
% Ny=20:0.25:26;
% Nz=0:0.25:6;

% % % box:-
% % % x=103:104
% % % y=23:24
% % % z=3:4
dxyz=0.02;
Nx=102-2*dxyz:dxyz:102+0.5+2*dxyz;
Ny=22 -2*dxyz:dxyz:22 +0.5+2*dxyz;
Nz=2  -2*dxyz:dxyz:2  +0.5+2*dxyz;
[ttc,ttr]=size(Nx);ttr^3

% ======================================
dxyz_refined = 0.01;
Nx_s_ileft = Nx(1):dxyz_refined:Nx(3);
Ny_s_ileft = Ny(1):dxyz_refined:Ny(end);
Nz_s_ileft = Nz(1):dxyz_refined:Nz(end);

Nx_s_iright = Nx(end-2):dxyz_refined:Nx(end);
Ny_s_iright = Ny(1):dxyz_refined:Ny(end);
Nz_s_iright = Nz(1):dxyz_refined:Nz(end);

Nx_s_jbottom = Nx(1):dxyz_refined:Nx(end);
Ny_s_jbottom = Ny(1):dxyz_refined:Ny(3);
Nz_s_jbottom = Nz(1):dxyz_refined:Nz(end);

Nx_s_jtop = Nx(1):dxyz_refined:Nx(end);
Ny_s_jtop = Ny(end-2):dxyz_refined:Ny(end);
Nz_s_jtop = Nz(1):dxyz_refined:Nz(end);

Nx_s_klow = Nx(1):dxyz_refined:Nx(end);
Ny_s_klow = Ny(1):dxyz_refined:Ny(end);
Nz_s_klow = Nz(1):dxyz_refined:Nz(3);

Nx_s_khigh = Nx(1):dxyz_refined:Nx(end);
Ny_s_khigh = Ny(1):dxyz_refined:Ny(end);
Nz_s_khigh = Nz(end-2):dxyz_refined:Nz(end);
% ======================================
Nx_s =
{Nx_s_ileft,Nx_s_iright ,Nx_s_jbottom,Nx_s_jtop ,Nx_s_
klow ,Nx_s_khigh};
Ny_s =
{Ny_s_ileft,Ny_s_iright ,Ny_s_jbottom,Ny_s_jtop ,Ny_s_
klow ,Ny_s_khigh};
Nz_s =
{Nz_s_ileft,Nz_s_iright ,Nz_s_jbottom,Nz_s_jtop ,Nz_s_
klow ,Nz_s_khigh};

dxyz = dxyz_refined;

% ====================================

% ====================================
total_current = 1;
currentno=3;

%% rosiori environment
%
=====================================================
========
wire_coordinate_rosiori
% onewire_Sept2016
%
=====================================================
========
% total_current=1;
%
=====================================================
========
for mode = 1:6
    Nx = Nx_s{mode};
    Ny = Ny_s{mode};
    Nz = Nz_s{mode};
    %
=====================================================
========
    ait_gendata_bxbybz_v3_dontuse
    %
=====================================================
========

    datestamp = datestr(datetime('now','format','dd-
MM-yyyy'));
    datestamp=strcat(datestamp(1:11),'-
',datestamp(13:14),datestamp(16:17),datestamp(19:20));

    %clear cluster1 ans


eval(sprintf('save %s_rosi_stdcur_parpool8.mat',datest
amp));
end
% end

Hx = BX{1}(:,:,3); Hy = BY{1}(:,:,3); Hz =
BZ{1}(:,:,3);
[NumberOfXPoints,NumberOfYPoints]=size(Hx);
for k=1:NumberOfXPoints
    for l=1:NumberOfYPoints
        H_mag(k,l) =
sqrt(Hx(k,l)^2+Hy(k,l)^2+Hz(k,l)^2);
    end
end
figure;surf(H_mag);  view(2)
%
=====================================================
=====================================================
=============================================
% ait_gendata_bxbybz
% START
=====================================================
=====================================================
=============================================
u0 = 4*pi*10^-7;
total_current = 1;
currentno=3;
Lwire={};origin_wire={};current_wire={};
for i=1:total_wire

eval(sprintf('Lwire{%d}=Lwire%d;origin_wire{%d}=origin
_wire%d;current_wire{%d}=current_wire%d;',i,i,i,i,i,i)
);
end

if length(Nx)==1
    dx=1;
else
    dx = Nx(2)-Nx(1);
end
if length(Ny)==1
    dy=1;
else
    dy = Ny(2)-Ny(1);
end
if length(Nz)==1
    dz=1;
else
    dz = Nz(2)-Nz(1);
end

lengthNx=length(Nx);lengthNy=length(Ny);lengthNz=lengt
h(Nz);

[X,Y,Z] = ait_gen_XYZ_axis(Nx,Ny,Nz,dx,dy,dz);

%cell to store current vs. height for B_mag
calculation :{current,height}
BX={}; BY={}; BZ={};

for k=1:total_current
    for a=1:lengthNx
        for b=1:lengthNy
            for c=1:lengthNz

BX{k}(a,b,c)=0;BY{k}(a,b,c)=0;BZ{k}(a,b,c)=0;
            end
        end
    end
end

datestamp = datestr(datetime('now','format','dd-MM-
yyyy'));
datestamp=strcat(datestamp(1:11),'-
',datestamp(13:14),datestamp(16:17),datestamp(19:20));

tStart = tic;
req_time_temp=0;rem_time_temp=0;
total_calc = total_current*total_wire;
```

```
currtimestamp = 'nil';cntr=0;
tElapsed2 = 0;
%parfor k=1:total_current

clc
disp(['------------------------------------------------
--------']);
disp(['Processing: ']);
disp([' >>  current ',num2str(1),' of
',num2str(total_current)]);
disp([' >>  wire    ',num2str(1),' of
',num2str(total_wire)]);
disp([' >>  mode    ',num2str(1),' of
',num2str(mode)]);
disp(['-.-.-.-.-.-.-.-.-.-.-.-.-.-.-.-.-.-.-,']);
disp(['Percentage Done = ', num2str(0),'%']);
disp(['Required time   = ', '---',' seconds']);
disp(['                  ', '---',' mins']);
disp(['Elapsed time    = ', '---',' seconds']);
disp(['                  ', '---',' mins']);
disp(['Remaining time  = ', '---',' seconds']);
disp(['                  ', '---',' mins']);
disp(['Timestamp (previous):  ','nil']);
disp(['Timestamp (latest)  :  ',
datestr(datetime('now','format','dd-MM-yyyy'))]);
disp(['-.-.-.-.-.-.-.-.-.-.-.-.-.-.-.-.-.-.-,']);

for k=1:total_current
    for i=1:total_wire
        cntr=cntr+1;
%         if(rem(cntr,floor(total_wire/3))==0)
        if(rem(cntr,1)==0)
            clc
            tElapsed = toc(tStart);
            perc_done = cntr*100/total_calc;
            req_time = tElapsed*100/perc_done;
            rem_time = req_time-tElapsed;
            prevtimestamp = currtimestamp;
            currtimestamp =
datestr(datetime('now','format','dd-MM-yyyy'));

            disp(['------------------------------------
--------------------']);
            disp(['Processing: ']);
            disp([' >>  current ',num2str(k),' of
',num2str(total_current)]);
            disp([' >>  wire    ',num2str(i),' of
',num2str(total_wire)]);
            disp([' >>  mode    ',num2str(mode),' of
',num2str(6)]);
            disp(['-.-.-.-.-.-.-.-.-.-.-.-.-.-.-.-.-.-.-,']);
            disp(['Percentage Done = ',
num2str(perc_done),'%']);
            disp(['Required time   = ',
num2str(req_time),' seconds']);
            disp(['                  ',
num2str(req_time/60),' mins']);
            disp(['Elapsed time    = ',
num2str(tElapsed),' seconds']);
            disp(['                  ',
num2str(tElapsed/60),' mins']);
            disp(['Remaining time  = ',
num2str(rem_time),' seconds']);
            disp(['                  ',
num2str(rem_time/60),' mins']);
            disp(['Timestamp (previous):
',prevtimestamp]);
            disp(['Timestamp (latest)  :
',currtimestamp]);
            disp(['-.-.-.-.-.-.-.-.-.-.-.-.-.-.-.-.-.-.-,']);
            disp(['Elapsed time for one point  = ',
num2str(tElapsed2),' seconds']);
            disp(['                                ',
num2str(tElapsed2/60),' mins']);


        end
        tStart2 = tic;
        [BX1,BY1,BZ1] =
ait_gen_B_fromwire(Lwire{i},origin_wire{i},Nx,Ny,Nz,X,
Y,Z,current_wire{i}(currentno),u0);
        tElapsed2=toc(tStart2);

        for a=1:lengthNx
            for b=1:lengthNy
                for c=1:lengthNz

BX{k}(a,b,c)=BX1(a,b,c)+BX{k}(a,b,c);

BY{k}(a,b,c)=BY1(a,b,c)+BY{k}(a,b,c);

BZ{k}(a,b,c)=BZ1(a,b,c)+BZ{k}(a,b,c);
                end
            end
        end
    end

%     if(rem(k,2)==0)
%
eval(sprintf('save %s_rosi_light_parpool8_midproc.mat'
,datestamp));
%     end
end

% END
=====================================================
```

```
=====================================================
=============================================
% % % working template PDE vs BSavat with box & hole
% % % version5: addition with locations for 3 holes
% % % version 6: correction on B=miuH calculations and
the sigma & miu values


clc
clear all
close all force

datestamp_start = datestr(datetime('now','format','dd-
MM-yyyy'));
% load('28-Sep-2016-164303_rosi_stdcur_parpool8.mat')
% load('27-Sep-2016-205352_rosi_stdcur_parpool8.mat')
% load('25-Mar-2017-
165545_3holes_rosi_lightcur_parpool8_maxcurrent_dxyz0p
02.mat')
%  load('2-nov-2016-
080900_3holes_rosi_stdcur_parpool8_dxyz0p02.mat')
% load('28-Oct-2018-
005025_rosi_lightcur_parpool8.mat')
load('28-Oct-2018-010012_rosi_stdcur_parpool8.mat')
% >> myCluster=parcluster('local');
N=myCluster.NumWorkers; poolobj=parpool(myCluster,2)
% myCluster=parcluster('local');
N=myCluster.NumWorkers; poolobj=parpool(myCluster,N)
% Nx
tic



% -- Finite-difference equation [C] --
omega = 2*pi*50;
h = dx;
sigma_aluminium = 3.5*10^7;
sigma_copper = 5.8*10^7;
sigma_air = 3*10^-15;
sigma_metal = sigma_copper;

u0 = 4*pi*10^-7;
u_air = 1;
u_metal = 1; %all metals miu = 1;

C_metal_complex =
complex(0,omega*sigma_metal*u0*u_metal*h^2);
C_air_complex   = complex(0,omega*sigma_air  *u0*u_air
*h^2);
C_metal = 1/(6 + C_metal_complex);
C_air   = 1/(6 + C_air_complex);
%C_air   = 1/(6 + 0);
A_cmetal = -1/C_metal;
A_cair = -1/C_air;

-1/C_metal;
-1/C_air;

% --  --  --  --  --  --  --  --  --  --  --  --  --

currentno=3;
counter=1;
total_current = 1;

for cellnum = 1:total_current
    % NOTE: B = miu*H ; H = B/miu
    Hx_surfinit{cellnum} = BX{currentno}/(u0*u_air);
    Hy_surfinit{cellnum} = BY{currentno}/(u0*u_air);
    Hz_surfinit{cellnum} = BZ{currentno}/(u0*u_air);

    BXi{cellnum} = BX{cellnum};
    BYi{cellnum} = BY{cellnum};
    BZi{cellnum} = BZ{cellnum};

    counter = counter+1;
end


% % filter only outair of box points

for cellnum = 1:total_current
    for k = 1:lengthNz
        for j = 1:lengthNy
            for i = 1:lengthNx
                if
((i==1||i==lengthNx)||(j==1||j==lengthNy)||(k==1||k==l
engthNz))

Hx_surf{cellnum}(i,j,k)=Hx_surfinit{cellnum}(i,j,k);

Hy_surf{cellnum}(i,j,k)=Hy_surfinit{cellnum}(i,j,k);

Hz_surf{cellnum}(i,j,k)=Hz_surfinit{cellnum}(i,j,k);
                else
                    Hx_surf{cellnum}(i,j,k) = 0;
                    Hy_surf{cellnum}(i,j,k) = 0;
                    Hz_surf{cellnum}(i,j,k) = 0;
                end
            end
        end
    end
end
% --  --  --  --  --  --  --  --  --  --  --  --  --


% -- create and insert value in [A] matrices
NoOfUnKnowns = lengthNx*lengthNy*lengthNz;
```

```
A = {zeros(NoOfUnKnowns, NoOfUnKnowns)};
b_x = {zeros(NoOfUnKnowns,1)};
b_y = {zeros(NoOfUnKnowns,1)};
b_z = {zeros(NoOfUnKnowns,1)};

% % metal box location
brd11 = 2;
brd12 = lengthNx-1;
ileft_m   = brd11; iright_m  = brd12;
jbottom_m = brd11; jtop_m    = brd12;
klow_m    = brd11; khigh_m   = brd12;
% % % ileft_m   = Nx(2); iright_m  = Nx(end-1);
% % % jbottom_m = Ny(2); jtop_m    = Ny(end-1);
% % % klow_m    = Nz(2); khigh_m   = Nz(end-1);

% % inner air location
brd21 = brd11+1;
brd22 = brd12-1;
ileft_inair   = brd21;        %index of outer surface
left side
iright_inair  = brd22;      %index of outer surface
right side
jbottom_inair = brd21;    %index of outer surface
Bottom side
jtop_inair  = brd22;          %index of outer surface
Top side
klow_inair  = brd21;          %index of outer surface
Bottom side
khigh_inair = brd22;        %index of outer surface
Top side
% % % ileft_inair   = Nx(3); iright_inair  = Nx(end-
2);
% % % jbottom_inair = Ny(3); jtop_inair    = Ny(end-
2);
% % % klow_inair    = Nz(3); khigh_inair   = Nz(end-
2);

% % Holes location
brd31j = 14;
brd32j = 17;

klow_hole1 = 7;     khigh_hole1 = 10;
klow_hole2 = 14;    khigh_hole2 = 17;
klow_hole3 = 21;    khigh_hole3 = 24;

% brd31k = klow_hole1;
% brd32k = khigh_hole1;
% brd31 = ceil(lengthNx/2)-ceil(lengthNx/5);
% brd32 = ceil(lengthNx/2)+ceil(lengthNx/5);
ileft_hole   = brd31j;   iright_hole = brd32j;
jbottom_hole = jtop_m;  jtop_hole   = jtop_m;
% ------------------------------------
% -------  FILL THIS IN!!!  --------
klow_hole    = klow_hole3;   khigh_hole  =
khigh_hole3;
hole_num=strcat('hole3');
% ------------------------------------
% % % ileft_hole   = Nx(23); iright_hole = Nx(23);
% % % jbottom_hole = Ny(2); jtop_hole   = Ny(2);
% % % klow_hole    = Nz(23); khigh_hole  = Nz(23);
% --  --  --  --  --  --  --  --  --  --  --  --  --

tStart = tic;
req_time_temp=0;rem_time_temp=0;
currtimestamp = 'nil';

for cellnum = 1:total_current
    Counter=1;
    for k = 1:lengthNz
        for i = 1:lengthNx
            for j = 1:lengthNy

                if rem(Counter,50)==0
                    clc
                    tElapsed = toc(tStart);
                    perc_done =
Counter*100/NoOfUnKnowns;
                    req_time = tElapsed*100/perc_done;
                    rem_time = req_time-tElapsed;
                    prevtimestamp = currtimestamp;
                    currtimestamp =
datestr(datetime('now','format','dd-MM-yyyy'));

                    disp(['Processing matrix A ...']);
                    disp(['   Current No. =
',num2str(cellnum),' of ',...
                        num2str(total_current)]);
                    disp([' (i,j,k) =
',num2str(i),',',num2str(j),',',num2str(k)]);
                    disp(['   Counter =
',num2str(Counter),' of ',num2str(NoOfUnKnowns)]);
                    disp(['   Percentage Done =
',num2str(perc_done),'%']);

                    disp(['   Required time:
',num2str(req_time),' seconds']);
                    disp(['   Elapsed time:
',num2str(tElapsed),' seconds']);
                    disp(['   Remaining time:
',num2str(rem_time),' seconds']);

disp('.....................................');
                    disp(['   Required time:
',num2str(req_time/60),' mins']);
                    disp(['   Elapsed time:
',num2str(tElapsed/60),' mins']);
                    disp(['   Remaining time:
',num2str(rem_time/60),' mins']);

disp('.....................................');

                    disp(['   Required time:
',num2str(req_time/60/60),' hours']);
                    disp(['   Remaining time:
',num2str(rem_time/60/60),' hours']);

disp('.....................................');
                    disp(['   Timestamp (previous):
',prevtimestamp]);
                    disp(['   Timestamp (latest)  :
',currtimestamp]);
                end

                %-----------------------------------
----------------
                % filter for the outter air
                if (    (i==1 || i==lengthNx)||...
                        (j==1 || j==lengthNy)||...
                        (k==1 || k==lengthNz))
                    %  ..............................
.................
                    A{cellnum}(Counter,Counter)=1; %
'A'=1 because the source location is where 'A' is
equal to 1

                    b_x{cellnum}(Counter,1) =
Hx_surf{cellnum}(i,j,k); % put source value to b_xyz
array
                    b_y{cellnum}(Counter,1) =
Hy_surf{cellnum}(i,j,k); % put source value to b_xyz
array
                    b_z{cellnum}(Counter,1) =
Hz_surf{cellnum}(i,j,k); % put source value to b_xyz
array

                else

                    b_x{cellnum}(Counter,1) = -
( Hx_surf{cellnum}(i-1,j,k) + ...

Hx_surf{cellnum}(i+1,j,k) + ...

Hx_surf{cellnum}(i,j-1,k) + ...

Hx_surf{cellnum}(i,j+1,k) + ...

Hx_surf{cellnum}(i,j,k-1) + ...

Hx_surf{cellnum}(i,j,k+1));
                    b_y{cellnum}(Counter,1) = -
( Hy_surf{cellnum}(i-1,j,k) + ...

Hy_surf{cellnum}(i+1,j,k) + ...

Hy_surf{cellnum}(i,j-1,k) + ...

Hy_surf{cellnum}(i,j+1,k) + ...

Hy_surf{cellnum}(i,j,k-1) + ...

Hy_surf{cellnum}(i,j,k+1));
                    b_z{cellnum}(Counter,1) = -
( Hz_surf{cellnum}(i-1,j,k) + ...

Hz_surf{cellnum}(i+1,j,k) + ...

Hz_surf{cellnum}(i,j-1,k) + ...

Hz_surf{cellnum}(i,j+1,k) + ...

Hz_surf{cellnum}(i,j,k-1) + ...

Hz_surf{cellnum}(i,j,k+1));

                    % filter for hole
                    if(     (i>=ileft_hole     &&
i<=iright_hole) &&...
                            (j>=jbottom_hole   &&
j<=jtop_hole)   &&...
                            (k>=klow_hole      &&
k<=khigh_hole)  )
                        %  ..........................
.....................

A{cellnum}(Counter,Counter)=A_cair;
                            % 'A' value depends on
material; no b_xyz because this is not source


                    % filter for the inner air
                    elseif( (i>=ileft_inair     &&
i<=iright_inair) &&...
                            (j>=jbottom_inair   &&
j<=jtop_inair)   &&...
                            (k>=klow_inair      &&
k<=khigh_inair)  )
                        %  ..........................
.....................

A{cellnum}(Counter,Counter)=A_cair;
                            % 'A' value depends on
material; no b_xyz because this is not source
```

```
                    % filter for the metal box
                    elseif( (i>=ileft_m     &&
i<=iright_m) &&...
                            (j>=jbottom_m   &&
j<=jtop_m)   &&...
                            (k>=klow_m      &&
k<=khigh_m)  )
                        %  ..........................
.....................

A{cellnum}(Counter,Counter)=A_cmetal;
                        % 'A' value depends on
material; no b_xyz because this is not source
                    else

A{cellnum}(Counter,Counter)=A_cair;
                        % the rest is considered
material = air
                        % 'A' value depends on
material; no b_xyz because this is not source
                    end

                    %
#####################################################
###########

                    if(j~=1)
                        A{cellnum}(Counter,Counter-1)
= 1;
                    end
                    if(j~=lengthNy)
                        A{cellnum}(Counter,Counter+1)
= 1;
                    if(i~=1)
                        A{cellnum}(Counter,Counter-
lengthNx) = 1;
                    end
                    if(i~=lengthNx)

A{cellnum}(Counter,Counter+lengthNx) = 1;
                    end
                    end
                    if(k~=1)
                        A{cellnum}(Counter,Counter-
lengthNx*lengthNy) = 1;
                    end
                    if(k~=lengthNz)

A{cellnum}(Counter,Counter+lengthNx*lengthNy) = 1;
                    end
                end

                Counter=Counter+1;          % counter
from 1 t0 MxN points
            end
        end
    end
end
toc;

A=A{1};
disp(' ');
disp('---------------------------------');
disp('---DONE: Processing matrix A ---');
disp('---------------------------------');
disp(' ');

% ------------------- %
%|%%%%%%%%%%%%%%%%%%%|%
%|%% CLEAN UP #1  %%|%
%|%%%%%%%%%%%%%%%%%%%|%
% ------------------- %
%

% % % % % % -- reshape matrices in single column
% % % % % w=0.9; max_it=1000; tol=1e-4; %max_it=100000
% % % % % for cellnum = 1:total_current
% % % % %     disp(['   Current No. =
',num2str(cellnum),'/',num2str(total_current)]);
% % % % %
% % % % %     Hx_surf{cellnum} =
reshape(Hx_surf{cellnum},NoOfUnKnowns,1);
% % % % %     Hy_surf{cellnum} =
reshape(Hy_surf{cellnum},NoOfUnKnowns,1);
% % % % %     Hz_surf{cellnum} =
reshape(Hz_surf{cellnum},NoOfUnKnowns,1);
% % % % %
% % % % % %     Hx_surfinit{cellnum} =
reshape(Hx_surfinit{cellnum},NoOfUnKnowns,1);
% % % % % %     Hy_surfinit{cellnum} =
reshape(Hy_surfinit{cellnum},NoOfUnKnowns,1);
% % % % % %     Hz_surfinit{cellnum} =
reshape(Hz_surfinit{cellnum},NoOfUnKnowns,1);
% % % % %
% % % % % % -- calculate for [H?_obsv_surf] on plate
and reshpe [H?_obsv_surf] array
% % % % %     disp('Start SOR for Hx');toc;disp('-----
----------------');
% % % % %
[Hx_obsv_surf{cellnum},errHx1,errHx2,iterHx,flagHx] =
sor(A,zeros(NoOfUnKnowns,1),...
% % % % %         b_x{cellnum},w,max_it,tol);
% % % % %     disp('Start SOR for Hy');toc;disp('-----
----------------');
% % % % %
[Hy_obsv_surf{cellnum},errHy1,errHy2,iterHy,flagHy] =
sor(A,zeros(NoOfUnKnowns,1),...
% % % % %         b_y{cellnum},w,max_it,tol);
% % % % %     disp('Start SOR for Hz');toc;disp('-----
----------------');
% % % % %
[Hz_obsv_surf{cellnum},errHz1,errHz2,iterHz,flagHz] =
sor(A,zeros(NoOfUnKnowns,1),...
% % % % %         b_z{cellnum},w,max_it,tol);
% % % % % --  --  --  --  --  --  --  --  --  --  --
--  --
% % % % % % % % % -- calculate for [H?_obsv_surf] on
plate and reshpe [H?_obsv_surf] array
% % % % % % % %     disp('Start SOR for
Hx');toc;disp('----------------------');
% % % % % % % %
[Hx_obsv_surf{cellnum},errHx1,errHx2,iterHx,flagHx] =
sor(A,Hx_surfinit{cellnum},...
% % % % % % % %         b_x{cellnum},w,max_it,tol);
% % % % % % % %     disp('Start SOR for
Hy');toc;disp('----------------------');
% % % % % % % %
[Hy_obsv_surf{cellnum},errHy1,errHy2,iterHy,flagHy] =
sor(A,Hy_surfinit{cellnum},...
% % % % % % % %         b_y{cellnum},w,max_it,tol);
% % % % % % % %     disp('Start SOR for
Hz');toc;disp('----------------------');
% % % % % % % %
[Hz_obsv_surf{cellnum},errHz1,errHz2,iterHz,flagHz] =
sor(A,Hz_surfinit{cellnum},...
% % % % % % % %         b_z{cellnum
},w,max_it,tol);
% % % % % % --  --  --  --  --  --  --  --  --  --  --
--  --
% % % % % %
% % % % % % -- reshape matrices in [column X rows]
% % % % % %
Hx_obsv_surf{cellnum}=reshape(Hx_obsv_surf{cellnum}, .
..
% % % % % %         lengthNx, lengthNy, lengthNz);
% % % % % %
Hy_obsv_surf{cellnum}=reshape(Hy_obsv_surf{cellnum}, .
..
% % % % % %         lengthNx, lengthNy, lengthNz);
% % % % % %
Hz_obsv_surf{cellnum}=reshape(Hz_obsv_surf{cellnum}, .
..
% % % % % %         lengthNx, lengthNy, lengthNz);
% % % % % end
tStart2 = tic;
for cellnum = 1:total_current
    disp(['   Current No. =
',num2str(cellnum),'/',num2str(total_current)]);
    disp('---------------------------------------');
% -- calculate for [H?_obsv_surf] on plate and reshpe
[H?_obsv_surf] array
    disp('Start Ax=B for Hx');toc(tStart2);
    disp(['Timestamp:
',datestr(datetime('now','format','dd-MM-yyyy'))]);
    disp('     -.-.-.-.-.-.-.-.-.-.-.-.-.-.-');
    Hx_obsv_surf{cellnum} = A\b_x{cellnum};
    disp('End   Ax=B for Hx');toc(tStart2);
    disp(['Timestamp:
',datestr(datetime('now','format','dd-MM-yyyy'))]);
    disp('---------------------------------------');
    disp('Start Ax=B for Hy');toc(tStart2);
    disp(['Timestamp:
',datestr(datetime('now','format','dd-MM-yyyy'))]);
    disp('     -.-.-.-.-.-.-.-.-.-.-.-.-.-.-');
    Hy_obsv_surf{cellnum} = A\b_y{cellnum};
    disp('End   Ax=B for Hy');toc(tStart2);
    disp(['Timestamp:
',datestr(datetime('now','format','dd-MM-yyyy'))]);
    disp('---------------------------------------');
    disp('Start Ax=B for Hz');toc(tStart2);
    disp(['Timestamp:
',datestr(datetime('now','format','dd-MM-yyyy'))]);
    disp('     -.-.-.-.-.-.-.-.-.-.-.-.-.-.-');
    Hz_obsv_surf{cellnum} = A\b_z{cellnum};
    disp('End   Ax=B for Hz');toc(tStart2);
    disp(['Timestamp:
',datestr(datetime('now','format','dd-MM-yyyy'))]);
    disp('---------------------------------------');
end

%% uuuuuuuuuuuuuuuuuuuuuuuuuuuuuuuuuuu
% FIRST HALF
%% uuuuuuuuuuuuuuuuuuuuuuuuuuuuuuuuuuu
for cellnum = 1:total_current

    % -- reshape matrices in [column X rows]

Hx_obsv_surf{cellnum}=reshape(Hx_obsv_surf{cellnum}, .
..
        lengthNx, lengthNy, lengthNz);

Hy_obsv_surf{cellnum}=reshape(Hy_obsv_surf{cellnum}, .
..
        lengthNx, lengthNy, lengthNz);

Hz_obsv_surf{cellnum}=reshape(Hz_obsv_surf{cellnum}, .
..
        lengthNx, lengthNy, lengthNz);
end

% % :::debug:::
% for cellnum = 1:total_current
%     b_x{cellnum}=reshape(b_x{cellnum}, ...
%         lengthNx, lengthNy, lengthNz);
```

```
% end
% % :::debug:::


% -- plot biot-savat & PDE
H_mag_inair={zeros(size(Hx_obsv_surf{1}))};
H_magnitude_BSavat={zeros(size(Hx_obsv_surf{1}))};
pdif={};
pdifmax={};
% for cellnum = 1:total_current
%     for k = 1:lengthNz
%         for j = 1:lengthNy
%             for i = 1:lengthNx
%                 H_mag_inair{cellnum}(i,j,k) =
sqrt(Hx_obsv_surf{cellnum}(i,j,k)^2 ...
%                 +Hy_obsv_surf{cellnum}(i,j,k)^2 ...
%                 +Hz_obsv_surf{cellnum}(i,j,k)^2);
%
%                 H_magnitude_BSavat{cellnum}(i,j,k) =
sqrt(BXi{cellnum}(i,j,k)^2 ...
%                 +BYi{cellnum}(i,j,k)^2 ...
%                 +BZi{cellnum}(i,j,k)^2);
%
%
pdif{cellnum}=(H_magnitude_BSavat{cellnum}-
H_mag_inair{cellnum})./H_magnitude_BSavat{cellnum};
%
pdifmax{cellnum}=max(pdif{cellnum}(:));
%
%             end
%         end
%     end
% end


% % Filter/ focus on inner air
% changelog: Hx_foc --> Hx_inair
% changelog: Hx_focmetal --> Hx_onmetal
H_mag_foc={zeros(size(H_mag_inair{1}))};
Hx_inair={zeros(size(Hx_obsv_surf{1}))};
Hy_inair={zeros(size(Hy_obsv_surf{1}))};
Hz_inair={zeros(size(Hz_obsv_surf{1}))};
H_mag_focmetal=H_mag_foc;
Hx_onmetal=Hx_inair;
Hy_onmetal=Hy_inair;
Hz_onmetal=Hz_inair;

% Filter only the inner air
for cellnum = 1:total_current
    for k = 1:lengthNz
        for j = 1:lengthNy
            for i = 1:lengthNx
                if(     (i>=ileft_inair     &&
i<=iright_inair) &&...
                        (j>=jbottom_inair   &&
j<=jtop_inair)   &&...
                        (k>=klow_inair      &&
k<=khigh_inair)  )
                    Hx_inair{cellnum}(i,j,k)        =
Hx_obsv_surf{cellnum}(i,j,k);
                    Hy_inair{cellnum}(i,j,k)        =
Hy_obsv_surf{cellnum}(i,j,k);
                    Hz_inair{cellnum}(i,j,k)        =
Hz_obsv_surf{cellnum}(i,j,k);
                    H_mag_inair{cellnum}(i,j,k)     =
sqrt(Hx_inair{cellnum}(i,j,k)^2 ...

+Hy_inair{cellnum}(i,j,k)^2 ...

+Hz_inair{cellnum}(i,j,k)^2);
                end
            end
        end
    end
end
% Filter only the metal box
for cellnum = 1:total_current
    counter=1;
    for k = 1:lengthNz
        for i = 1:lengthNx
            for j = 1:lengthNy
                if(     (i>=ileft_m     &&
i<=iright_m) &&...
                        (j>=jbottom_m   && j<=jtop_m)
&&...
                        (k>=klow_m      &&
k<=khigh_m)  )

Hx_onmetal{cellnum}(i,j,k)=Hx_obsv_surf{cellnum}(i,j,k
);

Hy_onmetal{cellnum}(i,j,k)=Hy_obsv_surf{cellnum}(i,j,k
);

Hz_onmetal{cellnum}(i,j,k)=Hz_obsv_surf{cellnum}(i,j,k
);
                    counter=counter+1;
                end
                if(     (i>=ileft_inair     &&
i<=iright_inair) &&...
                        (j>=jbottom_inair   &&
j<=jtop_inair)   &&...
                        (k>=klow_inair      &&
k<=khigh_inair)  )
                    Hx_onmetal{cellnum}(i,j,k)      =
0;
                    Hy_onmetal{cellnum}(i,j,k)      =
0;
                    Hz_onmetal{cellnum}(i,j,k)      =
0;
                end
                if(     (j>=ileft_hole     &&
j<=iright_hole) &&...
                        (i>=jbottom_hole   &&
i<=jtop_hole)   &&...
                        (k>=klow_hole      &&
k<=khigh_hole)  )
                    Hx_onmetal{cellnum}(i,j,k)      =
0;
                    Hy_onmetal{cellnum}(i,j,k)      =
0;
                    Hz_onmetal{cellnum}(i,j,k)      =
0;
                end
            end
        end
    end
end

dxyz = (dx+dy+dz)/3;

Nx_foc = Nx(ileft_inair):dxyz:Nx(iright_inair);
Ny_foc = Ny(jbottom_inair):dxyz:Ny(jtop_inair);
Nz_foc = Nz(klow_inair):dxyz:Nz(khigh_inair);
% % ------------------------------------------------
------------------
Nx_focmetal = Nx(ileft_m):dxyz:Nx(iright_m);
Ny_focmetal = Ny(jbottom_m):dxyz:Ny(jtop_m);
Nz_focmetal = Nz(klow_m):dxyz:Nz(khigh_m);
% % ------------------------------------------------
------------------


% % find proper scale
a1 = cell2mat(H_mag_inair);
a2 = cell2mat(H_magnitude_BSavat);
% PDE self scale
caxis_max1=abs(max(a1(:)));
caxis_min1=abs(min(a1(a1>0)));
% BSavat self scale
caxis_max2=abs(max(a2(:)));
caxis_min2=abs(min(a2(:)));
% PDE && BSavat scale
caxis_max3=abs(max([a2(:);a1(:)]));
caxis_min3=abs(min([a2(:);a1(:)]));
[Xq,Yq,Zq] = ait_gen_XYZ_axis(Nx,Ny,Nz,dx,dy,dz);
[Xq_foc,Yq_foc,Zq_foc] =
ait_gen_XYZ_axis(Nx_foc,Ny_foc,Nz_foc,dx,dy,dz);
[Xq_focmetal,Yq_focmetal,Zq_focmetal] =
ait_gen_XYZ_axis(Nx_focmetal,Ny_focmetal,Nz_focmetal,d
x,dy,dz);
[Xmesh,Ymesh,Zmesh] = meshgrid(Nx,Ny,Nz);

% caxis_max1temp=real(max(H_magnitude{1}(:)));
% caxis_min1temp=real(min(H_magnitude{1}(:)));
% caxis_max2temp=real(max(H_magnitude_BSavat{1}(:)));
% caxis_min2temp=real(min(H_magnitude_BSavat{1}(:)));


% % - plot quiver for PDE

quiverscale = 1;
dxyz = (dx+dy+dz)/3;
for cellnum = 1:total_current
    figure;
    quiver3(Xmesh,Ymesh,Zmesh,...
        abs(Hx_inair{cellnum}),...
        abs(Hx_inair{cellnum}),...
        abs(Hx_inair{cellnum}),quiverscale);
    axis([Nx(1)-2*dxyz Nx(end)+2*dxyz Ny(1)-2*dxyz
Ny(end)+2*dxyz Nz(1)-2*dxyz Nz(end)+2*dxyz])
    xlabel('X-axis'), ylabel('Y-axis'), zlabel('Z-
axis')
    title('plot quiver for PDE (inner air)');

    ait_draw_box_line
end

for cellnum = 1:total_current
    figure;
    q = quiver3(Xmesh,Ymesh,Zmesh,...
        abs(Hx_onmetal{cellnum}),...
        abs(Hy_onmetal{cellnum}),...
        abs(Hz_onmetal{cellnum}),quiverscale);
    axis([Nx_focmetal(1)-2*dxyz
Nx_focmetal(end)+2*dxyz ...
        Ny_focmetal(1)-2*dxyz
Ny_focmetal(end)+2*dxyz ...
        Nz_focmetal(1)-2*dxyz
Nz_focmetal(end)+2*dxyz])
    xlabel('X-axis'), ylabel('Y-axis'), zlabel('Z-
axis')
    title('plot quiver for PDE (metal)')

    ait_draw_box_line
end

for cellnum = 1:total_current
    figure;
    density = 1;
    streamslice(Xmesh,Ymesh,Zmesh,...
                abs(Hx_onmetal{cellnum}),...
                abs(Hy_onmetal{cellnum}),...
```

```
                abs(Hz_onmetal{cellnum}),...
                [Nx(2) Nx(end-1)],...
                [Ny(2) Ny(end-1)],...
                [Nz(2) Nz(end-1)],density);
    axis([Nx_foc(1)-4*dxyz Nx_foc(end)+4*dxyz
Ny_foc(1)-4*dxyz Ny_foc(end)+4*dxyz Nz_foc(1)-4*dxyz
Nz_foc(end)+4*dxyz])
    xlabel('X-axis'), ylabel('Y-axis'), zlabel('Z-
axis')
    title('plot quiver for PDE focus (on metal)')
    grid on
    ait_draw_box_line
end


% % % Hx_inair_inv = {zeros(size(Hx_inair{cellnum}))};
% % % Hy_inair_inv = {zeros(size(Hy_inair{cellnum}))};
% % % Hz_inair_inv = {zeros(size(Hz_inair{cellnum}))};
% % % H_mag_inair_inv =
{zeros(size(H_mag_inair{cellnum}))};
% % % Hx_inair_inv{cellnum}=
PDE_swapXYaxis(Hx_inair{cellnum},lengthNx,lengthNy,len
gthNz,total_current);
% % % Hy_inair_inv{cellnum}=
PDE_swapXYaxis(Hy_inair{cellnum},lengthNx,lengthNy,len
gthNz,total_current);
% % % Hz_inair_inv{cellnum}=
PDE_swapXYaxis(Hz_inair{cellnum},lengthNx,lengthNy,len
gthNz,total_current);
% % % H_mag_inair_inv{cellnum}=
PDE_swapXYaxis(H_mag_inair{cellnum},lengthNx,lengthNy,
lengthNz,total_current);
% % % for cellnum = 1:total_current
% % %     figure;
% % %     quiverscale = 1;
% % %     q = quiver3(Xmesh,Ymesh,Zmesh,...
% % %         abs(Hx_inair_inv{cellnum}),...
% % %         abs(Hy_inair_inv{cellnum}),...
% % %         abs(Hz_inair_inv{cellnum}),quiverscale);
% % %     axis([Nx(1)-2*dxyz Nx(end)+2*dxyz Ny(1)-
2*dxyz Ny(end)+2*dxyz Nz(1)-2*dxyz Nz(end)+2*dxyz])
% % %     xlabel('X-axis'), ylabel('Y-axis'),
zlabel('Z-axis')
% % %     title('plot quiver for PDE (inner air)');
% % %     ait_draw_box_line
% % %
% % %     density = 1;
% % %     streamslice(Xmesh,Ymesh,Zmesh,...
% % %
abs(Hx_inair_inv{cellnum}),...
% % %
abs(Hy_inair_inv{cellnum}),...
% % %
abs(Hz_inair_inv{cellnum}),...
% % %                             [Nx(3) Nx(end-
2)],...
% % %                             [Ny(3) Ny(end-
2)],...
% % %                             [Nz(3) Nz(end-
2)],density);
% % %     axis([Nx_foc(1)-4*dxyz Nx_foc(end)+4*dxyz
Ny_foc(1)-4*dxyz Ny_foc(end)+4*dxyz Nz_foc(1)-4*dxyz
Nz_foc(end)+4*dxyz])
% % %     xlabel('X-axis'), ylabel('Y-axis'),
zlabel('Z-axis')
% % %     title('plot quiver for PDE focus (inner air)
- meshgrid')
% % %
% % %     ait_draw_box_line
% % % end

% % - plot slices for PDE with mesh
for cellnum = 1:total_current
    xslice = [];
    yslice = [];
    zslice = 1:1:5;
    zslice = Nz;
    figure;
    title('plot slices for PDE with mesh');

s=slice(Xmesh,Ymesh,Zmesh,abs(H_mag_inair{cellnum}),xs
lice,yslice,zslice);
    view(3);
    xlabel('X-axis'), ylabel('Y-axis'), zlabel('Z-
axis')

    caxis([caxis_min1,caxis_max1]);

%     axis([Nx(1)-1 Nx(end)+1 Ny(1)-1 Ny(end)+1 Nz(1)-
1 Nz(end)+1])
    for n=1:length(s)

set(s(n),'alphadata',get(s(n),'cdata'),'facealpha','fl
at','edgecolor','none')
    end
end

% % - plot slices for PDE without mesh
for cellnum = 1:total_current
    xslice = [];
    yslice = [];
    zslice = 1:1:5;
    zslice = Nz;
    figure;
    title('plot slices for PDE without mesh');
    xlabel('X-axis'), ylabel('Y-axis'), zlabel('Z-
axis')

s=slice(Xmesh,Ymesh,Zmesh,abs(H_mag_inair{cellnum}),xs
lice,yslice,zslice);
    view(3);
    caxis([caxis_min1,caxis_max1]);

%     axis([Nx(1)-1 Nx(end)+1 Ny(1)-1 Ny(end)+1 Nz(1)-
1 Nz(end)+1])
    for n=1:length(s)

set(s(n),'alphadata',get(s(n),'cdata'),'facealpha','fl
at','edgecolor','none')
    end
    ait_draw_box_line
end


disp('---DONE---');
toc(tStart2)

datestamp_end = datestr(datetime('now','format','dd-
MM-yyyy'));
disp(['Start time : ',datestamp_start]);
disp(['End time   : ',datestamp_end]);

%% uuuuuuuuuuuuuuuuuuuuuuuuuuuuuuuuuu
datestamp = datestr(datetime('now','format','dd-MM-
yyyy'));
datestamp = strcat(datestamp(1:11),'-
',datestamp(13:14),datestamp(16:17),datestamp(19:20));
eval(sprintf('save %s_rosi_stdcur_dxdydz0p02_%s_v3.mat
',datestamp,hole_num));
%% uuuuuuuuuuuuuuuuuuuuuuuuuuuuuuuuuu
```

Appendix C: Publications

1. A. I. Tarmizi; Mihai D. Rotaru; Jan K. Sykulski. Electromagnetic compatibility studies within smart grid automated substations. Power Engineering Conference (UPEC), 2014 49th International Universities. 2014.
2. A. I. Tarmizi; Mihai D. Rotaru; Jan K. Sykulski. Magnetic field calculations within substation environment for EMC studies. 2016 IEEE 16th International Conference on Environment and Electrical Engineering (EEEIC).2016.
3. A. I. Tarmizi; R.H. Ramlee, Mihai D. Rotaru. Electromagnetic Compatibility Studies of Substation Environment using Finite Difference Method. International Journal of Engineering & Advanced Technology (IJEAT).2019.
4. A. I. Tarmizi; R. H. Ramlee; Hybrid Combination of Biot Savart Law and Finite Difference Method for Magnetic Field calculation within Substation's EMC Studies (Draft), IET High Voltage Journal.

Electromagnetic Compatibility Studies within Smart Grid Automated Substations

A. I. Tarmizi
University of Southampton, UK
Universiti Teknikal Malaysia Melaka
ait1g12@ecs.soton.ac.uk

Mihai D. Rotaru
University of Southampton, UK
mr@ecs.soton.ac.uk

Jan K. Sykulski
University of Southampton, UK
jks@soton.ac.uk

***Abstract*- Switching, fault currents, lightning and other transient phenomena produce electromagnetic fields that may disturb the normal functioning of a high voltage power substation. With the advent of the 'smart grid' – where electronic control and communication equipment are integrated within the substation – understanding of the electromagnetic environment and the resulting interferences is becoming very important. This paper uses an example of a particular 400/220kV substation in Romania to analyse its behaviour from the point of view of transient stability and faults. The results of the transient analysis in terms of currents will then be used to excite an electromagnetic model with the aim to predict the field distribution within the substation during the transient. These results will in turn be used to identify the EMI 'hot spots' within the substation.**

***Index Terms*-- EMI, fault analysis, smart grid, substation, transient stability.**

I. Introduction

Power systems need to operate under increasingly complex conditions and situations. The recent large implementation and penetration of renewable generation and demand have introduced new challenges to the operation of the electric grid. To cope with these challenging conditions the overall system's operation requires new and innovative approaches in order to enhance the performances of the power grid. One of the novel ways is the concept of a smart grid. Sensing nodes, communication networks and information systems are embedded and integrated into the power network to create a 'smart' grid that is able to manage almost autonomously all operating conditions by itself. A smart grid is a power system that enables real-time communication and control between the consumer and the utility such that the energy usage is optimised. It is able to consider different aspects, such as cost and technical and environmental constrains, when providing an optimum power supply to the customer. To operate in such a mode the smart grid will utilise digital information technology to create a more efficient, reliable and responsive network that is flexible. Communication within a smart grid will not be limited to that between the consumer and the utility only, but will include channels between digital relays, so that information could be exchanged between relays without necessarily involving the control centre. This type of communication networking will provide a self-managing capability that will allow the smart grid to develop different strategies in the protection and control of the system. The smart grid architecture aims to provide overall power network monitoring, create control strategies to maintain the system performance and security and reduce the cost of operation, maintenance and system availability planning. The control built within a smart grid will allow the flexibility to handle distributed resources, stochastic demand, to adapt to new conditions of operation and to respond in an optimal manner to smart appliances connected to the grid [1-7].

Consequently, a smart grid has the potential to improve the efficiency and reliability of the power delivery; however, due to its increased complexity and dependence on technologies that were not previously part of the power grid, the smart grid may be susceptible to factors that will affect negatively its normal functioning. Some of these factors result from Electromagnetic Interference (EMI). All power grid devices are exposed to electromagnetic (EM) fields of natural or man-made origin, radiated directly into devices or conducted via the power, signal or ground connections. A smart grid may contain a large number of data communication channels, in support of applications with divergent functions, which can all be degraded by electromagnetic interference. These functions have different reliability requirements, correlating with different levels of data flow reliability, and may require different radiated and conducted immunity levels [8].

Our research aims to develop the understanding of the electromagnetic environment in which the smart grid will function and identify possible EMC/EMI issues. EMC has to be considered to ensure continuous reliable operation in many locations where the smart grid equipment may operate. Components and devices in the smart grid system are subjected to a wide range of conducted and radiated noise sources that are disruptive to all electronic equipment.

The substations in a power network afford one of the most severe electromagnetic environments where the equipment of a smart grid has to function correctly and reliably. The term "substation" describes the physical location in the grid that contains transformers, circuit breakers, capacitor banks, voltage regulators, sensors, protective relays and other equipment necessary for controlling and distributing electric power. Substations provide critical interconnections and are located throughout the grid for generation (as part of a power plant), transmission and distribution systems, and for distributed generation (DG) projects. The primary voltages at these substations will vary depending on the location. These substations can be as simple as a few circuit breakers or include complex systems covering large areas. For the purpose of this EMI discussion, the substation EM environment is defined as an area of high EM fields, including transients from switching that are higher than those found in other portions of the distribution system. The

physical substation environment is generally the area bounded by a grounded fence around the substation yard and/or building and the area extending a few meters outside the fence [8]. Substations are very complex in their protection and control schemes.

The microprocessor-based protective relays have recently been replacing electromechanical ones, especially at major substations. These devices not only offer protection, but also act as intelligent electronic devices (IEDs) that perform control functions, metering, substation automation, etc. The communication between these devices is currently serial using copper wires; the trend, however, is to replace wires between devices with Station Bus technology using Ethernet IP connectivity over fibre-optic cable and to network communication protocols for new or expanded installations. The power line carrier (PLC) transmitters/receivers, microwave and optical fibre communication multiplexers used in conjunction with protective relays to provide pilot protection schemes are now IEDs.

In this work, we have analysed – through simulation – a high voltage substation. The aim was to build a simulation model capable of simulating the transient processes and phenomena that can produce EMC noise that may potentially affect the smart grid equipment within the substation. This paper has analysed the behaviour of a 400/220kv high voltage substation in Romania called Rosiori for the transient stability and fault analysis. The results of the transient analysis in terms of currents will be used as excitation in an electromagnetic model of the substation with the aim to find electromagnetic field distribution. These results will then be used to identify EMI 'hot spots' within the substation. The placement of the sensitive control electronic equipment will be optimized so that the hot spots are avoided, hence reducing the danger of equipment malfunction.

II. SMART GRID AUTOMATED SUBSTATION

In substations the power grid equipment is installed, such as transformers, circuit breakers, capacitor banks, voltage regulator protection relays, sensors and control equipment for power system operation. Currently, the majority of this conventional equipment relies on mechanical components. There is a trend, however, to replace electromechanically actuated relays with microprocessor based relays, especially in major substations. These new relays can act as intelligent electronic devices and perform extra duties, such as control and metering.

Substation automation systems are categorised into three hierarchical levels, which are found in most implementations as physical levels (Fig. 1) [8]. The levels are referred to as: the process level, the bay level and the station level. The process level refers to the individual power system equipment in the substation represented by the process interface, e.g. circuit breakers, transformers, electronic current transformers (ECT), electronic voltage transformers (EVT) and merging units. The bay level consists of bay protection and control IEDs hosting the related functions. The station level consists typically of the substation computer with central functions, human machine interface (HMI) and the gateway to the network control centre. The station and bay levels are connected by the station bus. The bay and process levels are nowadays still connected by a lot of parallel copper wires but in the near future, as the need for more information exchange increases, these will be replaced by a process bus. A comprehensive set of standards, the IEC61850 series, has been developed to define the requirements for such communication networks and systems in substations [9].

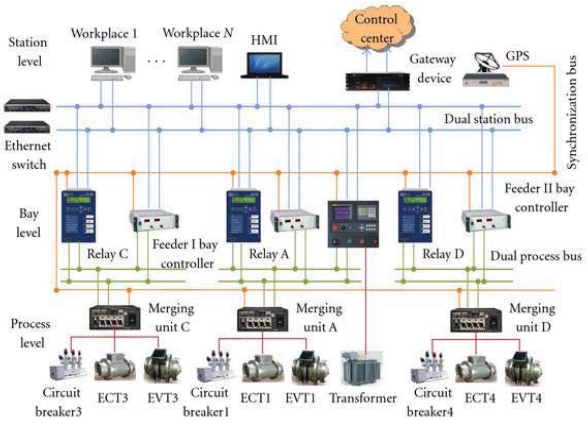

Fig. 1 The system architecture of a substation automation system [8]

Currently, most of the automated substations present a heterogeneous mixture of technologies where the modern IEC61850 structure works in parallel with an analog instrumentation channel serving a relay which will usually actuate an electromechanical protection device.

One of the important elements of an automatic substation is the merging unit (MU) (Fig 1). The merging units are analog to digital data collection devices which sample and digitize electrical quantities. The electrical quantities are analog or digital signals which are of interest. Analog quantities include voltage and current signals from potential transformers (PTs) and current transformers (CTs), transformer temperature signals from resistance temperature detectors (RTDs), transformer turns ratios from potentiometers, etc. Digital quantities include auxiliary contact outputs.

The MUs are placed physically close to the signals which they monitor. This arrangement minimises the potential for signal corruption under normal equipment exploitation. The MUs include usually a weatherised exterior suitable for outdoor and extreme physical conditions common in substations. Although these MUSs are tested to conform to standards such as IEC 60255-25, IEC 60255-22-4 and IEC 61000-4-3, this may not be enough as field levels than can exist within substations could be larger [11,14] than the ones specified by the above mentioned standards. Therefore, there is a need to develop methodologies and simulation tools that allow prediction and calculation of electromagnetic field emissions in such environments.

III. SUBSTATION SIMULATION MODEL

In this research, a specific case of a power substation located in Romania at Rosiori is used. Although at the

moment this substation is not integrated with IEDs, it will be useful to understand the electromagnetic environment in such a substation prior to installing the IDES.

As the first stage of this study, the substation was modelled using ERACS [17], a power system analysis software. There are several solvers available within ERACS: load flow, fault analysis, harmonic impedance and transient stability solvers. The main aim of this part of the study was to quantify and understand the transient currents that may occur within the substation equipment while different transient phenomena take place.

The substation consists of three outgoing feeders and one compensation coil, together with an autotransformer, at 400kV and three outgoing feeders on the 220 kV side. The details of the Rosiori 400/220 kV substation components are presented in Table 1 [12].

TABLE I
ROSIORI SUBSTATION COMPONENTS

Components of 400kV power station	
1	Overhead line Gadalin
2	Overhead line Mukachevo
3	Overhead line Oradea
4	400MVA Autotransformer 400/220 KV
5	100MVAr Reactance coil 400 KV
Component of 220kV power station	
1	Overhead line Vetis
2	Overhead line Baia Mare – double circuit

The results of the load flow simulation, and then transient stability studies while applying fault at each of the busbars as disturbances within the Rosiori substation, are detailed in the following sections.

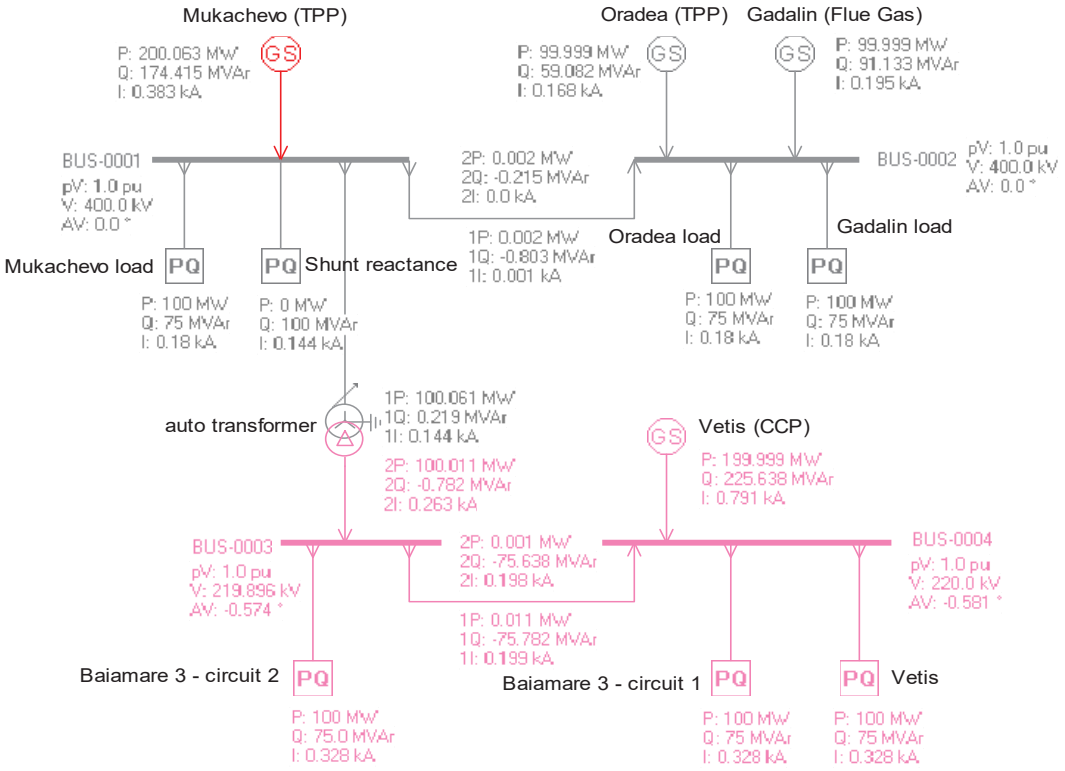

Fig. 2 Load flow analysis of Rosiori substation.

A. *Load Flow Analysis*

There are several purposes of load flow analysis, such as to calculate the steady state operation conditions of the power generation or transmission system for a given set of busbar loads; however, for the case under consideration the load flow analysis was necessary for the subsequent transient stability study. The results of the load flow analysis for the Rosiori substation are presented in Fig 2.

Based on the load flow analysis, the total real power generation (PG) is 600.74MW which is sufficient for real power demand at load (PL) of 600MW. The total generated reactive power (QG) is 564.796MVAr satisfying the necessary reactive power at the load (QL) of 550MVAr. Table II shows the summary of the results of the load flow analysis for the Rosiori substation using ERACS.

TABLE II
RESULT OF LOAD FLOW ANALYSIS

Loadflow			
PG:	600.061 MW	Vmx:	BUS-0003
QG:	550.269 MVAr	pVmn:	1.0 pu
PL:	600 MW	Vmn:	BUS-0004
QL:	550 MVAr	I3Fmx:	19.106 kA
PLO:	0.061 MW	3Fmx:	BUS-0004
QLO:	0.268 MVAr	I3Fmn:	12.644 kA
Base:	100 MVA	3Fmn:	BUS-0002
Hz:	50 Hz	Iter:	218
pVmx:	1.0 pu	Conv:	4.8578E-6

B. *Fault Analysis*

Under normal conditions of operation the maximum magnetic field intensity within 400 to 500 kV substations, such as Rosiori, is expected to be between 1.5 to 3 A/m [14]. This level of magnetic field intensity should be tolerated by the merging units. However, in the case of a short circuit fault, intensities as high as 160 A/m have been reported [14]. Such large magnetic field intensity values can damage electronic equipment such as MUs. To calculate the magnetic field one first has to calculate the fault current. In this work the fault analysis option within ERACS has been used to calculate the fault currents and voltages. The following scenarios have been simulated: a single phase to earth, phase to phase, two phases to earth, and a three phase short circuit fault. These faults are applied at all busbars in the circuit model. The summary of fault analysis results is presented in Table III. The maximum fault current observed for these simulations is when a phase to phase and two phases to earth faults are applied at BUS 3. For these cases the fault current magnitude is 12.306 kA.

TABLE III
RESULT OF FAULT ANALYSIS

Element	Fault type (kA)			
	Single phase to earth (kA)	Phase to phase (kA)	Two phase to earth (kA)	Three phase (kA)
Busbar 1	IL1: 10.299 IL2: 0 IL3: 0	IL1: 0 IL2: 7.796 IL3: 7.796	IL1: 0 IL2: 8.05 IL3: 9.189	IL1: 7.382 IL2: 7.382 IL3: 7.382
Busbar 2	IL1: 10.169 IL2: 0 IL3: 0	IL1: 0 IL2: 7.783 IL3: 7.783	IL1: 0 IL2: 8.001 IL3: 9.108	IL1: 7.378 IL2: 7.378 IL3: 7.378
Busbar 3	IL1: 0.001 IL2: 0 IL3: 0	IL1: 0 IL2: 12.306 IL3: 12.306	IL1: 0 IL2: 12.306 IL3: 12.306	IL1: 11.918 IL2: 11.918 IL3: 11.918
Busbar 4	IL1: 0.001 IL2: 0 IL3: 0	IL1: 0 IL2: 12.258 IL3: 12.258	IL1: 0 IL2: 12.258 IL3: 12.258	IL1: 11.866 IL2: 11.866 IL3: 11.866

C. *Transient Stability Analysis*

Following the fault analysis a transient stability analysis was undertaken. For such analysis the assumption is that the dynamics of the system is dominated by the transient behaviour of motor loads, generators and governors AVRs. This implies that transmission time delays and distribution network mesh time constants are negligibly small compared with the motor and the generator behaviour [13].

For the Rosiori substation case the results of the transient stability analysis simulations, when a three phase short-circuit fault has been applied to BUS 1, are presented in Fig. 3. The currents in each phase (L1, L2, L3) and the AC and DC components of the fault current are shown. As the data about the four generators connected to the system – Mukachevo, Oradea, Gadalin and Vetis – was not readily available for the transient stability simulation, typical average values of the synchronous-machines constants were assumed [16]. For the above situation the simulation results show that there is a sudden drop in power at 0.05s; however, the system tries to recover to a stable state. This will result in the oscillating transient state shown graphically in Figs 3, 4 and 5.

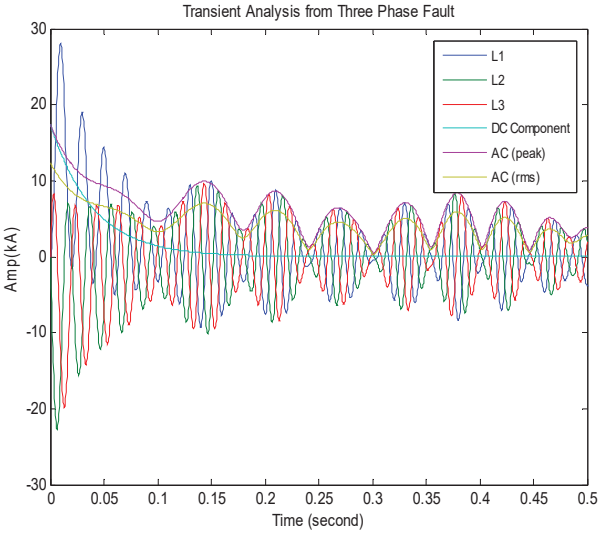

Fig. 3 Transient analysis results due to 3-phase fault at BUS 1.

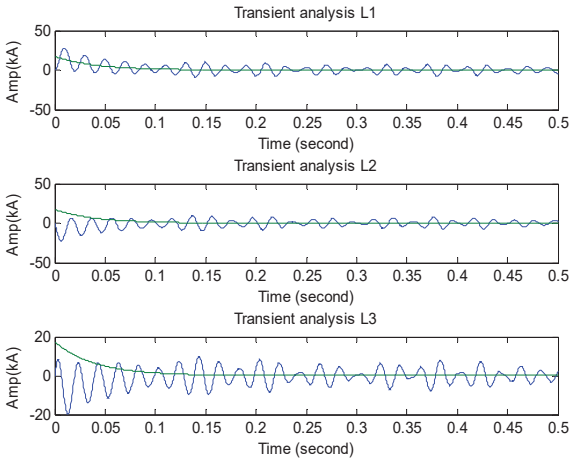

Fig. 4 Transient currents for each of the 3 phase (3phase fault at BUS 1)

From the point of view of the EMC/EMI analysis there is a need to understand not only the magnitude of the fault currents but also their harmonic content. Higher frequency currents are expected to be more detrimental in terms of coupling to other equipment within the substation. A Fast Fourier Technique (FFT) in Matlab was employed to determine the harmonic content of the transient currents obtained from the ERACS simulation. The results of the FFT analysis are summarised below in Fig. 6.

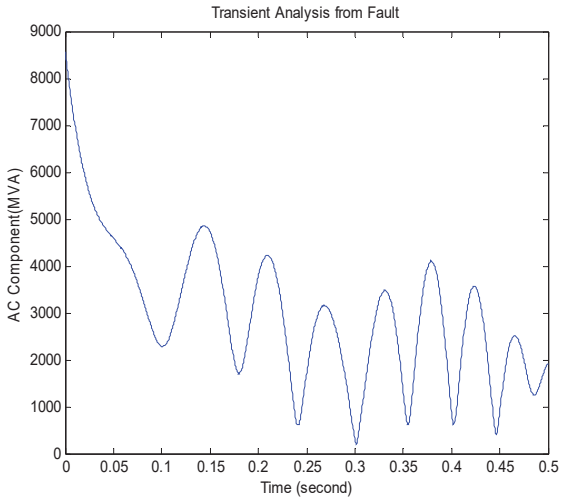

Fig. 5 AC component of the transient power

As shown in Fig. 6 the symmetrical component of the fault currents has the largest magnitude around 6 kA and the same frequency as the fundamental harmonic (50 Hz). The DC component of the asymmetrical fault currents has smaller amplitude of about 2.8 kA.

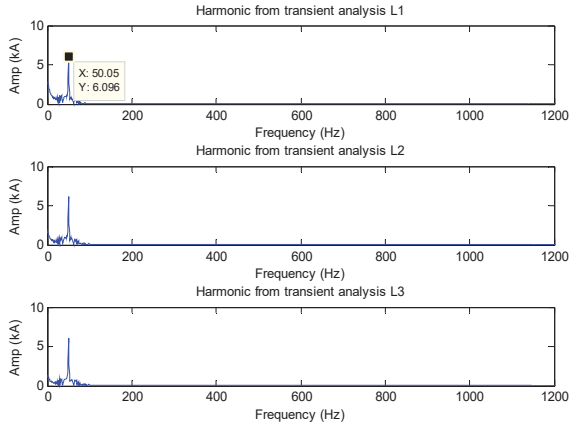

Fig. 6 Harmonic for each phase

It is clear from the results of the FFT analysis that there are no significant higher harmonic currents excited when a transient stability simulation is considered. Hence the only aspect that has to be considered from the EMC/EMI point of view is the magnitude of the currents and their flowing paths within the substation.

IV. Conclusions and Future Work

Fault current and transient stability simulations of the Rosiori substation were successfully completed using commercial package ERACS. The analysis assumed that the substation is connected to a large grid. The harmonic content of the asymmetrical fault currents calculated by ERACS was determined using the FFT analysis in Matlab. It has been shown that most of the power existent in the transient signal is either DC or the fundamental harmonic (50Hz), hence for EMC/EMI analysis the magnitude of the current will be the most important parameter. Going further the results of the transient analysis and fault analysis in terms of currents will be used in the future to excite an electromagnetic model of the Rosiori substation such that the electromagnetic field distributions within the substation will be obtained for these currents. These results will in turn be used to identify the EMI 'hot spots' within the substation. Another aspect that that will be studied is the transient effects when switching of a disconnector or a circuit breakers, especially in the case of inductive loads, takes place. The switching and disconnecting is expected to produce transient currents with much higher harmonic content which may couple significant energy through common-mode currents to electronic equipment installed in the substation switchyard.

References

[1] P. Zhang, F. Li, and N. Bhatt, "Next-generation monitoring, analysis, and control for the future smart control centre," *IEEE Trans. Smart Grid*, vol. 1, no. 2, pp. 186–192, 2010.

[2] M. Shahraeini, M. H. Javidi, and M. S. Ghazizadeh, "Comparison between communication infrastructures of centralized and decentralized wide area measurement systems," *IEEE Trans. Smart Grid*, vol. 2, no. 1, pp. 206–211, Mar. 2011.

[3] K. Vu, M. M. Begouic, and D. Novosel, "Grids get smart protection and control," *IEEE Comput. Appl. Power*, vol. 10, no. 4, pp. 40–44, 1997.

[4] R. Abe, H. Taoka, and D. McQuilkin, "Digital grid: Communicative electrical grids of the future," *IEEE Trans. Smart Grid*, vol. 2, no. 2, pp. 399–410, Jun. 2011.

[5] L. Fangxing, Q.Wei, S. Hongbin, W. Hui, W. Jianhui, X. Yan, X. Zhao, and Z. Pei, "Smart transmission grid: Vision and framework," *IEEE Trans. Smart Grid*, vol. 1, no. 2, pp. 168–177, Sep. 2010.

[6] Mhedi Kiani, and Maysam Ghovanloo, "The circuit theory behind coupled-mode magnetic resonance-based wireless power transmission," *IEEE Trans. On Circuits and Systems*, vol. 59, No. 9, pp. 2065-2074, September 2012.

[7] J. Medina, N. Muller, and I. Roytelman, "Demand response and distribution grid operations: Opportunities and challenges," *IEEE Trans. Smart Grid*, vol. 1, no. 2, pp. 193–198, Sep. 2010.

[8] EMII WG/ Galene Koepke (chair), "Electromagnetic Compatibility and Smart Grid Interoperability Issues" *SGIP Electromagnetic Interoperability Issues Working Group*, SMART GRID INTEROPERABILITY PANEL SGIP Electromagnetic Interoperability Issues Working Group SGIP Document Number: 2012-005, Version 1.0., December 5, 2012.

[9] Xiang Lu, Wenye Wang, and Jianfeng Ma, " Authentication and Integrity in the Smart Grid: An Empirical Study in Substation Automation Systems," *Hindawi Publishing Corporation International Journal of Distributed Sensor Networks Volume 2012, Article ID 175262, 13 pages doi:10.1155/2012/175262.*

[10] M. Olofsson, " Power Quality and EMC in Smart Grid," *10th Intenational Conference Electrical Power Quality and Utilisation,* 2009.

[11] Claudia Imposimato, Jean Hoeffelman, Anders Eriksson, W.H. Siew, Pieter H. Pretorius and Paul S. Wong " EMI CHARACTERIZATION OF HVAC SUBSTATIONS – UPDATED DATA AND INFLUENCE ON IMMUNITY ASSESSMENT," *CIGRE Working Group 36.04,* CIGRE 2002.

[12] D. N. FÎTA, L. Muresan, C. Cheleman, and M. Grebenisan, "The Modelling of Rosiori Power Station 400/220/20 KV Retechnologized of Transelectrica Company. The Simulation of the Permanent Regime With EDSA Programme," *6TH International Conference Electromechanical and Power Systems,* 2007.

[13] ERA Technology, "Power System Analysis Software -Technical Manual," 2005.

[14] M. K. Kostin, M. V. Matveye, A. Ovsyannikov, V.S.Verbin and S. Zhivodernikov "SOME RESULTS OF EMC INVESTIGATIONS IN RUSSIAN SUBSTATIONS," *36-103,* CIGRE 2002.
[15] J. C. Das, "Transients in Electrical Systems - Analysis, Recognition, and Mitigation" *The McGraw-Hill Companies*, Inc. 2010
[16] J.D. Glover, M.S. Sarma and T.J. Overbye, "Power System Analysis and Design", *Cengage Learning 2011*, Fifth ed., SI.
[17] ERACS, http://www.eracs.co.uk/

Magnetic field calculations within substation environment for EMC studies

A. I. Tarmizi
University of Southampton, UK
Universiti Teknikal Malaysia Melaka
ait1g12@soton.ac.uk

Mihai D. Rotaru
University of Southampton, UK
mr@ecs.soton.ac.uk

Jan K. Sykulski
University of Southampton, UK
jks@soton.ac.uk

***Abstract*— The electromagnetic environment within high voltage substations needs to be correctly predicted and quantified especially as more and more sensitive microelectronic devices are introduced in proximity to the switching devices in the switchyard. This trend will only increase with the advent of the 'smart grid'; therefore there is a need to re-evaluate the substation environment for EMC assessment, accounting for new scenarios. In this paper, the magnetic field distribution within a substation is calculated using an in-house developed numerical algorithm within Matlab. The flow of current in the substation is used as an input to the code and fields within the substation are then evaluated. The reported code can calculate the magnetic field distribution within an air insulated (AIS) high voltage substation under normal operating conditions as well as for the case of a lightning strike situation.**

Keywords*— EMC; magnetic field; Matlab; Digsilent PowerFactory; lightning current;

I. INTRODUCTION

The ability of an equipment or system to function satisfactorily in its electromagnetic environment without introducing intolerable electromagnetic disturbances to anything in that environment is known as Electromagnetic Compatibility (EMC) [1]. In a high voltage substation, while the components and equipment are operating, electric and magnetic fields are produced that might or might not cause interruption to the system; thus it is important to make sure that the system is compatible and immune to electromagnetic interferences [2, 3].

EMC in power systems is a topic which has been widely covered in literature. However, there has been limited work done on the EMC within an automated substation, especially in the context of a smart grid implementation. Substation automation is a term applied to an electrical substation that manages the operation between distributed intelligent electronic devices (IEDs) interconnected by communication networks [4]. This implies that microelectronic devices, such as microcontrollers and microprocessors, which provide the 'intelligence', are being installed closer to high voltage and high power switching devices within the switchyard of high voltage substations. In this context, it is important that the electromagnetic field distribution within a substation is well understood so that possible EMC hazards are minimised. Measurements and/or simulations can be employed to build a picture of the field distribution within the area of interest. Deciding on which method to use depends on many factors; however, in most of the published work, both approaches are used [5-8]. Usually computational methods are used to test cases that are difficult or impossible to be measured, such as lightning strikes; on the other hand, numerical methods are normally validated against a set of measurements [5].

Under normal operating conditions a high voltage substation system produces electric and magnetic fields at low frequency, 50Hz or 60Hz. However, high frequency fields can also be generated due to disturbances that occur in the system, such as switching and lightning strikes. According to [9] frequencies up to 30GHz can be generated by disturbances occurring naturally or due to man-made sources.

From a health and safety point of view, these generated fields should be within the range of health regulations and EMC standards, with different countries setting their own national standards. The majority of the national guidelines are set by the International Commission on Non-Ionizing Radiation Protection (ICNIRP) which is recognized by the World Health Organization (WHO) as a non-governmental organization that evaluates scientific results from all over the world. The limits recommended by the ICNIPR and WHO are summarized in Table I [10].

TABLE I. ICNIRP EXPOSURE GUIDELINES AT POWER FREQUENCY 50HZ

	Magnetic field intensity, H (A/m)	**Magnetic flux density, B (μT)**
Public exposure limits	80	100
Occupational exposure limits	400	500

II. CALCULATION OF MAGNETIC FIELDS WITHIN A SUBSTATION

Under normal operating conditions magnetic and electric fields exist around the current carrying equipment within the substation. It is expected that the highest magnitude of the fields will be observed around the paths that carry the highest currents. However, there are various factors affecting the level of the fields, such as current magnitude, phase spacing, bus height, phase configuration, distance from the source and the phase unbalance. It is rather difficult to predict the distribution of magnetic field in the substation environment using popular numerical methods, such as finite differences and finite elements, mainly because of the large size of the electromagnetic problem to be solved; these methods will struggle with meshing large domains such as the whole substation environment. We have employed directly the Biot-Savart Law because of its simplicity and computational efficiency. Obviously all components and equipment structure and dimensions need to be included.

978-1-5090-2320-2/16/$31.00 ©2016 IEEE

According to the Biot-Savart Law the magnetic field due to a current element of length *dl* is given by [11]

$$\bar{H} = \frac{I}{4\pi}\int_{l} \frac{\bar{dl} \times \bar{R}}{R^2} \quad (1)$$

A simple MATLAB routine was developed to calculate the field in three dimensions (3D) within the air environment. The total magnetic field intensity, *H*, at each position (*x, y, z*) and at any instant of time *t* is then given by

$$H(x,y,z,t) = \hat{x}H_x(t) + \hat{y}H_y(t) + \hat{z}H_z(t) \quad (2)$$

$$|H| = \sqrt{H_x^2 + H_y^2 + H_z^2}$$

with superposition applied at every location. To illustrate the approach a particular substation has been considered.

A. Substation structure and modelling assumptions

For this work, the layout of the Rosiori substation was provided by the Technical University of Cluj, Faculty of Electrotechnics. The substation consists of a 400kV double busbar with three outgoing feeders that connect to three loads and a shunt reactor which is a compensation coil. The autotransformer then steps down the voltage to 220kV and finally there are three outgoing feeders on the 220kV side [12]. One of the reasons that this particular substation was chosen was the availability of magnetic and electric field measurements [7] which will be used to validate the developed calculation model.

In order to make the modelling tool efficient we decided to focus on the main sources of the magnetic field and thus neglect the less important influences. The first simplification was to include only the conductors above the ground, with the substation busbars treated effectively as transmission lines and currents and voltages of each branch computed. All other equipment, as well as the insulators, are neglected and thus only the magnetic field produced by the conductors in the substation is considered. Although there are some differences in the results when compared with the case where more details are accounted for, as discussed in [13], the errors are relatively minor and hence the simplification is considered acceptable. In fact the main difference observed and reported in [12] is not in the overall field distribution but rather in the finer details of the results, such as the closeness of the maximum field to the substation equipment. If the field is to be calculated far enough from the current paths the assumption used here is justified.

Another important substation component which would normally be considered is the transformer. The transformers installed in substations, however, are usually very well shielded, so that most of their magnetic field is confined within their casing; consequently, their contribution to the magnetic field of the outer environment is relatively small. It would be very expensive computationally to simulate the whole transformer [14], therefore – for this particular research study – only the connections between the transformer terminals and the cables are considered. This simplification appears to be fully justified for the normal operation of the system, but may need to be reconsidered in the case of a lightning strike situation, especially when the strike is close to the transformer.

B. Modelling procedures

The algorithm consists of two main steps. First, the geometry (and topology) of the substation is introduced to identify all conducting paths. Each path is then divided into sub-segments in the *xyz* coordinate system and currents are applied to each conductor. This information would usually come from a power flow solution provided by appropriate modeller (such as PowerFactory [15]) for normal operating conditions. The Biot-Savart Law is then applied to calculate the magnetic field generated by the applied currents. For the illustrative example reported in this paper, a plane grid of 6674 calculation points is arranged for the substation environment for magnetic field calculations. Along the *x* axis the increment is a 3m interval (*x*+3) and for the *y* axis it is a 2m interval (*y*+2) as illustrated in Fig. 1. With this algorithm the density of the calculation points can be easily modified to focus on regions of higher interest.

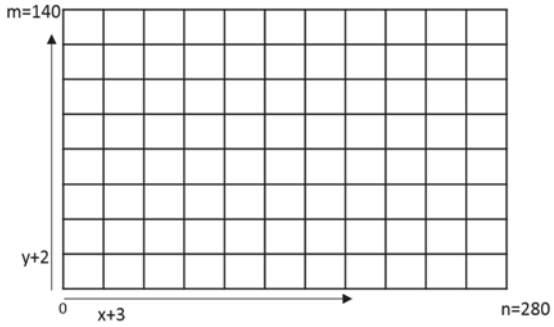

Fig. 1. A grid of points for magnetic field calculations for a substation.

The substation considered is 280m long, 140m wide and the conductors are located at the height of 12m above the ground (on the 400kV side). For such a large site, it takes almost 6 hours for a computer with Intel (R) Core (TM) 3.4GHz processor with 16GB of RAM to complete the magnetic field calculations for a matrix of points 94×71 in *x* and *y* axes, respectively. The generated magnetic field is studied at different levels from the ground by setting the height for *z* axis in the algorithm. In [16], the magnetic field was measured at three different heights based on the human body measurements, namely: the feet at 0m, the waist at 1m and the head at 1.75m. The computing times will obviously depend on the number of current inputs.

Two particular cases of magnetic field calculation have been considered. For the first case a normal distribution of three phase currents is assumed resulting from a load flow analysis. The second case introduces a lightning strike and associated current injected into substation conductors. Thus both the steady state and a particular disturbance have been considered. Although for the case of the lighting strike the assumptions introduced earlier on may be a little too restrictive, the results will nevertheless demonstrate the capability of the algorithm to cope with transient as well as steady-state currents. To show this capability a frequency domain analysis was also implemented and the results in terms of magnetic field intensity are presented and compared with the time domain analysis.

III. Magnetic Field Computational Results

A. Nominal input current

The Rosiori substation has the 400kV side connected to three loads, a shunt reactance and an auto transformer to step down the voltage to 220kV. The normal operating currents at frequency of 50Hz for each load, as listed in Table II, are used for the magnetic field calculations.

TABLE II. Operating currents of the Rosiori station 400kV side

Load Component	Operating current (A)
Load 1 (Mukacevo)	200
Load 2 (Oradea)	90
Load 3 (Gadalin)	28
Shunt Reactance	147

The magnetic field distribution can be evaluated at different heights from the ground, but for this particular substation this was calculated and plotted only at the height of 1.7m since the measurements were done at this height [6]. The predicted and experimental distributions will be compared in the context of the exposure limits.

The computed results for the normal operating currents are presented in Fig. 2. It shows that the predicted highest value of the magnetic field is 4.164A/m located along busbar 1, where it is connected to Load 1 with 200A. The measurements were reported in [5] and it is worth mentioning that the distribution of the magnetic field was obtained through more than 3000 test points scattered around the whole area of the substation. The meter was placed at 1.7m above the ground. The measurements were performed under normal working conditions and by monitoring the current flow in all bays. The highest magnetic field measured was 4A/m, thus the prediction is within 3.5% of the measured maximum, while both values are within the public exposure limits. The good agreement between the modelling and experiment increases confidence in the results and provides some justification for the assumptions made.

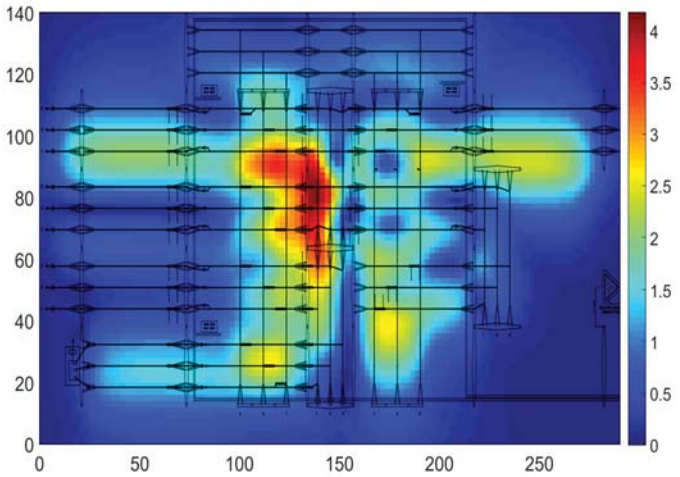

Fig. 2. The computed magnetic field distribution (in A/m) at the Rosiori substation at the height of 1.7m above the ground.

B. Input current with a single lightning pulse

In the second test, a single 200kA IEC62305-1 [17] lightning pulse with 19/459μs front and tail times was injected as a disturbance in the substation circuit as illustrated in Fig. 3.

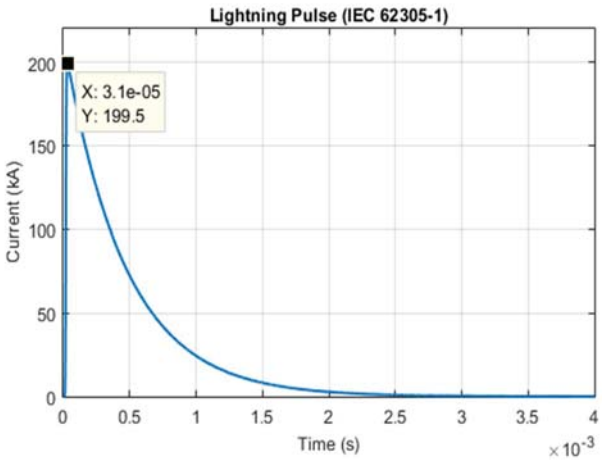

Fig. 3. IEC62305-1 lightning pulse injected to the substation.

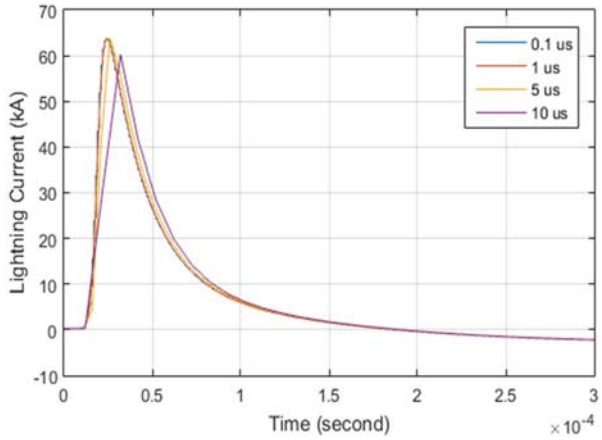

Fig. 4. Lightning current at one of the load (Mukachevo) for four different time steps.

Using the Power Factory software [15], the load flow in the substation was supplemented by an addition of a lightning pulse injected at 0s at one of the 400kV busbars. The time step of this transient analysis is one of the important parameters that needs to be correctly set to achieve meaningful results. The time step will influence the length of the simulation so it is important that it is not set to a very small value. To decide on a suitable time step value, several simulations with different time step were set up and run. The results in terms of the currents in one of the loads (Mukachevo) are shown in Fig. 4 for four different time steps: 0.1μs, 1μs, 5μs, and 10μs, respectively. It is clear that a 10μs time step is not sufficient and the peak current calculated using 5μs and 1μs steps is about 5% larger; moreover, the time at which the maximum current is reached is also different. When the time step was further reduced to 0.1μs no major differences were observed compared with the 1μs case. Consequently, for the simulations presented here, a 1μs time step was used.

The currents of each load with the lightning pulse were used as an input to predict the magnetic field distributions (Fig. 5). The highest current magnitude in the system at 0.02s was 64kA at Mukacevo. The charge conservation is enforced within the model by making sure that the total currents flowing in and out of the substation sum up to zero.

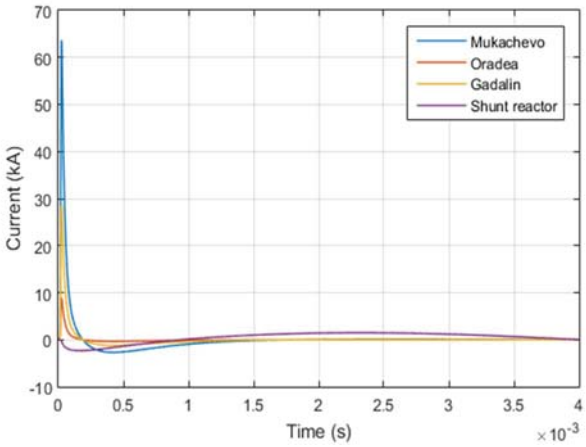

Fig. 5. The current waveforms when a lightning pulse is added.

The magnetic field distribution in the substation due to the lightning pulse can be considered in two different ways, in time domain and in frequency domain. Both approaches have been applied and compared.

1) Magnetic field calculation: the time domain approach

The current flow with a lightning pulse added varies in time as illustrated in Fig. 5, thus the magnetic field changes with time too. Since the lightning current is changing fast, the current element needs to be small enough to capture this fast transient situation; however, it has been found that a 1m long element is sufficient to yield good precision of the result. The time step used for this simulation was 1μs and the total time of the simulation 0.0003s. The highest magnetic field is plotted in Fig. 6 and is obtained at the time of 24μs. The field is plotted at 1.75m from the ground and the maximum is 1282A/m.

The magnetic field calculated shows that the maximum magnetic field value exceeds the public and the occupational exposure limit set by ICNIRP. The calculated magnetic field then could be used for further electromagnetic compatibility analysis. The field may be harmful to the equipment in the proximity of the hot spots shown in Fig. 6.

2) Magnetic field calculation: the frequency domain approach

In order to calculate the magnetic field in the frequency domain, Prony Analysis and Fast Fourier Transform (FFT), the frequency analysis tools from the Digsilent Power Factory, were used. Prony Analysis was used to decompose the signal into damped sinusoidal oscillations to determine the exact value of the important harmonic signals over a range of frequencies [15]. These results compare well with the existent data in the public domain that the induced currents due to the lightning strike have the frequency ranging from 100kHz to 120MHz [18]. The magnitude and frequencies decomposed from each three phase load currents using Prony Analysis are shown in Fig. 7. The important frequencies that were used in the magnetic field calculations are: f_1, the fundamental frequency at 50Hz, f_2 at 70kHz, f_3 at 100kHz, f_4 at 150kHz, f_5 at 200kHz, and lastly f_6 at 250kHz.

The model was then excited separately by each of these harmonics with their respective amplitude. The magnetic field for each frequency was then computed. Finally, the results were combined by adding all the field results in terms of *x*, *y* and *z* components from all the harmonics. A typical result is shown in Figs. 8 and 9.

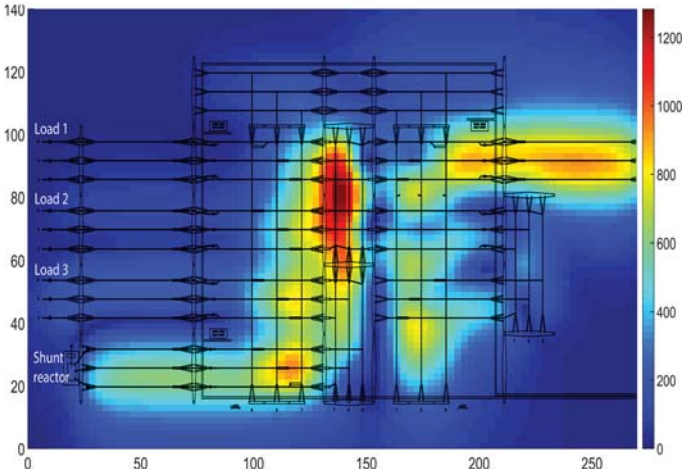

Fig. 6. Distribution of the magnetic field (in A/m) due to a lightning strike in time domain.

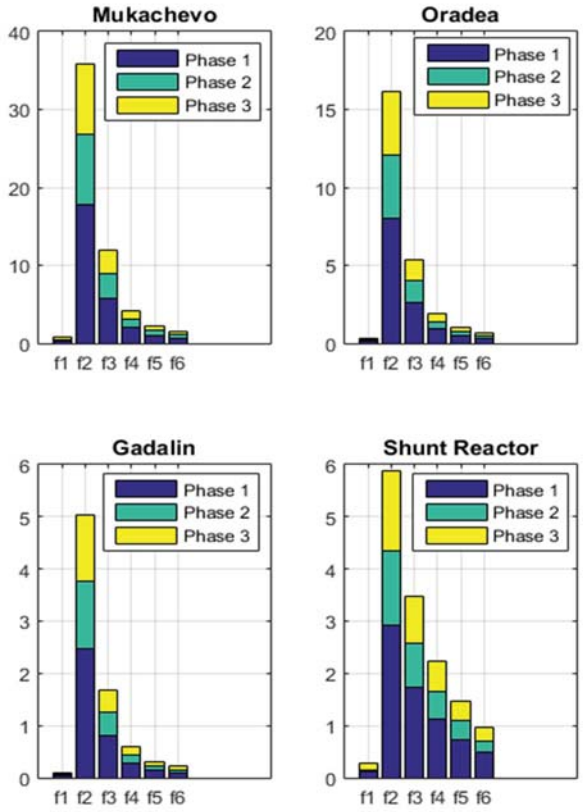

Fig. 7. The important harmonics of each three phase current at every load.

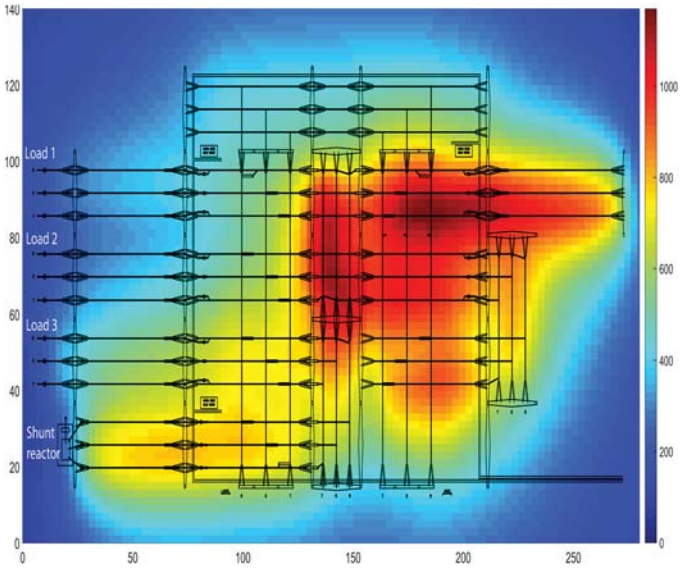

Fig. 8. Distribution of the magnetic field (in A/m) due to a lightning strike calculated using the frequency domain approach

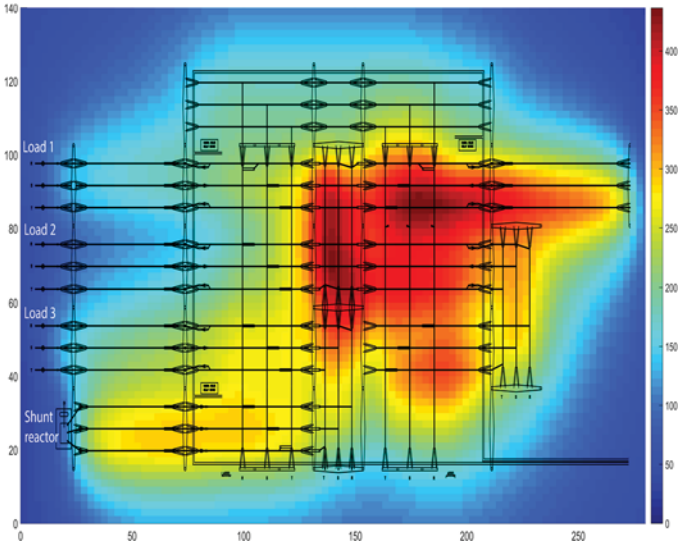

Fig. 9. Distribution of the magnetic field (in A/m) in frequency domain without a 70kHz harmonic.

The highest magnetic field computed using this approach is 1166A/m, this value being 9.04% smaller than the value obtained from the time domain analysis. The difference can be attributed to the fact that we are only considering six harmonics whereas in the time domain all the harmonics carrying power are accounted for. However, the approach allows us to separate the effects of each of these harmonics. For example, in Fig. 9 the magnetic field intensity plot without the 70kHz harmonic is presented: the maximum magnetic field only reaches 436.4A/m. Therefore if the 70kHz harmonic were to be filtered out a reduction of more than half could be achieved. This suggests that to protect sensitive electronic equipment in the substation environment an appropriate filter may be sufficient.

Both analyses, the time domain and frequency domain, predict the hot spot in the same location, which gives confidence in the proposed methodology and the computational tool. The hot spot for the Rosiori substation, studied here, is close to the connection towards the autotransformer. As demonstrated, this relatively simple approach allows the calculation of the magnetic field within the substation and could be used by the utilities companies to predict the field distribution following any disturbance and thus assist in the planning for the future substation refurbish or upgrade.

IV. Conclusion

In this paper, a simple computational approach has been proposed for predicting magnetic field distribution within the substation environment. The method has been verified through direct comparison with test results conducted at a particular substation during working conditions and good agreement is observed. For the normal operation conditions the maximum values of the magnetic field were found to be below public exposure limits. Using the same algorithm, the magnetic field was then calculated for the cases when a lightning pulse was injected to the substation as a disturbance. The model is able to calculate the magnetic field using two different approaches, in time domain and in frequency domain. Both methods yield very close results and predict that the maximum magnetic field value exceeds the public and the occupational exposure limit set by ICNIRP. For a lightning strike in the substation, a smaller time step in the current load flow analysis is required in order to predict the peek current magnitude and to capture the fast transient so that the magnetic field could be calculated accurately. Using the frequency domain approach facilitates the understanding of how each important frequency harmonic influences the field distribution within the substation and this can be used to design more efficient EMI protection for sensitive electronic and digital equipment.

Acknowledgment

The layout of the substation provided by the Technical University of Cluj, Faculty of Electrotechnics, Romania.

References

[1] Working Group C4.208, "EMC within Power Plants and Substations," CIGRE2013.

[2] U. M. Peterlin and T. Zivic, "Electromagnetic Compatibility Levels in Power Plants and Substations," IEEE International Symposium on Electromagnetic Compatibility (EMC), 2015.

[3] U. M. Peterlin, "Guidelines for Electromagnetic Compatibility Provision in Power Plants and Substations," International Symposium on Electromagnetic Compatibility (EMC Europe 2013), 2013.

[4] E. Csanyi. (2012). Smart Grid Concept and Characteristics.

[5] C. P. Nicolaou, A. P. Papadakis, P. A. Razis, G. A. Kyriacou, and J. N. Sahalos., "Measurements and Predictions of Electric and Magnetic Fields From Power Lines," Electric Power Systems Research, vol. 81, pp. 1107-116, 2011.

[6] C. Munteanu, G. Visan, and I. T. Pop, "Electric and Magnetic Field Distribution Inside High Voltage Power Substations. Numerical Modeling and Experimental Measurements," IEEJ Transactions on Electrical and Electronic Engineering, vol. 5, pp. 40-45, 2010.

[7] C. Munteanu, V. Topa, I. T. Pop, A. Racasan, and E. Merdan, "Advances on the Electromagnetic Field Distribution Analysis inside High Voltage Substations," International Universities' Power Engineering Conference (UPEC 2011), 2011.

[8] I. Said, H. B. Hussain, and V. Dave, "Characterization of Magnetic Field at Distribution Substations," 9th International Conference on Environment and Electrical Engineering (EEEIC), pp. 423 - 426, 2010.

[9] W. G. Duff, Fundamentals of Electromagnetic Compatibility. Gainesville, Va.: Interference Control Technologies, 1988.

[10] W. H. Organization, "What are electromagnetic fields? - Current standards," in Exposure to extremely low frequency fields, ed. http://www.who.int/peh-emf/about/WhatisEMF/en/index4.html: WHO Media centre, 2007.

[11] F. T. Ulaby, Electromagnetics for Engineer: Peason/Prentice Hall, 2005.

[12] D. N. FÎTA, L. Muresan, C. Cheleman, and M. Grebenisan, "The Modelling of Rosiori Power Station 400/220/20 KV Retechnologized of Transelectrica Company. The Simulation of the Permanent Regime With EDSA Programme," 6TH International Conference Electromechanical dan Power Systems, 2007.

[13] W. Krajewski, "Numerical Modelling of The Electric Field in HV Substations," IEE Proceedings - Science, Measurement and Technology, vol. 151, pp. 267-272, 2004.

[14] A. P. P. Charalambos P. Nicolaou, Panos A. Razisa, George A. Kyriacou, John N. Sahalos, "Simplistic numerical methodology for magnetic field prediction in open air type substations," Electric Power Systems Research, vol. 81, pp. 2120-2126, 2011.

[15] "DIgSILENT PowerFactory 15," in User Manual, 15 ed. Gomaringen, Germany: DIgSILENT GmbH, 2015.

[16] C. P. Nicolaou, A. P. Papadakis, P. A. Razis, G. A. Kyriacou, and J. N. Sahalos, "Experimental measurement, analysis and prediction of electric and magnetic fields in open type air substations," Electric Power Systems Research, vol. 90, 2012.

[17] I. E. Commission, "IEC 62305-1 International Standard," in Protection Against Lightning, ed, 2010.

[18] R. A. D. Marcus O. Durham, "Lightning, Transient & High Frequency Impact On Material Such As Corrugated Tubing. Frontiers of Power. ," 2008.

Electromagnetic Compatibility Studies of Substation Environment using Finite Difference Method

A. I. Tarmizi, R. H. Ramlee, Mihai D. Rotaru

Abstract*— The implementation of the smart grid system transformed the old substation into a new automated substation. All equipment and component installed in the high voltage substation need to be electromagnetically compatible with each other. Thus, the magnetic field distributed in the environment must be predicted and quantified. Furthermore, with the use of more sensitive microelectronic devices in the system, it creates a need to reassess the substation environment compatibility for current and future circumstances. In this paper, the calculation method used to determine magnetic field distribution within a substation environment has been reviewed. A new routine which allows the user to focus at a specific area of the substation and calculate the field has been developed in-house using Matlab. The new routine calculates the magnetic field using a finite difference approach and allows a much better field resolution to be achieved in a specific area of interest within the substation.

***Index Terms*— EMC; automated substation; smart grid; magnetic field; Matlab; Finite Different Method; Biot Savart Law**

I. INTRODUCTION

In a smart grid system, the is a new level of expectation for distribution automation. Substation automation is expected to expand dramatically with increased control of relays, capacitor banks, and voltage regulators along the feeder. The smart grid substations are expected to incorporate distributed energy resources, advanced metering infrastructure, as well as demand response functions. Achieving these goals requires three essential components: 1. Intelligent Electronic Devices (IED) for sensing, measuring and control of the equipment and network parameters; 2. A communication network to connect different components; 3. Software applications at various levels of the network, including the substation system that can manage the other pieces of the automation system [1-3]. All the equipment or systems above need to function satisfactorily in its electromagnetic environment without introducing intolerable electromagnetic disturbances to anything in that environment [4, 5]. In a high voltage substation, while the components and equipment are operating, electric and magnetic fields are produced that might or might not cause interruption to the system; thus, it is crucial to make sure that the system is compatible and immune to electromagnetic interferences [6-8].

Electromagnetic compatibility (EMC) studies in the substation area are more concern today than ever before. Although the EMC issues have been discussed widely in power systems, there has been limited work done on the EMC within the current implementation of the automated substation, especially in the context of a smart grid [9-11]. Thus, it is significant that the electromagnetic field distribution within a substation environment is well identified with the intention of the possible to reduced EMC hazards. To have a clear view of the magnetic distribution, the previous researcher has done mapping of the field distributed via site measurements [12-14] or simulations [15, 16]. Deciding on which approach to use are depends on many factors; however, both approaches, measurement and simulation have been used in previous research [17-19]. Since it is difficult and nearly impossible to measure the magnetic field distribution during disturbances occurrence, computational methods are used to predict and illustrate the real event. As discussed in the previously published work, Biot-Savart law can be employed directly to solve the electromagnetic problem that has a large size environment. To simplify the computational complexity and improve the efficiency a coarse mesh was applied [20]. However, to understand the field intensity and its distribution where the sensitive equipment may be installed within the substation a better resolution of the field solution is necessary. In this paper, an extension of the previous work is provided. A methodology that allows a details analysis on specific volumes in the substation environment based on the Finite Difference Method (FDM) is presented. The numerical algorithm has been developed in Matlab and can perform a detailed analysis of the magnetic field distribution within the specific region in the substation environment. This is would be giving the user or utility company information on the electromagnetic environment at a specific location within the substation and informed decision where to install the new equipment can be taken.

II. EMC LIMITATION GUIDELINES AND STANDARD

Limits guidelines and standards used to ensure that the substation environment is safe for human health and the equipment able to operates compatibly in the substation environment system. From a health and safety point of view, these generated fields should be within the range of health regulations and EMC standards. The International Commission sets the majority of the national guidelines on Non-Ionizing Radiation Protection (ICNIRP) which is recognised by the World Health Organization (WHO) which is a non-governmental organisation that assesses scientific outcomes from all over the world. The limits recommended

Manuscript received October 01, 2011. (Fill the Details)
A. I. Tarmizi, University of Southampton, UK, Universiti Teknikal Malaysia Melaka, UTeM (e-mail: aineizzati@utem.edu.my).
R. H. Ramlee, Universiti Teknikal Malaysia Melaka, UTeM
Mihai D. Rotaru, University of Southampton, UK.

Published By:
Blue Eyes Intelligence Engineering
& Sciences Publication Pvt. Ltd.

by the ICNIPR and WHO for human exposure limits of the magnetic field are published to be 80 A/m for public exposure and 400 A/m for occupational exposure [21].

For this research study will be focusing on the standard that applied directly to the equipment limitation to magnetic field disturbances at medium voltage and high voltage substation environment. In the substation environment magnetic field is dependent on the configuration of the high voltage line, load, fault condition. It is significant to know the field profile in the electromagnetic environment exposure towards equipment. Thus, the values of the magnetic field in the substation area from the standard will be used to compare the EMC as in Table I below.

TABLE I. VALUES OF THE MAGNETIC FIELD IN HIGH VOLTAGE SUBSTATION AREAS [22]

Substation	220kV	400kV
Under the bus-bars near the connection to a line carrying about 0.5 kA	14 A/m	9 A/m
In the relay room (kiosk)	Near event recorders at about 0.5 m distance: 3.3 A/m Near measurement voltage transformer: d = 0.1 m: 7.0 A/m d = 0.3 m: 1.1 A/m	
In the equipment room	Maximum 0.7 A/m	

III. MAGNETIC FIELD CALCULATION USING FINITE DIFFERENCE METHOD

To get a detailed analysis of a specific area in the substation, first, the coarse magnetic field distribution is computed using the methodology described in our previous work [20]. The volume of interest is then separated from the initial coarse solution, and a more detailed FDM is applied in this volume using the information already computed as the boundary condition. The details of this procedure are presented in the following sections.

A. Mathematical Description of FDM Equation for Magnetic Field Calculation

FDM is a numerical computational method used to solve linear partial differential equations. As we are interested in the magnetic field distribution, we need to consider the Ampere's law stated below (1):

$$\nabla \times \mathbf{H} = \mathbf{J}_e + \frac{\partial \mathbf{D}}{\partial t} \tag{1}$$

$\mathbf{J}_e$ is the conduction current density and $\frac{\partial \mathbf{D}}{\partial t}$ is the displacement current density respectively. For the case study here the displacement current density is considered to be negligible as the main field is produced by the current flowing at 50 Hz the grid frequency If fault currents produce the magnetic field, currents due to switching or currents due to lighting strike their higher harmonics may produce displacements currents that cannot be ignored, hence the solution provided here is not applicable. However, if the displacement current is ignored, a quasistatic case can be assumed. Finally, using Faraday's law in Equation (2) and Ohms law is written in its microscopical form in Equation (3) one can rewrite Equation (1) as Equation (4) which is an equation having one single variable namely magnetic field.

$$\nabla \times \mathbf{E} = -\mu_\circ \mu_r \frac{\partial \mathbf{H}}{\partial t} \tag{2}$$

$$\mathbf{J}_e = \sigma \mathbf{E} \tag{3}$$

The new problem that needs to be solved now is a second-order differential Equation (4) which is known as diffusion equation.

$$\nabla^2 \mathbf{H} = \sigma \mu_\circ \mu_r \frac{\partial \mathbf{H}}{\partial t} \tag{4}$$

The equation (4) can be written in three dimensions as follow:

$$\left[\frac{\partial^2}{\partial x^2} + \frac{\partial^2}{\partial y^2} + \frac{\partial^2}{\partial z^2}\right] \mathbf{H}^m_{(x,y,z,t)} = \sigma \mu_0 \mu_r \frac{\partial \mathbf{H}(x,y,z,t)}{\partial t} \tag{5}$$

The finite difference approximation for the spatial component of the Equation (5) in the three axes (*x*,*y*,*z*) is then:

$$\frac{\partial^2 \mathbf{H}^m_{(x,y,z)}}{\partial x^2} = \frac{\mathbf{H}_{(k+1,j,i)} - 2\mathbf{H}_{(k,j,i)} + \mathbf{H}_{(k-1,j,i)}}{\Delta x^2} \tag{6}$$

$$\frac{\partial^2 \mathbf{H}^m_{(x,y,z)}}{\partial y^2} = \frac{\mathbf{H}_{(k,j+1,i)} - 2\mathbf{H}_{(k,j,i)} + \mathbf{H}_{(k,j-1,i)}}{\Delta y^2} \tag{7}$$

$$\frac{\partial^2 \mathbf{H}^m_{(x,y,z)}}{\partial z^2} = \frac{\mathbf{H}_{(k,j,i+1)} - 2\mathbf{H}_{(k,j,i)} + \mathbf{H}_{(k,j,i-1)}}{\Delta z^2} \tag{8}$$

Similarly, the finite difference approximation of the time component of Equation (5) is shown below in Equation (9).

$$\sigma \mu_0 \mu_r \frac{\partial \mathbf{H}}{\partial t} = \sigma \mu_0 \mu_r \frac{\mathbf{H}^{m+1}_{(k,j,i)} - \mathbf{H}^m_{(k,j,i)}}{\Delta t} \tag{9}$$

If we let $\Delta x = \Delta y = \Delta z = \boldsymbol{h}$, the simplified equation can be written as follow:

$$\begin{aligned} \mathbf{H}^{m+1}_{(k,j,i)} = \mathbf{H}^m_{(k,j,i)} + C[&\mathbf{H}^m_{(k+1,j,i)} - 6\mathbf{H}_{(k,j,i)} \\ &+ \mathbf{H}_{(k-1,j,i)} + \mathbf{H}_{(k,j+1,i)} \\ &+ \mathbf{H}_{(k,j-1,i)} + \mathbf{H}_{(k,j,i+1)} \\ &+ \mathbf{H}_{(k,j,i-1)}] \end{aligned} \tag{10}$$

$$\begin{aligned} \mathbf{H}^{m+1}_{(0)} = \mathbf{H}^m_{(0)} + C[&\mathbf{H}^m_1 - 6\mathbf{H}^m_0 + \mathbf{H}^m_2 + \mathbf{H}^m_3 + \mathbf{H}^m_4 \\ &+ \mathbf{H}^m_5 + \mathbf{H}^m_6] \end{aligned} \tag{11}$$

After further simplification, the final equation stated in Equation (10) and the coefficient represented in Equation (11) can be written as below:

$$\mathbf{H}_0 = C(\mathbf{H}_1 + \mathbf{H}_2 + \mathbf{H}_3 + \mathbf{H}_4 + \mathbf{H}_5 + \mathbf{H}_6) \tag{12}$$

$$C = (6 + j\omega\sigma\mu_0 h^2)^{-1} \tag{13}$$

The application of Equation (12) and Equation (13) within the volume of interest area in the substation are illustrated in a uniform 3D mesh grid as in Fig. 1.

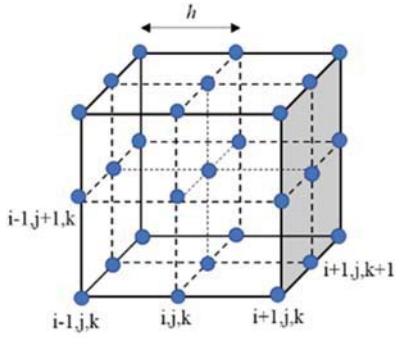

Fig. 1. Uniform mesh in 3-D grid point.

Published By:
Blue Eyes Intelligence Engineering
& Sciences Publication Pvt. Ltd.

B. Substation structure and modelling assumptions

The layout of the substation used in this research is generously provided by the University of Cluj Romania, Faculty of Electrotechnics. The Rosiori substation is a 400/220kV substation and is a major substation of the National Power System (SEN), located in the north of Romania. The substation consists of a 400kV double busbar steps down to 220kVwith three outgoing feeders [23]. One of the main reasons that this specific substation used in this research was the availability of magnetic and electric field measurements done by researchers in Cluj, Romania [7] which will be used to validate the developed calculation model. Fig. 2 shows that the computed results for the normal operating currents with the predicted highest value of the magnetic field are 4.164A/m which located along busbar 1, where it is connected to Load 1, drawing a 200A current as published in [20].

By referring to the coarse calculation which refereeing to overall magnetic field distribution from the previous calculation for the whole substation with larger mesh grid in Fig.2, the user chooses the volume of interest area as illustrated in Fig. 3. Once the volume of interest has been determined the size of the mesh has to be chosen. The details need to be plug-in the numerical calculation routine developed in Matlab.

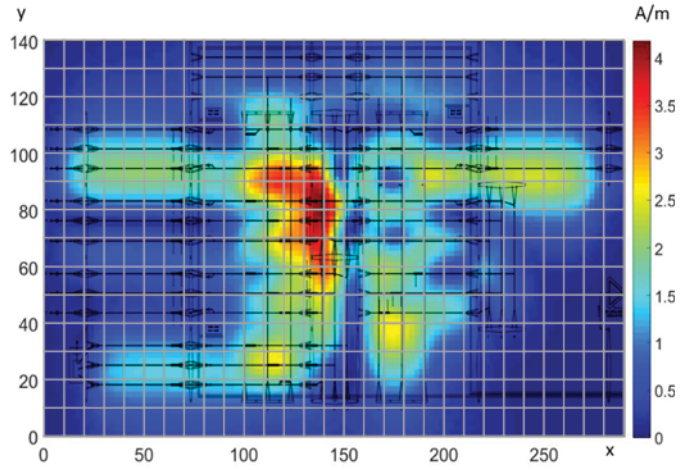

Fig. 2. The computed magnetic field (A/m) distribution at the Rosiori substation (in grid square cell) at the height of 1.7m above the ground.

The simulation model developed computes magnetic field within a volume of interest within the substation environment using the finite difference method in three dimensions (3D). The developed routine divides the subdomain of interest in cubic cells with space step of ***h*** as shown in Fig. 4. With this algorithm, the density of the calculation points can be easily modified to focus on regions of higher interest. The initial value of the calculated fields at the boundaries is assumed to be fixed due to the changes in the subdomain.

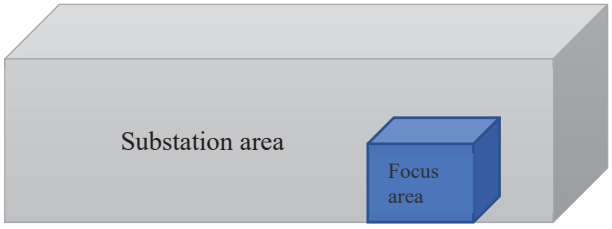

Fig. 3. Illustration of whole substation area and focus area

IV. FDM Calculated Result and Comparison with BSL Calculation Method

The calculated magnetic field for focus area was calculated using finite difference method (FDM) as shown in Fig. 4 with the highest magnetic field were estimated to be nearly 5A/m which is below ICNIPR exposure guideline [24]. The FDM result was compared with the field calculated using Biot-Savart Law (BSL) [20] as plotted in Fig. 5.

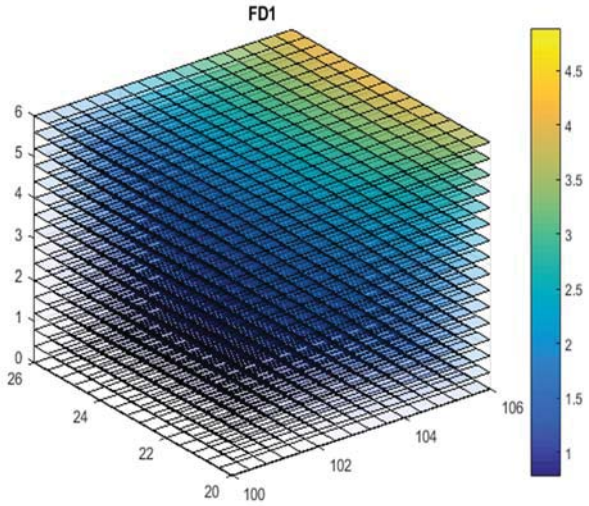

Fig. 4. Calculated magnetic field (A/m) at the focus area in the substation using Finite Difference Equation Method.

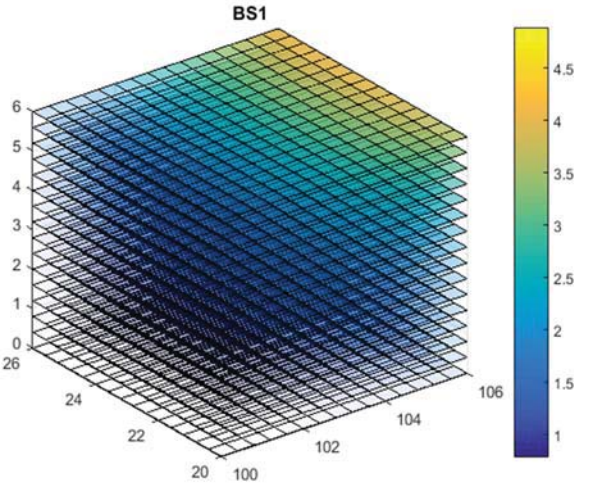

Fig. 5. Calculated magnetic field (A/m) at focus area in the substation using Biot Savart Law

The algorithm calculates the magnetic field start from initial value towards the inside for the whole area with the resolution of 0.02m for every axis (x,y,z). From both figures, it shows that the calculated value of **H** for both methods are almost the same, and it is difficult to do the comparative analyses. Thus, to get a better view, the percentage difference of the magnetic field between both calculation method was calculated.

The percentage differences for every point between FDM and BSL are calculated and plotted in Fig. 6. From the figure, it is clear that the initial magnetic field value which starts from outer points of the focus area is the same for both calculation method with 0% difference.

Published By:
Blue Eyes Intelligence Engineering
& Sciences Publication Pvt. Ltd.

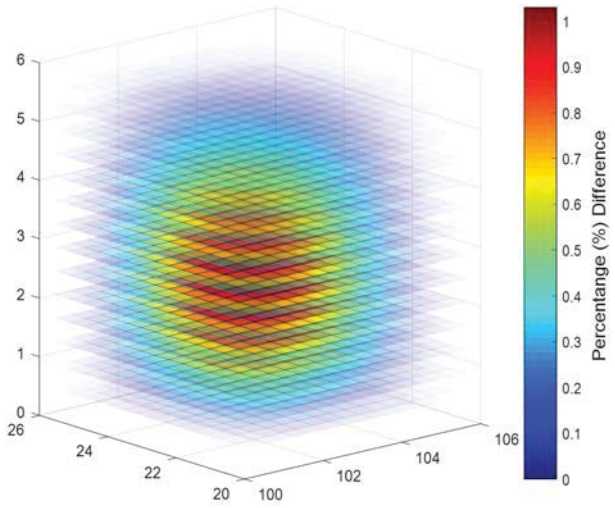

Fig. 6. The percentage indifferent between FDM and BSL

The differences between both approaches are getting more prominent as it calculates far apart from the initial value. It shows that the centre of the focus area has the highest with 1.01% percentage difference. To get a better view of the percentage difference between both numerical calculation method, a cross-section of the focus area (Fig. 6) at 2.8m ware plotted in Fig. 7 and Fig. 8. From both figures, it shows that the maximum value of percentage difference error is 1.012%. The percentage difference for both calculation methods gradually increases as it calculates the magnetic field towards the centre of the area. With the low percentage of difference, it is confident that both numerical methods can predict the magnetic field.

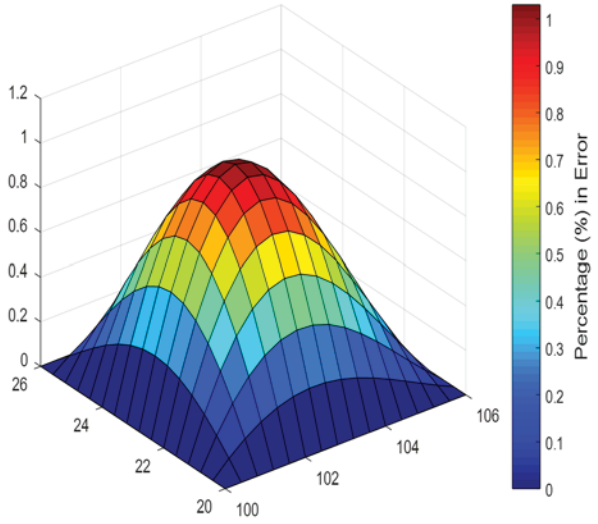

Fig. 7. Percentage difference at a cross-section of the focus area.

From the calculation result, there a few element comparisons that can be made between BSL and FDM. First, the BSL calculation takes more time to compute as the magnetic field was calculated directly from the source of current to the point of interest. The distance of the observation point to the conductor is changing. It is changing proportionally the calculated magnetic field induced by the current input. The calculation time could be reduced by setting the point of interest to be in a larger mesh. Thus, BSL is suitable to use to get an overall picture of the magnetic field distribution in the substation area with large mesh grid. In another hand, by using FDM, it can be used to predict the magnetic field by using the initial calculated value but for smaller grid mesh, which is needed to calculate for the whole focus area.

The combination of both calculation methods is the best for EMC studies in large substation area. It definitely will reduce the calculation time and the user able to choose the desired location with a preferable size of the mesh grid. Thus, it will allow the utility company to predict and determine the most suitable location to place the new equipment for the smart grid system.

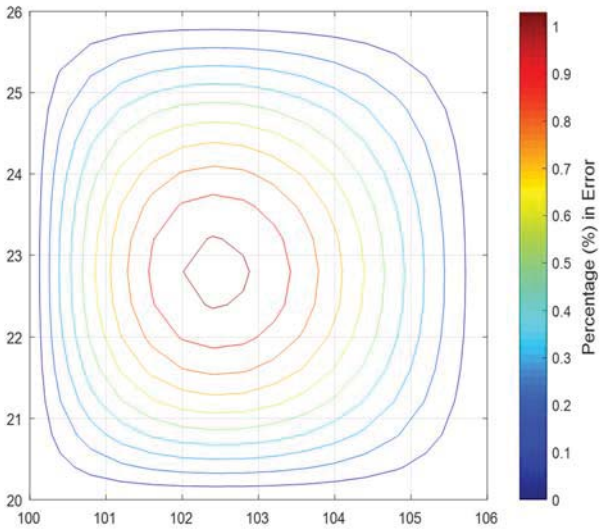

Fig. 8. Percentage difference at 2.8m cross-section of the focus area

V. Introduction of a Metal Box in the Substation Environment

There is another crucial justification to be made before installing new equipment in the substation. The equipment needs to be functional and connected to the substation within the optimum level and cost-friendly. To illustrate the real equipment that installs in the substation environment, a metal box model with holes which will demonstrate the cut off from the box for any connecting power supply and control buttons on the equipment. The magnetic field generated from the substation environment is expected to travel inside the equipment box. The parameter of the box that will be structured in the model is the dimension, location, and material of the desired by used. The box could be located at desired substation's environment. Ideally, the box should be located at the lowest magnetic field interference.

Using the calculation model, the size and location of this box can be adjusted to any measurement and could be set to anywhere in the substation environment to suite the user needs. For this particular case, the coordinate of the focus area chosen is located at [102,22,2]. As for the box dimension in the calculated model are set to be 0.5m for length, width, wide, and the thickness of the metal box is set to be 0.02m. The dimension of the box could be changed to any measurement that required to fit the equipment that will install in the substation, as illustrated in Fig. 9 below.

Published By:
Blue Eyes Intelligence Engineering
& Sciences Publication Pvt. Ltd.

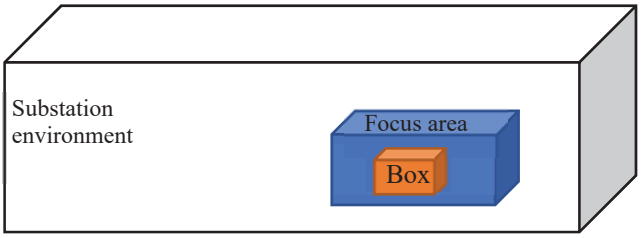

Fig. 9. Illustration of whole substation area and focus area

The same calculation method used, where developed FDM applied to every node in the mesh grid to calculate the magnetic field within the metal box. Fig. 10 shows that the grid or mesh in 2D where the cross-section of the metal box is illustrated. Every node (i,j,k) are divided to the region into a number of the subdomain. The blue mesh is set as a focus area which calculated earlier, the grey mesh will be the metal box and the white will be air. All parameter that associate to every node applied to the finite difference equation.

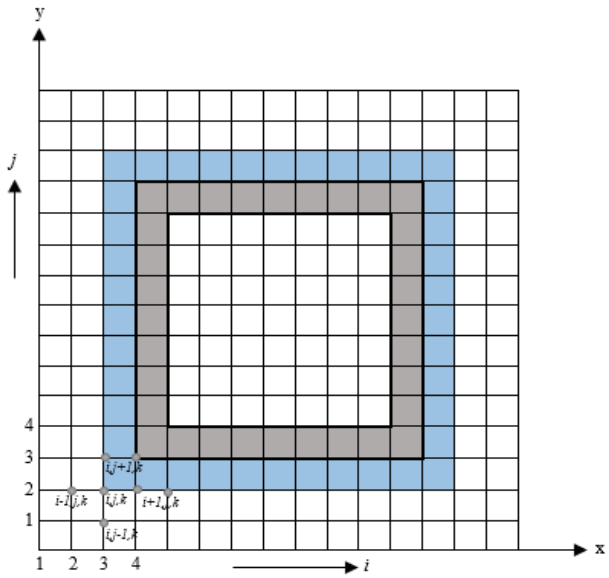

Fig. 10. Finite difference grid or mesh in 2D (cross-section) with a metal box

To illustrate the real equipment that will be installed in the substation environment, the metal box model as the equipment under test should have a cut opening on the surface, which generally for power supply connection or control button. The manufacturer will try to make it as small as possible to avoid any interference propagate into the equipment. Since the source of magnetic field interferences coming from the transmission line above the box, the cut opening on the box is located on the lowest position as illustrated in Fig. 11. The other parameter that needs to be considered is the material, which is the representative in the magnetic field equation as permeability, μ of material as shown in Equation (13).

With this calculation and prediction of the magnetic field within the operated substation, the result would be useful not only for safety assurance but it also will help utility company to design a newly automated substation or refurbish the old one with an optimum immunity level. The magnetic field generated from the substation environment flowing into the box through the cut opening and it is predicted that the magnetic field has higher field density at the opening of the box, and it will disperse within the area.

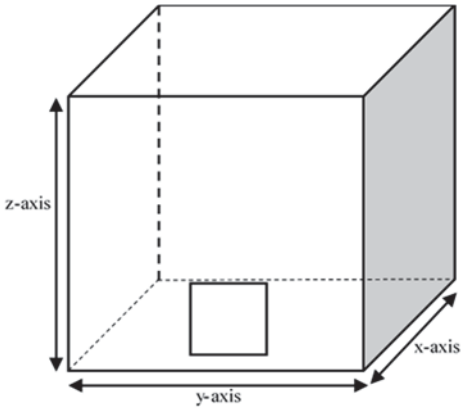

Fig. 11. Illustration of the box with an opening cut

A. *Computational Results and Discussion*

Based on the result of the calculation from the developed algorithm in Matlab, the magnetic field generated from the substation environment penetrate the box via the opening cut on the model box and the field travelled inside the box freely. The magnetic field was calculated for two different input current, which is during the normal operating current and lightning strike into the substation. The result shows the higher field density is located at the opening of the box as plotted in Fig. 12 and Fig. 13. Thus, the magnetic field generated from the substation environment able to enter in the box via any size and location of the cut opening on the metal box.

Based on the calculated magnitude of the magnetic field as listed in Table II, the predicted magnetic field during the substation's normal operation is below the safety guidelines exposure limit for health and safety, both public and occupational set by ICNIRP [24, 25] with 0.4A/m. In contrast with lightning event apply in the substation system, it shows that it is not fulfilling the recommended limits need to be 0.7A/m in the equipment room, where during the lightning event the magnetic field was calculated to be 854.5A/m. Thus, the substation environment is not a safe place for anyone. Nevertheless, the equipment in the substation is included at risk. The compatibility requirement set by IEC61000 [22, 26] within the substation environment needs to be fulfilled.

TABLE II. THE MAGNITUDE OF THE CALCULATED MAGNETIC FIELD

Substation condition	$\bar{H}$ (A/m)
Normal operation	0.4323
Lightning	854.505

Typically, during the lightning event, the protection system in the substation should be operated instantaneously to protect the equipment and component from lightning pulse flowing in. However, the magnetic field generated by this high current might cause electromagnetic compatibility issues in the system [27]. There was more power electronic equipment installed in the Smart Grid system with the latest development of smart grid substation [28, 29]. To ensure the system operate within the optimal compatibility level towards magnetic disturbances, it needs to satisfy the standard requirement by IEC61000 [22, 26].

Published By:
Blue Eyes Intelligence Engineering
& Sciences Publication Pvt. Ltd.

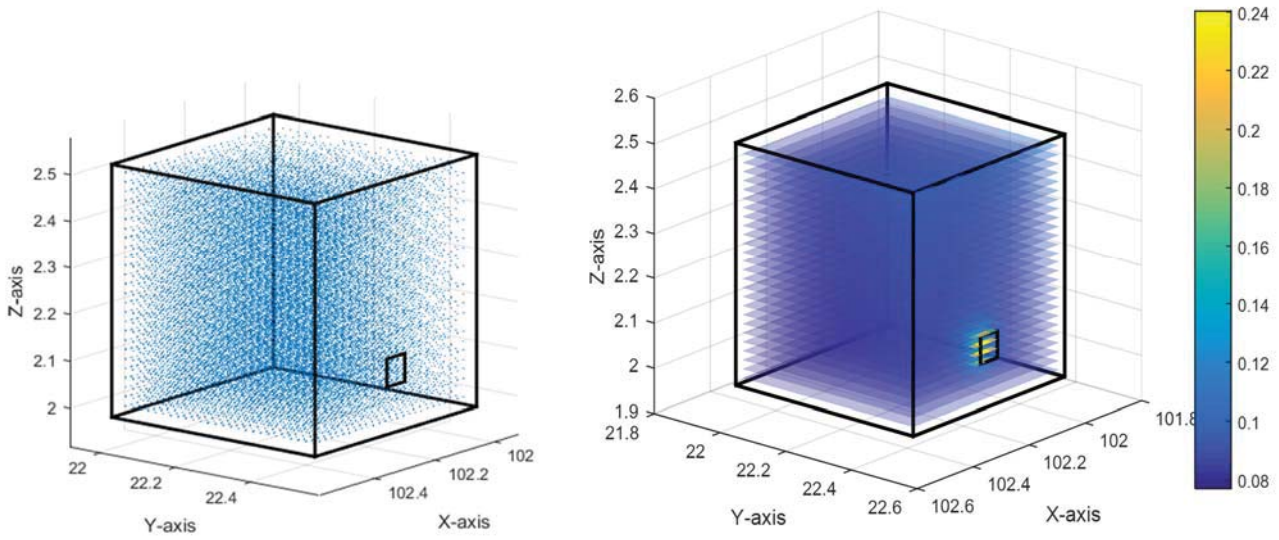

Fig. 12. Magnetic field (A/m) distributed inside the metal box with an opening during normal condition

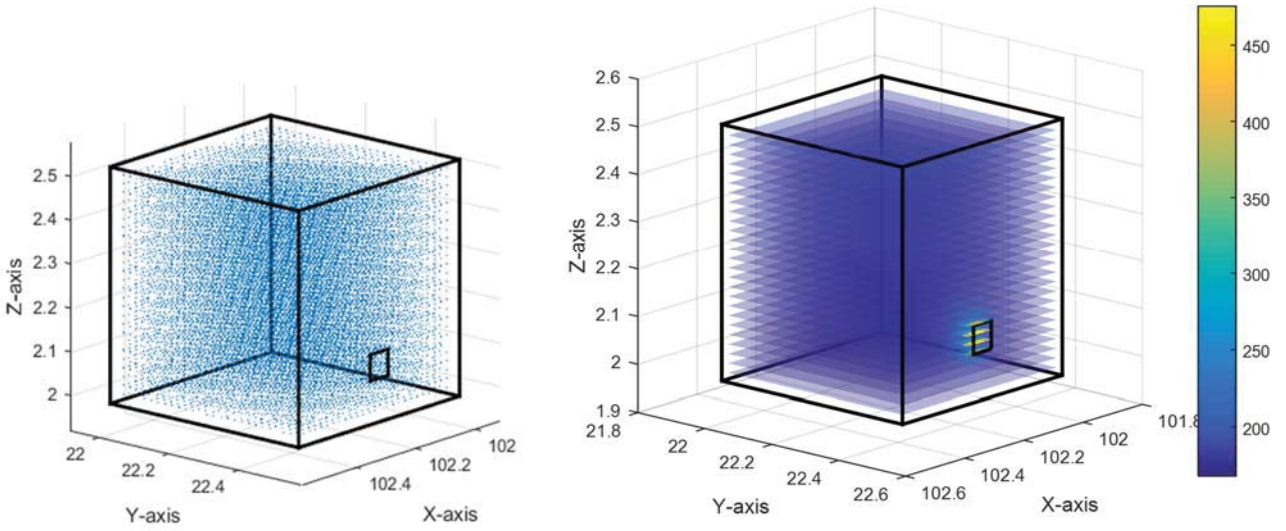

Fig. 13. Magnetic field (A/m) distributed inside the metal box with an opening during lightning

I. Conclusion

In this paper, the FDM equation has been introduced to calculate the magnetic field in the focus area within the substation environment. In result, the FDM compared with the previous work using BSL as discussed previous work on magnetic field calculation within the substation. With the low percentage differences between both methods shows that the calculation method is suitable to predict the magnetic distribution. The combination of both ways helps to achieve optimal simulation routine in predicting the magnetic field in the substation area with any current input. A model of metal box introduces in the simulation to represent the real equipment that will be installed in the focus area of the substation environment. The magnetic field distribution inside the box was calculated using FDM. The computed value is compared with the standard immunity or electromagnetic compatibility level of the equipment and help in the planning of the new equipment installed in the substation environment in future.

Acknowledgement

The layout of the substation provided by the Technical University of Cluj, Faculty of Electrotechnics, Romania and authors are grateful to Universiti Teknikal Malaysia Melaka for the financial support through Pusat Pengurusan Penyelidikan dan Inovasi (CRIM),

References

[1] E. Csanyi. (2012). *Smart Grid Concept and Characteristics*.
[2] A. Duffy and D. Heirman. (2012) Smart Grid and EMC Standards. *IEEE Electromagnetic Compatibility Magazine*.
[3] E. Chikuni, "Power System and Substation Automation."
[4] Working Group C4.208, "EMC within Power Plants and Substations," CIGRE2013.
[5] S. Bricker, T. Gonen, and L. Rubin, "Substation automation technologies and advantages," *IEEE Computer Applications in Power*, vol. 14, no. 3, pp. 31-37, 2001.
[6] U. M. Peterlin and T. Zivic, "Electromagnetic Compatibility Levels in Power Plants and Substations," *IEEE International Symposium on Electromagnetic Compatibility (EMC)*, 2015.

Published By:
Blue Eyes Intelligence Engineering
& Sciences Publication Pvt. Ltd.

[7] U. M. Peterlin, "Guidelines for Electromagnetic Compatibility Provision in Power Plants and Substations," *International Symposium on Electromagnetic Compatibility (EMC Europe 2013)*, 2013.

[8] U. M. Peterlin and T. Živic, "Electromagnetic compatibility levels in power plants and substations," in *2015 IEEE International Symposium on Electromagnetic Compatibility (EMC)*, 2015, pp. 266-270.

[9] SGIP Electromagnetic Interoperability Issues Working Group, "Electromagnetic Compatibility and Smart Grid Interoperability Issues," *Smart Grid Interoperability Panel*, 2012.

[10] P. F. Keebler. (2012) Meshing Power Quality and Electromagnetic Compatibility for Tomorrow's Smart Grid. *IEEE Electromagnetic Compatibility Magazine*.

[11] P. Kotsampopoulos *et al.*, "EMC issues in the interaction between smart meters and power electronic interfaces," *IEEE Transactions on Power Delivery*, vol. PP, no. 99, pp. 1-1, 2016.

[12] I. Said, A. S. Farag, H. Hussain, and N. A. Rahman, "Measurement of Magnetic Field from Distribution Substations in Malaysia," *Australasian Universities Power Engineering Conference (AUPEC 2004)*, 2004.

[13] W. Lihui, H. Jiayu, J. Jianfei, P. Fubin, and Y. Yubo, "Measurement of transient electromagnetic coupling and interference caused by disconnector operation in substation," *Measurement*, vol. 96, pp. 1-7, 1// 2017.

[14] A. S. Safigianni and C. G. Tsompanidou, "Electric- and Magnetic-Field Measurements in an Outdoor Electric Power Substation," *IEEE Transactions on Power Delivery*, vol. 24, no. 1, pp. 38-42, 2009.

[15] A. Weddemann, D. Kappe, and A. Hutten, "Hybrid FEM-BEM Approach for Two- and Three-Dimensional Open Boundary Magnetostatic Problems," 2011.

[16] T. Ling, W. Xiaoyu, Q. Liang, S. Lu, and Y. Fan, "Calculation of Power frequency Electric Field in HV Substation Using BEM," *Asia-Pacific Power and Energy Engineering Conference (APPEEC), 2011*, 2011.

[17] C. P. Nicolaou, A. P. Papadakis, P. A. Razis, G. A. Kyriacou, and J. N. Sahalos, "Experimental measurement, analysis and prediction of electric and magnetic fields in open type air substations," *Electric Power Systems Research*, vol. 90, pp. 42-54, 9// 2012.

[18] Y. Ma, G. G. Karady, J. R. Hunt, and B. L. Priest, "Measurement and Prediction of Electrical Substation Generated Electromagnetic Field," *IEEE Power and Energy Society General Meeting*, 2011.

[19] A. S. Safigianni and A. Kostopoulou, "Electric and Magnetic Field Measurements in an indoor Electric Power Substation," *Journal of Materials Processing Technology*, vol. 181, no. 1-3, pp. 126-130, 2007.

[20] A. I. Tarmizi, M. D. Rotaru, and J. K. Sykulski, "Magnetic field calculations within substation environment for EMC studies," in *IEEE 16th International Conference on Environment and Electrical Engineering (EEEIC)*, 2016, pp. 1-6.

[21] *What are electromagnetic fields? - Current standards*, 2007.

[22] *Electromagnetic compatibility (EMC)Part 4-8: Testing and measurement techniques — Power frequency magnetic field immunity test*, 2010.

[23] D. N. FÎTA, L. Muresan, C. Cheleman, and M. Grebenisan, "The Modelling of Rosiori Power Station 400/220/20 KV Retechnologized of Transelectrica Company. The Simulation of the Permanent Regime With EDSA Programme," *6TH International Conference Electromechanical dan Power Systems*, 2007.

[24] (2007, 23-Mac-2017). *Electromagnetic fields and public health - Exposure to extremely low frequency fields*. Available: http://www.who.int/peh-emf/publications/facts/fs322/en/

[25] *ICNIRP Guidelines For Limiting Exposure to Time-Varying Electric, Magnetic And Electromagnetic Fields (Up To 300 GHz)*, 1998.

[26] *IEEE Standard for Power Line Communication Equipment—Electromagnetic Compatibility (EMC) Requirements—Testing and Measurement Methods*, 2010.

[27] S. Gu, D. Li, X. Zeng, J. Su, Y. He, and Z. Zhao, "Analysis of the characteristics and impact of lightning on smart substations," in *2017 IEEE 5th International Symposium on Electromagnetic Compatibility (EMC-Beijing)*, 2017, pp. 1-6.

[28] Y. Yang, Z. Zhao, S. Gu, D. Li, and X. Zeng, "Analysis of the impact of direct lightning smart substation overhead ground wire on the station smart components," in *2016 Asia-Pacific International Symposium on Electromagnetic Compatibility (APEMC)*, 2016, vol. 01, pp. 927-929.

[29] Q. Song *et al.*, "Smart substation integration technology and its application in distribution power grid," *CSEE Journal of Power and Energy Systems*, vol. 2, no. 4, pp. 31-36, 2016.

Published By:
Blue Eyes Intelligence Engineering
& Sciences Publication Pvt. Ltd.